GEOLOGICAL SURVEY OF WESTERN AUSTRALIA

REPORT 30

PROFESSIONAL PAPERS

DEPARTMENT OF MINES
WESTERN AUSTRALIA

GEOLOGICAL SURVEY OF WESTERN AUSTRALIA

REPORT 30

PROFESSIONAL PAPERS

State Printing Division
Perth 1991

2474-1

MINISTER FOR MINES

THE HON. GORDON HILL, J.P., M.L.A.

DIRECTOR GENERAL OF MINES

D. R. KELLY

DIRECTOR, GEOLOGICAL SURVEY OF WESTERN AUSTRALIA

PHILLIP E. PLAYFORD

National Library of Australia Card Number and ISBN 0 7309 4400 X
ISSN 0508-4741
ISSN 0812-8952

Copies available from:
Director
Geological Survey of Western Australia
100 Plain Street
EAST PERTH, WESTERN AUSTRALIA 6004
Telephone (09) 222 3168

CONTENTS

The geology and hydrogeology of the Cowaramup borehole line Perth Basin, Western Australia

by S. J. Appleyard

ABSTRACT

The Cowaramup borehole line comprises nineteen bores at eight sites across the Perth Basin to the south of Busselton, Western Australia. The aggregate depth was 10 479 m; and the deepest bore (CL7A) was 1668 m deep.

Drilling has shown that the Sue Coal Measures (Early Permian), and the Cockleshell Gully, Yarragadee, and Parmelia Formations (Early Jurassic to Early Cretaceous) occur in major fault blocks, and are unconformably overlain by the Bunbury Basalt and the Warnbro Group (Early Cretaceous). The Parmelia Formation was recorded for the first time in the onshore Perth Basin near the eastern end of the borehole line.

The Warnbro Group is a multilayered aquifer consisting of a number of local flow systems superimposed on a weakly developed regional flow system. It is mainly shale, and contains only limited reserves of groundwater, except in the west, where the aquifer contains a larger percentage of sandstone. The groundwater in the Warnbro Group contains less than 500 mg/L total dissolved salts (TDS), but the concentration of dissolved iron usually exceeds 5 mg/L.

The Parmelia, Yarragadee, and the upper part of the Cockleshell Gully Formations, are sandstone and shale. These formations contain fresh groundwater between the Busselton and Darling Faults; and groundwater with a salinity of less than 1000 mg/L TDS extends to depths of between 800 and 1500 m below sea level.

The Sue Coal Measures consist of sandstone, shale, and coal; and contain fresh groundwater between the Dunsborough and Busselton Faults. Fresh groundwater occurs in two flow systems separated by a basement high; and extends to a depth of more than 500 m below sea level on both sides of a basement high.

The Yarragadee Formation and the Sue Coal Measures are major aquifers which are currently unexploited in the area.

KEYWORDS: Perth Basin, hydrogeology, geology, groundwater, stratigraphy

Introduction

The Cowaramup Line comprises nineteen bores at eight sites across the Perth Basin in the lower southwest of Western Australia at about latitude 33° 50' S (Figure 1); it is situated about 30 km south of the Quindalup Line (Wharton, 1981b). An aggregate depth of 10 479 m was drilled, and the deepest bore was 1668 m deep. The exploratory drilling was carried out as part of a long-term program to evaluate the deep groundwater resources of the Perth Basin.

Climate

The area has a mediterranean climate. Average annual rainfall ranges between 900 mm in the east and 1200 mm in the west, and 90% of the rain falls between April and October. The average annual evaporation is 1300 mm, and the mean daily temperature ranges from a maximum of 28°C in February to a minimum of 8°C in July.

Physiography and land use

The Cowaramup Line is on the Blackwood Plateau (Low, 1972), which ranges between 80 and 180 m above sea level. The plateau has a gently undulating surface covered by laterite and sand. It is bounded to the west by the Leeuwin– Naturaliste Ridge and to the east by the Darling Plateau.

Most of the Blackwood Plateau is covered by eucalypt forest. The western margin of the plateau has been cleared for agriculture; and some parts of the native forest have been replaced by pine plantations.

Investigation program

The Cowaramup Line (CL) bores were drilled by the Mines Department Drilling Branch—using mud-flush rotary drilling rigs—between November 1986 and April

TABLE 1. SUMMARY OF BORE COMPLETION DATA

Bore	Intrvl	AMG ZONE 50 East	AMG ZONE 50 North	Construction Start	Construction Finish	Total depth (m bns)	Elevation NS (m AHD)	Elevation TOC (m AHD)	Casing Depth (m bns)	Casing ID (mm)	Perforated interval (m bns)	Geol formtn	Status	Head (m AHD)	TDS (mg/L)	Airlift yield (m^3/d)
1A	1	334100	6250900	30NOV	21DEC	501	93.69	93.81	0 – 131.2	154	220 – 226	P	Obs	87.61	185	90
	2	....	....	....	....	....	....	....	109 – 500	102	456 – 462	P	Obs	86.18	230	35
W	....	....	....	20MAR	24MAR	25.5	94.21	....	0 – 12.6	102	12.6 – 18.7	Klw	Obs	94.64	340	184
2A	1	337600	6251300	28OCT	19NOV	759	144.59	145.45	0 – 759	154	270 – 276	P	Obs	38.73	320	3
	2	....	....	....	....	....	....	....	....	....	445 – 451	P	Abd	....	350	27
	3	....	....	....	....	....	....	....	....	....	725 – 731	P	Obs	30.04	540	33
C	....	....	....	14APR	19APR	101	144.62	145.30	0 – 100	50	94 – 100	Klw	Obs	82.44	<500	22
3A	1	344500	6250600	22SEP	16OCT	1025	134.21	135.06	0 – 1023	154	400 – 406	Juy	Obs	25.89	230	103
	2	....	....	....	....	....	....	....	0 – 1045	75	685 – 691	Jlo	Obs	24.93	220	36
B	....	....	....	16SEP	21SEP	199	134.41	135.40	0 – 174	154	175 – 181	Juy	Obs	25.98	170	230
W	....	....	....	09MAR	19MAR	100	134.33	134.68	0 – 84	102	84 – 90	Klw	Obs	65.30	....	....
4A	1	352400	6250900	27JUL	10SEP	1072	133.58	134.26	0 – 1072	102	175 – 181	Juy	Obs	26.45	470	84
	2	....	....	....	....	....	....	....	....	....	530 – 536	Juy	Abd	26.33	360	48
	3	....	....	....	....	....	....	....	....	....	855 – 861	Juy	Obs	25.00	300	2
W	....	....	....	18FEB	20FEB	30	133.12	133.37	0 – 20.5	102	21 – 27	Klw	Obs	121.43	220	36
5A	1	359300	6251300	14APR	09SEP	1500	178.13	179.09	0 – 986	154	220 – 226	Juy	Obs	26.62	720	5
	2	....	....	....	....	....	....	....	777 – 1499	102	765 – 771	Juy	Abd	....	230	150
	3	....	....	....	....	....	....	....	0 – 940.5	76	1450 – 1456	Jlo	Obs	26.85	850	61
B	_	....	....	25MAY	27MAY	166	178.30	179.14	0 – 165	102	150 – 156	Klw	Obs	31.02	200	5
C	....	....	....	15JUL	16JUL	70	178.23	179.17	0 – 64	102	64 – 70	Klw	Obs	155.07	600	103
6A	1	366000	6251000	09JUN	13JUL	1494	115.96	116.98	0 – 986	154	260 – 266	Juy	Obs	....	190	36
	2	....	....	....	....	....	....	....	940 – 1494	102	890 – 896	Juy	Abd	24.18	560	48
	3	....	....	....	....	....	....	....	0 – 940	76	1423 – 1429	Jlo	Obs	19.75	600	103
W	....	....	....	10FEB	12FEB	61	115.89	116.29	0 – 14.4	102	14.9 – 21	Klw	Ob	112.56	180	4
7A	1	374300	625190	12FEB	02APR	1668	110.47	111.40	0 – 987.5	154	222 – 228	Juy	Obs	....	370	48
	2	....	....	....	....	....	....	....	920 – 1653	102	850 – 860	Juy	Abd	25.40	180	63
	3	....	....	....	....	....	....	....	0 – 920	76	1512 – 1518	Jlo	Obs	23.75	320	125
W	....	....	....	03FEB	04FEB	41	110.38	110.78	0 – 29	102	29 – 32	Klw	Obs	91.71	400	44
8A	1	381200	6251100	13DEC	21JAN	1447.5	155.32	156.23	0 – 565.5	154	395 – 405	Juy	Obs	38.98	240	36
	2	....	....	....	....	....	....	....	520 – 1320	102	885 – 895	Juy	Abd	34.97	240	125
	3	....	....	....	....	....	....	....	0 – 475	76	1370 – 1380	Juy	Obs	22.96	180	12
B	....	....	....	29JAN	02FEB	170.4	155.36	156.24	0 – 170	102	160 – 166	Klw	Obs	70.79	320	125
C	....	....	....	04FEB	05FEB	49	155.35	156.25	0 – 49	50	14.9 – 21	Klw	Obs	135.86	165	12

NOTES: All bores except 2C and 8A were started and finished in 1987. Bore 2C started and finished in 1988; bore 8A started in 1986 and finished in 1987.

(bns) = below natural surface. (AHD) = Australian Height Datum. (NS) = natural surface. (TOC) = top of casing. (ID) = internal diameter. (Klw) = Warnbro Group. (Juy) = Yarragadee Formation. (Obs) = monitored interval. (Abd) = abandoned interval.

1988. At each site, a deep exploratory bore (designated "A") and a water-table bore (variously designated "B", "C" or "W") were drilled. At sites 3, 5, and 8, an additional bore was drilled to an intermediate depth. A wireline coring procedure was used for the shallow bore at site 2 (CL2C) in order to recover samples of coal.

Deep bores at sites 1 to 3 were drilled to total depth before being cased with 154 mm ID steel casing and pressure cemented. The shallow and intermediate bores were cased with 50 mm ID or 102 mm ID PVC or steel casing. A summary of drilling information and bore construction details is given in Table 1, and a more detailed account of investigation procedures and bore construction methods is given in Appleyard (1988).

The deep exploratory boreholes at sites 4 to 8 were drilled to an intermediate depth, cased with 154 mm ID steel casing and pressure cemented. Each bore was then drilled to total depth, and the bottom part of the hole was cased with 102 mm ID steel casing. This casing string was also pressure cemented.

Sludge samples were collected at three-metre intervals from each of the deep exploratory bores; they are stored at the GSWA Core Library. Each deep hole was geophysically logged on completion of drilling (Table 2); and sidewall cores for palynological dating were recovered from shale or siltstone beds in all deep bores except CL2A.

The casing in each of three intervals in each deep bore except CL1A was perforated with explosive charges to enable airlift sampling. The middle interval in each deep

TABLE 2. GEOPHYSICAL LOGS RUN IN DEEP BORES

LOG	*CL1A*	*CL2A*	*CL3A*	*CL4A*	*CL4A*	*CL6A*	*CL7A*	*CL8A*
Gamma	X	X	X	X	X	X	X	X
Normals Resistivity	X	X	X	X	X	X	X	X
Gamma-Gamma	X	X	....	X	X	X	X	X
Self Potential	X	X	X	X	X	X	X	X
Neutron	....	....	....	....	X	....	X	X
Point Resistance	X	X	X	X	X	X	X	X
Caliper	X	X	X	X	X	X	X	X
Temperature	X	X	X	X	X	X	X	X
Sonic	....	....	....	....	X	....	X	X

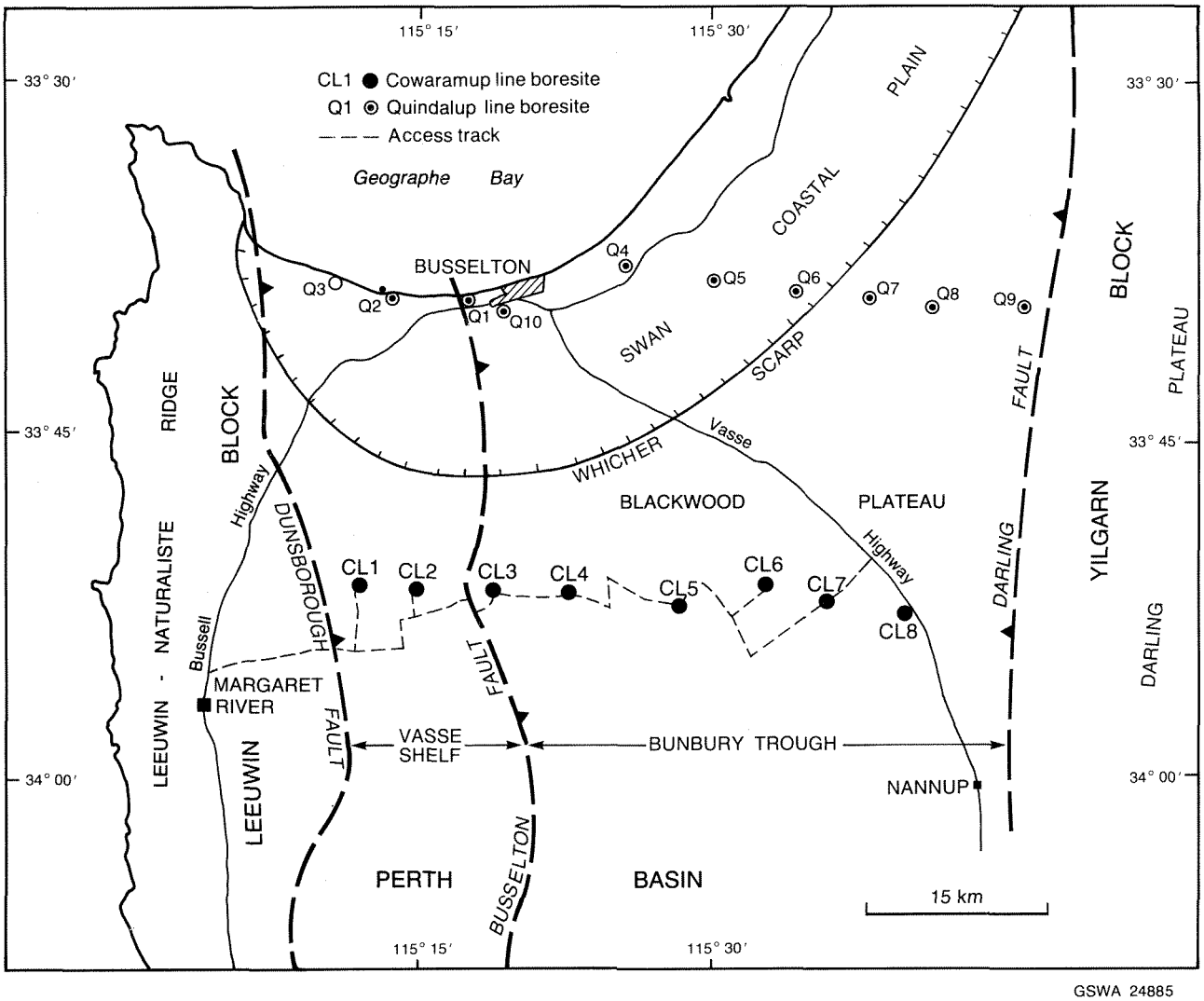

GSWA 24885

Figure 1. Location map.

bore was perforated first and was developed by airlifting until the water cleared and the salinity stabilized. Water samples were collected, and then the top and bottom intervals were perforated. The middle perforations were isolated with rubber packers and the top and bottom intervals were airlifted together, sampled, and constructed as a multiple level monitoring bore. Only two intervals were perforated in the deep exploratory bore at site 1, and this was also constructed as a multiple level monitoring bore.

Water samples collected from each perforated interval were analysed by the Chemistry Centre (Western Australia).

Geology

Setting

The Cowaramup Line bores were drilled in the southern part of the Perth Basin between the Leeuwin Block in the west and the Yilgarn Block in the east (Figure 1). The southern Perth Basin has been subdivided into two major structural units: the Bunbury Trough and the Vasse Shelf (Figures 1 and 2). The Bunbury Trough is a deep graben which probably contains at least 10 000 m of Phanerozoic sedimentary rocks (Playford et al., 1976). The Vasse Shelf is a fault block—lying between the Bunbury Trough and the Leeuwin Block—in which about 3 000 m of mostly Permian sedimentary rocks are preserved.

Stratigraphy

The formations intersected by the bores range in age from Early Permian to Cretaceous. The stratigraphic succession is summarized in Table 3 and the formations intersected are described below.

Sue Coal Measures

The Sue Coal Measures (Permian) were intersected in bores CL1A and CL2A; they consist of weakly to well-consolidated, fine- to coarse-grained sandstone along with some siltstone, shale, and seams of coal. The sandstone is light grey to brown, commonly clayey, and contains accessory garnet, feldspar, and heavy minerals. The sandstone intersected in CL2A was extremely hard and highly silicified—the silicification being possibly related to the nearby Wirring Fault.

TABLE 3. STRATIGRAPHY

Age	*Group/Formation*		*Maximum thickness intersected* (m)	*Lithology*	*Aquifer potential*
CRETACEOUS		WARNBRO GROUP	250 (CL2)	Shale, siltstone coal, sandstone	Confining bed minor aquifer
		UNCONFORMITY			
	Early	Bunbury Basalt	63 (CL7)	Basalt, shale	Confining bed
		UNCONFORMITY			
JURASSIC	Late	Parmelia Formation	70 (CL6)	Siltstone, shale, sandstone	Confining bed, minor aquifer
		Yaragadee Formation	1200 (CL7)	Sandstone, minor shale	Major aquifer
	Mid				
	Early	Cockleshell Gully Formation	690 (CL5)	Shale, sandstone, coal	Major aquifer
TRIASSIC	Late	Lesueur Sandstone	Not intersected	Sandstone	....
	Mid				
	Early	Sabina Sandstone	Not intersected	Sandstone	....
PERMIAN	Late	Sue Coal Measures	510 (CL2)	Sandstone, coal shale	Major aquifer
	Early				

The Sue Coal Measures unconformably overlie Precambrian basement and, on the Vasse Shelf, are unconformably overlain by the Warnbro Group. The maximum thickness intersected was 510 m in CL2A.

Several coal seams, which ranged in thickness between 0.1 and 1.9 m, were intersected in CL1A and CL2A. Palynological evidence (Backhouse, 1988e, 1988f) indicates that the Permian sediments belong to the Lower Stage 5b or 5c zones of Price (1983), and are younger than sediments in the Collie Basin. Highly sheared glacigene sediments were intersected in coal exploration hole RBCH8 (Fig. 2) in the basal part of the Permian sequence near site 1, and these may be equivalent in age to the Stockton Formation in the Collie Basin.

Cockleshell Gully Formation

The Cockleshell Gully Formation (Early Jurassic) was intersected at sites 3 to 7, and comprises interbedded sandstone and grey shale. The sandstone is weakly consolidated, moderately sorted, and contains medium- to coarse-grained quartz grains with interstitial clay. The shale is commonly silty and well consolidated.

The Cockleshell Gully Formation conformably overlies the Lesueur Sandstone; and is, in turn, conformably overlain by the Yarragadee Formation. The Cockleshell Gully Formation is about 1500 m thick in the Bunbury Trough (Playford et al., 1976), but the maximum thickness intersected by the Cowaramup Line bores was 690 m in CL5A. Limited palynological data suggest that the Cockleshell Gully Formation in this area was deposited in a non-marine environment.

Yarragadee Formation

The Yarragadee Formation (Middle to Late Jurassic) was intersected at sites 3 to 8. It consists of interbedded sandstone, shale, and siltstone. Sandstone is dominant and makes up more than 70% of the formation; it is generally cream to pale grey, and consists of weakly consolidated fine to very coarse subangular to subrounded quartz sand. Bright orange, ferruginous sandstone beds occurred in CL5A between depths of 500 and 700 metres. Garnet, feldspar, pyrite, and opaque heavy minerals, are common accessories in the formation. Shale beds in the Yarragadee Formation are commonly black to brown-grey and contain variable amounts of fine sand or silt.

The Yarragadee Formation occurs only in the Bunbury Trough, and the thickness of the formation ranges from 520 m in CL3A to more than 1200 m in CL8A. It conformably overlies the Cockleshell Gully Formation with a gradational contact, and is conformably overlain by the Parmelia Formation at sites 6 and 7. At site 5 and between sites 7 and 8, it is unconformably overlain by the Bunbury Basalt; elsewhere, the Yarragadee Formation is unconformably overlain by the Warnbro Group.

Palynomorphs from the Yarragadee Formation indicate a Middle or Late Jurassic age (Backhouse, 1987, 1988a–d, 1988g). Some samples have distinct assemblages which can be assigned to the bio-stratigraphic zones of Filatoff (1975) and Backhouse (1978) (Figure 2). The palynology of samples from the formation is consistent with a non-marine environment of deposition, and suggests that the formation thickens to the east.

Parmelia Formation

The Parmelia Formation (Late Jurassic–Early Cretaceous) was intersected in bores CL6A and CL7A. This was the first time this formation had been identified onshore in the southern Perth Basin (Backhouse, 1984), although reworked palynomorphs from the Parmelia Formation have been previously identified in the Quindalup Line bores Q7 and Q9 (Wharton, 1981b)

The Parmelia Formation consists of poorly consolidated clayey sandstone, siltstone, and shale. The formation is unconformably overlain by the Bunbury Basalt and the Warnbro Group. Palynological analysis indicates that the formation is non-marine to shallow marine in this area.

Bunbury Basalt

The Bunbury Basalt (Early Cretaceous) was intersected in bores CL5A, CL7A, and CL8A at depths of 72 to 174 m below natural surface. It is massive, aphanitic basalt with a maximum thickness of 63 m in CL7A. Two flows, separated by grey shale, were intersected in each deep bore. The basalt flows do not have extensive weathered margins in these bores. The Bunbury Basalt unconformably overlies the Yarragadee and Parmelia Formations, and is unconformably overlain by the Warnbo Group.

A sidewall core collected from shale at site 7 contained a sparse palynological assemblage, including the palynomorph *Fusiformacysta tumida* (Backhouse, 1988g), suggesting that the material between the basalt flows is contemporaneous with the Parmelia Formation.

Warnbro Group

Sediments assigned to the Warnbro Group were intersected in all Cowaramup Line bores. At sites 3 to 8, the sequence consists of grey, micaceous, and black, carbonaceous shale, and some coal and rare sandstone beds. At sites 1 and 2, the sequence consists of interbedded, poorly consolidated, fine- to coarse-grained sandstone and black, carbonaceous shale, with some glauconitic shale and coal seams. Data from coal exploration borehole RBCH8 (Fig.2) suggests that the proportion of sand in the Warnbro Group increases towards the Dunsborough Fault.

The Warnbro Group unconformably overlies the Sue Coal Measures, the Yarragadee and Parmelia Formations, and the Bunbury Basalt. It ranges in thickness from 250 m in CL2A to 72 m in CL7A. The top 3 to 6 m of the Warnbro Group sequence was lateritized during the Tertiary. The laterite consists of pisolitic gravel and mottled ferruginous, or white kaolinitic clay; the sand is commonly iron-stained, poorly sorted, and fine to coarse. Palynological analysis

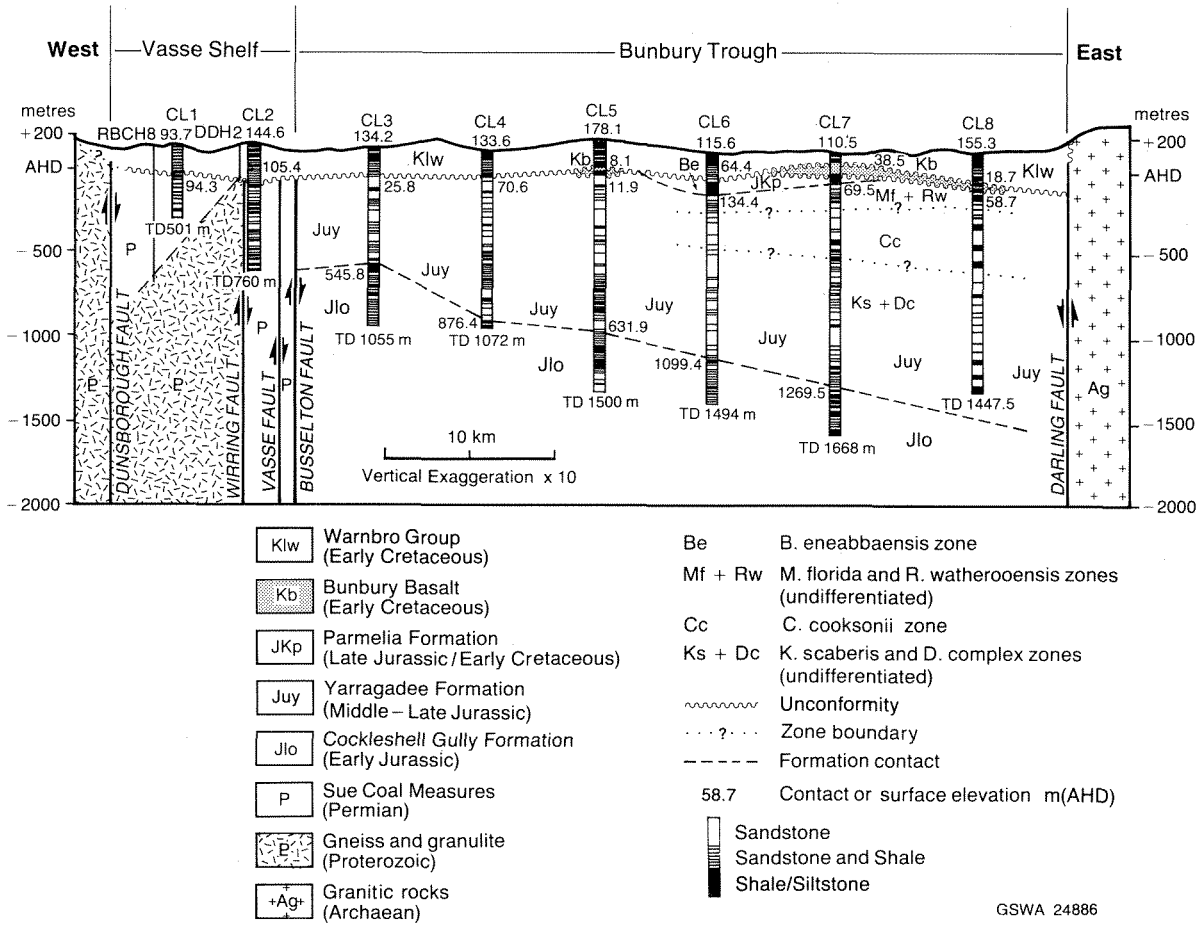

Figure 2. Geological cross section.

indicates that the Warnbro Group in this area is mainly non-marine, although the presence of glauconite is indicative of marine intercalations.

The Warnbro Group in the Cowaramup Line bores is probably an age equivalent of the Leederville Formation, although the rocks cannot be precisely zoned as they are mainly non-marine in origin. These rocks were previously identified as belonging to the Leederville Formation in the Busselton area (Wharton, 1982; Hirschberg, 1989).

Structure

The inferred structure is shown on a section through the Cowaramup Line bores (Fig. 2). The positions of formation boundaries shown in Figure 2 have been determined from the drilling data, and the positions of faults have been determined from seismic data (R.P. Iasky, personal communication, 1989).

Pre-Cretaceous rocks in the area are intersected by several north-trending faults. The Yarragadee and Cockleshell Gully Formations thicken and dip gently to the east, and are truncated in the west by the Busselton Fault. Permian sediments on the Vasse Shelf dip in a westerly direction and are truncated in the west by the Dunsborough Fault. The Warnbro Group unconformably overlies these sediments and is draped over the underlying fault blocks in a series of shallow synclines and anticlines (Cope, 1972).

Block faulting has produced a large basement high between sites 1 and 2, where the Warnbro Group rests directly on granitic rocks. Seismic evidence suggests that other block faults may occur in this area, and it is possible that the Dunsborough Fault consists of a large number of small step faults rather than being a simple normal fault.

Hydrogeology

Aquifer relationships

A section showing the vertical component of groundwater flow interpolated between the Cowaramup Line bores is shown in Figure 3. On the basis of isopotentials, three regional, structurally controlled, groundwater flow systems can be identified below the Cretaceous unconformity: one in the Yarragadee, Parmelia, and Cockleshell Gully Formations to the east of the Busselton Fault; a second in Permian sediments between the Wirring and Busselton Faults; and a third in Permian sediments to the west of the Wirring Fault. The Warnbro Group consists of

a large number of local flow systems related to the surface drainage pattern which are superimposed on a weakly developed regional flow system.

The base of the fresh groundwater flow system occurs in the Cockleshell Gully Formation. Groundwater flow in the Cockleshell Gully Formation is restricted by shale beds and by the clayey nature of the sandstone; and the groundwater salinity probably increases progressively with depth.

Two distinct flow systems occur in Permian sediments on the Vasse Shelf and are separated by a basement high between sites 1 and 2. Potentiometric levels between the Busselton and Wirring Faults are about 5 m higher than levels east of the Busselton Fault, indicating that the Busselton Fault acts at least as a partial hydraulic barrier. Similarly, potentiometric levels in the Sue Coal Measures to the west of the basement high are about 50 m higher than to the east of this structural feature, and it is unlikely that there is any groundwater flow between the two Permian flow systems near the Cowaramup Line. However, limited groundwater flow could take place across the Wirring Fault in other areas where the basement high is absent.

At site 1, the sandy nature of the Warnbro Group and the comparatively low vertical hydraulic gradient of 0.03 indicate that there is hydraulic connection between the Warnbro Group and the Sue Coal Measures, and it is likely that Permian rocks to the west of the basement high receive recharge from the overlying Cretaceous rocks.

Groundwater in the Sue Coal Measures east of the Wirring Fault probably flows north, and recharge probably only occurs where the Warnbro Group is more sandy.

Aquifers

Warnbro Group

The Warnbro Group is a multilayered aquifer system consisting of a number of local flow systems in the vicinity of the Cowaramup Line.

Downward heads (Fig. 3) indicate that groundwater in the Warnbro Group is recharged by rainfall, and that infiltration occurs through the laterite and sand capping. Water levels in the aquifer vary seasonally by up to 2 m in response to recharge. Groundwater flow is controlled by topography; and groundwater in local flow systems discharges into creeks and swamps throughout the area. Locally, confined conditions occur and CL1W has an artesian head of up to 1.8 m above ground level.

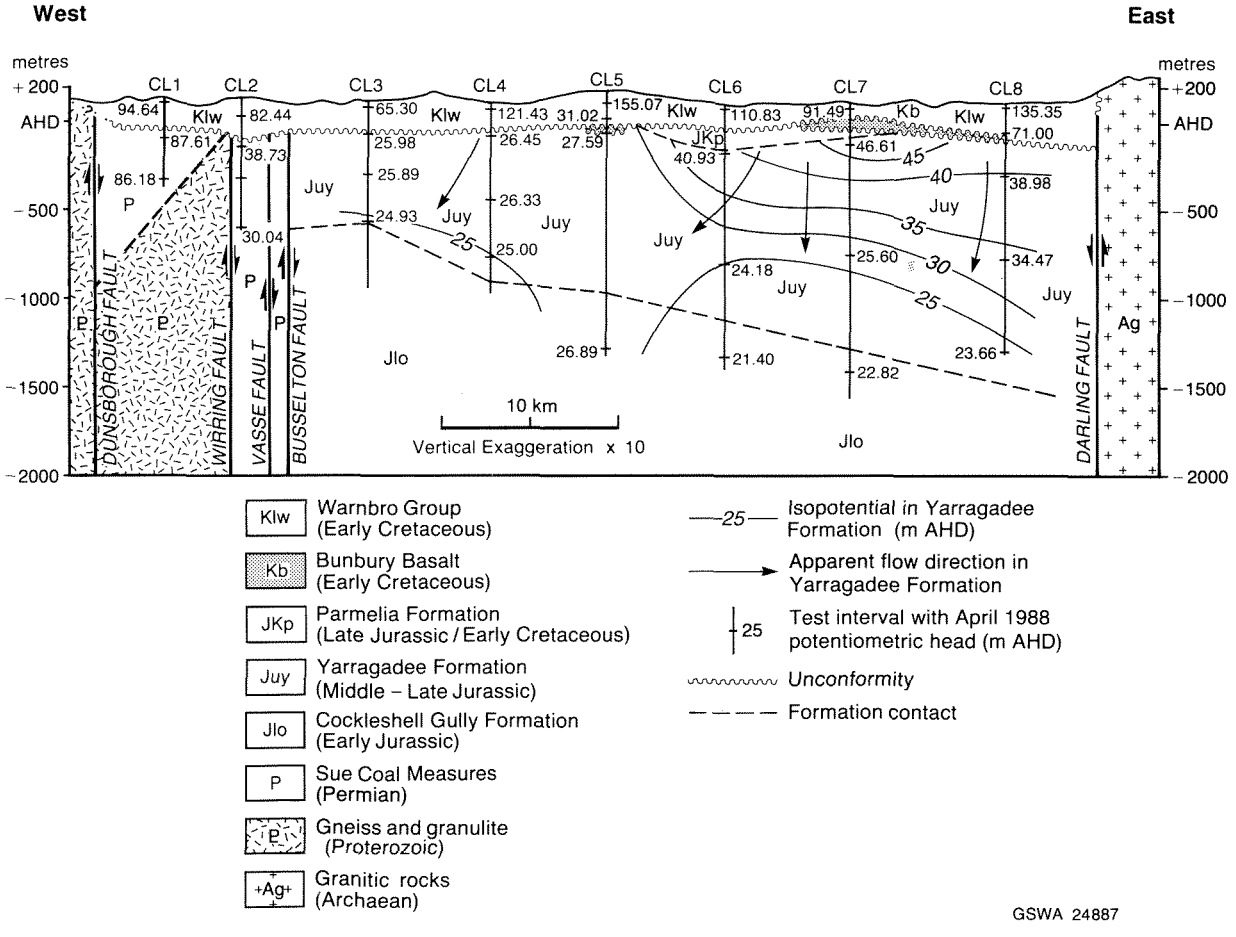

Figure 3. Isopotentials and apparent groundwater flow directions (April 1988).

Potentiometric levels in the Warnbro Group vary greatly both laterally and vertically, indicating that these sediments contain a number of distinct groundwater flow systems where the water table is controlled by topography (water-table elevations range from 65 to 156 m AHD), and where discharge to surface water bodies occurs. The potentiometric heads in bores in the Warnbro Group range from 1.8 m above ground level to 147 m below ground level, and heads generally decrease with depth. The vertical hydraulic gradient in the Warnbro Group is high and generally exceeds 0.1, making it impossible to directly compare heads of bores sunk to different depths in this aquifer.

The salinity of groundwater in the Warnbro Group in the area ranges from 165 mg/L to 600 mg/L and there is no simple relationship between salinity and bore depth or location. Water from the Warnbro Group generally contains in excess of 5 mg/L dissolved iron.

The Warnbro Group is only a minor groundwater source in the Bunbury Trough near the Cowaramup Line because of the large proportion of shale in the area. Some localized, high-yielding bores (such as CL5C) occur where there is a higher proportion of sand in the aquifer.

Larger supplies of groundwater can be obtained from this aquifer system to the west of the Wirring Fault where the Warnbro Group contains a significant amount of sandstone, especially near the Dunsborough Fault. Although this area has considerable development potential, Hirschberg (1989) noted that the Leederville Formation on the Vasse Shelf in the Busselton area to the north of the Cowaramup Line is shaly and contains only limited groundwater resources.

Yarragadee Formation

Recharge to the Yarragadee Formation probably occurs to the south of the Cowaramup Line, in areas where the formation is not covered by sediments of low permeability. However, the steep vertical hydraulic gradient in permeable sediments in the Yarragadee Formation beneath sites 6, 7, and 8, indicates that recharge may be occurring only a short distance south of the Cowaramup Line. The vertical hydraulic gradient in the Yarragadee Formation decreases to the west, and groundwater flow in this formation west of site 5 has almost no vertical component.

Groundwater flow in the Yarragadee Formation is predominantly to the north (Commander, 1982); there are only small components in the vertical and east-west directions. Hydraulic gradients are generally low and have a small vertical head component.

The salinity of groundwater in this formation varies from 180 mg/L to 900 mg/L, and is generally lowest in the middle of the aquifer where there are few shale beds. Fresh

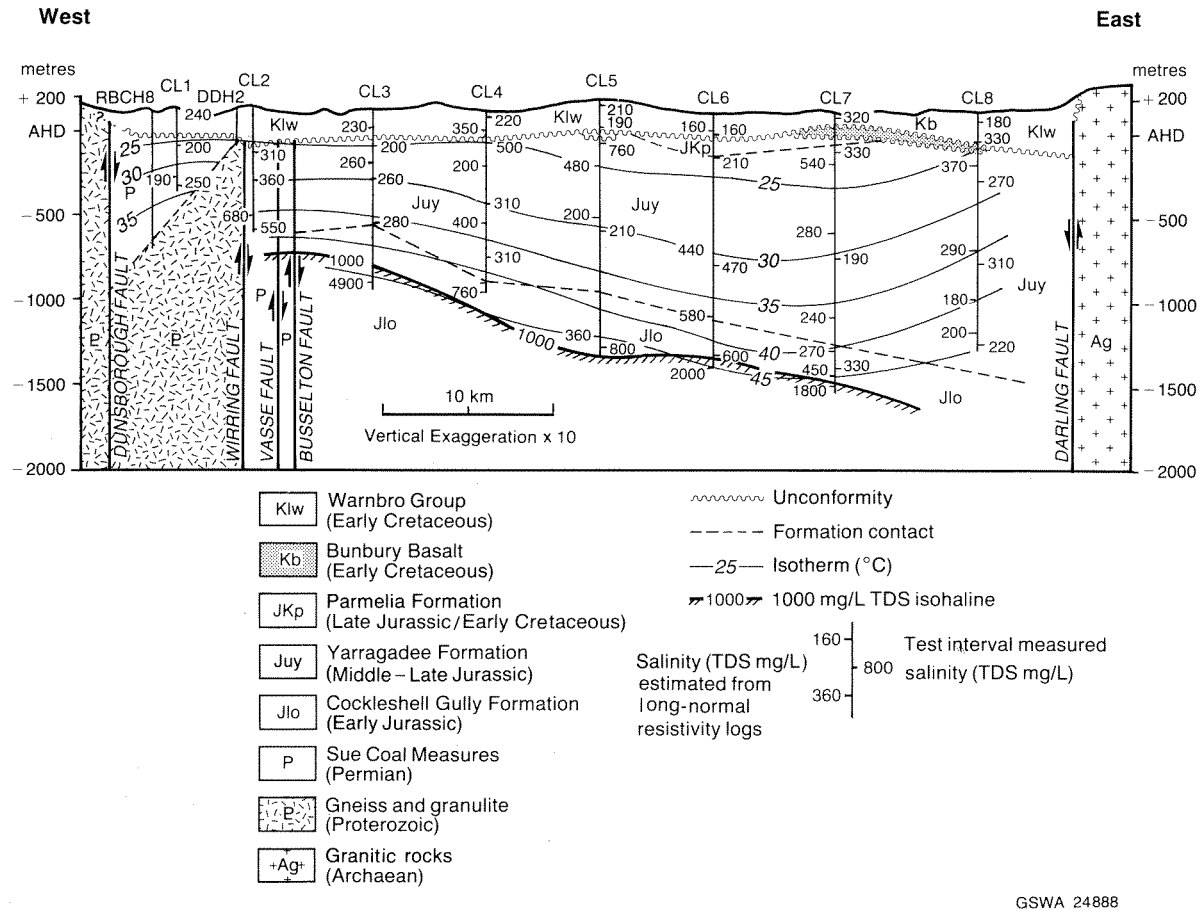

Figure 4. Groundwater temperature and geothermal temperature.

TABLE 4. CHEMICAL ANALYSES

(All concentrations expressed as Mg/L)

Bore	*GSWA no.*	*pH*	*TDS*	*Ca*	*Mg*	*Na*	*K*	*HCO_3*	*CO_3*	*Cl*	*SO_4*	*SiO_2*	*B*	*F*	*Fe(a)*
CL1A1	94138	6.6	200	6	6	38	10	41	....	65	8	47	<0.05	0.2	....
CL1A2	94139	8.6	250	11	3	70	6	136	0.17	48	12	27	<0.05	0.1	0.86
CL1W	94112	6.3	240	2	7	54	13	8	....	108	13	34	<0.05	<0.1	8.3
CL2A1	94135	8.6	310	5	<1	111	11	169	0.17	81	14	<1	0.07	0.1	....
CL2A2	94136	8.9	360	2	<1	141	8	259	0.60	53	10	1	0.14	<0.1	....
CL2A3	94137	8.9	550	2	<1	205	7	259	0.57	137	37	17	0.38	1.1	....
CL3A1	94131	7.7	260	21	6	50	18	133	....	67	14	13	0.04	0.2	8.3
CL3A2	94132	8.0	280	11	10	50	37	129	....	76	20	15	0.08	0.3	5.2
CL3B	94133	5.7	200	4	8	34	10	31	....	66	15	42	0.02	0.2	15
CL4A1	94126	8.1	500	91	13	62	10	258	....	132	37	21	0.03	0.1	3.2
CL4A2	94124	6.9	310	16	10	69	18	36	....	144	28	4	<0.05	0.2	70
CL4A3	94125	7.3	310	16	5	87	9	130	....	96	26	6	<0.05	0.2	1
CL4W	94113	7.4	220	2	7	54	6	56	....	71	14	34	0.06	0.2	17
CL5A1	94127	9.1	760	8	1	279	20	265	0.80	238	49	3	0.72	1.6	85
CL5A2	94115	7.1	210	6	4	44	25	38	....	90	7	13	0.05	<0.1	12
CL5A3	94128	8.4	800	10	1	284	16	282	0.17	274	50	14	1.00	2.4	37
CL5B	94116	7.4	190	15	4	42	10	34	....	90	9	2	0.05	0.1	49
CL5C	94121	6.0	210	2	5	50	9	10	....	90	16	34	<0.05	0.1	8.1
CL6A1	94118	7.9	210	9	6	44	11	94	....	50	16	28	0.03	0.2	4.1
CL6A2	94119	4.2	470	10	25	110	23	2	....	285	10	11	0.04	0.1	47
CL6A3	94120	8.7	600	<1	1	232	4	384	0.47	68	69	17	1.60	6.5	5
CL6W	94105	6.2	160	2	3	40	7	14	....	66	12	27	0.01	<0.1	NA
CL7A1	94109	7.4	330	24	10	77	11	143	....	102	17	18	0.07	0.1	5.9
CL7A2	94110	6.6	190	7	6	38	15	92	....	42	18	20	0.05	0.2	6
CL7A3	94111	7.4	330	2	1	115	9	155	....	92	17	19	0.12	0.3	1.9
CL7W	94106	6.0	320	5	12	82	7	8	....	165	16	28	<0.05	0.1	....
CL8A1	94102	7.5	270	13	9	62	10	122	....	70	23	17	0.04	0.2	....
CL8A2	94101	8.0	310	25	12	57	16	199	....	53	25	19	0.11	0.2	....
CL8A3	94103	7.6	220	2	6	43	30	83	....	59	17	18	<0.05	0.1	....
CL8B	94104	6.2	330	10	11	76	11	22	....	160	14	36	<0.05	0.3	....
CL8C	94107	6.4	180	1	5	38	7	31	....	59	10	44	0.02	0.1	....

NOTE: (a) — Fe represents total dissolved iron.

groundwater extends to depths of from -800 m AHD at site 3 to about -1500 m AHD at site 7, and the 1000 mg/L TDS isohaline (Fig. 4) closely follows the base of the Yarragadee Formation.

Sue Coal Measures

Groundwater in the formation is probably recharged from the overlying Warnbro Group, and groundwater flow is probably to the north. A large basement high between sites 1 and 2 has divided the aquifer into two distinct flow systems.

The salinity of groundwater in both flow systems of the Sue Coal Measures ranged from 200 mg/L to 680 mg/L TDS in bores CL1A and CL2A, and geophysical logs from RBCH8 (Fig. 2) indicate that the formation to the west of the basement high contains groundwater with a salinity of less than 1000 mg/L for its entire thickness.

The Sue Coal Measures form an important aquifer which was previously—on the basis of bores near the coast—thought to contain only brackish to saline groundwater (Wharton, 1981b).

Groundwater temperature

Temperature logs were run in all the Cowaramup Line deep bores several weeks after construction. These logs indicate that the geothermal gradient ranges from 1.8°C/100 m near site 7 in the Bunbury Trough, to 2.5°C/100 m near site 1 on the Vasse Shelf, where basement subcrops at a shallow depth. Isotherms are shown in Figure 4.

Hydrochemistry

Major ions

Water samples were collected from all Cowaramup Line bores and analysed for major ions (Table 4). The major ions are plotted as a percentage of their total milli-equivalent per litre concentrations on a trilinear diagram (Piper, 1944). This indicates two distinctive anionic compositions based on the proportions of HCO_3^- and Cl^- (Fig. 5). In most samples sodium is the principal cation.

Groundwater in the aquifers beneath the Cretaceous unconformity generally contains a much higher proportion of bicarbonate ion than water from the Warnbro Group,

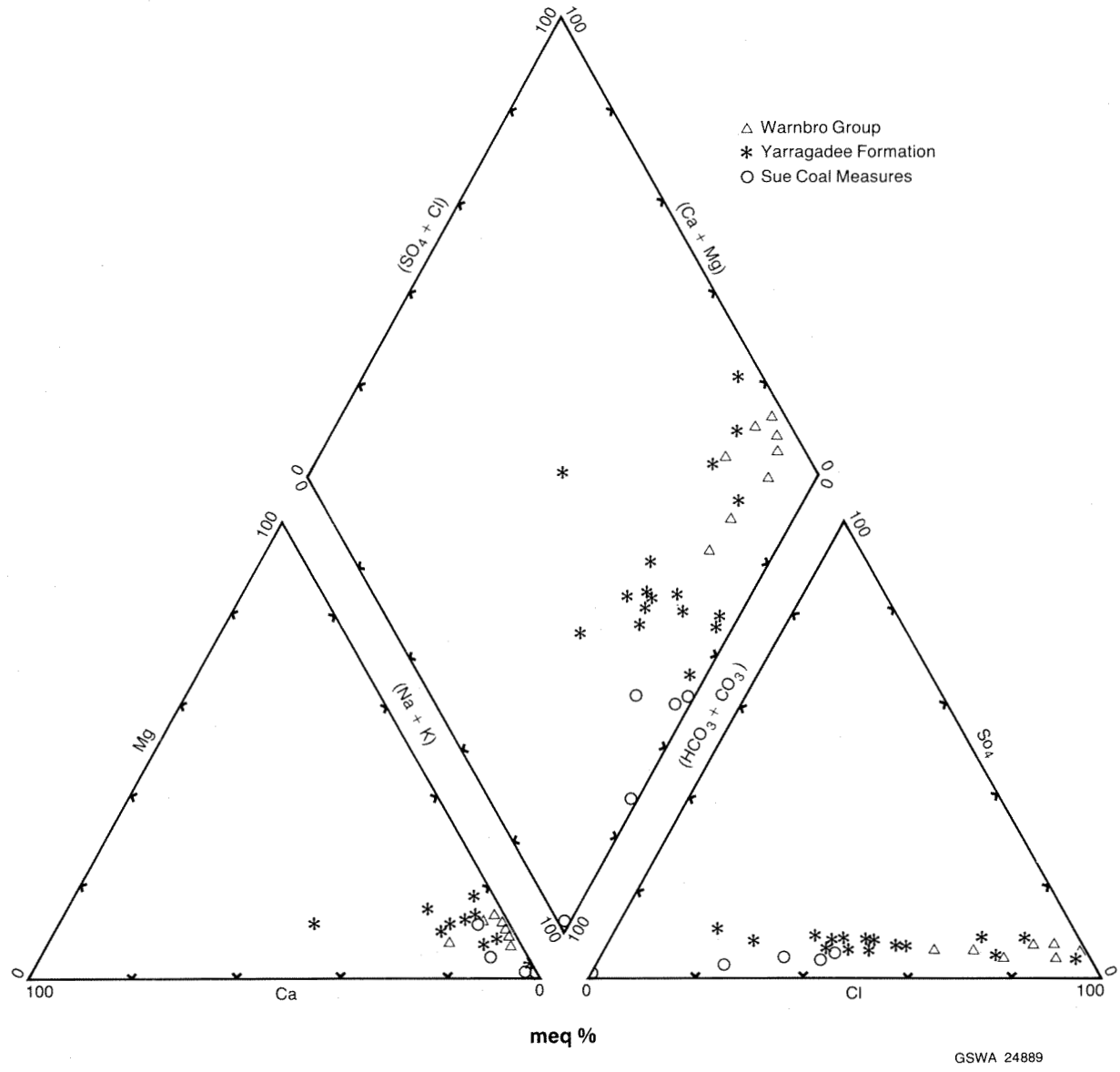

Figure 5. Piper trilinear diagram.

even though the total salinity is similar. The average mole ratio (HCO_3^-:Cl^-) for water samples in these formations was 1.00 compared to 0.16 for water from the Warnbro Group. Smith (1984) observed the same compositional difference between water from the Yarragadee Formation and the Warnbro Group in samples from deep bores from the Boyanup borehole line.

The high bicarbonate ion concentrations in the Yarragadee Formation and the Sue Coal Measure aquifers probably result from chemical reactions between the coal and carbonaceous shale and the groundwater. The major reactions producing bicarbonate ions are probably the oxidation of organic material by sulphate ions, and the diagenesis of lignite (Freeze and Cherry, 1979)

The composition of water samples from the Yarragadee Formation, whether collected from bores on the Cowaramup, Quindalup, Boyanup, or Picton Borehole Lines (Wharton, 1981a, 1981b; Smith, 1984), is relatively uniform; and there are no progressive changes in ionic composition or salinity. This suggests that interaction between groundwater and the sediment matrix in the aquifer is limited.

The anionic composition of groundwater at site 1 suggests that the upper part of the Sue Coal Measures in this area receives recharge from the overlying Warnbro Group. Figure 6 shows that groundwater in the Warnbro Group has an anionic composition dominated by chloride ion, whereas the lower part of the Sue Coal Measures has an anionic composition dominated by bicarbonate ion. The bore CL1A1 is monitoring the upper part of the Sue Coal Measures at site 1, and water from this bore has a composition midway between that of water from the Warnbro Group monitoring bore, CL1W, and that of water from CL1A2.

Dissolved iron

Groundwater containing high concentrations of dissolved iron can cause staining. It also requires treatment before it can be used as a potable supply. The recommended upper limit for dissolved iron in drinking water in Australia is 1 mg/L (NHMRC, 1980); and most of the samples from the Cowaramup Line that were analysed for iron exceeded this value. However, samples for iron analysis were collected during airlifting of bores, and are not necessarily representative of the actual concentrations in the aquifers.

Boron and fluoride

The recommended upper limit for fluoride ion concentrations in water in Australia is 1.5 mg/L (NHMRC, 1980), and recommended limits for fluoride ion and boron in water used for long term irrigation are 1 mg/L and 0.75 mg/L respectively (Lloyd and Heathcote, 1985). Concentrations of both fluoride ion and boron in excess of these guide-lines were recorded in water samples from the Cowaramup Line: the maximum concentrations were 6.5 mg/L and 1.6 mg/L respectively (Table 4).

Except at site 5, where the fluoride ion concentration at the top of the Yarragadee Formation exceeds 1 mg/L., high concentrations generally occur near the base of the fresh groundwater flow systems. A similar distribution exists for boron in groundwater beneath the Cowaramup Line.

High concentrations of both fluoride ion and boron in the area occur in groundwater which is alkaline (pH > 8), and generally occur where there is a large amount of shale or coal in the aquifer. These elements are probably leached from shales under the prevailing alkaline conditions; Wedepohl (1969) noted that fluoride ion especially is strongly desorbed from clay minerals under alkaline conditions. The strong relationship between boron and fluoride ion in the Cowaramup Line water samples is probably due in part to a common origin for these elements in groundwater, but may also indicate that these elements are associated in complexes such as BF_4^-.

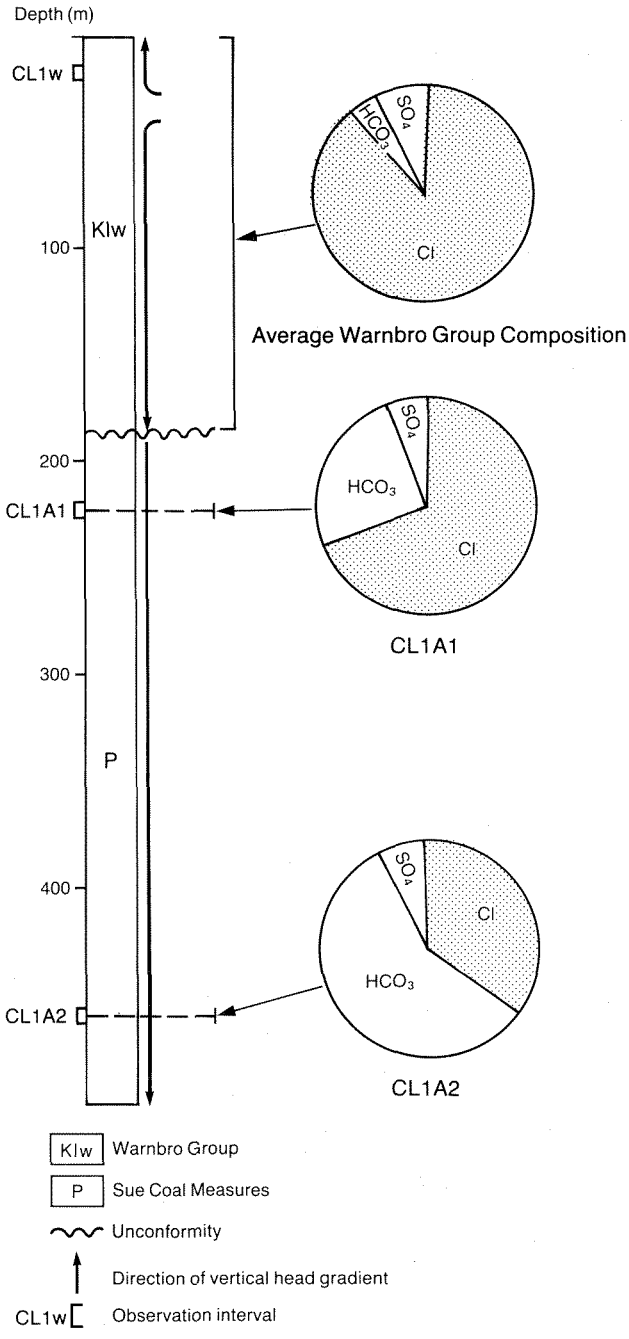

Figure 6. Variation of anionic composition with depth at site 1.

Conclusions

Drilling of the Cowaramup Line has provided new geological and hydrogeological information on a section across the Perth Basin south of Busselton.

Sediments of the Sue Coal Measures, Cockleshell Gully, Yarragadee and Parmelia Formations and of the Warnbro Group were intersected by drilling. This is the first recorded occurrence of the Parmelia Formation in the onshore southern Perth Basin.

Sediments below the basal unconformity of the Warnbro Group have been displaced by north-trending faults, which have created three major groundwater flow systems.

The most important groundwater flow system occurs in the Yarragadee Formation between the Darling and Busselton Faults, where fresh groundwater extends from -800 to about -1500 m AHD. Recharge to the Yarragadee Formation probably takes place to the south of the Cowaramup Line, as the overlying Warnbro Group is very shaly and has a low vertical permeability.

Two groundwater flow systems, which are separated by a basement high located between drilling sites 1 and 2, occur in sediments of the Sue Coal Measures west of the

Busselton Fault. These sediments were previously thought to contain brackish groundwater, but were found, in this area, to contain fresh groundwater. East of the basement high, fresh groundwater extends to more than -500 m AHD; west of this hydraulic boundary, to basement.

Both the Yarragadee and Sue Coal Measures aquifers contain very large reserves of fresh groundwater and are capable of substantial development.

The Warnbro Group, because it incorporates a large proportion of shale, contains limited fresh groundwater over much of the Cowaramup Line. The proportion of sand in the group increases in the west, adjacent to the Leeuwin Block; and it may be an important aquifer in this area.

Further drilling is required to the south of the Cowaramup Line to locate recharge areas and to provide the hydrogeological data necessary to fully evaluate groundwater resources in the region.

References

APPLEYARD, S. J., 1988, Bore completion reports for the Cowaramup Line bores: Western Australia, Geological Survey, Hydrogeology Report 1988/24 (unpublished).

BACKHOUSE, J., 1978, Palynological zoning of the Late Jurassic and Early Cretaceous sediments of the Yarragadee Formation, central Perth Basin Western Australia: Western Australia, Geological Survey Report Number 7.

BACKHOUSE, J., 1984, Revised Late Jurassic and Early Cretaceous stratigraphy in the Perth Basin: Western Australia, Geological Survey, *Professional Papers, Report 12, p. 1–6.*

BACKHOUSE, J., 1987, Palynostratigraphy of Cowaramup Line 8A: Western Australia, Geological Survey, Palaeontology Report 1987/11.

BACKHOUSE, J., 1988a, Palynology of Cowaramup Line 6A: Western Australia, Geological Survey, Palaeontology Report 1988/1.

BACKHOUSE, J., 1988b, Palynology of Cowaramup Line 5A: Western Australia, Geological Survey, Palaeontology Report 1988/2.

BACKHOUSE, J., 1988c, Palynology of Cowaramup Line 4A: Western Australia, Geological Survey, Palaeontology Report 1988/3.

BACKHOUSE, J., 1988d, Palynology of Cowaramup Line 3A: Western Australia, Geological Survey, Palaeontology Report 1988/4.

BACKHOUSE, J., 1988e, Palynology of Cowaramup Line 2A: Western Australia, Geological Survey, Palaeontology Report 1988/5.

BACKHOUSE, J., 1988f, Palynology of Cowaramup Line 1A: Western Australia, Geological Survey, Palaeontology Report 1988/6.

BACKHOUSE, J., 1988g, Palynology of Cowaramup Line 7A: Western Australia, Geological Survey, Palaeontology Report 1988/11.

COCKBAIN, A. E. and PLAYFORD, P. E., 1973, Stratigraphic nomenclature of Cretaceous rocks in the Perth Basin: Western Australia, Geological Survey, Annual Report 1972, p. 26–31.

COMMANDER, D. P., 1982, An outline of the groundwater resources of the Mandurah–Bunbury region: Western Australia, Geological Survey, Hydrogeology Report 2412.

COPE, R. N., 1972, Tectonic style in the southern Perth Basin: Western Australia, Geological Survey, Annual Report 1971, p. 46–50.

FILATOFF, J., 1975, Jurassic palynology of the Perth Basin, Western Australia: Palaeontographica, Abt. B, v. 154.

FREEZE, R. A. and CHERRY, J. A., 1979, Groundwater: New York, Prentice Hall Inc., 604 p.

HIRSCHBERG, K-J. B.,1989, Busselton shallow-drilling groundwater investigation: Western Australia, Geological Survey, Professional Papers, Report 25, p. 17–38.

LLOYD, J. W. and HEATHCOTE, J. A., 1985, Natural inorganic hydrochemistry in relation to groundwater: Oxford, Oxford Scientific Publications, 296 p.

LOW, G. H., 1972, Explanatory notes on the Phanerozoic rocks of the western part of the Collie 1:250 000 geological sheet, Western Australia: Western Australia, Geological Survey, Record 1972/10 (unpublished).

NHMRC (NATIONAL HEALTH AND MEDICAL RESEARCH COUNCIL), 1980, Desirable quality for drinking water in Australia.

PIPER, A. M., 1944, A graphic procedure for the geochemical interpretation of water-analyses: 25th Annual Meeting of the American Geophysical Union, Transactions, part 6, p. 914–923.

PLAYFORD, P. E., COCKBAIN, A. E., and LOW, G. H., 1976, Geology of the Perth Basin, Western Australia: Western Australia, Geological Survey, Bulletin 124.

PRICE, P. L, 1983, A Permian palynostratigraphy for Queensland, *in*, Permian Geology of Queensland: Geological Society of Australia, Queensland Division, p. 155–211.

SMITH, R. A., 1984, Geology and hydrogeology of the Boyanup bore line, Perth Basin: Western Australia, Geological Survey, Professional Papers 1982, p. 72–81.

WEDEPOHL, K. H. (ed.), 1969, Handbook of Geochemistry, Vol II/1: Berlin, Springer Verlag Press.

WHARTON, P. H., 1981a, Geology and hydrogeology of the Picton line of bores, Perth Basin: Western Australia, Geological Survey, Record 1981/2.

WHARTON, P. H., 1981b, The geology and hydrogeology of the Quindalup Borehole Line: Western Australia, Geological Survey, Annual Report 1980, p. 27–35.

Gold-bearing lateritic profiles at Mount Gibson, Murchison Province, Western Australia

by

R. Davy, R. M. Clarke[1], M. Sale[2] and M. Parker[3]

ABSTRACT

Mineralogical and multi-element chemical determinations of drill cuttings have been used to document the weathering profile and to examine the origin of gold in auriferous lateritic profiles in the Murchison Province of Western Australia.

The profiles comprise a thin, generally loose, surface cover; a hardened ferruginized horizon (ferricrete) now partly altered to silcrete and calcrete; and clay–saprolite overlying bedrock.

The ferricrete, the zone on which mining commenced, is formed largely of ferruginized nodules of altered rock cemented by a mixture of clay,iron oxides, calcrete, and silcrete. The nodules may be *in situ*, or they may have moved only a short distance from source; but the composition of the layer has been severely modified by chemical redistribution and by the introduction of calcrete and silcrete. The ferricrete may also contain eolian detrital material, which has possibly changed the concentration of "immobile" residual elements.

There has been no systematic enrichment of residual elements in the saprolite; the composition of this strongly leached material reflects, rather, the rock type from which the clay has been derived. Titanium and zirconium have been used to interpret the origin of the saprolite. Approximately two-thirds of the samples appear derived from mafic (high-magnesium) rocks, the remainder from felsic volcanic or metasedimentary rocks. This interpretation is in general agreement with known bedrock.

The ferricrete contains a mixture of remnant primary gold enclosed within the nodules, and secondary gold deposited in cracks and vugs and on the rims of nodules. Both primary and secondary gold are very fine grained, generally less than 5 μm in diameter. Gold in the saprolite is essentially residual, but may be leached.

Keywords: Mount Gibson, Murchison Province, laterite profiles, major elements, trace elements, gold

Introduction

Ferruginous laterite at the Mount Gibson Gold Mine, about 300 km north of Perth, has been investigated as part of a larger study of the relationships of laterite to underlying bedrock. Earlier studies have been carried out on laterites in the Darling Range in the Perth hinterland (Davy, 1979) and in the Boddington area, 120 km southeast of Perth, where laterite is both bauxitic and auriferous (Davy and El-Ansary, 1986). In this paper the near-surface massive-to-cemented "laterite" layer is called ferricrete; the full profile is referred to as a laterite profile.

The Mount Gibson mine is located at the southern end of a series of Archaean greenstone belts in the Murchison Province (Fig. 1). The southwestern portion of the greenstone belt which hosts the mine is an arcuate northwesterly trending sequence of metamorphosed volcanic rocks, hypabyssal intrusions, and banded iron-formation. Mafic rocks are dominant near the base of the sequence, but intermediate to felsic ones are more prominent in the mid to upper parts (Watkins and Hickman, 1990, plates 1 and 2). Minor gold discoveries were made in the early part of this century, and, more recently, the greenstone belt has been extensively explored for base metals.

In 1983, gold-bearing ferruginous nodules and nodular ferricrete were identified east of a line of small gold occurrences. Gold is present in the upper part of the laterite profile over a distance of 4 km; from north to south there are four separate prospects, Mount Gibson Well, Midway, Orion, and Tobias Find (Fig. 1). The last is named after a bedrock gold occurrence immediately west of the laterite and, with Orion, now forms the present Mount Gibson lateritic mining operation. When mining commenced, reserves of mineable lateritic ore, to a depth of 8 m, amounted to 5.5 Mt containing 1.66 g/t gold (El-Ansary and Sale, 1985).

The gold-bearing laterite lies on the eastern flank of a low north-trending ridge, which has a relief of approximately 20 m and a very gentle slope of about 1°. Isolated

[1]Chemistry Centre of W.A.
[2]Reynolds Australia Mines Pty Ltd
[3]Forsayth N.L.

exposures and small patches of rubble of mafic volcanic and intrusive rocks dot the ridge. Most rock is deeply weathered; and, below the ferricrete, the depth to fresh bedrock can be as much as 60 m. Much of the ferricrete is overlain by residual soil, alluvium, colluvium, or windblown sand. There is no permanent drainage; surface erosion is mainly by sheet wash after heavy (cyclonic) rains and, to a lesser degree, by wind action.

This study documents the lateritic profile and examines the origins of the ferricrete and the surface and near-surface gold. It does not address the relationship between the auriferous laterite and the basement gold deposits which have been discovered since the commencement of this study.

Samples have been taken from rotary-drill cuttings along four traverses: one traverse at Mount Gibson Well; one at Midway; and the remaining two at Orion. The holes sampled are shown on Figure 1; co-ordinates given are those of the early exploration grid. Each sample represents a 3 m vertical interval in the holes which generally terminated in competent but partly weathered bedrock. Numbering is from the surface, thus 856.1 is the uppermost sample from hole 856.

The samples were submitted for X-ray diffraction and chemical analysis at the Chemistry Centre (W. A.). Determinations were made of major oxides, 29 trace elements, and the pH of a sample–water slurry. These analyses have been supplemented by microscopic examination of selected heavy-mineral assemblages from weathered clays, and of thin sections of bedrock. A few samples have been examined by scanning electron microscopy (SEM). Minerals identified, methods of chemical analysis and details of results are presented in Davy et al. (1989).

Laterite profile

A generalized sketch of the laterite profile (Fig. 2) shows 4 zones. In ascending order these are: bedrock, clay, ferricrete and loose cover. The complete profile ranges from 10 to 100 m thick, but is usually between 20 and 30 m.

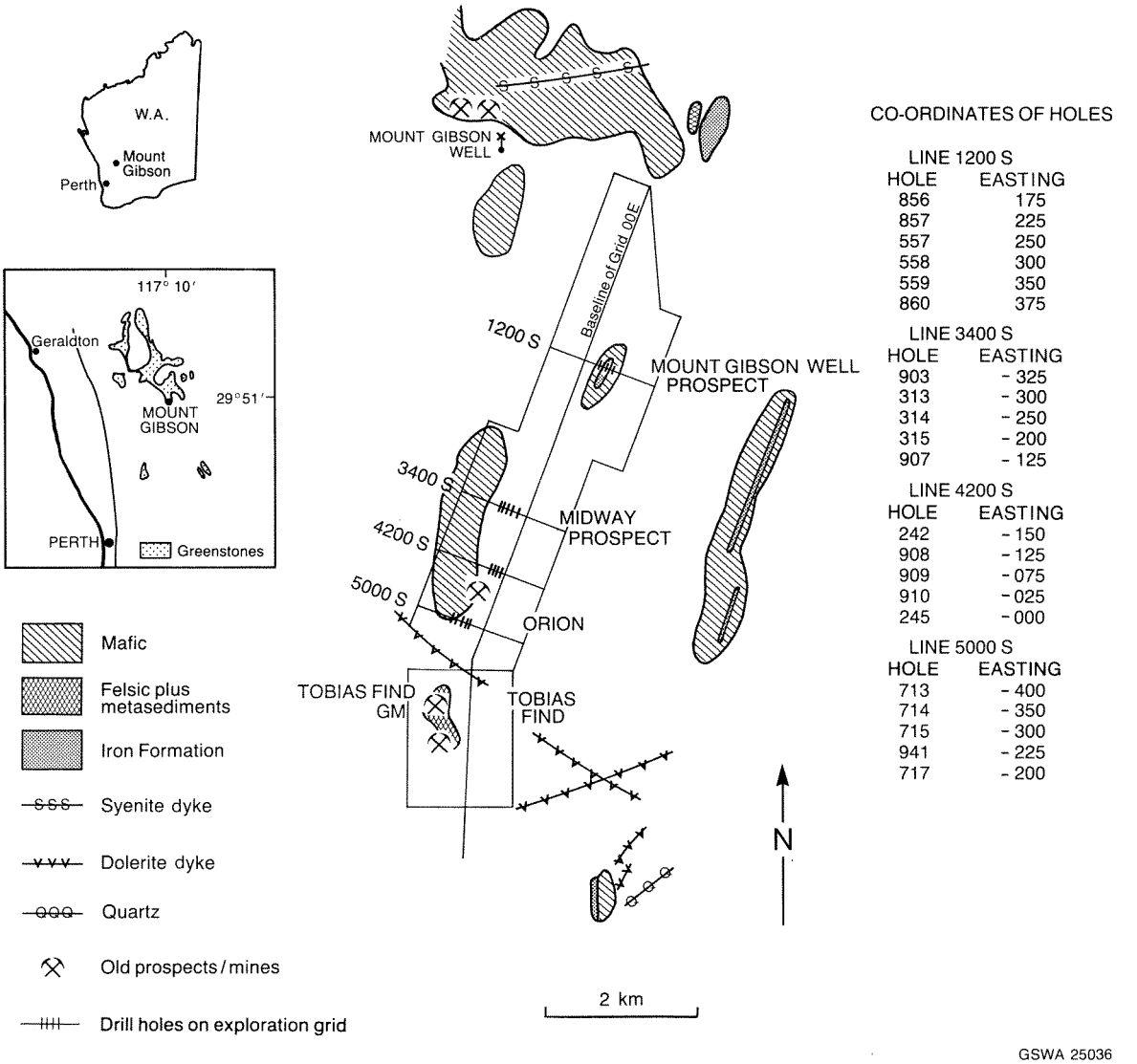

Figure 1. Location and geology of the Mount Gibson area, and drill holes sampled.

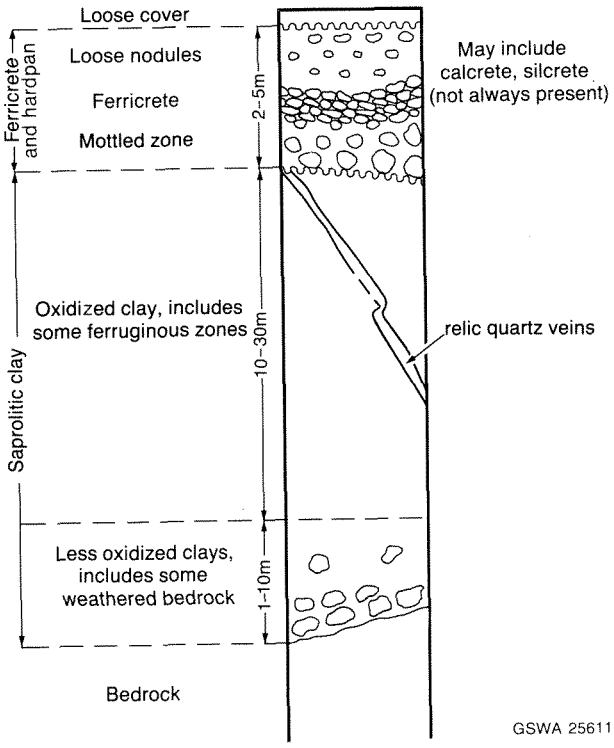

Figure 2. Generalized weathering profile at Mount Gibson. As samples were received in powder form, those described as ferricrete may include loose nodules and, rarely, mottled material, as well as true ferricrete.

Bedrock

Bedrock is of a series of former mafic to felsic volcanics, dolerite, and metasediments. All rocks have been metamorphosed to the lower amphibolite facies. Mafic rocks are now amphibolites, but some fragments retain traces of the original volcanic (basaltic), hypabyssal (doleritic) or fragmental (?tuffaceous) textures. Felsic volcanics include tuff and porphyritic rhyodacite–rhyolite. Probable metasediments include mica schist, garnetiferous mica schist, and iron-formation.

Clay

The clay zone is saprolite. Pits dug through ferricrete show that the clay retains primary rock textures. Relic phenocrysts of quartz and silicified feldspar are visible in what once was felsic volcanic rock; veins of quartz extend, without angular deflection through the clay to the base of the ferricrete. A few veins even extend through the ferricrete.

There are two subzones in the clay. The chief differences between these subzones are the lower oxidation state and the recognizable fragments of more or less weathered rock in the lower zone. Near the very bottom of the clay, these fragments of bedrock are relatively fresh. The lower

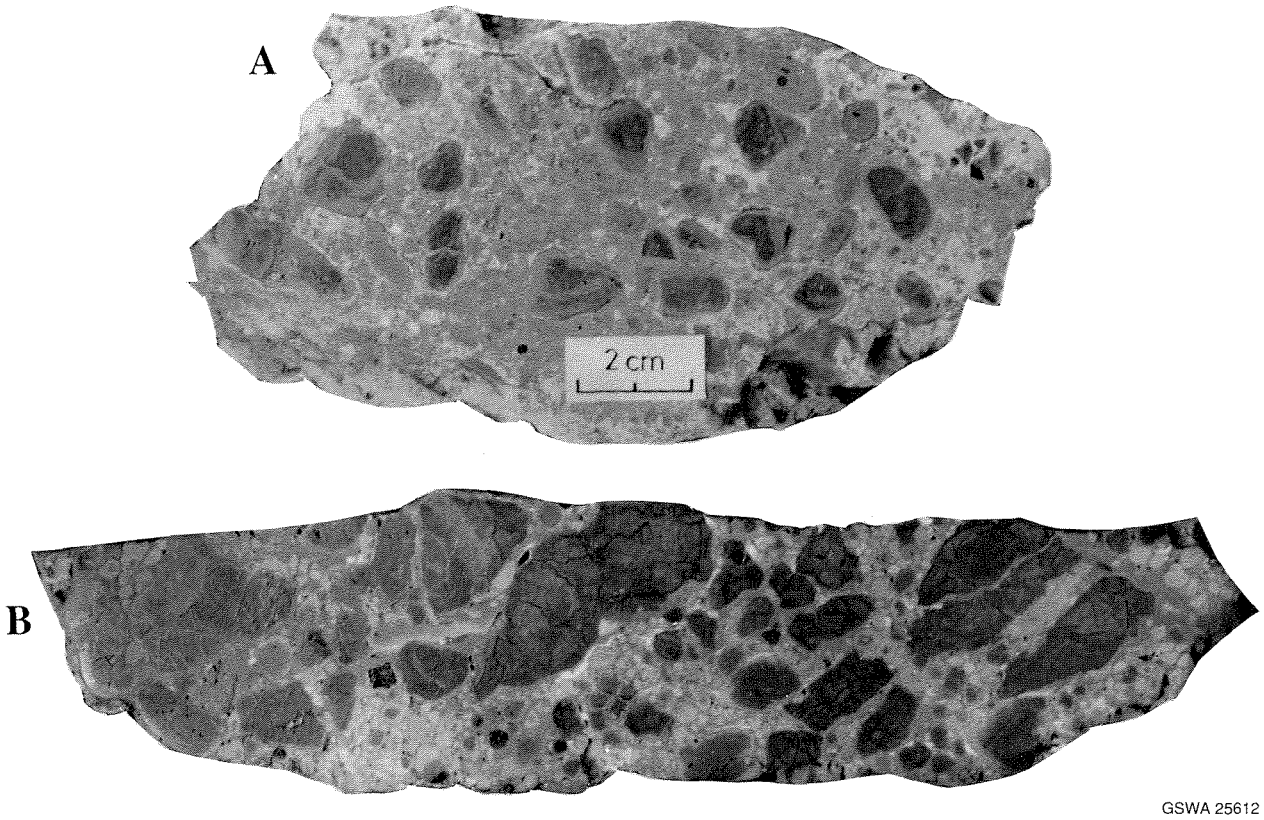

Figure 3. Polished specimens of ferricrete. A—Contains small rock relics with pronounced secondary surface skins in a matrix of carbonate and clay. B—Contains nodular relics of dark ferruginized rock; lighter, smaller limonitic nodules; and rare iron oxide pellets in a matrix of iron-rich clay. The last-deposited mineral is opal (white).

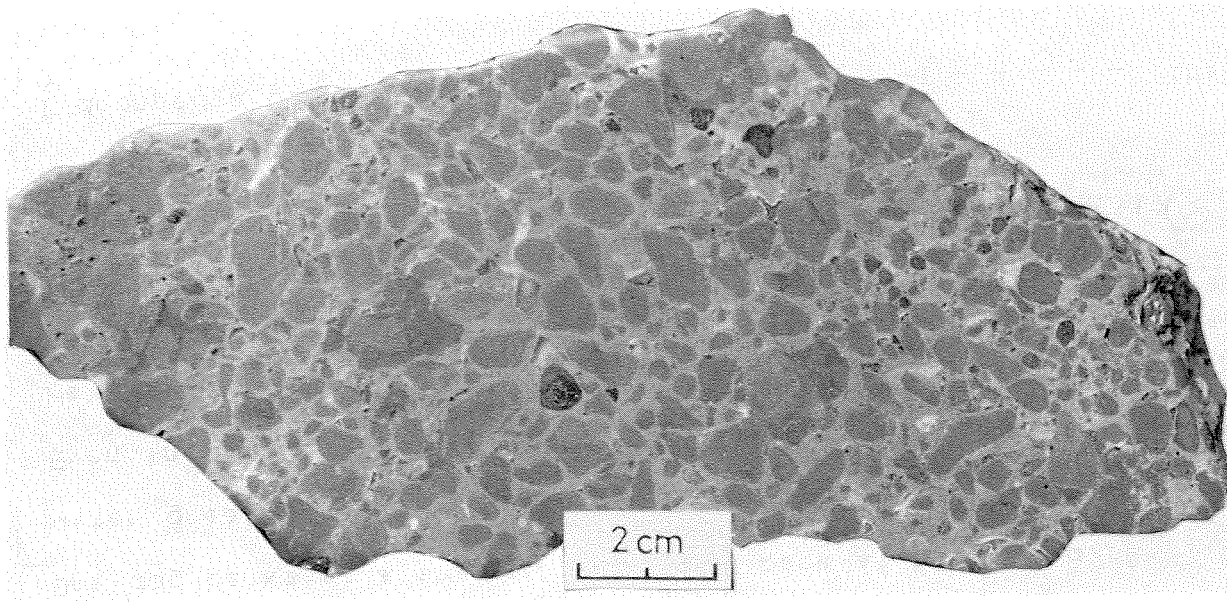

GSWA 25613

Figure 4. Polished specimen of ferricrete with 1–2 cm relics of ferruginized rock and isolated secondary iron oxide pellets in iron-rich clay. Minerals in cracks include carbonate, opal, and manganese dioxide.

GSWA 25614

Figure 5. Sheeted silica (silcrete) within poorly cemented nodules.

clays are normally grey to pale green, but in some places an oxidized iron-rich horizon just above the boundary between weathered and fresh rock probably reflects the passage of groundwaters along joints or other fractures.

The transition between the subzones is reflected in a change of colour from grey or green, to brown, yellow, or cream. In cuttings it normally occurs within a single three-metre interval. The upper clay is normally buff to cream.

In places, relic quartz veins are accompanied by dark ferruginous zones; the latter may be derived from primary sulphides.

A mottled zone between the clay and ferricrete is not always present. In most places, the clay–ferricrete contact is a horizontal fracture which may have been a sheet joint, and the contact is sharp. Occasionally, weakly ferruginized saprolite with blotchy colours passes gradually upwards into ferricrete. In places, lightly ferruginized siliceous clay surrounds blocks of more thoroughly ferruginized saprolite.

Ferricrete

The ferricrete is composed mainly of nodules that are cemented together, and is overlain in most places by loose

GSWA 25615

Figure 6. Sheeted carbonate (calcrete) within ferricrete.

GSWA 25616

Figure 7. Carbonate on vertical fracture surfaces in ferricrete, deposited from downward-moving waters.

nodules. There is a mixture of sub-rounded to semi-angular nodules and fragments of altered and ferruginized rock (some retaining traces of porphyritic texture); rounded to subangular grains of unzoned maghemite or hematite; limonite- or clay-rich grains cemented by some combination of clay, iron oxide–hydroxide, silica, and carbonate; and a few pisolites (Figs 3 and 4).

Most nodules are composed of altered ferruginized rock with a yellow- or red-brown ochreous skin (or cutan), often 2–3 layers thick, of oxide minerals and clay. The ferruginized rock comprises up to 90% of the nodule. The cutan may be discontinuous or partly destroyed. Many nodules show some penetration along cracks or fractures by the same material that forms the cutan. Cemented nodules are generally slightly larger (up to 100 mm in diameter) than those of the overlying loose material.

The ferricrete has been affected by later "hardpanization". Sheets of silcrete and calcrete have been deposited along sub-horizontal solution channels (Figs 5 and 6), and are rarely more than 15 cm thick. In a few places, deposition of carbonate from vertically moving vadose solutions occurred after formation of the horizontal sheets (Fig. 7). Some initially ferruginized nodules have been attacked and partly or wholly replaced by carbonate and small amounts of clay (Figs 8 and 9).

GSWA 25617

Figure 8. Partial replacement of ferricrete by carbonate.

GSWA 25618

Figure 9. Extensive replacement of ferricrete by carbonate.

GSWA 25619

Figure 10. Ferricrete with tree root, showing zone of loosened nodules.

The upper surface of the ferricrete is irregular. In places, loose nodules fill depressions within the ferricrete—depressions which could have been formed by tree roots or enhancement of original joints, or which merely reflect disaggregation surfaces above which dissolution of the cement has taken place. Tree roots of the present day produce pipe-like zones of loose nodules within the ferricrete (Fig. 10). At a few sites, nodules fill what may have been erosional channels (Figs 11 and 12).

The loose nodules are normally between 5 mm and 50 mm in diameter and tend to be rounded. True pisolites, defined as sub-spherical secondary accretionary pellets largely composed of concentric layers of secondary oxides –hydroxides, are rare and are invariably small (usually less than 5 mm in diameter). Most have a small lithic remnant as nucleus. Some rounded "pseudo-pisolites" are composed of clay impregnated with iron oxides. Matrix material includes clay, powdery carbonate, and sand. These loose nodules probably constitute a transition between the ferricrete proper and overlying material from other sources.

Ferricrete at the Mount Gibson Well prospect (line 1200 S) includes patches of gossan. Boxwork gossans have also been recorded in the pit floor at Orion.

Loose cover

The loose cover is dominated by grains of quartz, but contains variable amounts of remnant ferruginized rock fragments, red-stained clay, grains of iron oxide–hydroxide (including pisolites), carbonate, and organic remains. Residual soils contain the highest proportion of altered and

GSWA 25620

Figure 11. Loose nodules filling possible erosional channel in ferricrete.

ferruginized rock fragments and more abundant clays; they occur mainly on the ridge west of the main gold-bearing area. Colluvial and windblown soils are quite similar; both contain sand, minor clay, and sporadic iron-rich nodules. Most quartz grains are covered with a film of iron oxides. The loose cover is usually thin (less than 0.5 m), but ranges up to 4 m in the opencast mine area (Parker, 1987); it thickens to the northeast.

No further work has been carried out on this loose material.

Mineralogy

Lists of the minerals determined by X-ray diffraction, and of heavy minerals identified in the clay zone are given in Davy et al. (1989). This section summarizes the findings. Some minerals in ferricrete have been identified mineragraphically or by the electron microscopy. Bedrock mineralogy has been determined in part petrographically, in part by X-ray diffraction.

Bedrock

In fresh bedrock the dominant minerals are all metamorphic in origin; they include quartz, amphibole, feldspar (both plagioclase and K-feldspar), epidote, mica, and chlorite. Ilmenite is the most common opaque mineral, but most fresh rock contains some sulphide (pyrite). At the Mount Gibson Well prospect, iron-rich sphalerite, galena, and, more rarely, chalcopyrite and marcasite are also present.

Mafic rocks are now largely composed of hornblende, plagioclase, and subordinate quartz; some also contain tremolite, anthophyllite, or cummingtonite. Probable tuffaceous mafic rocks (e.g. sample 714.11) contain a slightly larger proportion of quartz. The abundance of tremolite and chlorite in many mafic rocks suggests an origin as high-magnesium basalt. In a few samples biotite is abundant. One possible ultramafic (high-magnesium) rock analysed (sample 941.15, line 5000 S) has the unusual mineralogy of tremolite and a small amount of quartz and coarse kaolinite. Biotite, and the coarse kaolinite, in such rocks may be of metasomatic origin.

Metapelite has been metamorphosed to quartz–mica–chlorite schist: some contains garnet; a small amount, cordierite. Iron-formation is composed of quartz, grunerite and (oxidized) magnetite. Felsic volcanics (or tuff) contain phenocrysts of plagioclase (or K-feldspar) and hornblende or (biotite) in a groundmass of feldspar, quartz, and mica. Felsic tuff and amphibolite at the Mount Gibson Well prospect both contain blastic tourmaline.

Whilst not common, siderite is the only carbonate found in bedrock. A rare blue muscovite occurs at the bottom of hole 717 on line 5000 S.

Many bottom-of-hole samples are not wholly fresh. Weathering is shown by iron-staining and the presence of fine-grained kaolinite, much of which has pseudomorphed feldspar.

Clay

At the bedrock–clay interface, amphibole, epidote–clinozoisite, biotite, chlorite, and most feldspar of the bedrock, have been transformed into clay minerals.

GSWA 25621

Figure 12. Detail of Figure 11, showing reduced size of loose nodules.

The most common minerals in both clay subzones are, in order of abundance, kaolinite, quartz, and goethite. Kaolinite is the first clay mineral formed from all felsic rocks and from many mafic rocks. However, smectite and vermiculite are the first clay minerals formed from some mafic rocks; these are normally converted to kaolinite higher in the profile. Muscovite, representing residual primary mica, is prominent over metasedimentary rocks; it disintegrates to sericite only near the top of the clay. Illite is sometimes present as an alteration product of biotite. Jarosite, as an oxidation product of partly replaced sulphide, is widespread in trace amounts near the base of some holes. Hematite sometimes occurs in the lower part of the clay zone; but goethite is more abundant, and occurs throughout. Traces of talc and anthophyllite occur in two holes (941 and 717) on line 5000 S at Orion.

In the clay zone, fine-grained gold occurs in three environments: in veins with quartz and iron oxide–hydroxide, in ferruginized patches, and disseminated in clay.

Heavy minerals in the clay zones include spessartine (yellow), almandine (pink or colourless), tourmaline, and zircon. There are two main varieties of tourmaline: one has

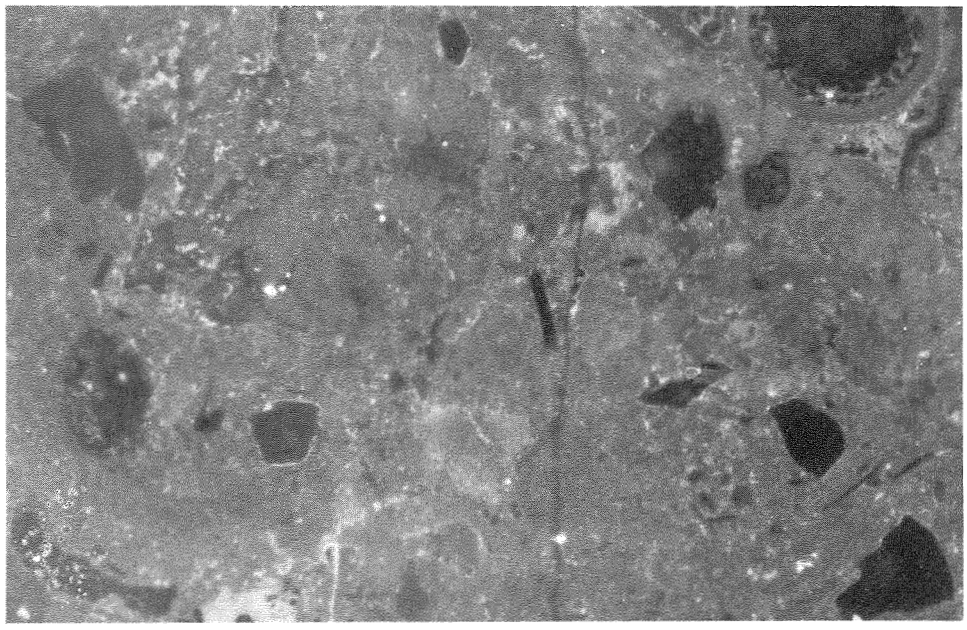

GSWA 25622

Figure 13. Gold particles in ferricrete on margins of nodules and in internodular matrix; field of view, 0.5 mm.

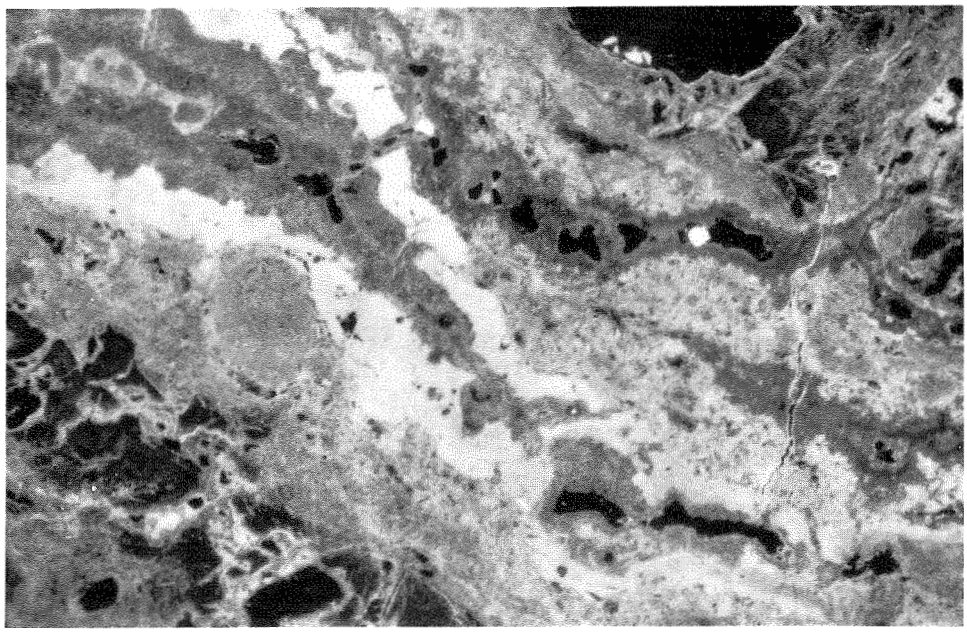

GSWA 25623

Figure 14. Gold particles in cavities within ferricrete; field of view, 0.5 mm.

brown–blue pleochroism; the other, olive brown–green pleochroism. Apatite is present in clay at Mount Gibson Well. Brown and mauve rutile and barite are present in line 5000 S. Barite is also present in one sample from line 3400 S.

Ferricrete

In most places the ferricrete contains, in order of decreasing abundance, kaolinite, goethite, relic quartz, and hematite. However, large areas contain calcrete, some of which is magnesian, and silcrete. There is a marked decrease in the crystallinity of silica compared to that in the clay zone. Traces of sericite or muscovite are common. Ilmenite and sphene, present in mafic rocks, have been replaced by leucoxene.

Dendritic patchy manganese dioxide coats some voids; elsewhere veinlets of opal fill cracks in the ferricrete.

Unusual minerals in a few surface or near-surface samples include small amounts of feldspar, amphibole, and barite; and gibbsite is present at the surface at two points on line 4200 S (Orion). A barium–strontium phosphate and a lead bromide mineral were detected in one sample of ferricrete.

In the ferricrete, gold occurs as single particles within nodules, in amorphous iron hydroxide on the rims of, or between, nodules, and in goethite-rich veins. Most individual grains are less than 5 μm in diameter. Gold, which occurs as sub-equant rounded grains, fine specks, rare elongate platelets, "wires", and as inclusions within quartz (Figs 13 and 14), is dispersed throughout the nodules. Grains of gold in veinlets are normally elongate, and small grains of crystalline gold were observed in vug-like cavities (Fig. 15).

Primary mineralization

Primary mineralization appears in three main environments:

(a) Auriferous quartz-rich veins which, from their present content of iron, were probably originally sulphidic. Such veins appear to be more common at Orion than further north.

(b) At Mount Gibson Well, sulphide mineralization with some gold, occurs in felsic metavolcanics and related tuff, and metasediment. Here the origin appears, at least in part, premetamorphic, as the sulphide grains form part of the metamorphic granoblastic texture.

(c) Mineralized shear zones (Kneebone, 1980).

Chemical composition

Chemical analyses of all examined samples are given in Davy et al. (1989).

Bedrock

Despite incipient alteration of some samples, most bedrock retains enough primary features for recognition of the general rock type. Many mafic rocks have a low-K tholeiitic composition, but others are unusual in having a high (to over 2%) content of K_2O in association with more normal mafic values for other major oxides. One hole (908, line 4200 S) ended in iron-formation containing over 17%

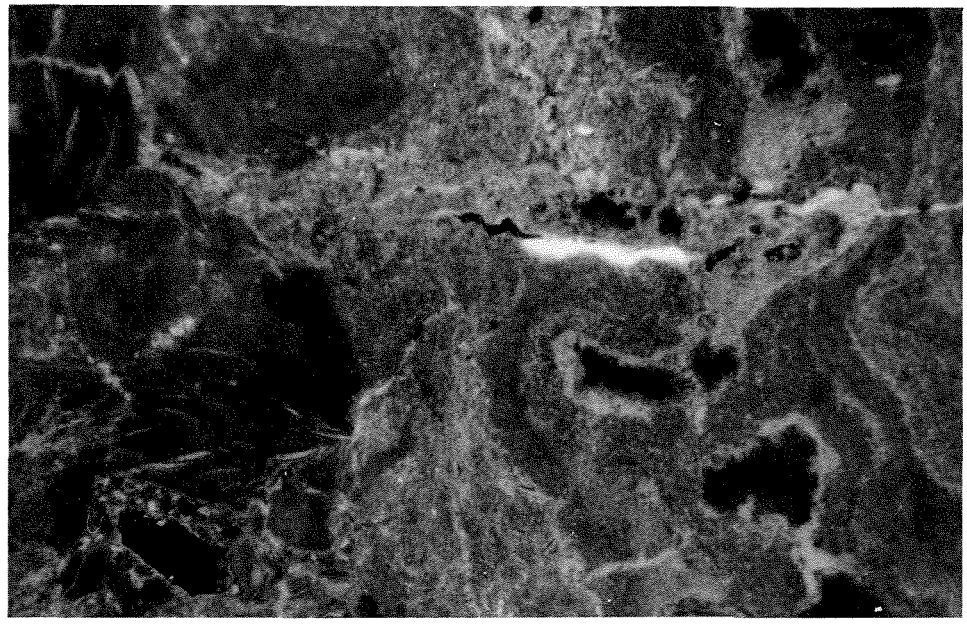

GSWA 25624

Figure 15. Late-formed gold in veinlet in ferricrete; field of view 0.2 mm.

Fe. Some felsic volcanics are highly (more than 3% K_2O and less than 0.5% Na_2O) potassic; others contain very little K_2O. Typical compositions are given in Table 1.

The tremolite–kaolinite rock referred to earlier (sample 941.15), contains high MgO, Fe_2O_3, and Cr, but low SiO_2. This sample also contains anomalous Cu (610 ppm), Pb (88 ppm), and Zn (780 ppm), while the K_2O content (0.4%) is high for a high-magnesium rock.

Clay

The greatest chemical changes in the profiles occur between bedrock and saprolite. Above this interface, CaO, MgO, Cd, and Sr, have been almost totally leached; Ce, Co, La, Mn, Ni, and Y, have been partly leached; Fe has been oxidized; and loss on ignition (LOI) and Al_2O_3 have increased. Though much Na_2O is lost at the interface, significant amounts (normally 0.1 – 0.5%) remain. Potassium oxide, SiO_2 and TiO_2 apparently remain little changed at the boundary, and other components display no consistent pattern. In some holes, Ce, Co, La, Ni, M,n and Y, are concentrated near the base of the clay.

There is little obvious chemical change at the boundary between oxidized and less oxidized clays. There is no evidence of a progressive increase in concentration of residual elements upwards, and no systematic compositional trends of enrichment or depletion are discernible within either of the upper or lower clay zones. This is illustrated in Figure 16, where all clay samples are believed to be derived from the same (mafic) rock. Most changes of composition are abrupt and define "blocks" which suggest

TABLE 1. COMPOSITION OF TYPICAL BEDROCK SAMPLES

	242.20	*245.17*	*314.20*	*315.17*	*856.13*	*857.18*	*903.19*	*908.17*	*910.21*	*941.15*
					(per cent)					
SiO_2	68.4	57.1	50.8	50.0	73.9	54.7	47.8	38.2	71.6	45.7
Al_2O_3	9.5	17.1	16.7	14.9	12.7	11.7	15.7	12.7	14.6	15.6
Fe_2O_3(a)	10.4	9.4	12.0	13.2	4.1	13.7	14.2	27.2	2.7	17.5
MgO	1.7	4.8	6.3	4.0	0.60	2.0	8.1	2.1	1.8	8.7
CaO	0.49	1.6	4.8	3.8	0.02	0.42	1.1	1.4	0.19	0.25
Na_2O	0.86	0.87	1.2	0.44	0.36	1.2	0.63	0.46	0.28	0.53
K_2O	0.39	1.1	0.3	2.3	3.2	2.2	1.2	0.48	3.5	0.41
TiO_2	0.22	0.79	0.86	1.9	0.07	0.95	1.1	0.37	0.26	0.54
P_2O_5	0.01	0.09	0.08	0.21	0.03	0.08	0.10	0.02	0.08	0.05
MnO	0.11	0.09	0.25	0.33	0.17	0.23	0.18	0.60	0.06	0.11
LOI	7.6	7.3	8.2	7.9	4.6	10.8	9.9	18.2	4.5	10.7
					(parts per million)					
Ag	17	0.6	0.4	17	0.6	42	1.4	<0.1	0.6	0.1
As	<10	35	<10	50	130	555	<10	<10	25	<10
Au	3.25	<0.01	<0.01	0.62	<0.01	1.6	0.36	2.1	0.02	0.19
Ba	219	435	105	520	695	220	520	115	500	90
Bi	<10	<10	<10	40	<10	<10	<10	<10	<10	<10
Cd	30	3	<2	20	<2	30	2	3	<2	3
Ce	34	<526	28	31	35	7	22	38	5	22
Cl	1400	1300	2200	1100	1800	10000	2600	1300	500	700
Co	1280	145	165	55	10	55	60	135	20	80
Cr	595	280	685	415	145	210	530	365	65	1120
Cu	1280	150	130	235	75	530	460	35	20	610
Ga	7	17	16	20	19	20	19	10	18	14
La	<5	5	11	16	23	17	13	5	24	12
Mo	<5	<5	<5	<5	<5	<5	<5	<5	<5	<5
Nb	<5	<5	<5	5	10	<5	<5	<5	<5	<5
Ni	365	395	210	100	35	95	145	135	45	300
Pb	1050	15	50	395	360	5940	10	10	25	90
Rb	35	50	20	125	130	50	45	20	285	20
Sb	<10	<10	<10	<10	<10	75	<10	<10	<10	<10
Sc	20	50	35	40	2	20	30	30	5	30
Sn	<5	<5	<5	10	<5	<5	<5	<5	<5	<5
Sr	<5	10	35	40	5	10	<5	15	10	5
Th	13	<10	<10	17	14	17	<10	<10	<10	<10
U	<2	<2	<2	3	2	2	2	<2	7	<2
V	125	300	240	405	10	195	250	200	30	145
W	7600	<10	330	85	<10	55	20	<10	<10	11
Y	5	8	22	37	22	29	12	26	9	18
Zn	2320	660	305	950	480	1990	140	365	90	790
Zr	20	55	90	160	75	80	105	25	150	45

KEY: 242.20 = Mineralized metasediment. 245.17 = Intermediate metasediment or tuff. 314.20 = Mafic rock (amphibolite). 315.17 = Mafic metasediment or tuff. 856.13 = Felsic tuff. 857.18 = Mineralized mafic tuff. 903.19 = Potash metasomatized mafic rock. 908.17 = Iron-formation. 910.21 = Felsic tuff or metasediment. 941.15 = Hydrothermally altered ultramafic rock.

NOTE: (a) = Total iron expressed as Fe_2O_3.

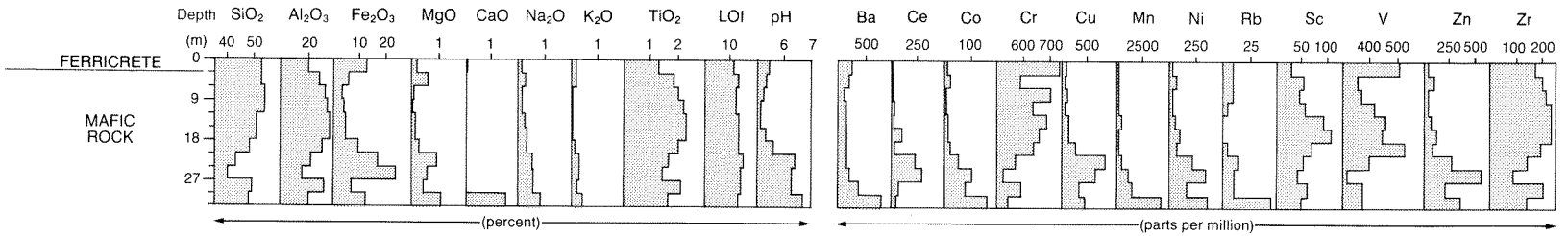

GSWA 25625

Figure 16. Element profiles in hole 714. Apart from first two samples, all are interpreted as having a mafic origin. Total iron is given as Fe_2O_3; depth increment, 3 m.

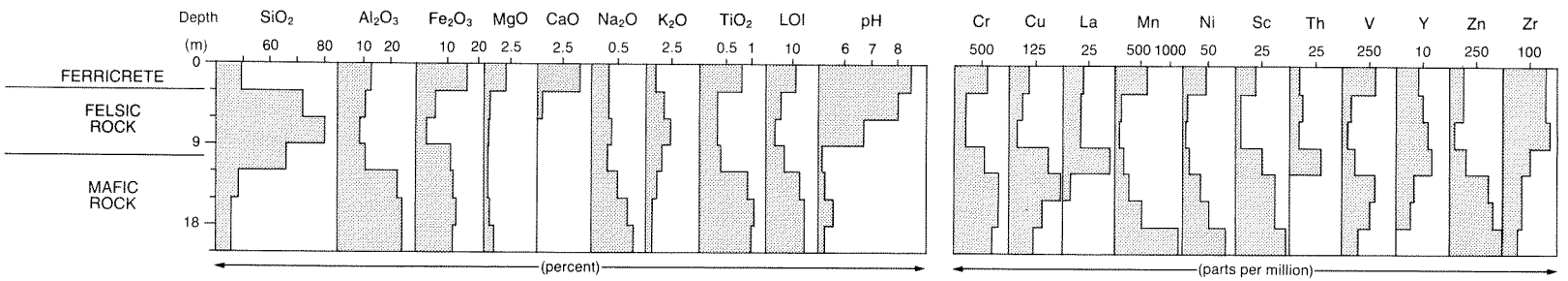

GSWA 25626

Figure 17. Element profiles in hole 557, showing ferricrete with calcrete (sample 1–2), clay derived from felsic rock (samples 3–4), and clay derived from mafic rock (remainder). Total iron is given as Fe_2O_3; depth increment, 3 m.

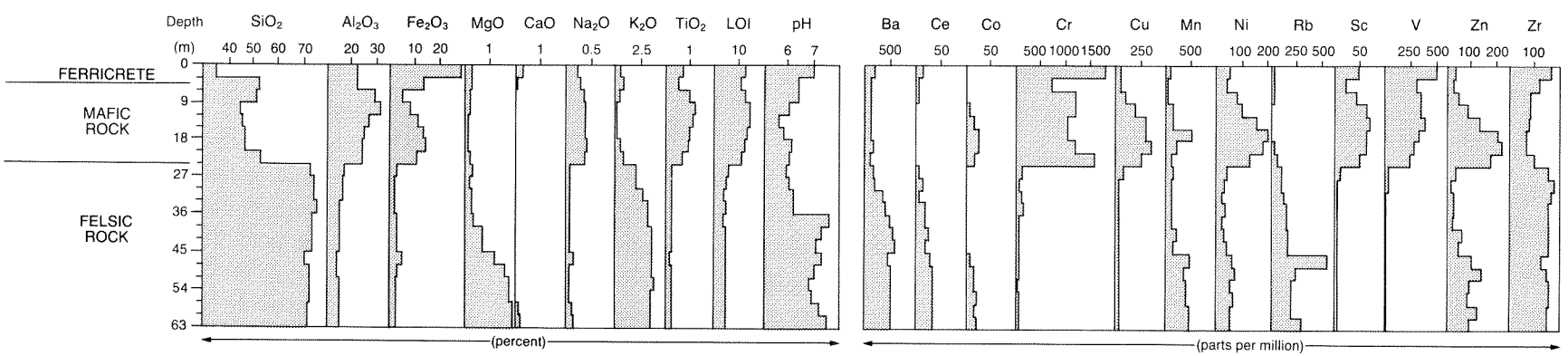

GSWA 25627

Figure 18. Element profiles in hole 910, showing weakly calcretized ferricrete (samples 1 and 2) overlying clay from mafic rocks (samples 3–8) and passing into clay derived from felsic metasediment (samples 9–16) then the metasediment itself. Total iron is given as Fe_2O_3; depth increment, 3 m.

TABLE 2. REPRESENTATIVE SAMPLES OF CLAY, FERRICRETE, AND CALCRETE

	Clay										*Calcrete and ferricrete*				
	242.13	*245.8*	*313.2*	*314.5*	*315.10*	*717.10*	*857.9*	*903.13*	*908.8*	*908.14*	*315.2*	*856.1*	*907.1*	*908.1*	*909.2*
	(per cent)														
SiO_2	55.0	58.5	56.6	48.7	73.3	74.3	74.7	52.1	47.4	37.4	48.2	23.1	25.9	29.6	25.7
Al_2O_3	29.0	25.6	16.6	28.6	14.4	15.3	14.2	19.2	24.8	14.8	13.2	7.3	18.5	25.9	21.0
Fe_2O_3(a)	2.7	3.1	13.3	8.1	3.8	2.9	2.6	13.0	14.1	32.1	25.5	8.8	41.7	22.5	38.5
MgO	0.14	0.15	0.25	0.14	0.39	0.28	0.34	1.1	0.15	0.88	0.20	7.8	0.23	0.57	0.24
CaO	0.01	0.01	0.58	0.08	0.09	0.01	<0.01	0.11	0.01	0.06	0.13	21.6	0.29	3.1	0.65
Na_2O	0.44	0.29	0.41	0.45	0.21	0.12	0.25	0.69	0.37	0.57	0.23	0.33	0.16	0.24	0.19
K_2O	0.22	0.57	0.38	0.52	2.9	1.7	2.6	1.6	0.07	0.29	0.93	0.49	0.11	0.14	0.06
TiO_2	0.66	1.2	0.46	0.89	<0.01	0.25	0.13	1.4	0.64	0.46	1.3	0.41	1.3	1.3	0.97
P_2O_5	0.03	0.04	<0.01	0.03	0.04	0.05	0.03	0.04	0.04	0.07	0.02	0.03	0.02	0.01	0.04
MnO	0.03	0.10	0.02	0.03	0.09	0.03	0.01	0.03	0.02	0.10	0.03	0.04	0.03	0.01	0.03
LOI	12.5	11.0	11.2	12.6	4.5	5.4	4.7	10.5	12.6	12.1	8.7	30.4	10.3	16.9	12.7
	(parts per million)														
Ag	<0.1	<0.1	<0.1	0.1	0.1	1.1	<0.1	0.1	0.1	0.1	0.1	<0.1	0.6	1.7	1.0
As	<10	35	<10	45	15	<10	720	<10	10	10	60	205	25	75	30
Au	1.8	<0.01	<0.01	<0.01	0.57	0.50	<0.01	0.30	0.20	0.10	0.03	0.56	0.71	1.0	0.65
Ba	75	115	305	95	425	500	380	710	55	135	345	160	145	380	105
Bi	<10	<10	<10	45	<10	<10	<10	<10	<10	<10	<10	<10	<10	<10	<10
Cd	<2	<2	<2	2	<2	<2	<2	2	2	8	2	<2	3	3	3
Ce	10	16	6	24	11	28	38	93	<5	34	11	14	16	28	<5
Cl	3500	1600	2600	3800	900	700	2200	3100	2700	1900	1700	1900	500	700	500
Co	10	10	5	10	<5	5	<5	20	5	200	<5	10	9	10	5
Cr	785	210	2430	465	185	200	95	540	1010	545	555	390	1930	1580	495
Cu	90	205	330	90	75	80	80	265	120	170	80	90	45	45	175
Ga	28	29	16	25	22	21	19	23	19	11	24	10	41	36	16
La	11	16	<5	32	<5	26	27	42	<5	22	7	13	9	18	<5
Nb	7	<5	<5	<5	9	7	7	<5	<5	<5	<5	<5	<5	6	<5
Ni	95	40	45	55	15	45	20	75	45	440	20	40	55	50	30
Pb	145	860	<5	255	310	15	840	100	25	20	30	55	45	35	30
Rb	155	45	20	60	140	70	105	90	<5	30	35	25	5	10	<5
Sb	<10	<10	<10	<10	<10	<10	25	<10	<10	<10	<10	<10	<10	<10	<10
Sc	88	58	38	29	9	12	4	40	61	40	22	12	60	52	48
Sn	5	<5	<5	50	8	<5	<5	<5	<5	<5	6	<5	5	<5	6
Sr	<5	10	15	<5	10	<5	35	10	<5	5	<5	285	10	85	35
Th	<10	<10	<10	25	<10	<10	20	<10	<10	<10	10	<10	25	15	<10
U	3	<2	<2	<2	4	<2	3	2	<2	<2	2	3	2	4	2
V	280	475	225	240	45	80	15	315	345	260	475	120	925	495	430
W	<10	<10	<10	40	<10	<10	<10	43	<10	<10	<10	<10	<10	75	<10
Y	3	5	2	3	11	10	16	40	2	105	3	9	5	10	3
Zn	40	260	40	155	60	40	85	120	65	1 040	40	225	35	45	55
Zr	60	90	60	110	50	165	85	130	50	30	140	70	205	175	100

KEY: 242.13 = After mafic rock with mineralized quartz vein. 245.8 = After metasediment of intermediate composition. 313.2 = After possible ultramafic rock. 314.5 = After mafic ?metasediment or tuff. 315.10 = After garnet-bearing metasediment. 717.10 = After weakly mineralized dacitic tuff. 857.9 = After sulphide-bearing dacite (?tuff). 903.13 = After high-K variety of mafic rock. 908.8 = After mafic rock. 908.14 = After weakly mineralized metasediment. 315.2 = Ferricrete over felsic rock. 856.1 = Calcrete. 907.1 = Ferricrete with possible ultramafic affinities. 908.1 = Mixed ferricrete and calcrete. 909.2 = Ferricrete over mafic rock.

NOTE: (a) = Total iron expressed as Fe_2O_3.

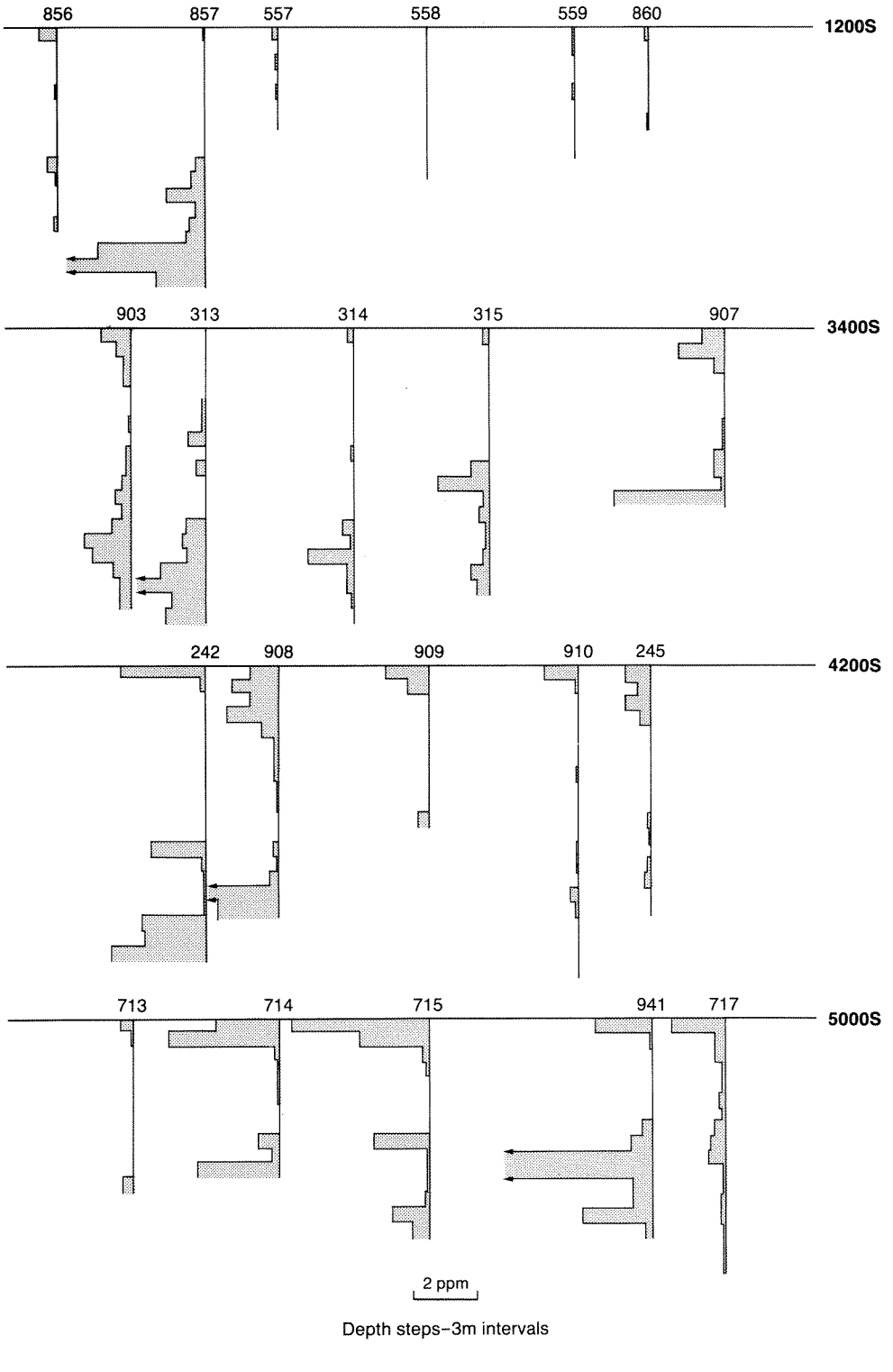

Figure 19. Gold distribution in lines sampled.

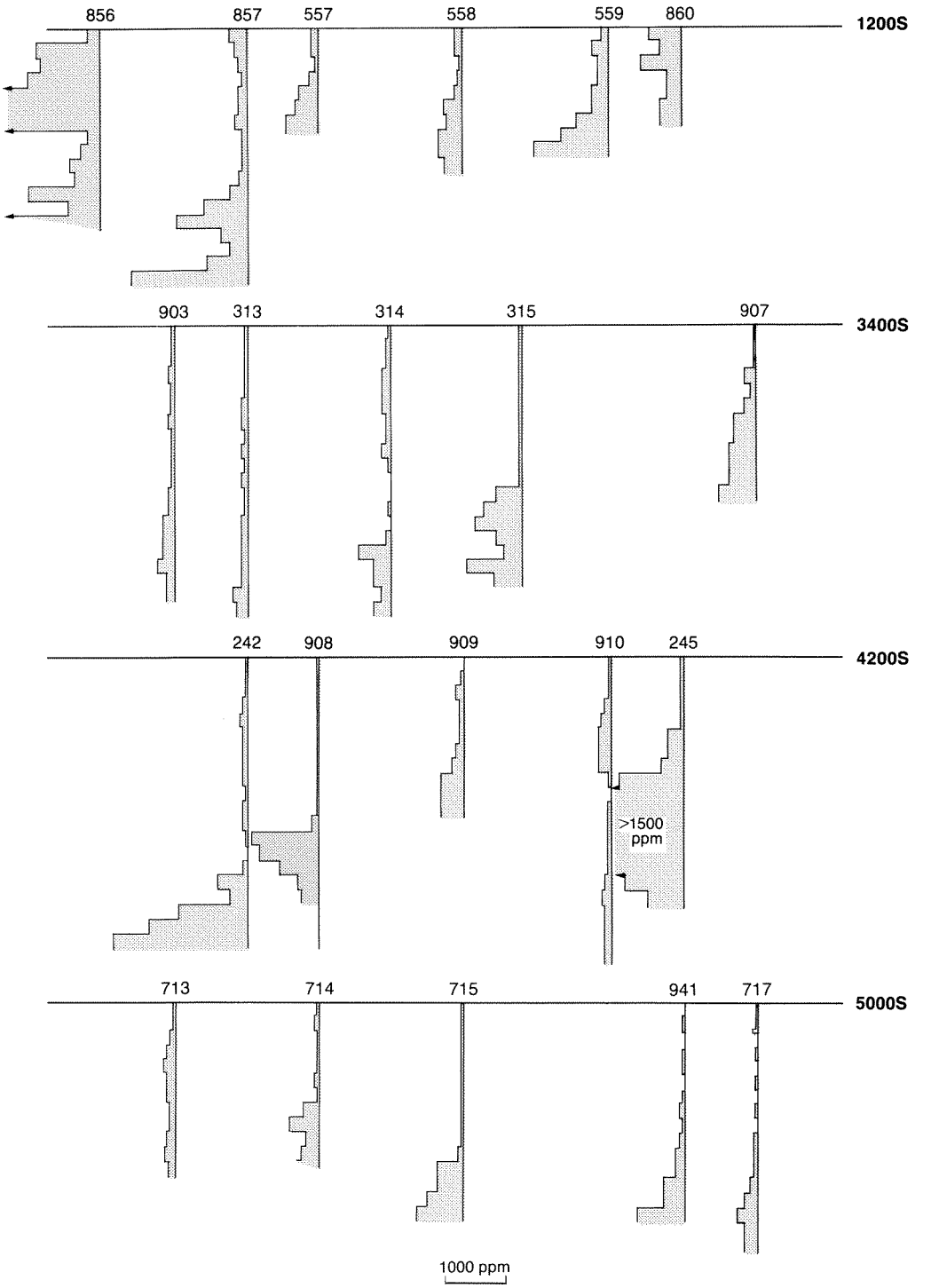

Figure 20. Zinc distribution in lines sampled.

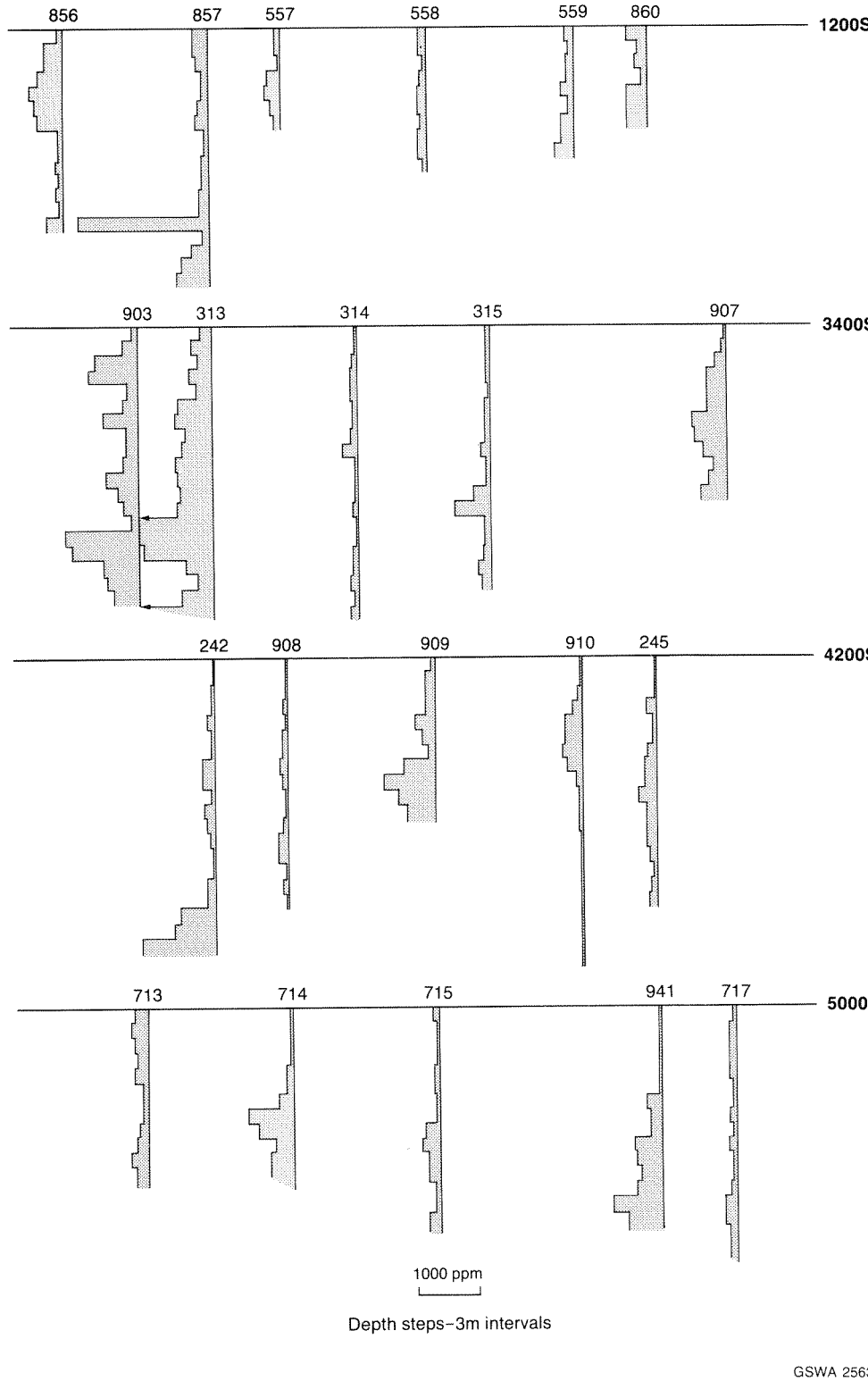

Figure 21. Copper distribution in lines sampled.

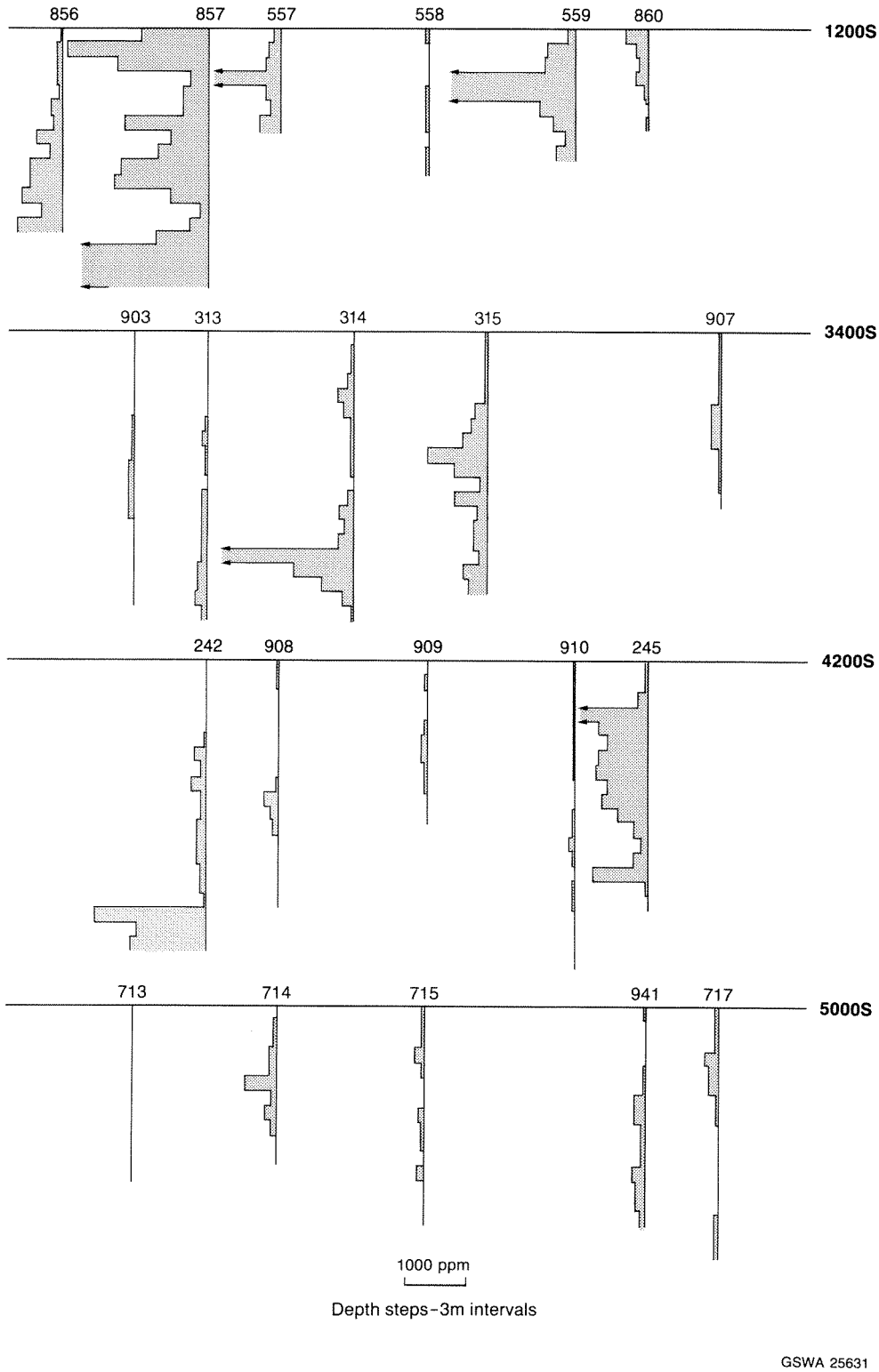

Figure 22. Lead distribution in lines sampled.

original differences in rock types (Figs 17 and 18). Tests, using concentrations of supposedly immobile components, have been applied to the clays to try to identify the original rocks (next section).

Some typical compositions for samples from the clay zone are given in Table 2.

Ferricrete

As expected, since carbonates are present, samples from ferricrete, in particular the uppermost sample in each hole, show marked increases in CaO, MgO, Sr and, rarely, MnO, compared with the underlying clay. In the ferricrete, iron is strongly enriched, SiO_2 is generally markedly depleted, and Al_2O_3 and TiO_2 slightly depleted compared with clay. The Fe_2O_3 content is generally between 15% and 30%, but reaches a maximum of 42%. Gossanous ironstone at Mount Gibson Well also reaches a maximum of 42% Fe_2O_3. Silica must have been even more depleted at some time prior to the late-stage resilicification. Most mica breaks down in the ferricrete, resulting in loss of potassium relative to the clay; however, where mica is absent from the clay, concentrations of K_2O vary little between clay and ferricrete and may even increase slightly in the ferricrete. Representative analyses of ferricrete and calcrete are given in Table 2.

TABLE 3. GROUNDWATER SAMPLES

(Results expressed in parts per million)

	GSWA Sample				
	82135	*82136*	*82137*	*82138*	*82141*
pH	7.5	3.9	3.7	6.5	7.3
"Major" components:					
Ca	88	138	17	398	279
Mg	329	1 240	1 900	1 390	744
Na	3 140	11 200	13 900	11 000	6 600
K	98	358	439	433	172
Fe	21	19	16	51	1.6
$(CO_3)^{2-}$	<2	<2	<2	<2	<2
$(HCO_3)^-$	310	<2	<2	127	507
Cl^-	5 370	20 300	25 000	20 090	11 700
$(SO_4)^{2-}$	603	2 280	4 010	2 280	1 670
$(NO_3)^-$	1	1	6	<1	3
SiO_2	30	104	100	42	56
"Minor" components:					
Al	0.3	42	12	0.1	<0.1
Au	<0.1	0.01	0.02	<0.01	<0.01
B	2.2	7.2	6.7	5.9	5.8
Co	0.04	0.09	0.14	0.06	0.05
Cr	0.08	0.03	0.02	0.02	0.01
Cu	0.03	0.05	0.16	0.03	0.02
F	0.3	<0.1	<0.1	<0.1	0.1
Li	0.08	0.13	0.14	0.05	0.12
Mn	0.73	1.0	1.8	5.5	5.4
Ni	<0.01	0.04	0.15	<0.01	<0.05
Pb	<0.05	0.27	0.29	<0.05	<0.05
Zn	0.08	0.13	0.13	0.03	<0.01

KEY: Sample number = (Local Grid) 82135 = (4600S, 175W) 82136 = (2000S, 400E) 82137 = (1000S, 750E) 82138 = (1600S, 150E) 82141 = (7400S, 50W).

NOTE: Total iron expressed as Fe_2O_3.

Gold is enriched in ferricrete, even when not detectable at the 10 ppb level in underlying clay. "Residual" elements, such as Cr, Th, V, and Zr, also tend to be more abundant in ferricrete—especially in the lower part of the zone—than in clay. The amount of Sc is normally higher in ferricrete than in clay immediately below, though maxima can occur anywhere in the profile. For most other trace elements there is little difference in composition between clay and ferricrete.

Metalliferous associations

Whilst Tobias Find was already known as a gold occurrence, the Mount Gibson Well and Orion prospects were originally prospected by North Prospecting Pty Ltd, North Flinders Mines Ltd, and Australian Anglo-American Prospecting Pty Ltd for base metals (B. Fehlberg, written comm.). The analyses confirm a primary regional metalliferous association which includes Au, Ag, As, Bi, Cu, Pb, Sb, W, and Zn, but which has different characteristics in each of the prospects. Arsenic, Ag, Sb, and Pb, have their highest values at Mount Gibson Well; Cu is prominent at Midway and the northern part of Orion, whilst W is highest at Orion. Maximum values of Pb (1.2% over 3 m) and Zn (0.3% over 3 m) occur at Mount Gibson Well, and the maximum value for W (0.76% over 3 m) occurs at Orion.

Silver has been leached from ferricrete and clay, but traces are retained in gossan at Mount Gibson Well. Arsenic and Sb, where they are present in bedrock, are retained in the profile; there is significant As on all lines except 5000 S; however, Sb is only prominent on line 1200 S. Bismuth and W are commonly close to, or below, the limit of detection (10 ppm): despite isolated higher values occurring above bedrock, these elements may be largely leached from the ferricrete and clay.

The distributions of Au, Cu, Pb, and Zn on each of the four lines sampled are presented in Figures 19–22. Figure 19 shows the consistent near-surface distribution pattern of gold at Orion, and the near-bedrock distribution on lines at Mount Gibson Well and Midway. A feature of almost all profiles is the lack of Au in the central to upper part of the saprolite.

Figures 20–22 reveal differences in both primary distribution and secondary dispersion of the base metals. Primary distributions near the bottom of holes suggest that all three base metals are only present together in anomalous quantities at the base of holes 857 and 242. The figures show that leaching of Zn from the saprolite (Fig. 20) has been more extensive (deeper) than that of Cu (Fig. 21). The amounts of both Cu and Zn trapped or retained in the ferricrete do not reflect the presence of mineralization at depth. Leaching patterns for Pb (Fig. 22) are less clear, but

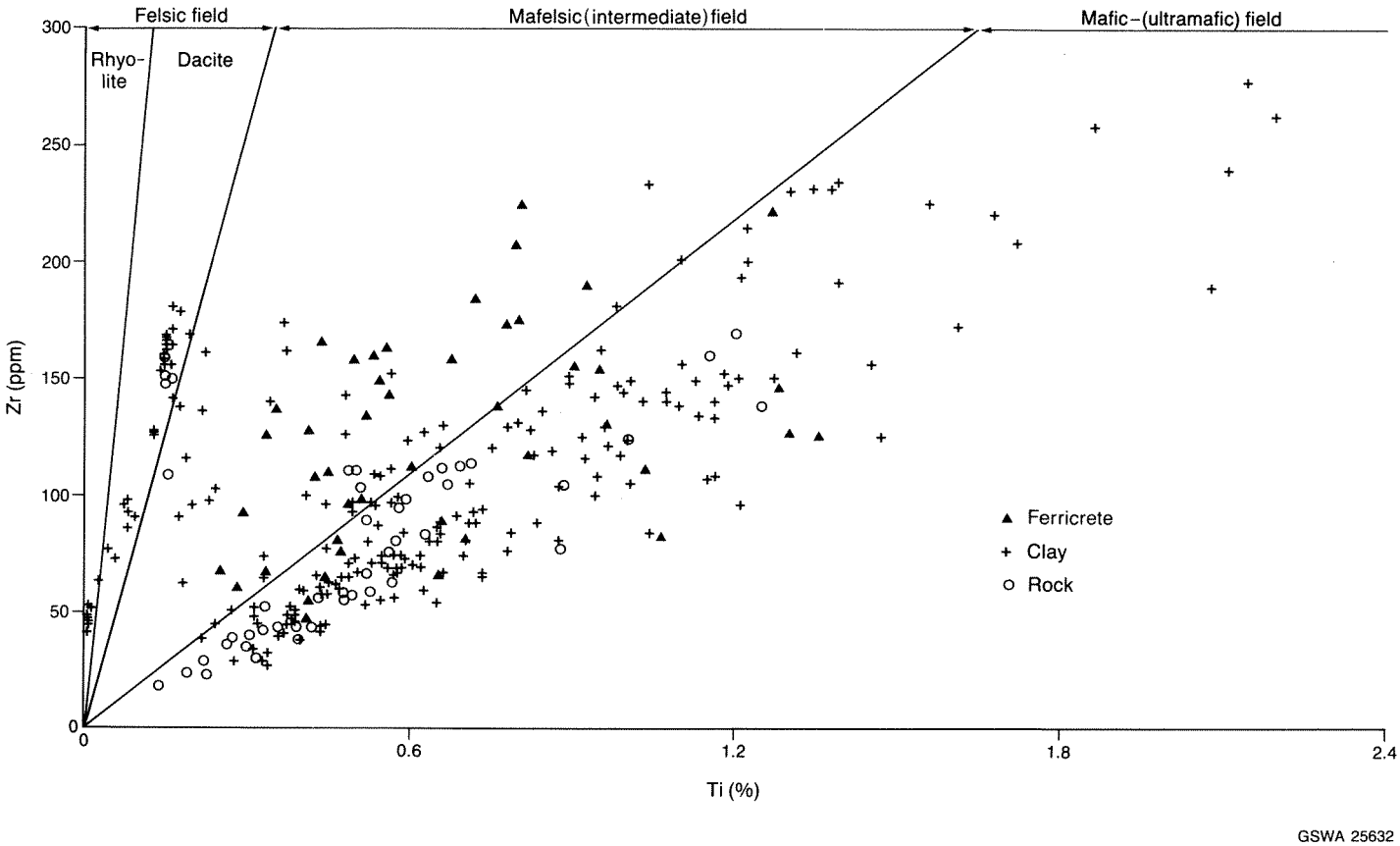

Figure 23. Zirconium–titanium plots for all samples collected from the Mount Gibson study area. Fields after Hallberg (1984).

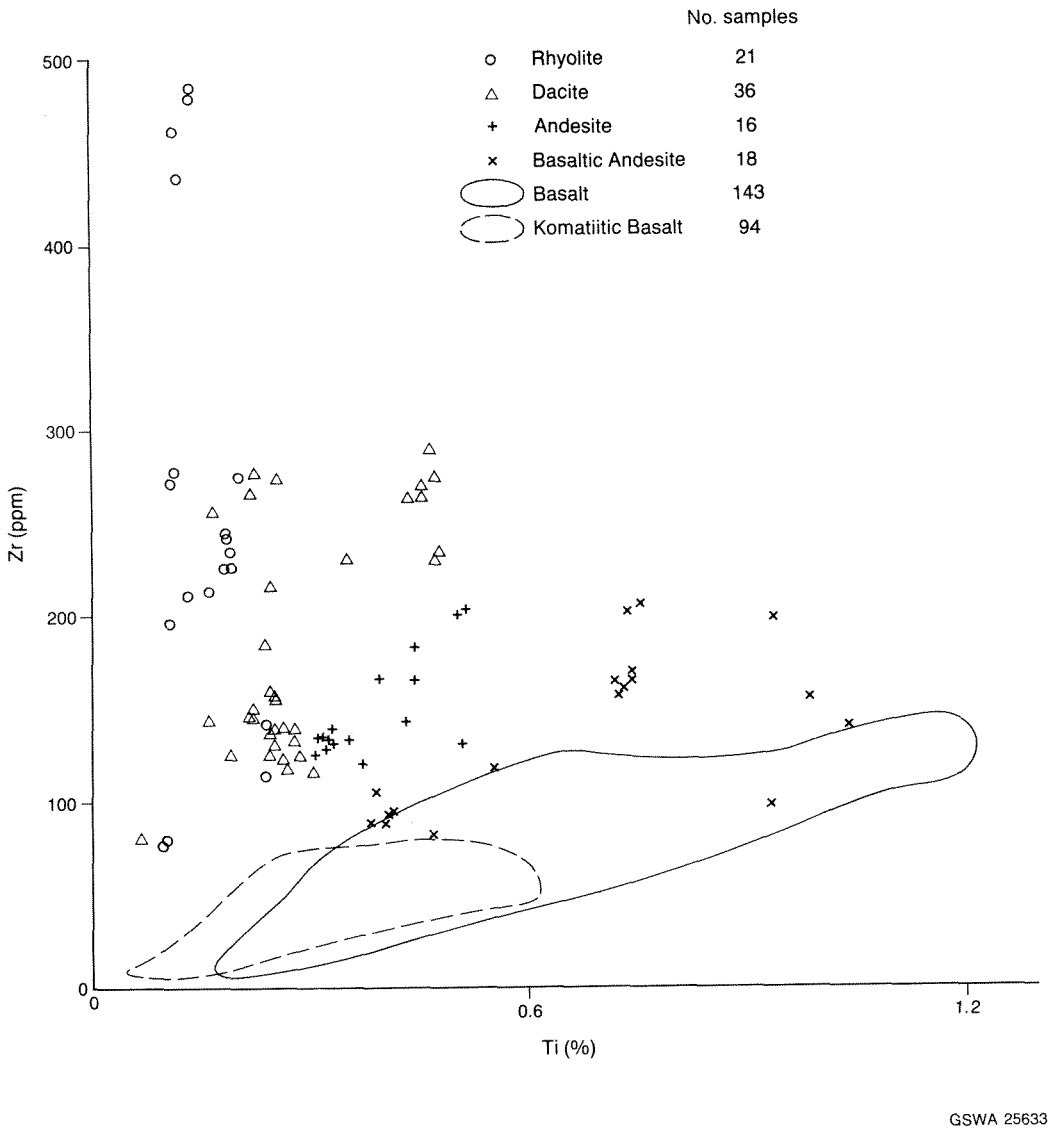

Figure 24. Zirconium–titanium plot for bedrock samples from the Murchison Province. Data from Watkins and Hickman (1990).

suggest that near-surface leaching has been effective in all but the northernmost line (Mount Gibson Well). This line (1200 S) also retains more Zn near the surface than other lines.

Tin and U are not considered part of the mineralizing assemblage. Values are low: maxima are 49 and 8 ppm respectively. Most samples with Sn at or about 10 ppm seem to relate to possible metasediments, and most detectable U may relate to felsic rocks in general.

Composition of groundwaters in the Gibson area

The compositions of some waters from the Gibson area are given in Table 3. Total dissolved solids in the mine area range from about 1% to a maximum of 4.6%, and the sampled waters are generally slightly less saline than normal sea-water (3.5%). The pH ranges from 3.7 to 7.0. The waters are chloride-rich: the content of chloride ions varies from 0.5% to 2.5%. Sulphate concentrations are about one tenth of chloride concentrations. Carbonate and bicarbonate ions are present in the neutral waters at low levels. In the more acid waters Al and Fe are clearly soluble. In neutral water Al is virtually absent, but Fe is variable; it reaches a maximum of 51 ppm in water of pH 6.5. This is slightly above normal maximum solubility for iron at this pH (Hem, 1970), and the iron is probably partly in either colloidal or chelate form. Manganese and boron both appear mobile in all waters. Other trace elements are soluble at the parts per billion level: there are higher values in the more acid water, where Au is present at about 10 ppb; and Pb, Cu, Co, Li, Ni, and Zn, are about 10 times higher. Uranium (<30 ppb) is not detectable.

Source rocks for weathered material

Clays

Hallberg (1984) used the less mobile elements Ti and Zr to classify samples taken from weathering profiles developed *in situ* according to possible rock types. All samples collected for this project have been plotted on a titanium–zirconium diagram (Fig. 23). Samples at Mount Gibson show values which may be interpreted to suggest that about two-thirds of their source rocks were either mafic or ultramafic; a lesser number of samples have a felsic origin; and a few, an intermediate origin. Other "immobile" elements, such as V and Sc, also show values which generally support the type of source rock indicated by the titanium–zirconium diagrams. Further general support for this interpretation is provided by the bedrock samples, which plot in parts of the diagram appropriate to their interpretation.

Figure 24 compares data from Mount Gibson with equivalent data (Watkins and Hickman, 1990) from 800 samples of fresh bedrock collected over the whole Murchison Province. Though in the Murchison Province, the boundaries between mafic, intermediate and felsic rocks may differ slightly from those suggested by Hallberg (1984), most clays at Mount Gibson have been derived from mafic rock, and a lesser amount from felsic rock.

This method of discrimination does not separate mafic from ultramafic rocks, but Hallberg (1984) suggested that Cr has potential for separating ultramafic from mafic rocks, since ultramafic rocks normally have high Cr but low TiO_2 and Zr values.

Many samples within the mafic field of the titanium–zirconium diagram have quite high (>500) ppm Cr. There are a number of samples on lines 3400 S and 4200 S with values in the 1000–2000 ppm range. Only nine samples (from three holes) exceed 2000 ppm Cr. Of these, two samples from hole 313, and one from 907, have low Ti and Zr consistent with an ultramafic origin; the others have TiO_2 >1% and Zr >100 ppm, which alteration from, or contamination by, a high-magnesium basalt. No chromite was observed in bedrock or heavy fractions, and SEM traces suggest that Cr was once in mica or iron oxides. It is probable that most samples with Cr in excess of 500 ppm were originally basalt or high-magnesium basalt, or have had Cr introduced during metamorphism.

Biotite-rich mafic rocks are represented by clays which have a high K_2O content but otherwise normal mafic values.

In general, apart from Ti and Zr, elements such as Si, Al, Cr, Ni, Sc, Th, and V, can be used to distinguish clays after

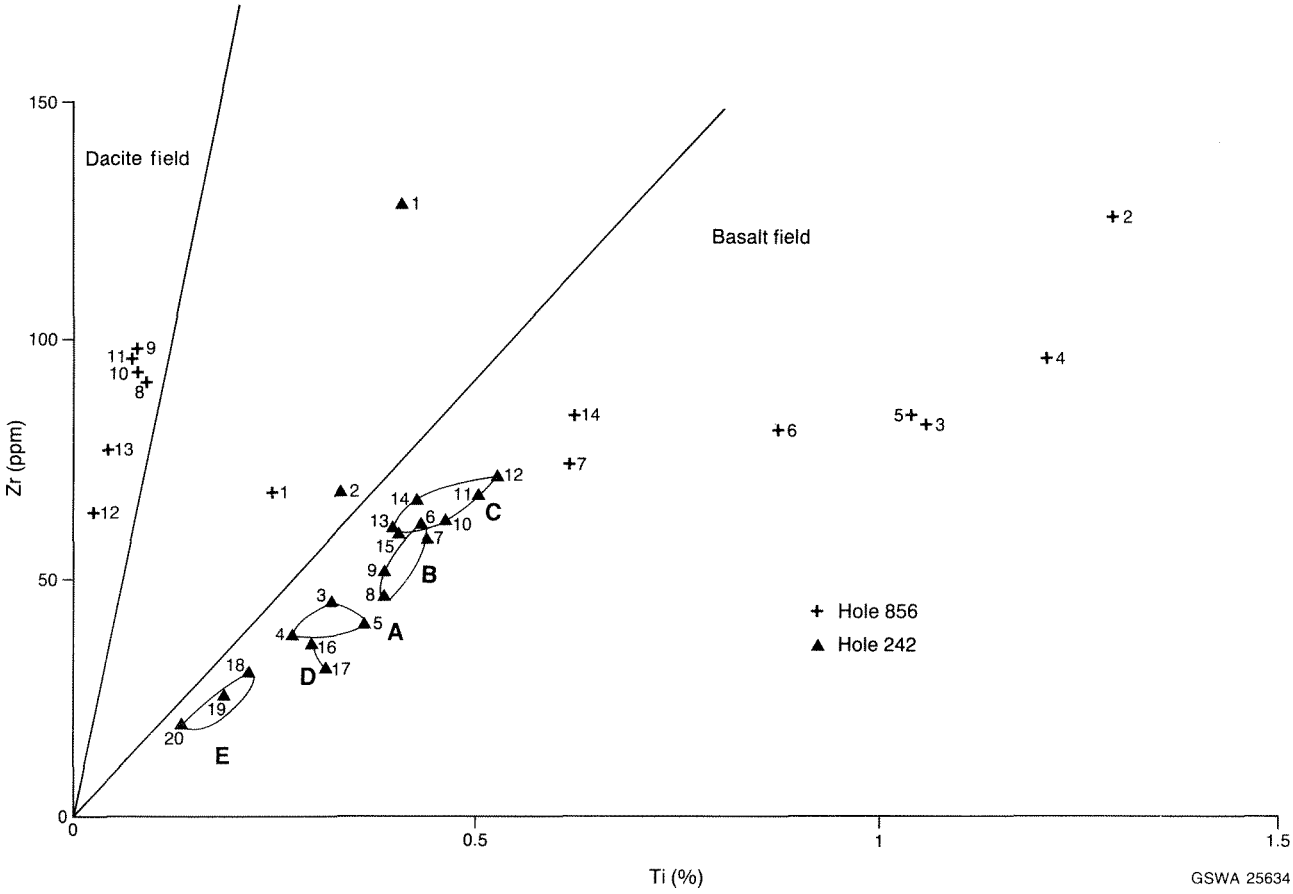

Figure 25. Zirconium–titanium plot for holes 242 and 856. In hole 242 samples 1 and 2 are of ferricrete, whilst A, B, C, D, and E, are clusters formed by successive samples: A, B, C, and D, are interpreted to have a derivation from mafic rock, whilst E may represent a mafic metasediment or tuff. In hole 856 samples 1–3 are ferricrete with calcrete; 4–7 and 14 are interpreted to have a mafic and 8–13 a felsic derivation.

mafic rocks from those after from felsic rocks. A comparison is given in Table 4. Some samples, which have compositional variations outside this framework, may contain thin units of a different rock-type; for example, a generally mafic unit may contain a thin metasediment. The presence of quartz veins in clay derived from mafic rock is generally marked by unusually high SiO_2 (and indications of mineralization); other properties are normal for mafic clays.

No unequivocal chemical distinction between clays derived from felsic volcanic rock and those derived from felsic epiclastic sediments has been found. However, based on comparisons with thin sections of fresh rock, almandine garnets identified in the heavy fractions of the clays have been taken as *prima facie* evidence of derivation from former sediments. Clay derived from former amphibole-rich iron-formation maintains its high content of Fe and low content of trace elements.

Figure 25 is a titanium–zirconium diagram for holes 242 and 856. Hole 242 is believed to intersect mainly mafic rocks, but rock at the bottom of this hole may be a metasediment or tuff; hole 856 passes through a mixture of mafic and felsic rocks. If the two uppermost samples (ferricrete) in this diagram are ignored, samples from 242, though mafic in character, cluster into five groups (labelled, in order downhole, A–E) defined by different absolute amounts of Ti and Zr. Other "residual" components which show similar clusters on bivariant plots, include SiO_2, Al_2O_3, Cr, Ga, and Sc (Fig. 26). The significance of the clusters is unclear, but they may reflect separate units (flows, sills, tuffs, etc).

Ferricrete

Figure 25 shows the uppermost, iron-rich, samples of the two holes plotting as though they were intermediate rocks, in contrast to samples lower in the holes. Similar plots for other holes show the same pattern of difference between near-surface and deeper samples. Since there is no other evidence to suggest derivation from intermediate

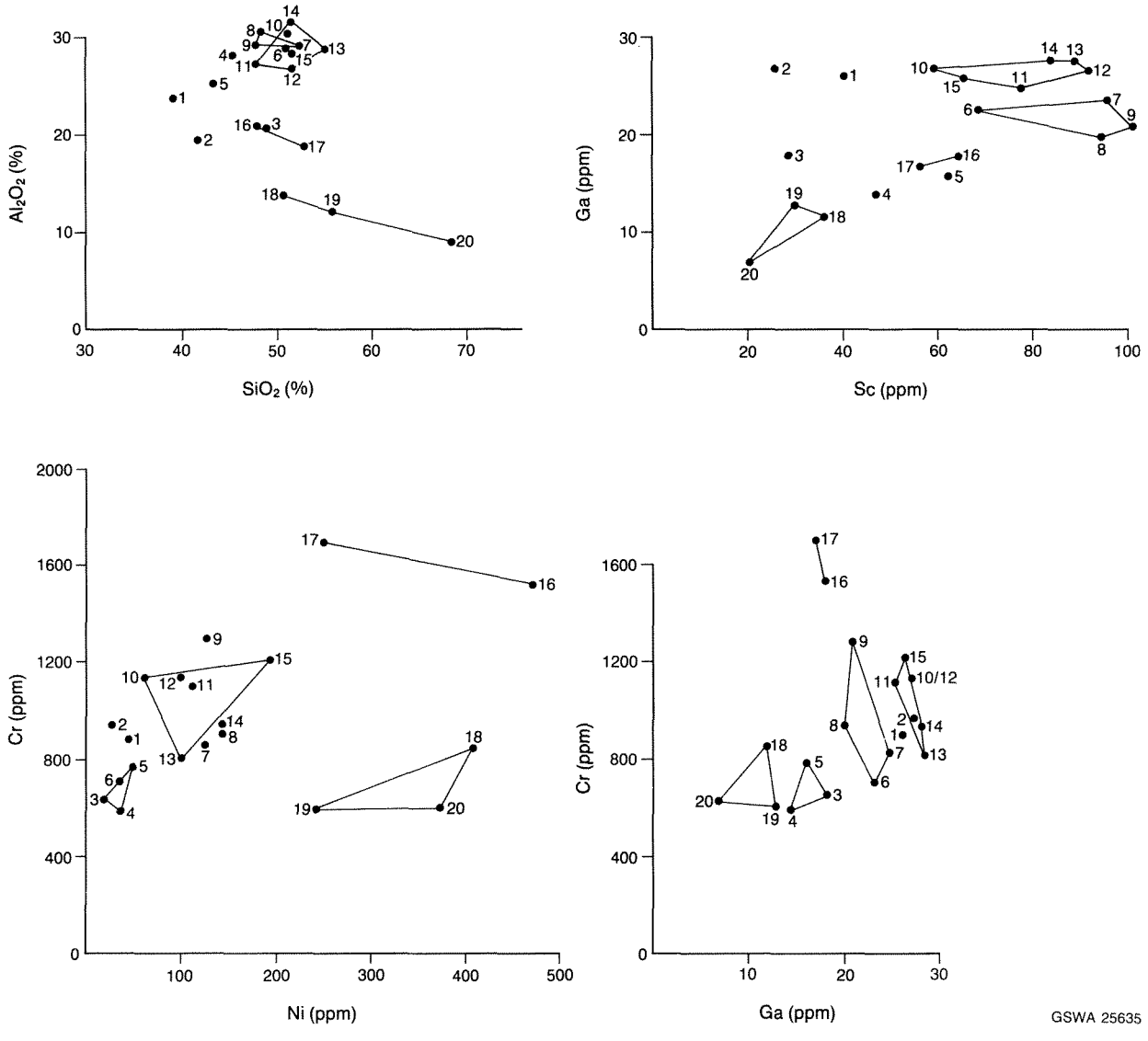

Figure 26. Bivariant (X–Y) plots showing the use of Al_2O_3, SiO_2, Cr, Ga, Ni, and Sc, in identifying possible units within hole 242.

TABLE 4. RANGES OF COMPOSITION FOR TYPICAL CLAYS DERIVED FROM VARIOUS ROCKS

	Mafic rocks	*Felsic rocks*	*Meta-sediments*
	(per cent)		
SiO_2	45 – 55	65 – 75	65 – 75
Al_2O_3	15 – 30	10 – 15	12 – 16
Fe_2O_3(a)	>10	<10	1.5 – 10
TiO_2	0.7 – 2	0.2 – 0.5	(b)<0.3
	(parts per million)		
Cr(c)	>150	<200	<10 – 230
Ni(d)	>50	<70	10 – 60
Sc	20 – 45	<20	<20
Th	<10	10 – 20	<10 – 18
V	200 – 500	<150	10 – 90
Zr	<150	>70 – 200	40 – 180

NOTES: (a) Total iron expressed as Fe2O3. (b) Most 0.2 ppm. (c) Most <100 ppm. (d) Nickel has commonly been depleted by leaching near surface.

rocks, and concentrations of other elements require alternative origins, it appears that titanium–zirconium diagrams are not applicable to ferricretes.

The Ti–Zr composition of the ferricrete may result from a mixture of source materials; or, alternatively, one or other element has been chemically mobile.

Chromium has been mobile in ferricrete. SEM traces across nodules show the late migration of Cr into cracks in the nodules (Figs 27 and 28). Further evidence of possible chemical mobility in ferricrete and, perhaps, the upper part of the clay zone, is found in Ga:Al_2O_3 ratios. In the lower parts of the profiles this ratio is relatively constant. On the crest of the low ridge west of the mineralization, the constancy is maintained through to the surface; but downslope, the ratio becomes increasingly erratic near the surface (Fig. 29), and suggests lateral movement of at least one component. Because the movement of Ga relative to Al_2O_3 is now well established (Burton and Culkin, 1972; Shiller, 1988); and because Ga is in general more soluble than, and moves further than Al: it is probable that Ga is the element that has moved.

Discussion

Origins of the profiles

The relic quartz veins and porphyritic texture identify both parts of the clay zone as residual saprolite. Lack of deflection of the veins where exposed in working faces implies that weathering and leaching of these zones has been essentially isovolumetric. Silica, and other components, have been depleted in the conversion of bedrock to saprolite; but, unlike some other described lateritic profiles (Buol et al., 1973, for example), there has apparently been no further de-silicification upwards. There has been no systematic increase in concentration of residual elements upwards in the clay zones; major changes in composition of the clays reflect changes in the primary rock type.

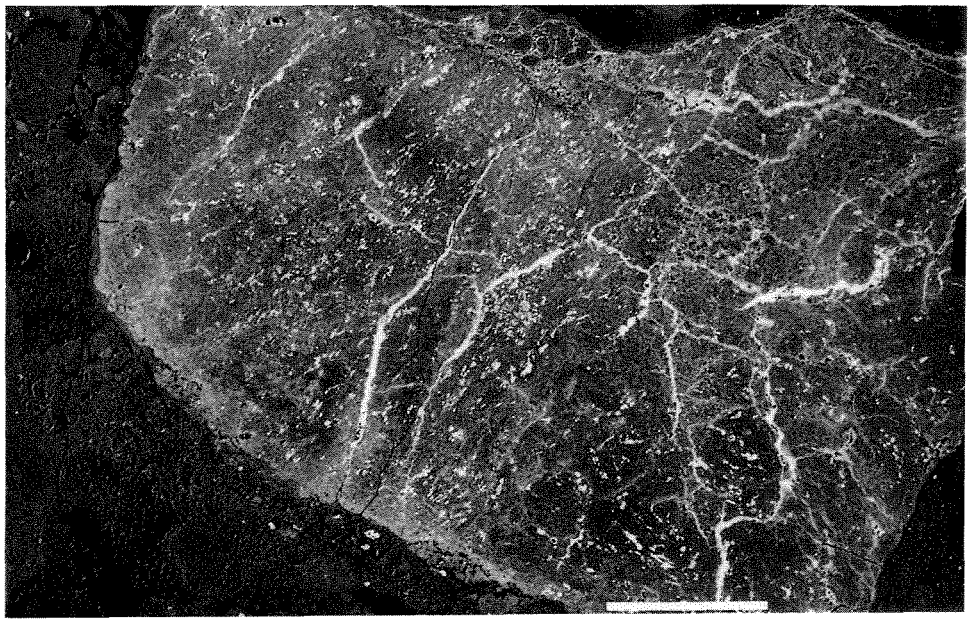

GSWA 25636

Figure 27. Electron micrograph showing nodule of suspected altered volcanic rock. A bulk elemental scan shows major Si > Al > Fe, minor Ti and traces of Cr. Bar length is 1 mm.

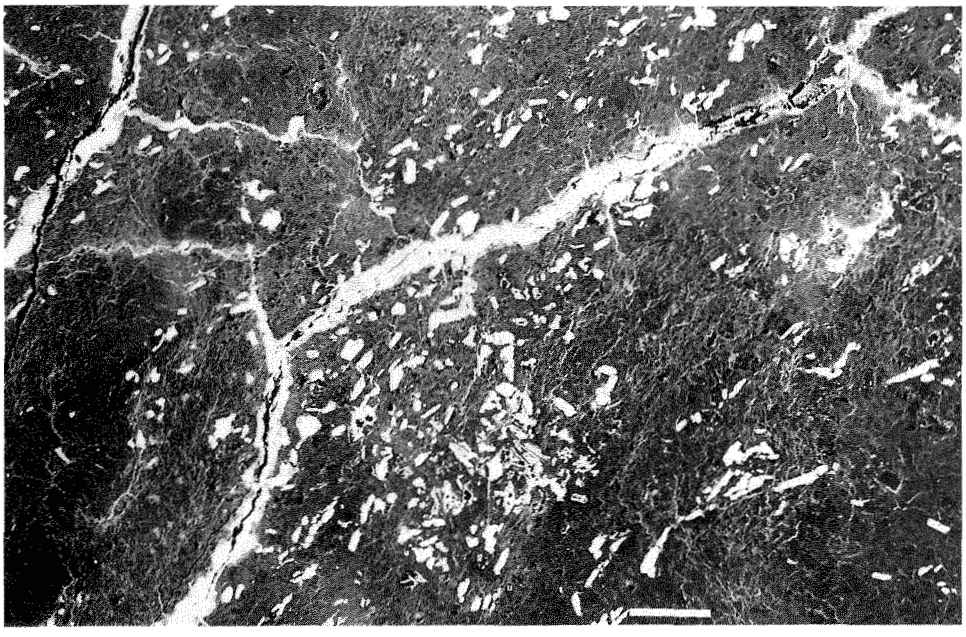

GSWA 25637

Figure 28. Detail of Figure 27, showing the distribution of veins (of iron "oxide" and traces of Al, Si, and Cr) and ilmenite crystals within the nodule. Chromium is restricted to the veins. Bar length is 0.1 mm.

The ferricrete has been more drastically modified. There were substantial volume changes during the formation of the nodules, and the ferricrete is a condensed part of the profile. The distribution of gold in the ferricrete, particularly at Orion, is only slightly greater in areal extent than the limits of known bedrock mineralization, and the nodules are believed to be substantially residual. There has, however, been extensive later chemical modification—including corrosion of the ferruginized nodules, and the precipitation of calcrete and silcrete—as part of the process of "hardpanization". Horizontal sheets of calcrete were probably precipitated from laterally moving ground water, vertical sheets from evaporation of rainwater.

Brimhall et al. (1988) have presented arguments that eolian transport has introduced substantial amounts of clay, rutile, zircon, and other detrital minerals, to the caprock bauxites of the Darling Scarp area southeast of Perth. Their finding of a suite of introduced metals (Fe, Al, Zr, Ti, Cr, and Mo) in bauxitic caprock, may help explain some of the

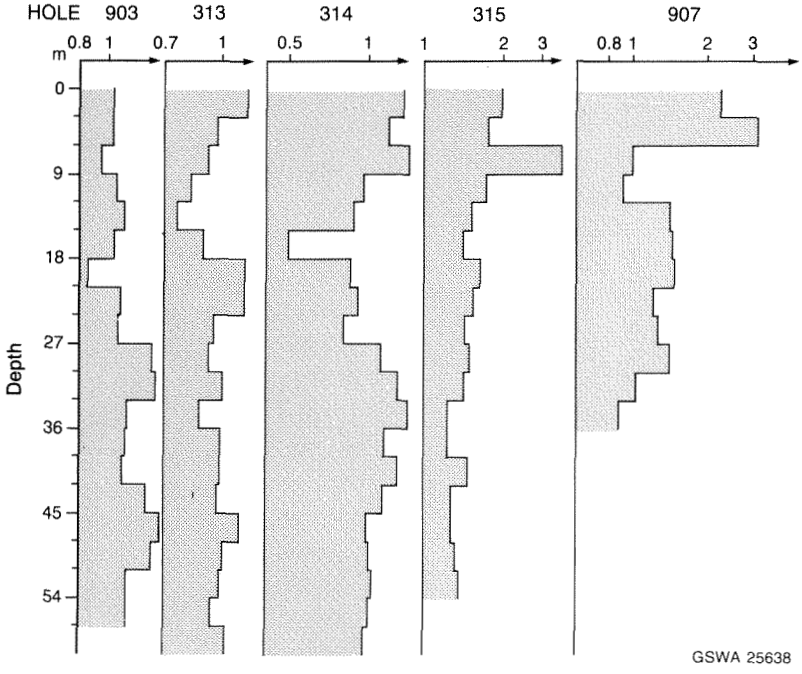

Figure 29. Gallium (ppm)–alumina (%) ratios for holes on line 3400 S, plotted on semi-logarithmic scale, showing increasing near-surface variations in the ratio from west to east (down slope).

unusual mineral properties and chemical patterns of the ferricrete at Mount Gibson. Thus, the trace amounts of feldspar and amphibole identified by X-ray diffraction may have been mechanically introduced by either eolian or colluvial transport: if the former, the source may be at some distance in the direction of the prevailing winds; if the latter, a possible source is rock cropping out on the ridge west of the auriferous laterite. Heavy minerals were not separated from ferricrete: as a result, minerals hosting Ti and Zr were not examined, but it appears that the chemical patterns could represent a mixture of residual enrichment, chemical redistribution, and eolian admixture. Clay of windblown origin, like the residual clays in the upper clay zone, is likely to be kaolinitic and should not materially affect the $Ga:Al_2O_3$ ratio. Near-surface variations in this ratio, therefore, may truly reflect chemical redistribution. Chromium also shows clear evidence for chemical redistribution into cracks, whatever its ultimate origin.

No attempt has been made to determine the full sequence, or timing, of events leading to the formation of the lateritic profiles as they now exist. The original ferruginization probably took place, in response to tropical or subtropical weathering, at a (then) stable water table and was apparently accompanied by severe leaching of underlying material. Almost certainly, the ferruginized layer was once more massive and less nodular than now.

Induration took place in a post-ferruginization weathering stage after the water table had dropped. At some later time, the ferruginized layer was attacked, mainly along desiccation cracks and fractures such as joints and cleavage planes; as a result, a mixture of poorly crystalline iron oxides and/or hydroxides and clay has formed at the edge of the fractures. The minerals are so intimately mixed that the resolution of individual grains is impossible, and the mixture appears homogeneous under the SEM: it seems that the iron and clay may have been co-precipitated from a "gel" phase.

The appearance of gold within this material may be due to some chemical redistribution, or to inclusion of gold deposited in the ferruginized layer at its formation.

The multiple layering on the surface of nodules (Fig. 3) may indicate a number of periods of deposition, and the partial absence of some layers periodic dissolution (possibly as a result of pressure solution). The iron oxide and clay mixture, along with carbonates and silica, currently cements the nodules, but is itself under chemical attack. Carbonated rainwater and tree roots which, according to Drake (1964), have highly acid surfaces, promote this attack (Fig. 10). Should the ferricrete become exposed at the surface, the potential for incorporation of eolian grains, and for the loosened nodules to be transported mechanically, is increased.

Origin of gold in weathered profile

Gold is present in bedrock, especially at Mount Gibson Well and Midway (lines 1200 S and 3400 S, Fig. 19). It is restricted to those areas with sulphides or quartz veins. Primary gold may contain significant silver, though no mineralogical analysis has been carried out; Ag is present with gold at the base of hole 857 at Mount Gibson Well (Ag to 129 ppm and Au to 6.7 ppm).

Gold in saprolite is also localized and essentially residual; there has been no mechanical redistribution, and the extent of chemical redistribution appears small.

Gold in nodules also appears primary. However, the gold is silver-poor and has no significant correlations (at the 95% probability level) with other trace elements of economic interest; bullion derived from it contains 99.7% Au, 0.2% Ag, and remnant base metals (Anon, 1988). Though many nodules may be physically *in situ*, the gold may have been leached of silver relative to its primary composition (Mann, 1984).

Some nodules, where loosened from the ferricrete, may have been mechanically transported short distances, giving rise to further local redistribution of gold.

The remainder of the gold, in coatings, vugs, and cracks, has been reprecipitated from groundwater. Principles for moving gold (with iron) by ferrolysis and reprecipitation at a water table (Mann, 1983) are consistent with observed features at Mount Gibson. The detection of dissolved Au in groundwater (Table 3) implies that the processes of dissolution and reprecipitation continue to operate.

In summary, gold in the saprolite has been subject to local leaching, and chemical and redistribution. Gold in ferricrete may be dispersed somewhat more widely, because of additional mechanical redistribution, than that in the saprolite below.

Mobility of other elements

Elements such as Ca, Mg, and Sr, have been almost completely leached from the weathered profile, but small amounts of these elements have been reprecipitated as calcrete. The depletion of Na has probably been underestimated because leaching would be partly offset by addition of salt from rainwater and subsequent concentration by evaporation. Elements, such as Co, Mn, and rare earths, have been leached from the upper parts of the profile, but some proportion has been reprecipitated near the oxidation –reduction interface towards the base of the saprolite. Base metals have been variably, but generally extensively, leached. The low pH and high metal content of some ground waters suggest that leaching is continuing at the present time. It is probable that none of the "residual" elements is completely immobile: each appears locally re-distributed rather than removed from the area; the concentration of some elements may even have increased in the ferricrete by eolian accretion.

The full extent of elemental movement during weathering is difficult to determine. Measurements on core give the bulk density of fresh rock as 2.8–3.0 t/m^3 in contrast to the bulk density—as measured at the mine—for saprolitic clay (2.05 t/m^3) and ferricrete (2.35–2.6 t/m^3). These last results are very low in view of the known mineralogy, and samples from which these figures were obtained must have contained an unusually high proportion of voids.

Assuming that the estimates of bulk density are correct and that initial weathering can be regarded as isovolumetric, immobile elements in the saprolite should have values approximately 1.4 times their equivalent bedrock values. However, since each profile normally intersects several units derived from different rock-types, comparison of a specific unit as it changes from fresh rock to saprolitic clay is not possible in some holes, and is restricted to a few metres in others. If conclusions drawn from titanium–zirconium diagrams are correct, only two of the twenty-one holes studied (714 and 715) intersect a single rock type through the whole thickness of the saprolite. The analytical data suggest that Al, Ti, Cr, Ga, Sc, V, and Zr, though locally redistributed, are still among the least mobile elements. Where such redistribution is not significant, the saprolite:rock ratios for these elements are generally between 1.1 and 1.2. These lower figures are more consistent with an expected bulk density close to 2.5. Silica commonly retains a saprolite:rock ratio of about 1, as does K_2O where mica is retained; evidently a loss of about 20–30% of these oxides has occurred. Little Fe has been lost from the lower clay zone (where the saprolite:rock ratio is about 1) but more has been lost from the upper subzone.

As the ferricrete contains a significant proportion of exotic material, the gain or loss of elements at the clay–ferricrete interface cannot be estimated.

Comparison with the Boddington gold deposit

The Mount Gibson lateritic gold deposit can be compared with that at Boddington, 400 km to the south, using Davy and El-Ansary (1986) and Monti (1987) as the main sources of data on the latter deposit (Table 5).

Some differences in the chemical compositions of the two profiles are related to the nature of the source rock (for example, a K-rich source and K-alteration may be more prominent at Mount Gibson). However, many differences in the nature of the profiles probably reflect variations in the climatic and geomorphological regimes in the two areas. Thus the ferruginous nature of the laterite at Mount Gibson compared to the bauxitic laterite at Boddington may be a function of different drainage characteristics at the two deposits; bauxite at Boddington occurs in an area of higher relief and better drainage than Mount Gibson. Waterlogging is believed to promote lateritization rather than bauxitization (Mann, 1983).

The differences in the position of the gold within the indurated layer may be a function of the thickness of the weathered profile and the mechanisms by which gold has been mobilized and reprecipitated. Ferrolysis has already

TABLE 5. COMPARISON OF MOUNT GIBSON AND BODDINGTON DEPOSITS

Mount Gibson	*Common*	*Boddington*
	Gold is present in laterite	
	The weathering profiles are superficially similar	
	Most gold is very fine grained, and there are few nuggets	
	Alkaline earth elements are almost totally leached	
	Cobalt and manganese tend to concentrate near the base of the clay	
	Much primary gold occurs in quartz veins.	
Laterite is ferruginous		Laterite is bauxitic
Calcrete is present		Calcrete is absent
Gold present in loose nodules		No gold in nodules
Gold concentrated at top of ferricrete		Gold concentrated at base of hardcap and top of underlying zone
Copper in surface laterite non-diagnostic of extent of gold mineralization		Copper at 50 mm in uppermost metre fo laterite defines extent of gold mineralization
Kaolite abundant in ferricrete		Minor trace kaolinite in hardcap
No trend to lateritic enrichment in saprolite		Lateritic enrichment evident in saprolite
Gold in saprolite in primary position		Gold in saprolite partly remobilized
Leaching of Na from saprolite "incomplete"		Leaching of Na from saprolite severe
Associated metals in laterite includes As, Cr, Cu, Pb, and W		Associated metals in laterite include Cu, Mo, and W
Primary mineralization possibly hydrothermal and related to shear zones		Primary mineralization essentially porphyry copper type (Symons et al.,1988)

been mentioned as one possible mechanism for the redistribution of gold. The groundwater at Mount Gibson (Table 3) is substantially more saline than that at Boddington (Monti, 1987), facilitating the formation of $AuCl_4^-$ complexes and thus promoting migration. Gold may also be mobilized by plants (Butt, 1988). Acid solutions around roots dissolve gold, draw it up into the plant system and subsequently release it to the ground via leaves, dead wood, etc. Local redistribution may then transfer gold some way down the profile; the final position depending on the depth to which either mechanical penetration occurs, or solutions are carried. Higher rainfall at Boddington than at Mount Gibson may have washed organic gold compounds further into the profile before decomposition occurred.

Primary gold at Mount Gibson, like that enclosed within the ferricrete nodules, is presumed to be very fine grained; it may be partly protected by quartz. However, it is surprising that secondary gold forms no significant nuggets for there are abundant nuclei onto which mobilized gold might have precipitated. Possibly, small grains of gold, co-precipitated with iron, have been protected from further solution and reprecipitation by a coating of iron oxide.

Implications for exploration

The Mount Gibson and the Boddington areas together highlight some of the problems of gold exploration in lateritic terrains. The best indicator of near-surface mineralization is gold itself. Although gold may be present in a lateritic profile, it is not always located in the same part of the profile. This means that before a general sampling procedure is established, an orientation investigation is necessary.

Elements in the ferricrete, such as Cr, Nb, Th, Ti, V, and Zr, give some indication of bedrock, but not as much as if the weathered profile were wholly residual. Elements, such as As, Cu, Pb, W, and Zn, which can be anomalous in surface ferricrete, seem merely to indicate the general area of (or even, potential for) mineralization rather than the position of specific veins or mineralized horizons. Where mineralization occurs on the crest of a ridge, as at Mount Gibson Well, the weathered profile contains less exotic material and the surface gossans better reflect the subsurface mineralization. Arsenic, which elsewhere is a useful indicator for Au (Mazzucchelli and James, 1966; Boyle and Jonasson, 1973; Boyle, 1974), is more prominent at Mount Gibson Well than at Orion, so this element may be better used as an indicator of sulphides than of gold.

Conclusions

The bedrock at Mount Gibson is a suite of mafic volcanic and hypabyssal rocks, felsic volcanic and felsic metasedimentary rocks. Some volcanic rocks are tuffaceaous. Primary mineralization occurs as a mixture of mineralized quartz veins, mineralized shear zones and stratabound sulphide. Anomalous elements include Ag, As, Au, Bi, Cu, Pb, Sb, W, and Zn.

The ore-bearing complex has been deeply weathered; this has resulted in extensive leaching and the formation of a ferruginized layer, which was later converted into hardened ferricrete. Clay between fresh rock and the base of the ferricrete is saprolitic, but shows no systematic enrichment of residual components. Though many mobile elements have been leached away, the composition of the saprolite retains key characteristics of the unweathered parent rock, and approximately two-thirds of the rocks appear to have a mafic or high-magnesium origin. Components leached from the bedrock–saprolite interface include MgO, CaO, Na_2O, and Sr. To some extent CaO and MgO have been reintroduced near surface, whilst loss of Na_2O may be partly concealed by redeposition from groundwater. Elements which tend to be leached from the top of the saprolite, but which are moderately concentrated in the lower part of the saprolite (in the less oxidized clay or at the boundary between the subzones), include Ce, Co, Cu, La, Mn, Ni, Y, and Zn. Iron and potassium oxides are variably retained; K_2O particularly where it occurs in micas. Alumina and TiO_2 have been generally immobile in saprolite but approximately 30% of SiO_2 has been lost.

In the ferricrete, residual ferruginized nodules of primary rock have been cemented by various precipitates from groundwater. Since the formation of the ferricrete, part of its cement has been replaced by silica or carbonate, particularly the latter; this has resulted in the beginning of a replacive calcrete.

Though much of the ferricrete is now covered by thin, (partly transported) soil, it may once have been exposed, and may have incorporated colluvium or windblown detritus. The present ferricrete may, therefore, have a very mixed origin.

Gold in the ferricrete is a mixture of primary—but leached—gold, and gold which has been dissolved and reprecipitated. It is generally very fine grained and has probably been protected from further dissolution and reprecipitation—and the formation of nuggets—by co-deposition with, and a coating of, iron oxides or hydroxides.

At Mount Gibson Well the ferruginized layer is partly gossanous in origin.

Intense leaching means that, over most of the area, there are no specific indicator elements for Au or base metals at the surface. However, arsenic may be a useful general indicator of the presence of sulphides. In the few parts of the area with clearly residual soils and gossans, mineralization, including gold, is indicated by anomalous concentrations of As, Au, Cu, Pb, Sb, and Zn. In the more normal ferricrete these elements, together with W, may be weakly anomalous, but gold is its own best indicator element.

Acknowledgements

It was through the agency and enthusiasm of Mohamed El-Ansary, then exploration manager for Reynolds Australia Mines Pty Ltd, that this project was initiated. Dr R. D. Gee, the present exploration manager, has continued to

provide support and encouragement. Reynolds Australia Mines Pty Ltd provided the drill cuttings from which most data of this paper have been generated. Ms Penny Line photographed Figures 13–15 on behalf of the Mount Gibson Gold Project Joint Venture Partners.

References

ANON. 1988, Technical information on the Mt. Gibson gold project: Notes for the Geological Survey of Western Australia Murchison field excursion, April 1988, Mt Gibson Gold Project, 13 p.

BOYLE, R. W., 1974, Elemental associations in mineral deposits and indicator elements of interest in geochemical prospecting: Canada, Geological Survey, Paper 74–45.

BOYLE, R. W. and JONASSON, I. R., 1973, The geochemistry of arsenic and its use as an indicator element in geochemical prospecting: Journal of Geochemical Exploration, v. 2, p. 251–296.

BRIMHALL, G. H., LEWIS, C. J., AGUE J. J., DIETRICH, W. E., HAMPEL, J., TEAGUE, T., and RIX, P., 1988, Metal enrichment in bauxites by deposition of chemically mature aeolian dust: Nature, v. 333, p. 819–824.

BUOL, S. W., HOLE, F. D., and McCRACKEN, R. J., 1973, Soil genesis and identification: Ames, Iowa State University Press, 360 p.

BURTON, J. D. and CULKIN, F., 1972, Gallium, *in* Handbook of geochemistry, *edited by* K. H. Wedepohl: Springer-Verlag, Heidelberg.

BUTT, C. R. M., 1988, Genesis of lateritic and supergene gold deposits in the Yilgarn Block, Western Australia, *in* Bicentennial Gold 88: Geological Society of Australia, Abstracts no 22, p. 359–364.

DAVY, R., 1979, A study of laterite profiles in relation to bedrock in the Darling Range near Perth, W. A.: Western Australia, Geological Survey, Report 8, 87 p.

DAVY, R., CLARKE R. M., and SALE M., 1989, Gold-bearing lateritic profiles at Mount Gibson, Murchison Province—Analytical and mineralogical data: Western Australia, Geological Survey, Record 1989/18.

DAVY, R., and EL-ANSARY M., 1986, Geochemical patterns in the laterite profile at the Boddington gold deposit, Western Australia: Journal of Geochemical Exploration, v. 26, p. 119–144.

DRAKE, M., 1964, Soil chemistry and plant nutrition, *in* Chemistry of the soil, *edited by* F. E. Bear: New York, Van Nostrand Reinhold, p. 395–444.

EL-ANSARY, M., and SALE, M., 1985, The Mt Gibson gold project: Reynolds Australia Mines Pty Ltd, (unpublished).

HALLBERG, J. A., 1984, A geochemical aid to igneous rock type identification in deeply weathered terrain: Journal of Geochemical Exploration, v. 20, p. 1–8.

HEM, J. D., 1970, Study and interpretation of the chemical characteristics of natural water: United States, Geological Survey, Water-supply paper 1473.

KNEEBONE, B. K., 1980, Orion/Mount Gibson Well prospect—Report to the Mines Department, W. A., of results of exploration of mineral claims for the period May to August 1977: Australian Anglo-American Prospecting Pty Ltd (unpublished).

MANN, A. W., 1983, Hydrochemistry and weathering on the Yilgarn Block, Western Australia—Ferrolysis and heavy metals in continental brines: Geochimica and Cosmochimica Acta, v. 47, p. 181–190.

MANN, A. W., 1984, Mobility of gold and silver in lateritic weathering profiles—Some observations from Western Australia: Economic Geology, v. 79, p. 38 - 49.

MAZZUCHELLI, R. M. and JAMES C., 1966, Arsenic as a guide to gold mineralization in laterite-covered areas of Western Australia: Institution of Mining and Metallurgy, London, Transactions, v. 75, p. B286–294.

MONTI, R., 1987, The Boddington lateritic gold deposit, Western Australia—A product of supergene enrichment processes: Perth, University of Western Australia, Geology Department and University Extension, Publication 11, p. 355–368.

PARKER, M., 1987, Geology of high-grade ore zones within laterite, Mt. Gibson gold project: Mt. Gibson Gold Project (unpublished).

SHILLER, A. M., 1988, Enrichment of dissolved gallium relative to aluminium in natural waters: Geochimica et Cosmochimica Acta, v. 52, p. 1879–1882.

SYMONS, P. M., ANDERSON, G., BEARD, T. J., HAMILTON, L. M., REYNOLDS, G. D., ROBINSON, J. M., and STALEY, R. W., 1988, The Boddington gold deposit, *in* Bicentennial Gold 88: Geological Society of Australia, Abstracts 22, p. 56 - 61.

WATKINS, K. P. and HICKMAN, A. H., 1990, Geological evolution and mineralization of the Murchison Province, Western Australia: Western Australia, Geological Survey, Bulletin 137.

Geology, mineralization, and origin of the Mount Clement gold and lead prospects Ashburton Basin

by

R. Davy, R. M. Clarke[1], A. M. Thorne, and D. B. Seymour[2]

ABSTRACT

The informally named Mount Clement "Main" and "Eastern" prospects occur within low-grade metasedimentary rocks of the 2.0 Ga Ashburton Basin. Mineralization of the Main prospect is hosted by a conformable lens of chert, ferruginous chert, and dolomitic siltstone, within deep-water marine sandstone, siltstone, and mudstone, of the Ashburton Formation. Fine-grained gold, silver, and subordinate arsenic, bismuth, copper, lead, and antimony, occur in stratigraphically controlled gossans, breccias, talc-rock, and ferruginized siliciclastic rocks in the lower third of the prospect. Mineral assemblages include polymetallic arsenates, silver halides, gold, and primary sulphides (arsenopyrite, pyrite, tetrahedrite–tennantite). Primary gold is silver-rich (18% Ag), but secondary gold is silver-poor. Field relationships, coupled with host-rock lithology and geochemistry, suggest that the mineralization of the Main prospect succession is a submarine hot-spring deposit of mixed syngenetic and epigenetic mineralization.

At the Eastern prospect, a sulphide-bearing assemblage occupies a fracture which has resulted from dextral wrenching of the Ashburton Formation. It is characterized by anomalous levels of silver, arsenic, gold, copper, molybdenum, antimony, and tin, which may have been derived, in part, by the leaching of wall rock.

Similar assemblages of trace elements at the two prospects suggest that both early and late mineralization tapped a common source. Metal-bearing fluids were probably released during burial metamorphism of the supracrustal sequence, and subsequently transported along major fractures.

Keywords: epithermal deposits, hot springs, arsenic minerals, gold, trace elements, geochemistry, Ashburton Basin.

Introduction

The informally named Mount Clement "Main" prospect is a small gold–silver–copper(–arsenic) deposit in the Precambrian Ashburton Basin, southwestern Pilbara (Figs 1, 2). It is located 20 km southwest of Wyloo Homestead and 8.5 km southeast of Mount Clement (22° 15' S, 116° 07' E). The Main prospect has been the subject of major investigations by mining companies since its discovery by Ronald William Prothero, a kangaroo shooter, in 1973 (B.H.P 1975; Doust, 1984). On the basis of its geological setting, distinctive mineralogy, and geochemistry, several workers have interpreted the mineralization of the Main prospect as an ancient subaqueous hot-spring deposit (Newmont, 1981, 1982; Doust, 1984).

This paper describes and interprets the geology and geochemistry of the Main prospect, and summarizes the geology of a second deposit, the Eastern prospect, which is 2 km southeast of the main orebody. The relevance of the Mount Clement-style mineralization to exploration for precious metals elsewhere in the Ashburton Basin is also discussed.

Information presented in this work was obtained by geological mapping at 1:40 000 scale and detailed sampling of the prospect area. Four hundred samples were collected from surface exposures and excavations and from more than 50 drill holes (Figs 2, 3, 4). Depths of samples in drill holes are given in Davy et al. (1989).

One hundred thin sections and 35 polished mounts were examined petrographically. Uncommon minerals were identified by X-ray diffraction analysis; supplemental analyses by energy-dispersive X-ray analysis were made using a scanning electron microscope at the Western Australian Institute of Technology (now Curtin University). Deuterium isotope determinations on talc were made at the University of Tasmania. Cobalt, copper, lead, manganese, nickel, and zinc, were determined by atomic-absorption spectrophotometry at the Geological Survey of Western Australia. All other determinations were carried out by the Chemistry Centre (W.A.). X-ray fluorescence analysis was used on samples of pressed powder for all elements except gold, and some silver (determined by fire assay), and lithium, molybdenum, and the remaining silver (determined by atomic absorption). Details of analytical methods are given in Davy et al. (1989).

The geometric means of analyses for selected trace elements in the principal rock types at Mount Clement are given in Table 1. The geometric mean was chosen in preference to the arithmetic mean because a small number of samples have disproportionately high values. A full listing of the results of geochemical analyses is given in Davy et al. (1989).

[1]Chemistry Centre (W.A.)
[2]Geological Survey of Tasmania

TABLE 1. PARTIAL ANALYSES OF ROCKS, MOUNT CLEMENT AREA

(Geometric means for selected elements, in parts per million unless otherwise noted)

	Hydrothermal sequence											*Eastern prospect*		
	A	*B*	*C*	*D*	*E*	*F*	*G*	*H*	*I*	*J*	*K*	*L*	*M*	*N*
Sample size	50	2	23	18	30	23	15	9	71	32	27	8	6	8
Ag	<1	135	(a)41	(a)14	(a,b)1	1.7	<1	<1	(b)1	<1	<1	14	<1	1
As	42	6.9%	2.3%	(a)2398	(a)3244	(a)6325	(a)1103	13	2184	572	345	3.6%	1444	8.5%
Au	<0.1	0.1	(a)4.4	(a)0.26	(a)0.26	(b)0.15	(b)0.13	<0.1	(b)0.11	<0.1	<0.1	0.20	<0.1	0.13
Ba	377	<25	42	(a)67	75	54	87	<25	115	286	294	68	429	149
Bi	(c)<15	275	70	(a,c)<20	(d)	(e)	(c)<20	<15	(c)<10	(c)<20	(c)<20	(c)<10	(c)<20	(c)<14
Ce	74	22	(b)9	15	(a)29	13	32	6	(a)33	60	59	26	63	21
Co	(c)8	....	(c)7	(c)14	(c)16	(c)9	(c)<5	....	(c)15	(c)13	(c)12	(c)<5	(c)10	(c)<5
Cr	(c)87	<10	(c)<10	(c)18	(c)51	(c)<10	(c)39	<10	(c)20	(c)40	(c)23	(c)28	(c)97	(c)25
Cu	57	1.1%	1660	(a)528	104	158	113	6	(a)118	(a)55	44	182	78	90
Ga	15	2	(c)<5	(c)3	(c)<5	(c)<2	(c)<5	<2	(c)<5	(c)12	6	(c)11	(c)16	(c)10
Hg	(c)0.08	1.9	(c)2.2	....	(c)0.3	(c)0.04	....	....	(c)0.06	....	....	(c)0.08	....	....
La	40	10	6	15	18	9	(a)16	(b)5	20	30	26	<20	41	<20
Li	....	....	....	(c)5	....	....	(c)9	....	(c)9	(c)25	<5	....	....	....
Mn	643	215	(a)95	(a)100	(a)178	250	101	1402	(a)221	(a)450	(a)489	34	340	37
Mo	(c)<5	<5	<5	<5	(a)<5	<5	(c)<5	<5	(c)<5	(c)<5	(c)10	(c)6	(c)<5	(c)<5
Nb	12	<5	<5	<5	<5	<5	<5	<5	<5	8	6	5	13	<5
Ni	33	17	23	31	14	18	17	7	21	31	25	11	33	6
Pb	27	72	43	51	69	101	(a)77	12	(a)130	50	(a)32	1.7%	99	266
Rb	113	7	<5	(a)<5	<5	(a)<5	<5	<5	<5	37	40	19	151	13
Sb	(a,b)10	1200	426	(a)131	(a)39	104	(a)91	<10	(a)96	21	9	9360	46	727
Sc	(c)11	<5	(c)<5	(c)<5	(c)<5	(c)<5	(c)<5	<5	(c)6	(c)13	(c)<10	(c)<5	(c)<15	(c)<5
Sn	(a)<10	<10	(a,b)7	(a)<10	(a)<10	<10	<10	<10	(b)5	(a)<10	<10	45	15	9
Sr	27	10	19	20	14	19	14	25	26	29	25	8	26	7
Th	17	87	(a)32	(a,b)11	10	(a,b)14	12	<5	11	14	11	17	19	13
U	1	1	(a)2	(a,b)2	(a)2	(a)2	1	1	3	1	(b)1	<1	(b)2	<1
V	70	12	9	29	21	11	45	9	32	58	34	32	97	30
W	....	....	(a,c)<10	(c)14	(c)<10	(c)<10	(c)<19	....	(c)17	(c)<10	....	(c)<10	(c)<10	(c)80
Y	25	<5	10	20	16	14	20	7	24	28	23	43	31	23
Zn	65	150	34	107	41	75	46	16	102	69	59	16	60	14
Zr	159	<10	<10	(a,b)17	15	<10	21	(c)10	23	95	74	27	181	44

KEY: A = Barren siltstone–mudstone. B = Sulphide. C = Gossan. D = Talc. E = Ironstone. F = Breccia. G = Quartz-hematite rock. H = Dolomite. I = Ferruginous silicified clastics of LMZ. J = Siltstone and mudstone of LMZ. K = Conglomerate, siltstone, and mudstone of UBZ. L = Eastern prospect. M = Weakly mineralized clastic sediments near Eastern prospect. N = Quartz-scorodite veins.

NOTES: (a) Rare high values. (b) Many samples at less than detection levels. (c) Sample size less than stated—for details see Davy et. al. (1989) (d) Surface sample size 12—for <20 ppm; drill sample size 5—for 144 ppm. (e) Surface sample size 5—for 20 ppm; drill sample size 8—for 47 ppm.

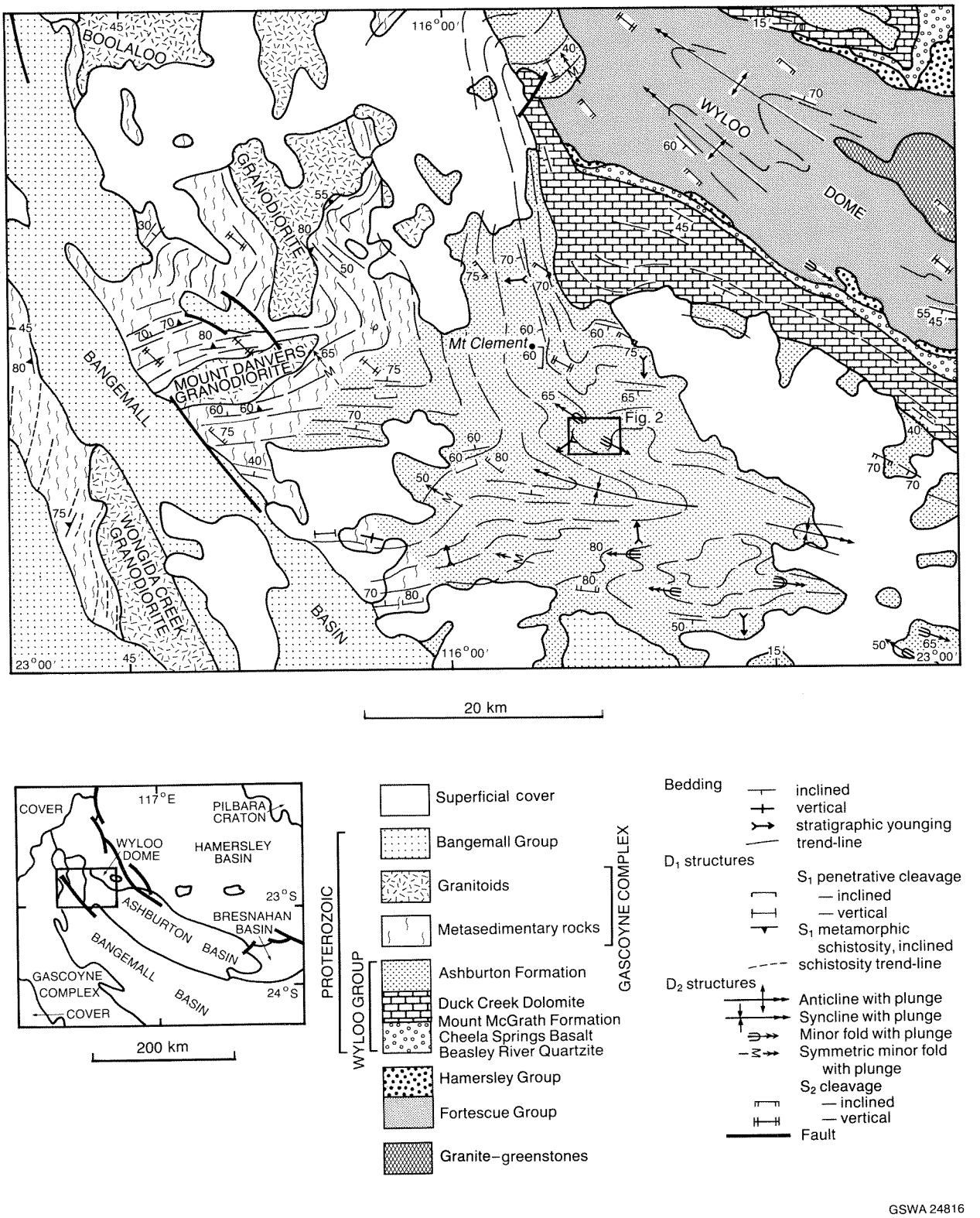

Figure 1. Regional geological setting of the western Ashburton Basin showing the location of the Mount Clement area.

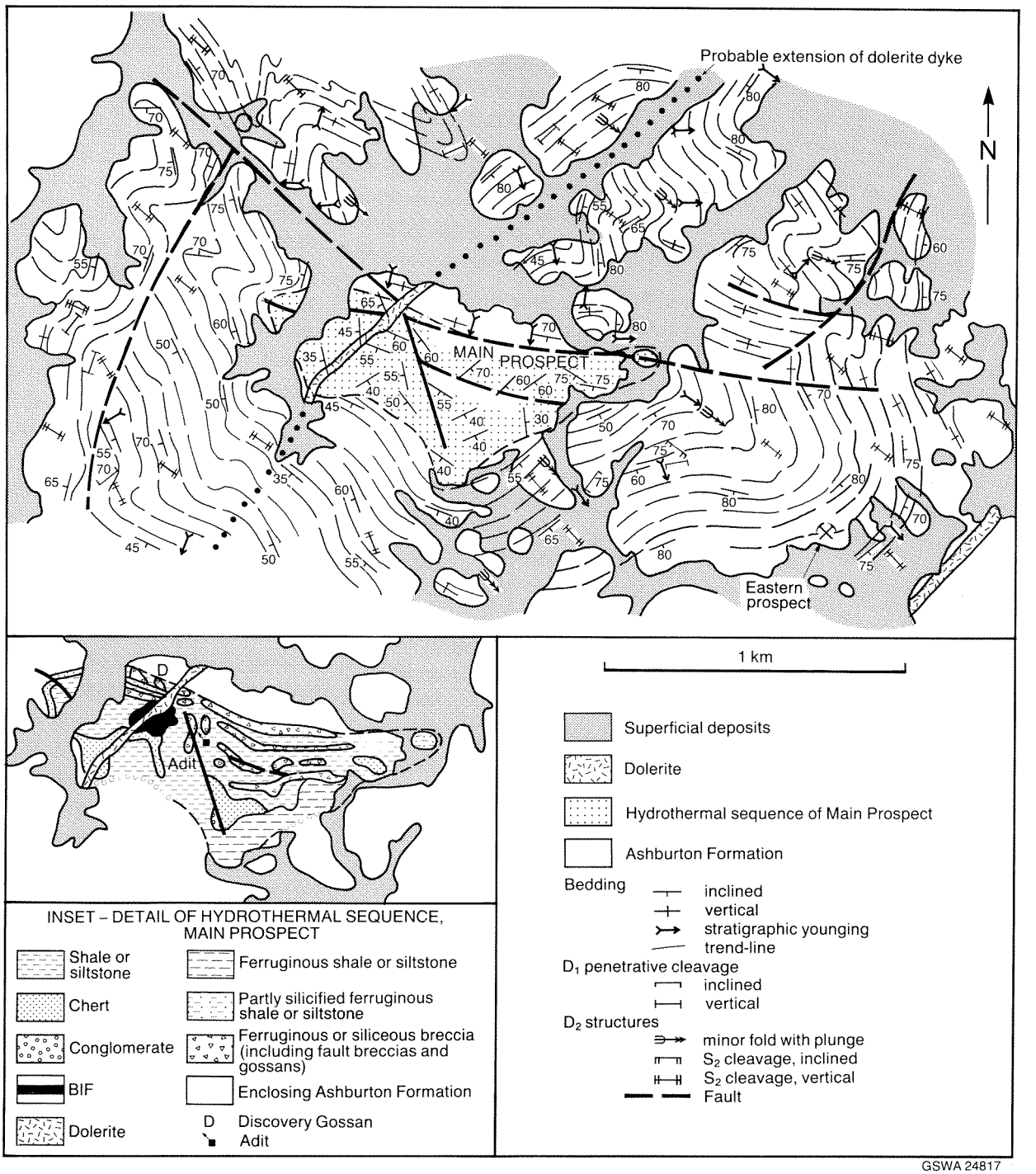

Figure 2. Local geological setting of the Mount Clement Main and Eastern prospects.

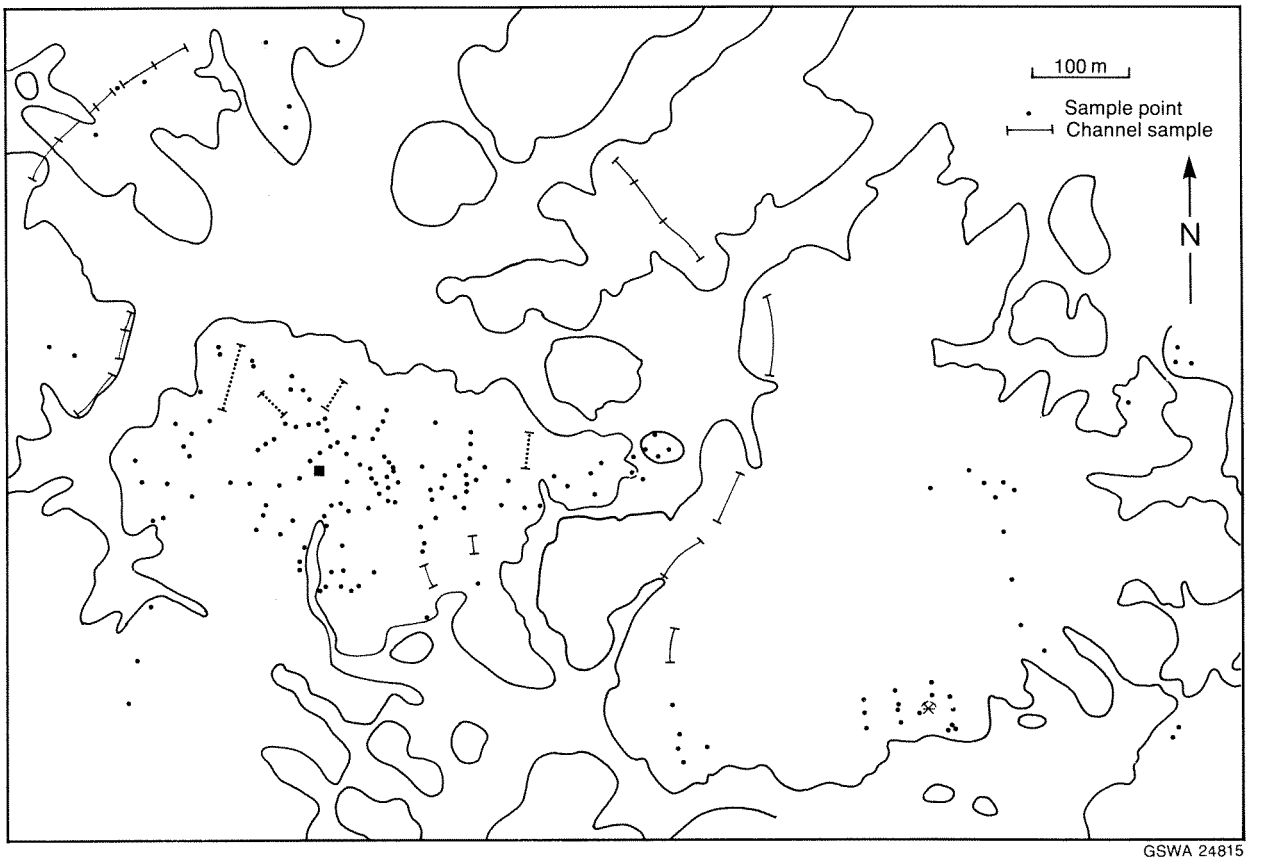

Figure 3. Sample localities.

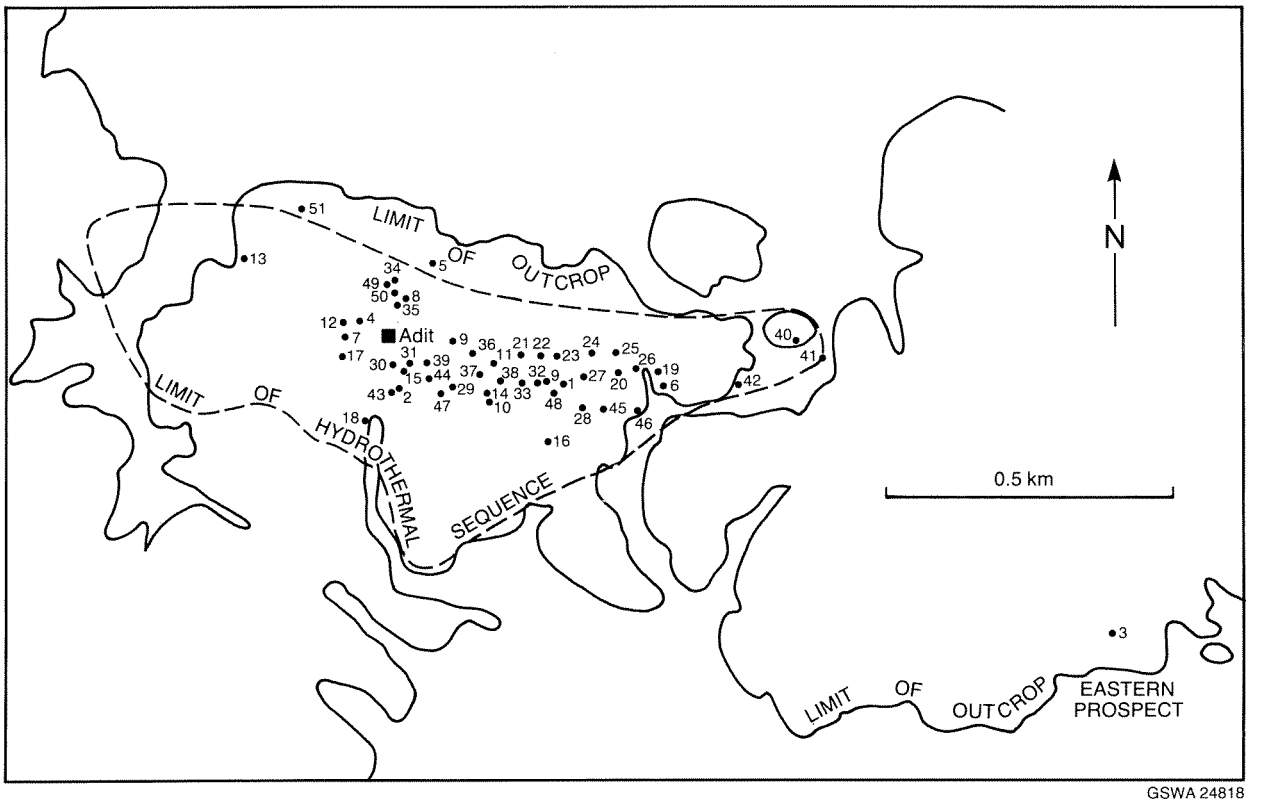

Figure 4. Drill locations at the Main prospect. The position of hole 3 at the Eastern prospect is shown on Figure 3.

Geological setting

The Mount Clement prospects are in the Ashburton Basin, an arcuate belt of Proterozoic metasedimentary and metavolcanic rocks that flanks the southern and western margins of the Hamersley Basin (Fig. 1). The Wyloo Group (2.0 Ga) is the principal stratigraphic unit of the Ashburton Basin (Thorne and Seymour, 1991). It unconformably overlies the Mount Bruce Supergroup of the Hamersley Basin (Trendall, 1979), and comprises a lower succession of marginal-marine to offshore-shelf rocks (Beasley River Quartzite to June Hill Volcanics), and an upper assemblage of deep-marine rocks (Ashburton Formation) (Fig. 1). The Wyloo Group is unconformably overlain by the Capricorn Formation and the Mount Minnie, Bresnahan, and Bangemall Groups (Thorne and Seymour,1991).

Both the Main and the Eastern prospects are hosted by mudstone, siltstone, and subordinate thin- to medium-bedded, partly conglomeratic, sandstone of the Ashburton Formation. The mudstone is composed of phyllosilicates (muscovite–sericite, biotite, and chlorite) and small amounts of quartz and opaques. The siltstone consists of rounded grains of quartz and feldspar, and minor amounts of chert, quartzite, and mudstone, all set in a mica-quartz matrix. The sandstone contains, in decreasing order of abundance, quartz, plagioclase, and small amounts of microcline, muscovite, biotite and chlorite, tourmaline, zircon, apatite, ilmenite, and pyrite. Diagenetic pyrite occurs locally. Primary carbonate was not observed in outcrop, but is present at depth in the Main prospect.

The Ashburton Formation has undergone two phases of post-Wyloo Group and pre-Bangemall Group deformation (D_1 and D_2). Interference between southwesterly trending F_1 folds and northwesterly trending F_2 folds has resulted in an upward-facing, large-scale dome-and-basin geometry in the Mount Clement area (Fig. 2). Bedding dips are steep (greater than 45°) to vertical. F_2 folds are generally associated with a strong S_2 penetrative cleavage. An S_2 crenulation cleavage has resulted in areas where S_2 is superimposed upon an S_1 slaty cleavage. Host rocks were subjected to lower greenschist-facies metamorphism during the interval between D_1 and D_2. In the Mount Clement area, the Ashburton Formation is cut by two northeast-trending, post-D_2, dolerite dykes (Fig. 2). The smallest of these is 40–50 m wide, and intersects the Main prospect succession. Although highly altered, it is unmineralized. The second dyke is over 50 m wide and crops out 400 m southeast of the Eastern prospect. In places, this dyke contains up to 50% quartzite and granitic xenoliths. Neither the groundmass nor the xenoliths are mineralized.

Surface weathering has resulted in the oxidation and replacement of sulphides and some phyllosilicates by iron oxide (or hydroxide); the alteration of rock matrix to kaolinite, smectite, and secondary quartz; and the formation of liesegang rings. Outside the prospect areas, the weathered profile over barren country rock is often relatively shallow, and data from drill holes suggest that entirely fresh rock is reached less than 30 m below the surface. In a few places, sulphides can be collected from the surface.

Main prospect

The interbedded clastic and chemical rocks that host the mineralization at the Main prospect will be referred to informally as the "hydrothermal sequence"; strictly, this

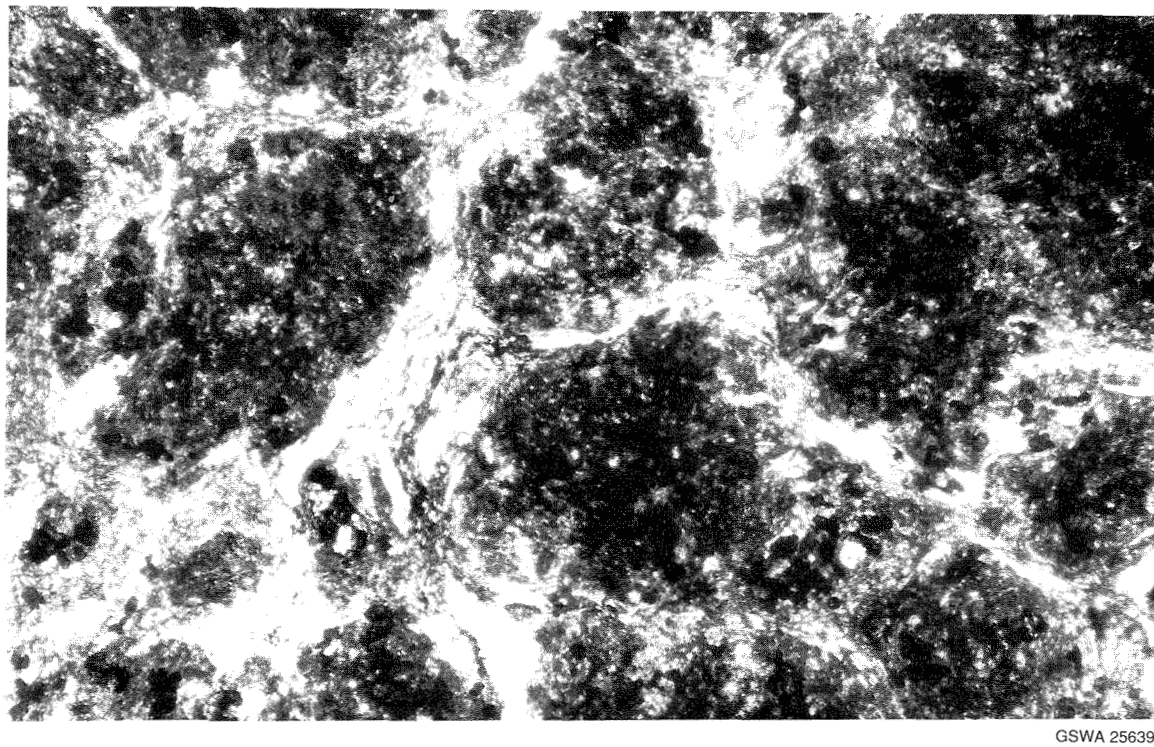

GSWA 25639

Figure 5. Talc (colourless) replacing dolomite (grey); sample from adit. Long axis is 3.2 mm.

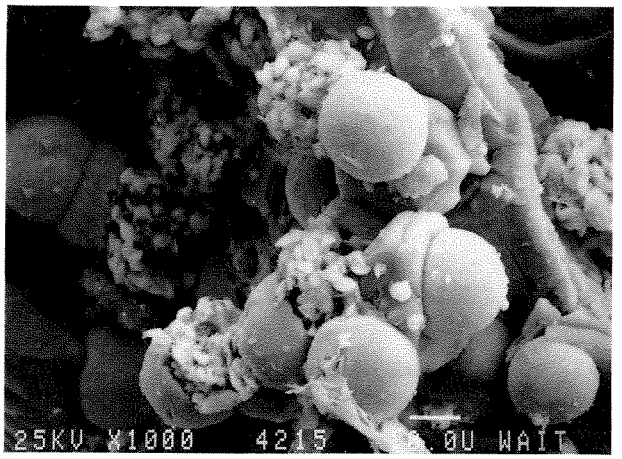

GSWA 25640

Figure 6. Iron oxide spheroids in ferruginous siltstone; hole 33 at 65 m. Scale bar 10 μm

sequence comprises clastic rocks overprinted by hydrothermal alteration and some chemical deposits of hydrothermal origin. They are clearly distinguishable on aerial photographs by their craggy outcrop, which contrasts with the more rounded topography of the unaltered Ashburton Formation. The hydrothermal sequence forms a lenticular to triangular body with a strike length of about 1.2 km and a maximum thickness of 400 m (Fig. 2). Its base is marked by a laminated talc which rests conformbly upon barren siltstone. The top of the sequence is defined by a discontinuous quartz-pebble-bearing siliceous siltstone.

The hydrothermal sequence can be divided into a Lower Mineralized Zone (LMZ), which contains all the known mineralization, and an Upper Barren Zone (UBZ). The LMZ includes iron-rich rock (cherts, altered siltstones, and breccias), talc-rich rocks, dolomite, and sulphide lenses; whereas the UBZ contains white chert, quartz-pebble-bearing siltstone and conglomerate. Both LMZ and UBZ contain unmineralized siltstone and mudstone which are indistinguishable from similar rocks in the enclosing Ashburton Formation.

Recrystallized dolomite, containing little or no siliciclastic detritus, occurs below the weathered profile in the LMZ. Locally the dolomite is veined or impregnated with quartz, tourmaline, chlorite, albite, calcite, and arsenopyrite. Traces of dolomite are present in most siltstones recovered from deeper drill holes in the LMZ and UBZ. These dolomite-bearing rocks typically contain clinochlore and phlogopite.

Talc partly replaces dolomite in some sub-surface samples (Fig. 5), and also forms thick, laminated masses near the base of the LMZ. Some talc bodies are virtually monomineralic: others are impregnated with quartz (nodules up to 0.2 m across), iron oxides, arsenopyrite and coarsely crystalline kaolinite.

Primary rocks, dominated by chemically deposited iron oxides, range from banded hematite–quartz iron-formation (BIF), through powdery laminated chert–hematite to hematitic siltstone. Layering in these rocks appears to be primary; however, most of them have been recrystallized. Ferruginized siltstone from hole 33 (Fig. 6) contains microspheres and octahedra of hematite, the latter after magnetite. Similar octahedra are also present in iron-formation.

Clastic rocks that have been ferruginized and silicified by the processes of alteration occur widely throughout the hydrothermal sequence, particularly in the vicinity of major bedding planes. Ferruginized siltstones are more abundant in the LMZ. They contain iron oxides and hydroxides, both as pseudomorphs after sulphide, and as cavity fillings. Silicification is most apparent in the UBZ, and, in places, has resulted in the almost total replacement of the primary minerals.

Breccias comprise white to off-white siliceous fragments, up to 5 cm in diameter, set in a ferruginous chert matrix. Four stratabound bodies of breccia, each as much as 10 m thick, crop out in the hydrothermal sequence east of the adit (Fig. 2), and are conformable with the enclosing strata. In contrast, the bodies of breccia that occur to the north and west of the adit cross-cut bedding. There is no evidence of faulting related to either conformable or discordant breccias.

Cherty rocks containing little iron occur mainly in the UBZ. Some are cryptocrystalline silica; but most consist of microcrystalline quartz with a polygonal, granoblastic texture.

Though now recrystallized, much "chert", especially the large mass south of the adit (Fig. 2), appears to be primary, and has layers of slightly different grain size that indicate original bedding. However, the occurrence of detrital quartz and mica suggests that some chert may be silicified siltstone. This interpretation is supported by field evidence which shows that, locally, some chert grades laterally into unaltered siltstone.

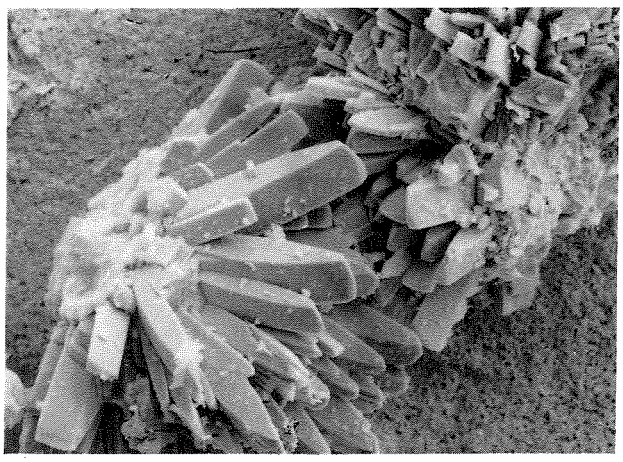

GSWA 25641

Figure 7. Conichalcite crystals in gossanous siltstone; hole 33 at 44 m.

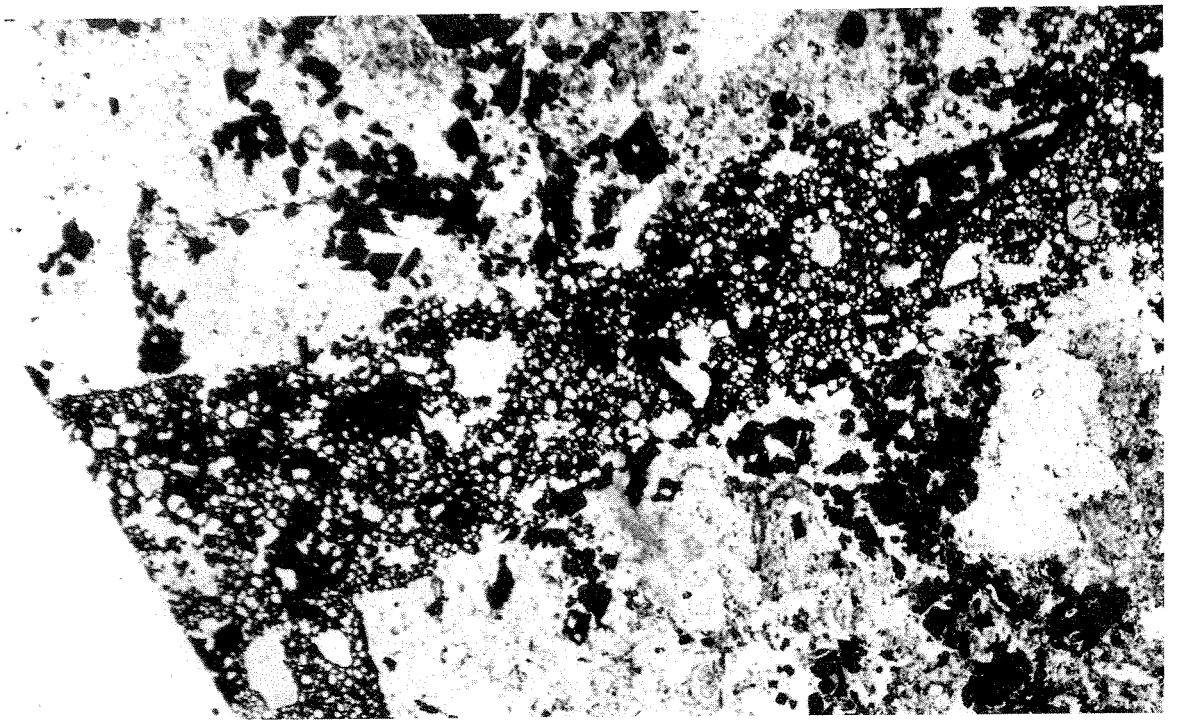

GSWA 25642

Figure 8. Mineralized breccia showing scorodite in matrix, in part replacing arsenopyrite; surface sample, second lowest breccia east of adit. Long axis is 9.8 mm.

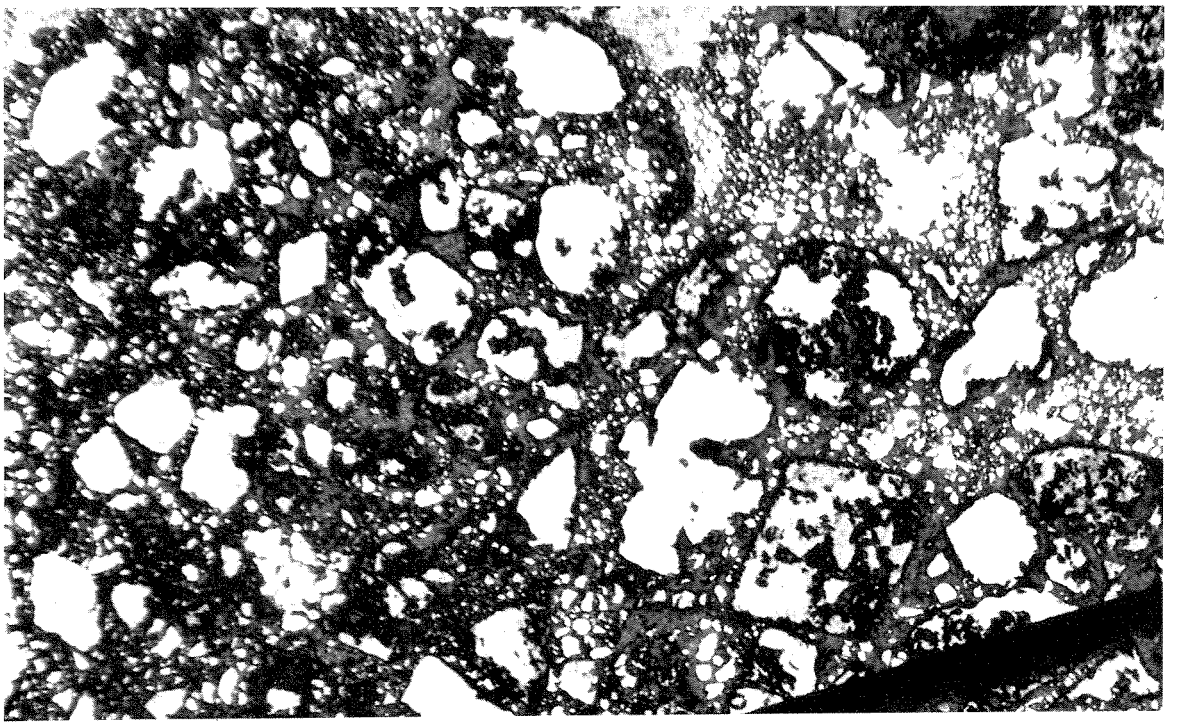

GSWA 25643

Figure 9. Gossanous breccia with quartz (white) and interstitial fine-grained scorodite. Some quartz has been replaced by the matrix, and pseudomorphs after sulphides are present. Long axis is 9.8 mm.

Main prospect mineralization

Most of the significant mineralization, which is associated with a suite of secondary, polymetallic oxidates—mainly arsenates—occurs in the LMZ. The mineralized zone is oxidized to a depth of more than 100 m at the Main prospect—considerably deeper than is the case for barren host rocks. Mineralization is generally stratabound, although, locally, conichalcite (Appendix; Fig. 7) occurs in minor, cross-cutting fractures.

The two central conformable chert breccia bodies east of the adit (Fig. 2) are strongly mineralized. Their outcrop includes gossanous areas, which display boxwork textures (after sulphides) and are characterized by a distinctive assemblage of green arsenate minerals (Appendix). The abundance of scorodite and arseniosiderite, and the texture of the boxworks, indicate that the dominant sulphide precursors were arsenopyrite and subordinate pyrite (Figs 8 and 9).

Substantial sulphide mineralization has only been observed in one drill hole (DDH 4), which is located 100 m west of the adit entrance (B.H.P, 1976). Massive arsenopyrite occurs between 99.5 m and 102.5 m. Remnants of this massive material, examined during the course of this study, were found to consist of arsenopyrite rimmed with arseniosiderite and quartz, and to be cut by quartz–talc veinlets. In a gossanous zone immediately above the massive sulphide, covellite and digenite rim residual arsenopyrite.

Disseminated arsenopyrite, accompanied by gold and silver, is still retained by talc–quartz–phlogopite rock at a depth of 86 m in DDH 43A. Traces of pyrite, pyrrhotite, and chalcopyrite, are associated with otherwise barren siliceous dolomite and siltstone in DDH 16.

Traces of gold have been recorded from all rock-types in the LMZ. Low values (less than 0.5 ppm) have been recorded from clay-rich horizons, dolomite, and iron-formation, whereas moderate values (up to 4.3 ppm) were obtained from some apparently unaltered siltstones and

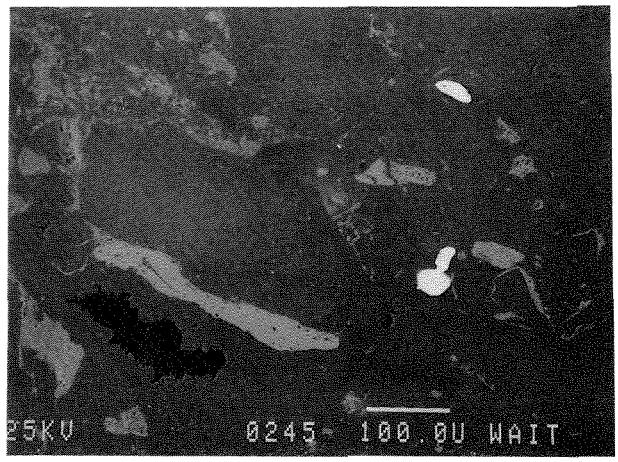

GSWA 25645

Figure 11. Typical argentiferous gold from the "discovery gossan": gold (bright) and chenevixite (light grey) in quartz. Scale bar 100 µm.

their ferruginized equivalents. Most of the anomalous, and all of the highest, gold values were recorded from chert breccia, gossan, massive talc, and ironstone (Davy et al., 1989, Table 3). Newmont (1981) obtained a value of 4.2 ppm Au from the massive sulphide between 99.5 and 100.8 m in DDH 4. The gold was described as free and fine grained (less than 30 µm). Flattened or elongate grains of gold, up to 250 µm across, have been recorded from the discovery gossan (Fig. 10, 11, 12). They occur locked in quartz or chalcedony, or in goethite pseudomorphs after sulphide. A typical analysis of the gold shows it to contain 18–20% Ag and 2% Fe. Gold from 37 to 38 m in DDH 33 contains no detectable silver; it occurs as "leaf gold" in microcrystalline quartz in breccia, and is probably of secondary origin.

Primary sulphides other than arsenopyrite, pyrite, and (traces of) chalcopyrite, have not been identified; however, the presence of significant silver, antimony, and copper

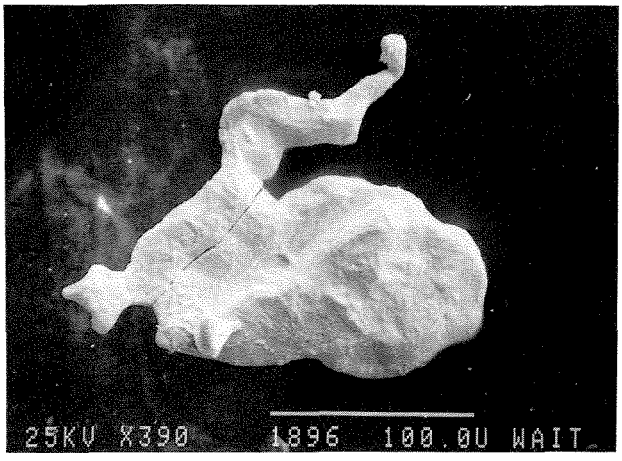

GSWA 25644

Figure 10. Argentiferous gold grain extracted from the "discovery gossan". Scale bar 100 µm.

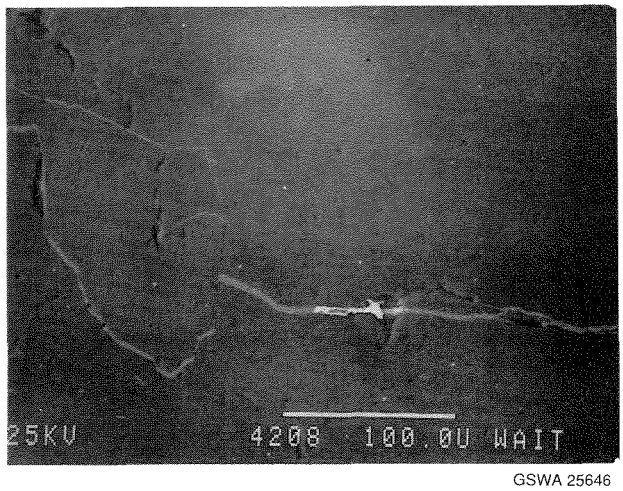

GSWA 25646

Figure 12. Silver-free secondary gold, and scorodite, in crack in late-stage quartz–tourmaline vein; hole 33 at 37.5 m. Scale bar 100 µm.

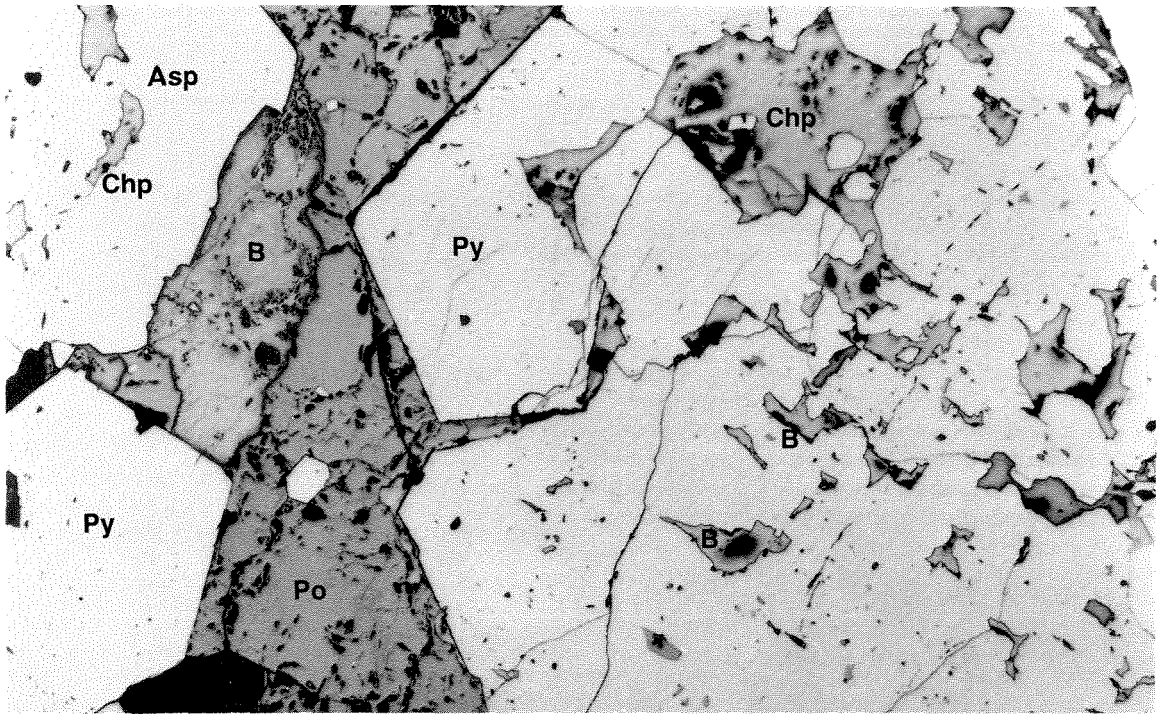

GSWA 25647

Figure 13. Sulphides typical of the Eastern prospect mineralization: pyrite (py) and arsenopyrite (asp) containing inclusions of chalcopyrite (clp) and boulangerite (bo). Pyrrhotite (po) in crack. Long axis is 1.37 mm.

suggests that a sulphosalt of the tetrahedrite–tennanite series could once have been present (B.H.P., 1976). Traces of this mineral, together with native bismuth, were reported from the discovery gossan. Most copper now occurs in chenevixite or conichalcite; whereas silver has been converted to halide, or has entered secondary copper arsenates. Antimony is associated with goethite, or occurs with lead in bindheimite.

Eastern prospect

The mineralization of the Eastern prospect crops out in a linear zone, 1 km long, and sub-parallel to the strike of the enclosing Ashburton Formation. It is approximately 400 m higher in the stratigraphic sequence than the main prospect. Mineralization is confined to a 3 m wide siliceous zone that cuts the bedding at about 5°. A locally developed gossan is dominated by scorodite, secondary lead minerals (chiefly bindheimite, carminite, and, philipsbornite), and several minerals of the jarosite and alunite groups.

Sulphides were encountered below a depth of 3 m in the single hole (DDH 3) drilled at this prospect. Sulphides and sulphosalts identified are (in order of decreasing abundance): arsenopyrite, pyrite, pyrrhotite, boulangerite, galena, chalcopyrite, and ullmanite (Appendix). Pyrite is the dominant mineral below a depth of 33 m. Mineralization occurs in irregular, cross-cutting veins less than 1 cm wide; it is accompanied by sparry quartz and traces of chlorite, muscovite, berthierine, calcite, apatite, and tourmaline. Dynamic recrystallization, which resulted from shearing, has locally produced small, discrete pods of sulphide. Disseminated boulangerite–chalcopyrite mineralization occurs within millimetre-thick veins of undeformed, fine-grained polygonal quartz.

Textural relationships suggest the earliest sulphur-bearing mineral was boulangerite, followed by chalcopyrite, pyrite and pyrrhotite, and arsenopyrite. It is possible, however, that the paragenesis is more apparent than real, and may reflect the ability of arsenopyrite, pyrite, and pyrrhotite, to form blastic grains at the expense of other sulphides and sulphosalts (Fig. 13).

The host sandstone, siltstone, and mudstone, contain fine- and (rarely) coarse-grained, disseminated pyrite and arsenopyrite. Sulphide depletion occurs in mudstone adjacent to the mineralized zone. Pressure shadows of quartz and biotite, elongated in the plane of S_2, fringe sulphide grains in siltstone.

Veins in country rock

Prominent cross-cutting veins occur 1 km east of the Main prospect (Fig. 2). They are green, and contain abundant scorodite (after arsenopyrite) in a saccharoidal quartz matrix. One vein, which strikes east-northeast, carries traces of boulangerite.

Several unmineralized quartz veins crop out northwest of the Main prospect. They include a set of quartz-chlorite tension-gash fillings, which are *en echelon* to the main

northwest-trending fault. West and southwest of the Main prospect, a series of small pods, up to 10 m long, marks the line of a southwest-trending fault.

None of these outcrops has been tested by drilling.

Geochemistry

Main prospect

Geometric means of the concentrations of elements in each of the major rock-types are shown in Table 1. Barren country rock is characterized by high barium, cerium, chromium, gallium, lanthanum, niobium, rubidium, vanadium, and zirconium. The abundances and ratios of these elements have been used to determine whether the rock-types within the LMZ are wholly or partly detrital, or are chemical in origin. Gossan, ironstone, chert-breccia, talc, BIF, quartz-hematite rock, and dolomite, have generally low values for the above trace elements. Mudstone and siltstone of the LMZ are compositionally very similar to barren country rock; but higher values for arsenic, lead, and antimony, and lower values for barium, calcium, gallium, manganese, niobium, rubidium, thorium, vanadium, and zirconium, indicate weak alteration. In contrast, highly altered, ferruginized and silicified samples of mudstone and siltstone from the LMZ are impoverished in the detrital component. Rubidium has been depleted to the extent that it is not detectable in most of the more altered samples.

The LMZ is characterized by abundant arsenic and a patchy distribution of economically important metals (silver, gold, bismuth, copper, lead, and antimony). Table 2 gives percentages of samples, from the various lithologies of the LMZ, that contain anomalous amounts of the above elements. For comparison, Table 2 presents similar data for rocks of the UBZ. These data illustrate the patchiness of the mineralization in the LMZ: only rarely are more than half the samples of a given rock anomalous; and, in the case of dolomite, the proportion of anomalous samples is very low. More gossans are anomalous in silver, gold, bismuth, copper, and antimony (and arsenic) than are other rock types (Table 2); they also provide the highest absolute values of these elements (Davy et al., 1989). Table 2 illustrates some separation between the elements: lead is only rarely anomalous in talc or gossan, but these rocks contain most of the anomalous silver and copper values. Antimony and bismuth occur in most rock types, but bismuth is restricted to gossans and breccias.

Other elements which may have been introduced or affected by the mineralizing event include cerium, mercury, lanthanum, thorium, uranium, tungsten, and zinc (Table 2). Values of 200–1500 ppm cerium (as compared to a maximum of 150 ppm in barren country rock) were obtained from mineralized rocks in the LMZ. The concentration of cerium (and lanthanum) is normally very low in gossans, breccias, and talc; and the rare high values for these elements may simply indicate local redistribution. Up to 50 ppm of thorium is commonly present in country rock, but values of 100–600 ppm have been obtained from gossans. Tungsten has not been detected in unmineralized samples, but values of 520 ppm and 115 ppm were obtained

TABLE 2. ANOMALOUS SAMPLES AT MAIN PROSPECT

(Stated as percentage of samples analysed for given rock type.)

	T	*A*	*C*	*D*	*E*	*F*	*G*	*H*	*I*	*J*	*K*
Sample size(a)		50	23	18	30	23	15	9	71	32	27
Ag	10	0	70	50	10	13	0	0	3	3	0
As	1000	4	96	72	73	87	40	0	76	41	26
Au	0.5	0	87	22	37	30	13	11	15	3	0
Ba	500	42	4	22	0	9	20	0	14	34	37
Bi	30	0	65	23	24	46	14	0	11	4	0
Ce	200	0	0	0	17	0	7	0	6	3	0
Cu	500	2	61	44	10	9	13	0	13	3	0
La	100	0	0	0	10	0	7	0	6	3	0
Mn	1000	22	13	11	17	22	7	7	21	38	37
Pb	500	0	9	0	23	17	20	0	34	13	4
Sb	50	12	83	67	40	74	73	0	68	28	7
Sn	15	10	17	17	0	0	7	0	4	3	0
Th	50	0	39	11	20	17	20	0	13	3	0
U	5	0	26	17	27	26	7	0	25	9	4
Zn	250	0	9	22	3	26	13	0	35	3	14

KEY: T = Threshold values (ppm). A = Barren siltstone–mudstone. C = Gossan. D = Talc. E = Ironstone. F = Breccia. G = Quartz–hematite rock. H = Dolomite. I = Ferruginous silicified clastics of LMZ. J = Siltstone and mudstone of LMZ. K = Conglomerate, siltstone, and mudstone of UBZ.

NOTE: (a) Except for Bi, where sample sizes were 48, 23, 13, 17, 13, 14, 9, 55, 25, and 27 respectively.

A

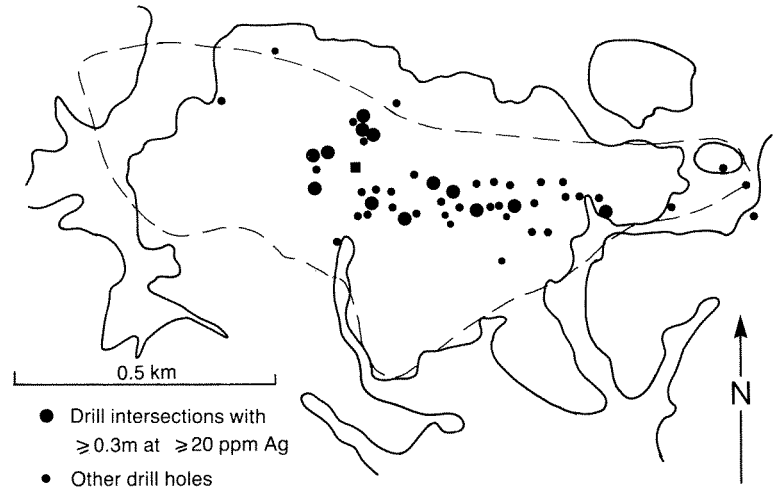
0.5 km
N
Drill intersections with
≥0.3m at ≥20 ppm Ag
Other drill holes

B

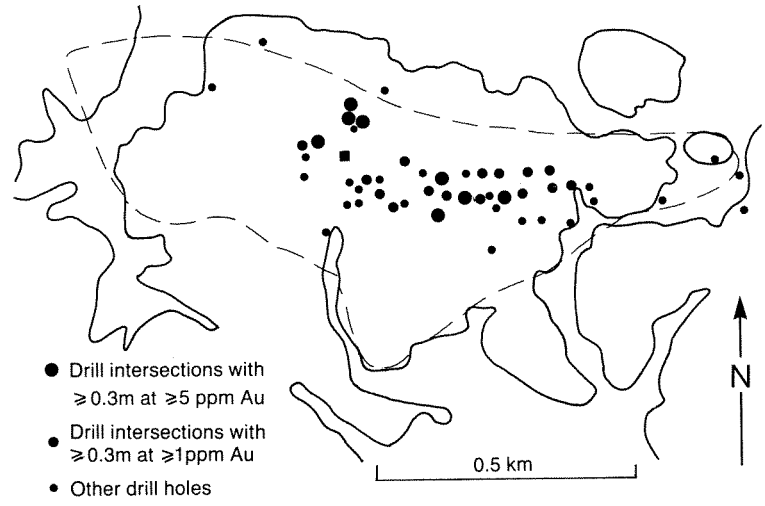
Drill intersections with
≥0.3m at ≥5 ppm Au
Drill intersections with
≥0.3m at ≥1ppm Au
Other drill holes
0.5 km
N

C

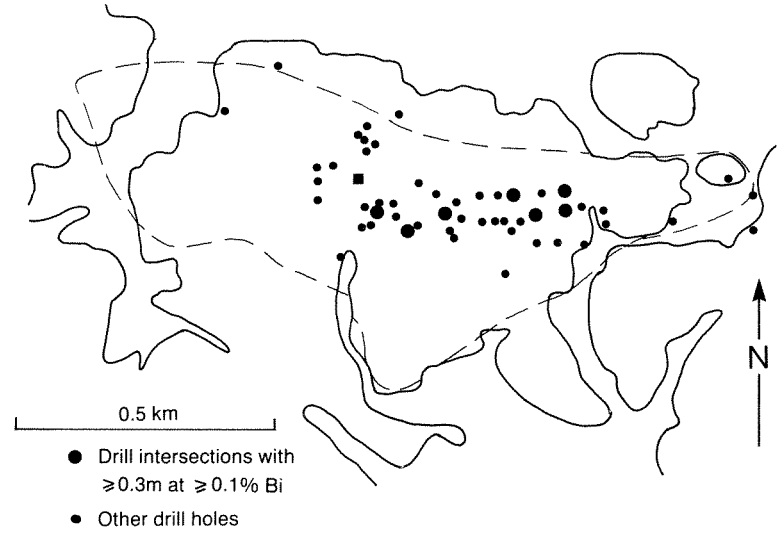
0.5 km
N
Drill intersections with
≥0.3m at ≥0.1% Bi
Other drill holes

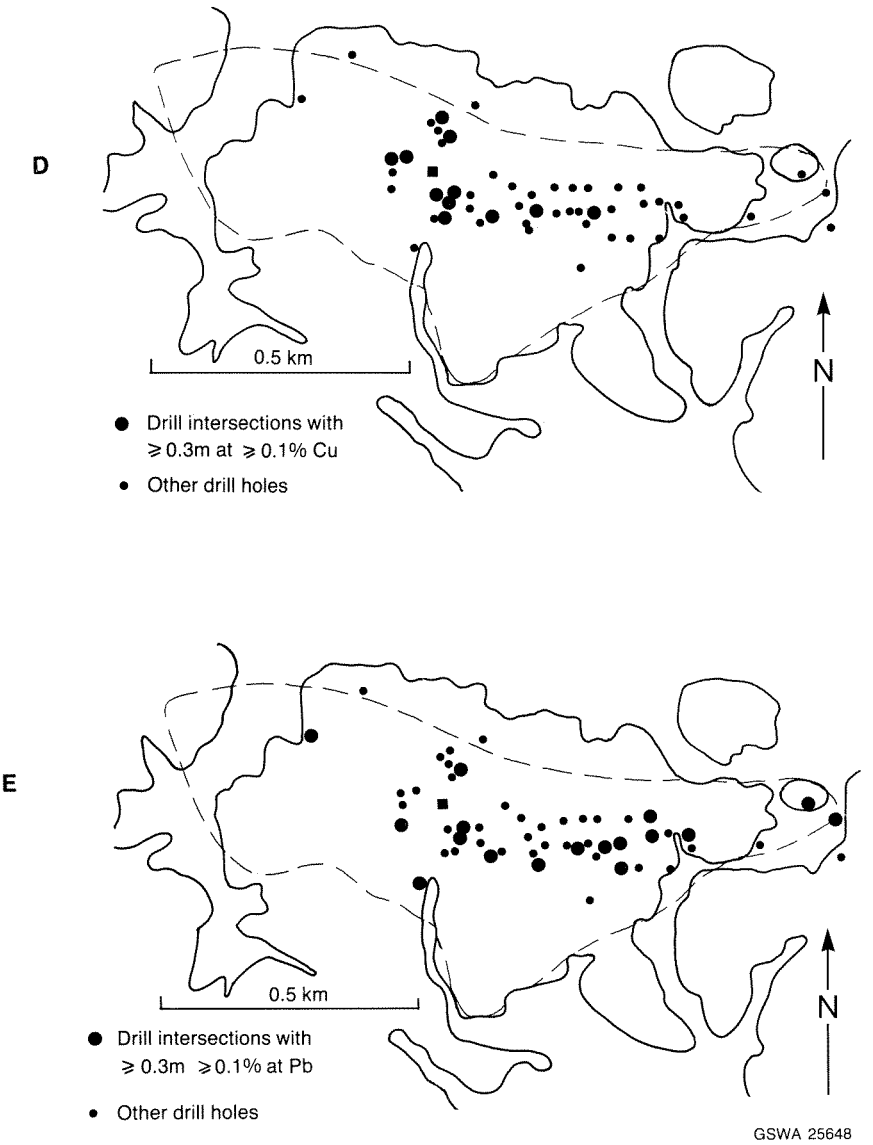

Figure 14. Distribution of anomalous metals in drill holes: A — Silver. B — Gold. C — Bismuth. D — Copper. E — Lead.

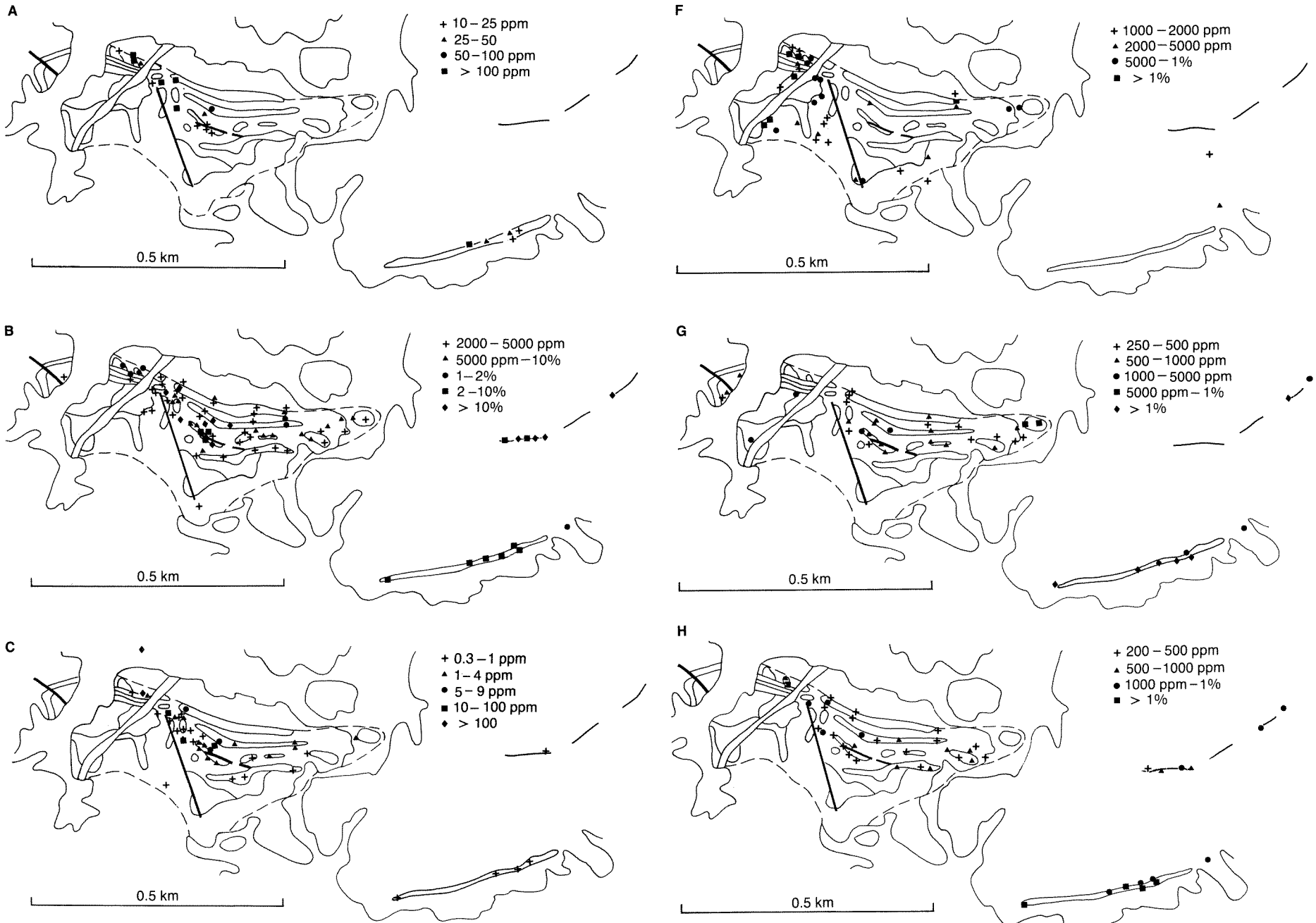
A
+ 10 – 25 ppm
▲ 25 – 50
● 50 – 100 ppm
■ > 100 ppm
0.5 km
B
+ 2000 – 5000 ppm
▲ 5000 ppm – 10%
● 1 – 2%
■ 2 – 10%
◆ > 10%
0.5 km
C
+ 0.3 – 1 ppm
▲ 1 – 4 ppm
● 5 – 9 ppm
■ 10 – 100 ppm
◆ > 100
0.5 km
F
+ 1000 – 2000 ppm
▲ 2000 – 5000 ppm
● 5000 – 1%
■ > 1%
0.5 km
G
+ 250 – 500 ppm
▲ 500 – 1000 ppm
● 1000 – 5000 ppm
■ 5000 ppm – 1%
◆ > 1%
0.5 km
H
+ 200 – 500 ppm
▲ 500 – 1000 ppm
● 1000 ppm – 1%
■ > 1%
0.5 km

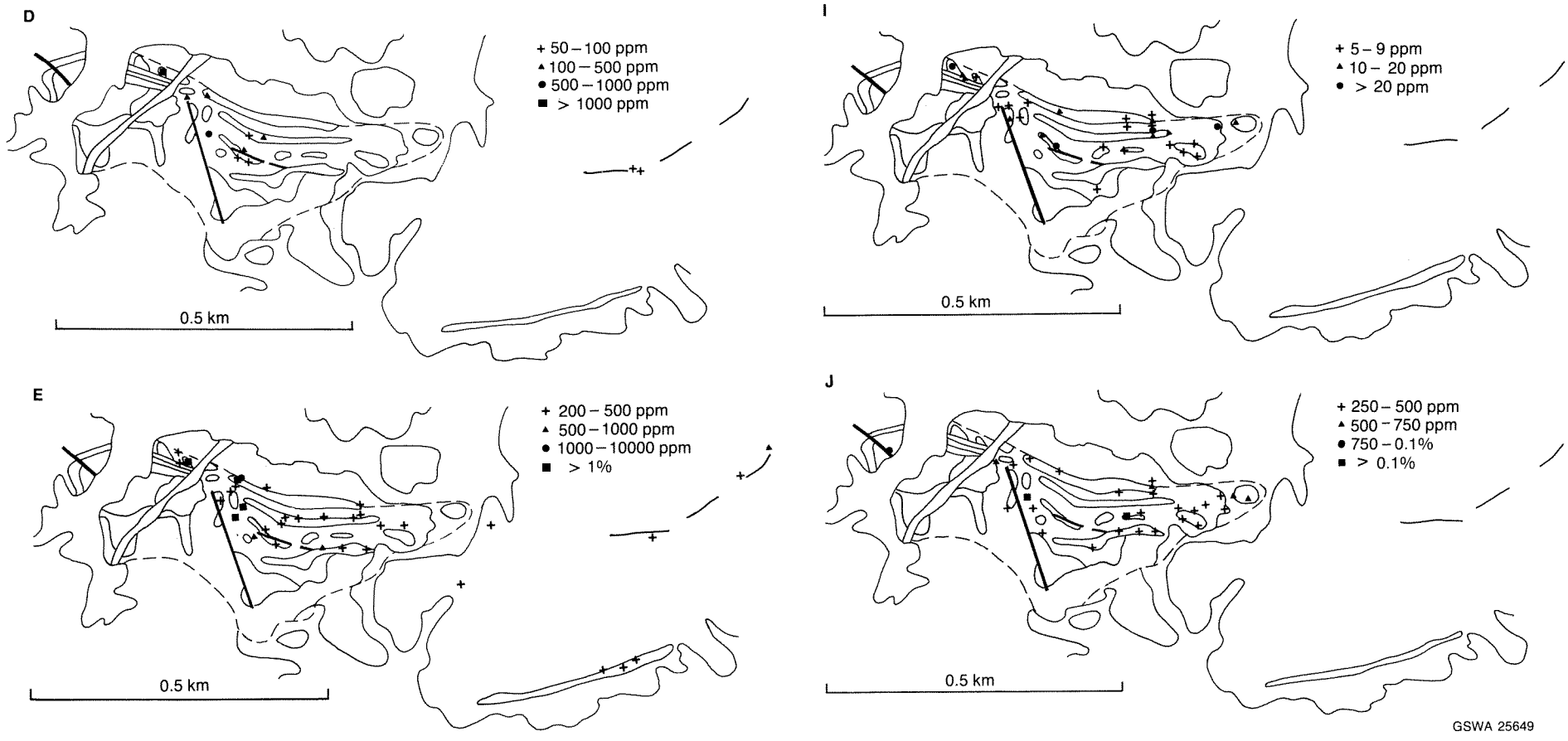

Figure 15. Distribution of anomalous metals in surface samples: A — Silver. B — Arsenic. C — Gold. D — Bismuth (incomplete data). E — Copper. F — Manganese. G — Lead. H — Antimony. I — Uranium. J — Zinc.

from a gossan and a ferruginous siltstone respectively. Background levels for zinc are less than 250 ppm; however, some mineralized samples contain in excess of 1000 ppm. Uranium has a maximum value of 35 ppm; yet all but one sample with values over 5 ppm occur in the LMZ. Only seventeen samples were analysed for mercury; gossans and massive sulphide remnants contain up to 5.6 ppm and 2.2 ppm respectively of mercury; other rocks contain less than 0.2 ppm.

Data from drill holes which intersect at least 0.3 m of precious or base metal suggest a poorly defined zoning of elements (Figs 14A–14E). These figures show that gold values over 5 ppm are restricted to two areas; copper values greater than 0.1%, to three areas; and bismuth greater than 0.1%, to one area. Silver values greater than 20 ppm are more widely distributed: the greatest enrichment occurs immediately north and west of the main adit. Lead values greater than 0.1% are centred upon an area to the southeast of the adit; high values have not been recorded from the lowest levels of the LMZ or the major gossans.

Anomalous values of silver, arsenic, gold, bismuth, copper, lead, antimony, uranium, and zinc, in surface samples also show an areal and stratigraphic zonation (Figs 15A–15J); they are highest in the breccia and gossan zones at the eastern end of the prospect. In contrast, manganese is more abundant in the less altered rocks of the UBZ.

These data suggest relatively little surface leaching. Direct comparison of drill material with surface samples is, however, difficult, because of the irregular distribution of the mineralization and the lack of subsurface material from unmineralized areas. The only elements which appear to be significantly leached, and then only from siltstone and mudstone, are bismuth and copper. Conversely there is no obvious enrichment of immobile elements—e.g. chromium, vanadium, and zirconium—in the weathered zone. Manganese forms local concentrations on the surface and at depth, and it is not clear to what extent leaching has affected the distribution of this element.

Eastern prospect

The Eastern prospect is anomalous in arsenic, lead, and antimony (Table 1). These elements are accompanied by minor amounts of copper, manganese, and antimony, but gold is barely detectable.

Quartz–scorodite veins

Quartz–scorodite veins are characteristically very high in arsenic, and contain significant lead and antimony (Table 1). Silver, gold, copper, and tin, are present in amounts just above detection limits.

Discussion

The mineralization of the Main prospect is widely considered to be hydrothermal. Newmont (1981, 1982) interpreted the prospect as a Galapagos-style exhalation deposit; but Doust (1984, p. 114) favoured the more general view that the deposit had been formed as a result of exhalation and precipitation in a submarine environment. Data presented in this work lend support to the interpretation that the Main prospect is an epithermal deposit (Lindgren, 1933; Silberman and Berger, 1985). Evidence in favour of the more specific interpretation as a hot-spring deposit is, however, equivocal.

The mineralization of the Main prospect pre-dates the D_1 deformation and subsequent metamorphism to lower greenschist facies. This, coupled with the conformable, sediment-hosted style of the mineralization, the host-rock lithology, and the lack of quartz veining, favours a syngenetic near-surface origin for the hydrothermal sequence of the Main prospect. Chert, banded iron-formation, and dolomite, occur interbedded with typical siliciclastic rocks, such as mudstone and siltstone, of the Ashburton Formation and are interpreted as the products of chemical sedimentation from a mixed exhalative–marine source. Ferruginized and silicified siltstone contains reduced levels of trace-elements characteristic of the detrital components compared with those of their unaltered equivalents in the Ashburton Formation. Initial trace-element ratios are still preserved, however, and suggest that these siliceous rocks formed either as a syngenetic exhalite in which there was a minor detrital component, or as an epigenetic replacement after siliciclastic siltstone.

Mineralization has resulted in significant enrichment of silver, arsenic, gold, copper, mercury, lead, antimony, uranium, tungsten, and zinc: elements which are known to be abundant in other epithermal deposits (e.g. Weissberg et al., 1979; Silberman and Berger, 1985). High thallium values are also characteristic of epithermal mineralization. Although this element was not analysed for in the present work, Doust (1984) reported up to 50 ppm thallium in surface ironstone and siltstone from the LMZ at the Main prospect. High levels of bismuth and thorium, such as occur in the LMZ, have not been reported from other epithermal deposits. Conversely, barium, manganese, and molybdenum, which are often anomalous in other epigenetic deposits, are present at generally low levels in the Main prospect.

The Main prospect, as exposed, presents essentially a cross-section through the deposit. The current outline of the hydrothermal sequence probably reflects tectonic shortening and thickening as a result of D_1 and D_2 deformation. The apparent thickness is also exaggerated because the topographic surface cuts the deposit at 45–60°. Nevertheless, deformation has not been so severe that primary layering and the fundamental shape of the deposit have been obliterated

The bodies of quartz-breccia within the LMZ may be analogous to the hydrothermal breccias of modern hot-spring environments. Those occurring east of the main adit are conformable with the Ashburton Formation and show no evidence of fault-related shearing. Low levels of siliciclastic contamination suggest that the breccias originated as (siliceous) chemical precipitates; high values of manganese and strontium in some samples suggest that the original rock had a significant carbonate component.

No large feeder conduit is exposed; but the shape of the Main prospect succession suggests that one might have been located about 150 m northwest of the adit, close to the discovery gossan; it may well have occupied the fracture that is now occupied by the dolerite dyke. Breccias east of the adit appear to radiate from this area, and the cross-cutting chert exposed west of the adit may have been a local feeder for siliceous deposits in the upper UBZ. The presence of breccias at different stratigraphic levels and locations within the LMZ suggests that hydrothermal activity was episodic, and that the position of the feeder vent may have changed with time.

The Ashburton Formation is a 5–10 km thick succession of deep-marine siliciclastic and chemical deposits (Daniels, 1975; Gee, 1979; Thorne and Seymour, 1991). It might be expected, therefore, that a high hydrostatic pressure would have inhibited explosive activity in the vents. However, on the basis of the composition of emerging fluid, Bischoff and Pitzer (1985) calculated that, for vents at 2.3 km depth (23 MPa hydrostatic pressure) which have fluid temperatures of 380–400°, boiling occurs well below the sea floor. Considerable over-pressurization could, therefore, be expected in a confined system; and this may have been the driving force for explosive brecciation at Mount Clement.

Hydrothermal activity at Mount Clement was accompanied by tourmalinization, albitization, and the development of coarse-grained kaolinite and talc. Deuterium isotope ratios in talc at the base of the hydrothermal sequence enable some estimate of the temperature of the hydrothermal fluid to be made (Taylor, 1974). Mount Clement deuterium isotope ratios (δD) fall between $-63‰$ and $-80‰$ where:

$$\delta D = \frac{R_{(sample)} - R_{(SMOW)}}{R_{(SMOW)}} \times 1000$$

and R = D/H isotopic ratio

SMOW = Standard Mean Ocean Water

The "recorded values of δD imply a lack of isotopic equilibrium with sea-water (where $\delta D = 0‰$ by definition), and suggest formation through the agency of a metamorphic or hydrothermal fluid of δD composition $-40‰$ to $-50‰$ at temperatures of 300–400°C, using the muscovite–water deuterium/hydrogen fractionation figures" (D.C. Green, written communication, 1984). The interpretation is that the talc formed by the reaction of a hot fluid with dolomite or dolomitic mudstone–siltstone. The association of pyrite and arsenopyrite indicates a maximum temperature of 491°C for the ore-forming fluids (Clark, 1960). Temperatures of 300–490°C are consistent with values deduced for other hydrothermal ore-forming fluids (e.g. Solomon and Walsh, 1981).

Other alteration features, of less certain origin, observed at Mount Clement include:

- Massive arseniosiderite and scorodite which lack textural evidence of formation from arsenopyrite.
- Development of scorodite along cracks and vugs.
- Growth of coarse-grained, polygonal and granoblastic chert.
- Cavity development to depths of 100 m.
- Silicification of primary minerals of breccia.

These features could be the result of supergene alteration, including weathering. However, similar phenomena at Carlin, Nevada, are interpreted as the product of oxidation and acid leaching in a surface or near-surface, hot-spring environment (Hausen, 1967; Radtke, 1985). At Mount Clement, an acid hydrothermal environment is indicated by the presence of coarsely crystalline kaolinite, while oxidizing conditions are suggested by the presence of primary magnetite and hematite. The present contrast in depth of alteration between the Main prospect and country rock may also reflect primary oxidation rather than subsequent weathering. Alteration features which are almost certainly the result of recent weathering include: oxidation of pyrite; formation of cryptocrystalline silica; and the development of fine-grained kaolinite in both the hydrothermal sequence and country rock.

Comparison with modern hydrothermal systems is difficult because most recent examples occur in subaerial volcanic terrains or oceanic rifts. No description of modern hot springs in a submarine-fan environment has been located.

Modern thermal systems in New Zealand have a surface expression at least as large as that at Mount Clement Main prospect. Most have multiple springs. For example, hot ground at Orakeikorako occurs in two lobes, measuring approximately 1.3 km by 0.9 km and 1.0 km by 0.6 km, each of which contains abundant hot springs (Lloyd, 1972). The Waiotapu geothermal system is actively precipitating precious metals; gold, arsenic, and antimony, are dominant in separate springs. Hydrothermal argillization of surface materials can be detected more than 1.1 km from the mineralization, and the whole system extends more than 4 km (Lloyd, 1959; Hedenquist and Henley, 1985). Drilling at Waiotapu indicates minor precious and base-metal mineralization to depths of 300 m below the surface.

Hydrothermal eruptions are not uncommon; an eruption in 1951 at Lake City, California, has been described by White (1955). Hydrothermal breccias similar in thickness and areal distribution to those occurring at the Main prospect have been documented by several workers including Lloyd (1959, 1972), Nairn and Solia (1980), and Hedenquist and Henley (1985), and are discussed in detail by Nelson and Giles (1985). At Kawerau, New Zealand, Nairn and Solia (1980) recorded hydrothermal eruption debris—up to 8 m thick—scattered with decreasing fragment size and thickness over a radial distance of 1.5 km. In the

Orakeikorako (New Zealand) hydrothermal system, eruptions have occurred from a number of craters; and breccias contain fragments up to 0.1 m in diameter set in a finer grained matrix (Lloyd, 1972). Breccias of various ages have been reported from Waiotapu, New Zealand (Hedenquist and Henley, 1985). Hedenquist (1986, p.98) describes the deposits as made up of "poorly sorted fragments which are matrix supported, angular to subrounded, and often veined; bedding is unusual except in the distal portions of deposits". Though the stratabound breccias at Mount Clement are recrystallized, their size and thickness, and the fragment size, are consistent with modern hydrothermal breccias.

The 300 m long body of massive chert in the UBZ at Mount Clement can be interpreted as having formerly been siliceous sinter. Though its primary textures have been obscured by recrystallization, its geometry and lithology, and its capping of thin discontinuous conglomerate, are consistent with a chemical deposit which formed a mound (lens) within clastic sediments. Modern sinters in New Zealand can have this form, e.g. Ohaaki Pool (Browne and Lloyd, 1986). At Orakeikorako, the Umukuri sinter is as much as 20 m thick, and formerly covered 1 km^2 (Lloyd, 1972). Chert southwest of the adit at Mount Clement may have a similar origin.

It is doubtful if the mineralization at the Main prospect was wholly syngenetic. Though a spring may have been active, most mineralization may have been originally deposited below the sea floor and subsequently introduced to its present location by eruption. The situation may be analogous to that at Carlin, Nevada, where Radtke (1985) sees mineralization as associated with a hot spring; whereas Bagby and Berger (1985) postulated that the gold ore was deposited at least 1 km below the surface.

Drilling has encountered only one intersection of massive sulphide, although gossanous zones indicate that such mineralization was formerly more widespread. Small grains of sulphide enclosed in quartz are disseminated throughout much of the LMZ, but most of the mineralization occurs in the form of oxidate minerals. The abundance of scorodite and other compound oxides, coupled with the virtual absence of sulphate minerals and presence of primary magnetite, hematite, and siderite, suggests that sulphur levels waned as the hydrothermal environment evolved. The presence of primary magnetite and hematite in association with sulphide suggests that the oxygen fugacity ($\log_{10} fO_2$) was between -35 and -40, and that the temperature was in excess of 250°C (Large, 1977; Franklin et al., 1981). Heald-Wetlaufer et al. (1983), Bonham and Giles (1983), and Bonham (1986), identify several low-sulphur precious-metal epithermal deposits hosted by volcanic rocks. Although volcanic rocks have not been identified at Mount Clement the deposit may be of this general type.

Sediment-hosted precious metal deposits of hydrothermal non-volcanic origin are typically formed in carbonaceous silty dolomite, limestone, and calcareous siltstone and claystone (Bagby and Berger, 1985). In many instances these rocks have been subjected, variously, to silicification, decalcification, argillization, and carbonatization. Supergene alteration is dominated by oxidation: numerous oxides and sulphates have been formed, and fine-grained gold has been separated from its primary sulphide host. Trace elements commonly enriched during this alteration include: arsenic, barium, mercury, antimony, and thallium. Bagby and Berger (1985) recognized two forms of hydrothermal non-volcanic deposit: a Carlin type, where pod-like zones of mineralization are difficult to distinguish from host rock; and a jasperoid type, where most mineralization is concentrated in jasperoid, quartz veins, or related siliceous rocks. Each of these types may be subdivided depending on whether the deposit is gold- or silver-rich.

The Main prospect, though it cannot be confidently assigned to either of these two types of hydrothermal deposit, has many of the features of this style of mineralization: silty, carbonatized host rock; fine-grained gold; silicification, argillization, and decalcification, as the main alteration features; an appropriate association of trace elements (possibly excepting barium); and abundant base-metal and arsenic oxidate minerals. In addition, many of the silicified rocks qualify as jasperoids—defined by Lovering and Heyl (1974, p. 48) as epigenetic rock bodies " formed largely by fine-grained chert-like siliceous replacements of a pre-existing rock"; they are distinguished from chert, which is a "siliceous rock formed at or near the time of sedimentation". In view of the large amount of silver in some of the talc and gossan, the Main prospect probably qualifies as a silver-rich deposit.

In summary—and on the basis of mixed clastic and chemical sedimentation, stratabound breccias, and chert "sinter" in the UBZ — the hydrothermal sequence of the Main prospect is interpreted as a hot-spring deposit. The proposed sequence of events (Figs 16A–16E) for the formation of this hydrothermal sequence is:

(a) Tectonic disruption of a subsiding marine basin created a conduit for hydrothermal fluids. Initial deposition of chemical sediments (carbonates) occurred at the same time as clastic sedimentation. Precipitation of massive dolomite coincided with a period of low clastic input (Fig. 16A)

(b) Increased hydrothermal activity was accompanied by precipitation of precious metals and copper at depth.

(c) Local sealing of the vent, accompanied by increasing fluid temperatures, produced extreme over-pressurization and phreatic eruption. Subsequent mineralization precipitated from hydrothermal fluids and was largely confined to the hydrothermal breccias. Vent sealing and explosive brecciation occurred a further three times; most mineralization was introduced to its present position during the second and third eruptions (Figs 16B and C).

(d) The passage of hot hydrothermal fluids through the lower parts of the sequence caused slight albitization of the host rock, and altered part of the early-formed carbonate to talc. Silver precipitation accompanied the formation of talc (Fig. 16C).

(e) The hydrothermal system reached maximum temperatures between eruptions three and four. As temperatures waned, iron, manganese, and silica, continued to be precipitated in the upper part of the

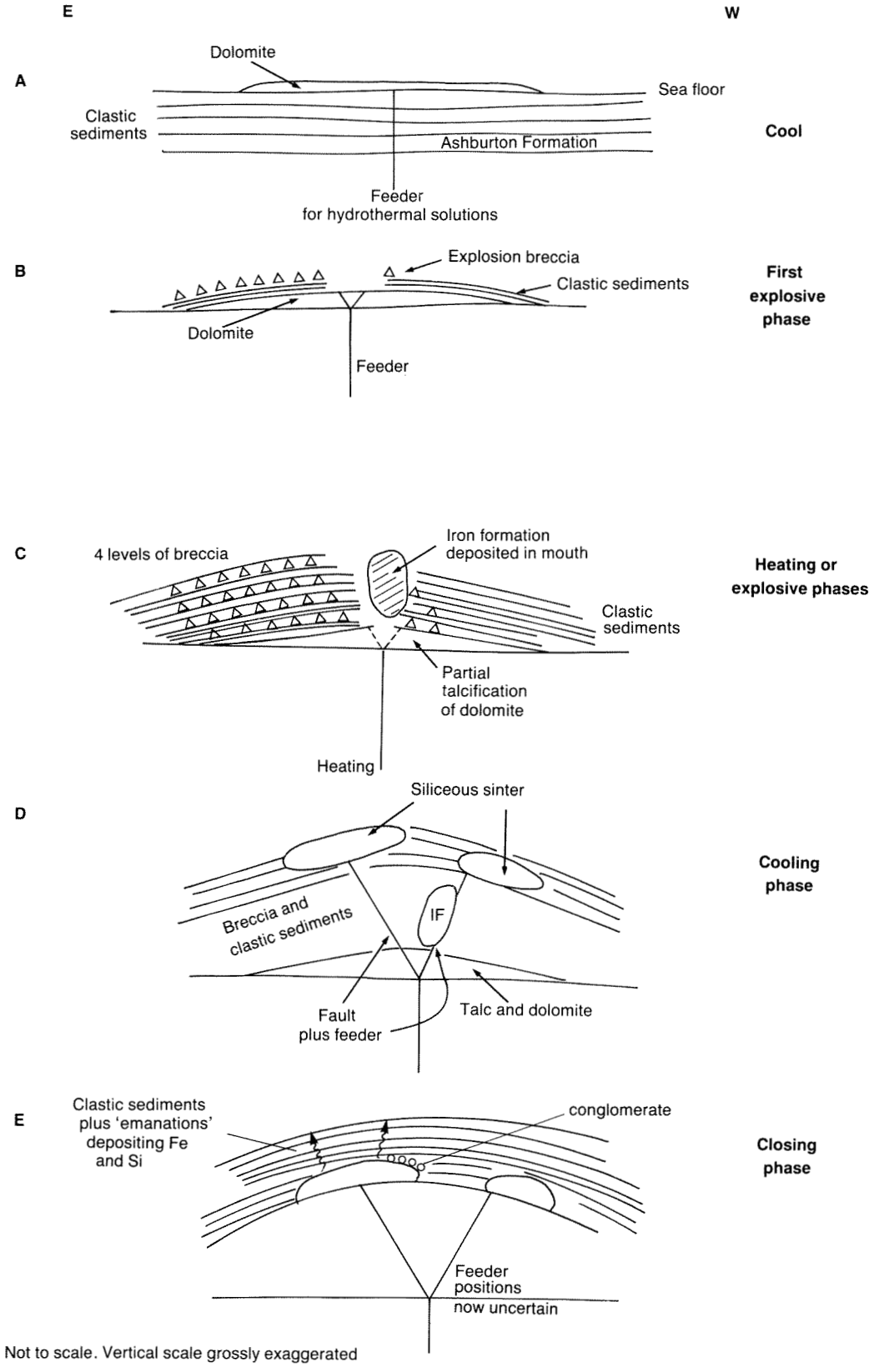

Figure 16. Diagrammatic sketch of the possible development of the hydrothermal sequence at the Main prospect: A — Beginning of spring. B — First explosive phase; heating period. C — Situation at close of fourth explosive phase; maximum heating in phases two and three. D — Cooling phase; deposition of barren silica. E — Final, waning phase.

sequence, and clastic sedimentation became dominant except in the vicinity of the main spring. Lower in the hydrothermal sequence, conditions became more oxidizing and there was some remobilization of early mineralization (Fig. 16D).

(f) In the dying phases of activity, clastic sedimentation dominated, but a small volume of hydrothermal fluid added traces of silica, manganese, and iron, to the sediments (Fig. 16E).

Eastern prospect and quartz–scorodite veins

Mineralization at the Eastern prospect occurs in fractures that formed during the latter part of the D_2 deformation and is, therefore, younger than syngenetic enrichment in the Main prospect. Thorne and Seymour (1991) noted that most of the known mineral occurrences in the Ashburton Basin are sulphide-rich, and are associated with faults and veins formed during the D_2 dextral wrenching event. At the Eastern prospect, sulphur required for precipitating base metals seems to have been derived in part from the enclosing host-rock, as country rock adjacent to the vein is depleted in sulphide.

The quartz–scorodite veins cross-cut D_1 structures and early D_2 folds. It is probable that they are related to wrench faults, formed during late D_2 deformation (Thorne and Seymour, 1991) and thus have affinities with the Eastern prospect mineralization.

Mineralization in the Ashburton Basin

Small quantities of gold, silver, copper, and lead, have been extracted from the Ashburton Basin since the latter part of the nineteenth century. Most deposits are vein-hosted sulphides (gold occurs with pyrite or arsenopyrite) associated with major west-northwesterly to north-northwesterly trending dextral wrench faults and their related synthetic and antithetic shears (Thorne and Seymour, 1991). The only examples of pre-D_2, mineralization, other than at Mount Clement, occur at Yarraloola, where copper sulphides formed in a distal volcanogenic–sedimentary setting (Marston, 1979), and at Mount Stuart where weak stratiform lead mineralization is associated with felsic volcanic tuff (Doust, 1984).

Descriptions of prospects and mines in the Ashburton Basin (Simpson, 1926; Blockley, 1971; Marston, 1979; Doust, 1984) suggest that, though gold, copper, and lead, have been the dominant elements of commercial interest, accessory to anomalous amounts of silver, arsenic, bismuth, antimony, thallium, uranium, and zinc, are also common. These elements are associated with both early (pre-D_1) and late (post-D_2) deposits, and suggest a common source for the mineralization. Doust (1984) suggested that formation waters within the thick basin succession gained metals as lithic fragments underwent burial metamorphism. Additional metal-rich connate brines, pressurized by structural loading or igneous intrusion, may also have entered the system along lines of deep crustal weakness. Thorne and Seymour (1991) interpreted the Wyloo Group as an active-margin to foreland-basin succession which was laid down and deformed during continental crustal collision between the Pilbara and Yilgarn cratons. This environment, in which rapid subsidence and sedimentation was accompanied by significant horizontal shortening, would have promoted fracture development, over-pressurization, and fluid movement, in the crustal and supracrustal succession.

Syngenetic hydrothermal sequences such as the Mount Clement Main prospect, and late-stage wrench fault systems are important targets for future mineral exploration in the Ashburton Basin. To date, no other examples of a Main prospect style of mineralization have been reported. The surface expression of the Main prospect is marked by a distinctive ferruginous gossan that contains a variety of copper–arsenic minerals. The absence of gold nuggets in the area around the prospect suggests the discovery of further examples of this style of mineralization may depend upon the recognition of other gossanous outcrops, coupled with sampling for appropriate trace elements (Thorne and Seymour, 1991). High levels of arsenic are associated with mineralization at Mount Clement and elsewhere in the Ashburton, but are not specific to gold. Anomalous levels of silver, arsenic, gold, bismuth, cerium, copper, mercury, lanthanum, lead, antimony, tin, thorium, thallium, uranium, tungsten, and zinc, have been recorded at Mount Clement, but it is not known if this association has any significance in a regional context.

Conclusions

The Main prospect at Mount Clement lies within a lens of oxidized and silicified siliciclastic and chemical rocks, which are generally conformably confined within the Ashburton Formation. The lower part of the lens (LMZ) contains anomalous levels of silver, arsenic, gold, bismuth, cerium, copper, mercury, lanthanum, lead, antimony, thorium, thallium, uranium, tungsten, and zinc. The upper part of the lens (UBZ) is extensively silicified and ferruginzed, and is characterized by anomalous manganese.

On the following bases, the Main prospect is interpreted as a sediment-hosted, deep-marine, hot-spring deposit:

(a) the lithology and stratabound nature of the deposit, coupled with the lack of quartz veining;

(b) the overall size and shape of the deposit, which is consistent with modern hot-spring deposits;

(c) the four stratabound mineralized breccia zones within the LMZ, whose properties are consistent with brecciation in a hydrothermal system;

(d) deuterium-isotope data from talc, which suggests mineralizing-fluid temperatures of 350–400°C; and

(e) trace-element assemblages which are similar to those of other sediment-hosted epithermal deposits.

The Eastern prospect at Mount Clement is a sulphide-bearing fill in a fracture that formed as a result of dextral wrenching after the deposition of the Ashburton Formation. It is characterized by anomalous levels of silver, arsenic, gold, copper, molybdenum, antimony, and tin, which may have been derived, in part by leaching of wall rocks.

Similar trace-element assemblages in the Main and Eastern prospects suggest that both early and late mineralization tapped a common source. Metal-bearing fluids were probably released during burial metamorphism of the supracrustal sequence, and subsequently transported along major fractures. These fractures were either formed, or reactivated, during continental crustal collision between the Pilbara and Yilgarn Cratons.

The discovery of further examples of Mount Clement-style mineralization may depend upon the recognition of other ferruginous copper-arsenic gossans, or upon the identification of areas with anomalous silver, arsenic, gold, bismuth, copper, mercury, lead, antimony, tin, thorium, thallium, uranium, tungsten, and zinc.

Acknowledgements

The authors thank John White, John Dow, Dave Sargeant, and staff of Norseman Gold Mines NL for constructive discussion in the early stages of the project. Mallina Mining, Western Mining Corporation, and Norseman Gold Mines NL, provided access to the drill cuttings and core. On-site facilities were provided by Norseman Gold Mines.

Appendix

Minerals identified at the Mount Clement prospects

Unoxidized "ore" minerals

Arsenopyrite occurs in both massive and disseminated forms; where the matrix is soft, e.g. in talc, perfect crystals, some with butterfly or interpenetrating twins, are present. There has been replacement by supergene copper sulphides.

Pyrrhotite is present in both hexagonal and monoclinic phases; most is granular, and lacks crystal form; however, hexagonal plates occur at the Eastern prospect.

Pyrite is relatively uncommon, and is subordinate to both arsenopyrite and pyrrhotite.

Chalcopyrite is a minor constituent preserved in chert or quartz.

Boulangerite ($Pb_5Sb_4S_{11}$) occurs as disseminated fibrous crystals and massive granular aggregates at the Eastern prospect.

Jamesonite ($Pb_4FeSb_6S_{14}$): an iron-rich variety is present at the Eastern prospect.

Galena is associated in minor amounts with boulangerite at the Eastern prospect.

Gold: none has been observed in fresh sulphide, but it occurs in Main prospect gossans as very small flat or elongate grains, or as "paint"or "leaf" in fractures. "Primary" gold contains Ag and Bi.

Oxidized "ore" minerals

Scorodite ($FeAsO_4.2H_2O$) is ubiquitous at both prospects; boxworks indicate pseudomorphous replacement of arsenopyrite and pyrite. Euhedral grains present in cavities in quartz.

Arseniosiderite ($Ca_3Fe_4(AsO_4)_4(OH)_6.3H_2O$) appears to be pseudomorphous after scorodite, at the Main prospect, no well-developed crystals.

Chenevixite ($Cu_2Fe_2(AsO_4)_2(OH)_4.H_2O$) occurs as earthy masses at the Main prospect in many shades of green.

Conichalcite ($CaCu(AsO_4)(OH)$) occurs at the Main prospect mainly as emerald-green acicular-botryoidal crusts lining fractures.

Digenite/covellite replace arsenopyrite in oxidized zone.

Cornubite ($Cu_5(AsO_4)_2(OH)_6$) occurs as rare greenish-blue botryoidal grains associated with chenevixite.

Unidentified copper-silver arsenate discovered by scanning electron microscope analysis in the Main prospect, has not been seen optically, and may be a new mineral.

Philipsbornite ($PbAl_3H(AsO_4)_2(OH)_6$) occurs as compact greyish-yellow masses at the Eastern prospect. Unlike the holotype this variety has high Sb.

Bindheimite ($Pb_2Sb_2O_6(O,OH)$) occurs as brown vitreous to resinous masses with philipsbornite at the Eastern prospect.

Jarosite ($KFe_3(SO_4)_2(OH)_6$) occurs in veins and crusts at the Eastern prospect.

Plumbogummite ($PbAl_3(PO_4)_2(OH)_5.H_2O$) occurs as very small grains, mixed with quartz in siliceous ironstone and gossan at the Eastern prospect.

Chlorargyrite ($AgCl(Br,I)$) has been observed in talc, quartz and carbonate at the Main prospect.

Iodoargyrite ($AgI(Cl)$) is associated with secondary gold at the Main prospect.

Carminite ($PbFe_2(AsO_4)_2(OH)_2$) occurs as pseudomorphs after pyrite in the Eastern gossan.

Ullmanite ($NiSbS$) occurs in trace amount in the Eastern prospect.

Gangue minerals

Goethite is abundant in gossans; boxwork textures indicate pseudomorphous replacement of pyrite or arsenopyrite; occasionally it contains anomalous As, Sb, and, at the Main prospect, Bi.

Gypsum and anhydrite have been detected in trace amounts at the Main prospect in some gossans and siltstones.

Talc/dolomite: talc, and talc partly replacing dolomite, contains silver minerals and arsenopyrite, and can be regarded as gangue.

Epidote has been observed in a gossan at the Main prospect, where it is closely associated with arseniosiderite, and possibly replaces scorodite.

Quartz in narrow veins and segregations is present at both prospects; it usually has a fine-grained granular texture and, only rarely, the coarse-grained sparry texture of hydrothermal veins.

Chlorite commonly has anomalous polarization colours; it is the second most abundant gangue mineral at the Main prospect.

Muscovite is a minor constituent of some veins.

Apatite is present in cavities representing former arsenopyrite.

Tourmaline in the form of pale-blue crystals of ?dravite, occurs in some veins at the Main prospect.

Rutile occurs as clusters of anhedral grains and needles with lead minerals.

Ilmenite occurs unusually as needles in some places at the Main prospect.

"Berthierine" is dark brown, coarsely crystallized pleochroic mineral, associated with chlorite; XRD shows the mineral to have serpentine structure and X-ray pattern similar to berthierine—$(Fe,Mg)_{2-3}(SiAl)_2O_5(OH)_4$.

Host rock minerals

Quartz: microquartzitic or novaculite texture is common.

Albite is detrital in clastic sediments, and is also present in hydrothermal veins with quartz and biotite.

Microcline is a minor detrital constituent of siltstones and shales.

Orthoclase occurs as disseminated grains in metamorphosed shale.

Tourmaline is a common detrital mineral; it is pleochroic from green to brown, rarely to blue.

Zircon is rare in detrital sediments.

Talc occurs in the mineralized sequence only, where it is usually associated with other Mg-rich minerals including chlorite and phlogopite.

Chlorite is mostly of metamorphic origin; its optical properties are very variable.

Muscovite is the most common mica; it is usually fine-grained (sericitic).

Phlogopite is usually porphyroblastic, and is abundant in dolomitic siltstone.

Biotite is partly retrograded to chlorite.

Hornblende is ferrohastingsitic, rich in Al and Fe; it is metamorphic or metasomatic in origin.

Tremolite occurs in metamorphosed siliceous dolomite.

Garnet occurs at Main prospect where it is metamorphic or metasomatic in origin; the variety is spessartine-almandine, with a minor proportion of andradite molecule.

Kaolinite occurs in the hydrothermal association with talc; in other places it is a weathering product.

Montmorillonoid clays are associated only with talc.

Vermiculite occurs with illite and quartz in greenish-white spots in schists, and may represent former cordierite.

Interstratified clay occurs in altered biotite schist.

Dolomite is partly recrystallized to marble; some is siliceous; some is partly altered to talc.

Other carbonates: magnesite is present as an alteration product at the surface; siderite is present in BIF; calcite is present as a minor component in veins and tension gashes.

Magnetite is rare;, it has been more abundant, but most is altered to hematite.

Hematite is common in the Main prospect in siltstones, quartz-hematite rock and BIF; much is secondary, but a proportion may be primary.

Carbon: finely dispersed opaque material, consistent with carbon, occurs as laminae in some talc-rich rocks.

Pyrite is relatively abundant as disseminated grains within silt- and mudstone country-rock; syngenetic pyrite is generally coarser and better formed.

References

BAGBY, W. C. and BERGER, B. R., 1985, Geologic characteristics of sediment hosted, disseminated precious metal deposits in the western United States, *in* Geology and geochemistry of epithermal systems, *edited by* B. R. Berger and P.M. Bethke: Society of Economic Geologists, Reviews in Economic Geology, v. 2, p. 169–202.

B.H.P. Co., Ltd., 1975, Report for the year 1974 on mineral claims 08/2201-08/2203, 08/2218-08/2224 and GML's 08/52-08/56, Ashburton Goldfield, Western Australia: unpublished report to the W.A. Mines Department for the year ended 31 December 1974.

B.H.P. Co., Ltd., 1976, Mineral claims 08/2201-08/2203, 08/2218-08/2224 and GML's 08/52-08/56, Ashburton Goldfields, Western Australia: unpublished report to the W.A. Mines Department for year ended 31st December 1975.

BISCHOFF, J. L., and PITZER, K. S., 1985, Phase relations and adiabats in boiling seafloor geothermal systems: Earth Planetary Science Letters, v. 75, p. 327–338.

BLOCKLEY, J. G., 1971, The lead, zinc and silver deposits of Western Australia: Western Australia, Geological Survey, Mineral Resources Bulletin 9.

BONHAM, H. F. Jr., 1986, Models for volcanic-hosted epithermal precious metal deposits—A review, *in* Volcanism, hydrothermal systems and related mineralization: International Volcanological Congress, Symposium 5, Auckland, Proceedings p. 13–17.

BONHAM, H. F. Jr. and GILES, D. L., 1983, Epithermal deposits—The geothermal connection: Geothermal Resources Council, Special publication 13, p. 257–262.

BROWNE, P. R. L. and LLOYD, E. F., 1986, Water-dominated geothermal systems and associated mineralization: New Zealand Geological Survey, Record 11.

CLARK, L. A., 1960, The Fe–As–S system—Phase relations and applications: Economic Geology, v. 55, p. 1345–1381 and p. 1631–1652.

DANIELS, J. L., 1975, Gascoyne Province: Western Australia, Geological Survey, Memoir 3, p. 107–113.

DAVY, R., CLARKE, R. M. C. and SEYMOUR, D. B., 1989, Geochemical data from the Mount Clement gold and lead prospects, Ashburton Basin, Western Australia: Western Australia, Geological Survey, Record 1989/16.

DOUST, G., 1984, Stratiform polymetallic sulphide mineralization—An exploration perspective for the Ashburton Basin, Western Australia: James Cook University, M.Sc. thesis (unpublished).

FRANKLIN, J. M., SANGSTER, D. M., and LYDON, J. W., 1981, Volcanic-associated massive sulphide deposits: Economic Geology, 75th Anniversary Volume, p. 485–627.

GEE, R. D., 1979, Structure and tectonic style of the Western Australian shield: Tectonophysics, v. 58, p. 327 - 369.

HAUSEN, D. M., 1967, Fine gold occurrence at Carlin, Nevada, *cited by* W. C. Bagby and B. R. Berger, 1985: Columbia University, Ph.D. thesis, 166 p.

HEALD-WETLAUFER, P., HAYBA, D. O., FOLEY, N. K., and GOSS, J. A., 1983, Comparative anatomy of epithermal precious and base-metal districts hosted by volcanic rocks: U.S.A., Geological Survey, Open-file report 83-710, p. 16.

HEDENQUIST, J. W., 1986, Hydrothermal eruptions in the Waiotapu geothermal system, New Zealand—Their cause, breccia deposits and hydrological effect, *in* Volcanism, hydrothermal systems and related mineralization: International Volcanological Congress, Symposium 5, Auckland, Proceedings p. 98.

HEDENQUIST, J. W., and HENLEY, R. W., 1985, Hydrothermal eruptions in the Waiotapu geothermal system, New Zealand—Their origin, associated breccias and relation to precious metal mineralization: Economic Geology, v. 80, p. 1640–1668.

LARGE, R. I., 1977, Chemical evolution and zonation of massive sulphide deposits in volcanic terrains: Economic Geology, v. 72, p. 549–572.

LINDGREN, W., 1933, Mineral deposits (4th edn): New York, McGraw-Hill, 930p.

LLOYD, E. F., 1959, The hot springs and hydrothermal eruptions of Waiotapu: New Zealand Journal of Geology and Geophysics, v. 2, p. 141–176.

LLOYD, E. F., 1972, Geology and hot springs of Orakeikorako: New Zealand, Geological Survey, Bulletin 85, 164p.

LOVERING, T. G. and HEYL, A. V., 1974, Jasperoid as a guide to mineralization in the Taylor Mining District and vicinity, near Ely, Nevada: Economic Geology, v. 69, p. 46–58.

MARSTON, R. D., 1979, Copper in Western Australia: Western Australia, Geological Survey, Mineral Resources Bulletin 13.

NAIRN, I. A. and SOLIA, W., 1980, Late Quaternary hydrothermal explosion breccias at Kawerau geothermal field, New Zealand: Bulletin Volcanologique, v. 43, p. 1–13.

NELSON, C. E. and GILES, D. L., 1985, Hydrothermal eruption mechanisms and hot spring gold deposits: Economic Geology, v.80, p. 1633–1639.

NEWMONT PROPRIETARY LTD, 1980, 1979 Annual report on Mt. Clement prospect, Western Australia: Unpublished report to the W.A. Mines Department.

NEWMONT PROPRIETARY LTD, 1981, 1980 Annual report on Mt. Clement prospect, Western Australia: Unpublished report to the W.A. Mines Department.

NEWMONT HOLDINGS PTY LTD, 1982, 1981 Annual report on Mt. Clement prospect, Western Australia: Unpublished report to the W.A. Mines Department.

RADTKE, A. S., 1985, Geology of the Carlin gold deposit, Nevada: U.S.A., Geological Survey, Professional Paper 1267, 124p.

SILBERMAN, M. L. and BERGER, B. I., 1985, Relationship of trace-element patterns to alteration and morphology in epithermal precious-metal deposits, *in* Geology and geochemistry of epithermal systems, *edited by* B.R. Berger and P.M. Bethke: Society of Economic Geologists, Reviews in Economic Geology, v. 2, p. 203–232.

SIMPSON, E. C., 1926, The minerals of the Ashburton and Gascoyne valleys, *in* A geological reconnaissance of part of the Ashburton drainage basin, *by* H. W. B. Talbot: Western Australia, Geological Survey, Bulletin 85, p. 72–108.

SOLOMON, M. and WALSHE, J. L., 1981, The formation of massive sulfide deposits on the sea floor: Economic Geology, v. 74, p. 797–813.

TAYLOR, H. P. Jr.,1974, The application of oxygen and hydrogen isotope studies to problems of hydrothermal alteration and ore deposition: Economic Geology, v. 69, p. 843–883.

THORNE, A. M. and SEYMOUR, D. L., 1991, The geology of the Ashburton Basin: Western Australia, Geological Survey, Bulletin 139.

TRENDALL, A. F., 1979, A revision of the Mount Bruce Supergroup: Western Australia, Geological Survey, Annual Report 1978, p. 63 –71.

WEISSBERG, B. G., BROWNE, P. I. L., and SEWARD, T. M., 1979, Ore metals in active geothermal systems, *in* Geochemistry of hydrothermal ore deposits, *edited by* H.L. Barnes : New York, John Wiley and Sons, p. 738–780.

WHITE, D. E., 1955, Violent mud-volcano eruptions of Lake City hot-springs, northeast California: Geological Society America, Bulletin, v. 66, p. 1109–1130.

LAMPNORM
A scheme for calculating the normative minerals of lamproites

by

J. D. Lewis

ABSTRACT

The CIPW norm calculation is inappropriate for lamproites as a result of the peculiar K_2O- and TiO_2-rich nature of the magma and the consequent abundance of K_2O- and TiO_2-rich minerals. Rocks with abundant modal leucite are reported as quartz- and orthoclase-normative. A scheme has been devised to calculate only the minerals actually present in lamproites, and to report excess SiO_2 as a remainder. LAMPNORM calculates leucite, phlogopite, potassic richterite, diopside, olivine, and the minor minerals priderite, wadeite, chrome spinel, apatite, calcite and barite. LAMPNORM is particularly oriented towards the lamproites of the West Kimberley Province, but may be modified for other groups with differing mineralogy.

Keywords: Lamproite, norm calculation.

All "norm" calculations recast the chemical analysis of a rock into a number of standard, or "normative" minerals, according to a fixed set of rules. The result is that rocks of similar bulk chemistry but different cooling histories, or degrees of alteration, can be compared by considering their ideal, or normative mineralogy rather than their actual, or modal mineralogy. The original scheme of Cross, Iddings, Pirsson, and Washington (1903) —the CIPW norm—was devised in conjunction with a complex nomenclature for a chemical and mineralogical classification of igneous rocks. The artificiality of the classification, and the cumbersome nomenclature, ensured that the scheme was not widely adopted, but the norm calculation itself, and a number of concepts embodied within it, proved popular with petrologists and are still widely used. For example, the concept of silica saturation of a rock, the term "mafic" to group the ferromagnesian minerals, and "perpotassic" to describe rocks in which K_2O is greatly in excess of Na_2O, are all derived from the CIPW classification of igneous rocks.

The essential features of the CIPW calculation are as follows:

(a) All normative minerals are anhydrous—thus, hornblende and biotite are not calculated in the norm.

(b) All normative minerals have a fixed composition.

(c) For a given analysis, all mafic minerals have the same magnesium/iron ratio.

(d) All mafic minerals are free of Al_2O_3, which is combined only in feldspar and feldspathoid minerals.

(e) Quartz is incompatible in the norm with olivine and feldspathoid minerals.

Using these principles, the various oxides are allocated to form minerals in a particular sequence, beginning with apatite and calcite, followed by the feldspars, ilmenite, magnetite, and hematite, and ending with the mafic minerals diopside and hypersthene. If at the end of this calculation there is insufficient SiO_2 to satisfy the equation, then hypersthene, albite, and orthoclase, are successively "desilicated" to form olivine, nepheline, and leucite, until the equation balances. Details of the rules for calculating the CIPW norm are given in Johannsen (1939) and Hutchison (1974).

The resulting CIPW norm is still basically an aid to the classification of rocks, distinguishing between suites of rocks that are oversaturated or undersaturated in SiO_2, or that fulfil any other particular mineralogical criteria useful to the petrologist. The norm is also useful for emphasizing the mineralogical variation that may result from quite subtle changes in chemistry; and the normative minerals—e.g. quartz, orthoclase, and albite—are often plotted on triangular diagrams to show variation within a suite of rocks.

The original CIPW system was designed for the common range of basaltic and gabbroic compositions, and the resulting norms for rocks of this composition show close correspondence with the modal mineralogy of coarse-grained, slowly cooled gabbroic rocks. Other rock types, such as picrite, pyroxenite, peridotite, and dunite, which consist essentially of those minerals calculated in the CIPW norm, also show close correspondence between the calculated and actual mineralogy, although the small amounts of K_2O show up in the norm as orthoclase, a mineral not usually found in ultrabasic rocks.

In less magnesian rocks, in which the modal mafic mineralogy includes hornblende or biotite, the CIPW norm is less satisfactory. For granites and related rocks, the feldspar proportions compare well with the modal mineralogy, but biotite is represented by normative hypersthene, and hornblende-bearing varieties often contain diopside in the norm.

A number of minor variations have been made by some authors to the CIPW calculation, to exclude calcite from the norm, or to report TiO_2 as rutile rather than sphene, but these do not make a significant difference to the result. Similarly, the molecular norm proposed by Niggli (1954), is easier to calculate but differs only in reporting the norm in molecular per cent rather than weight per cent. The only significantly different normative scheme is that of Barth (1955), which allows MgO and FeO to be calculated as biotite + riebeckite, or actinolite + riebeckite + edenite (= hornblende), where appropriate. For granitic rocks the Barth "Mesonorm", reporting biotite, is more appropriate to the modal mineralogy, and less likely to over-estimate orthoclase. For intermediate igneous and metamorphosed basic rocks, such as amphibolite, the Barth Mesonorm, set to calculate hornblende, provides a realistic estimate of the mineralogy. Complete schemes for calculating both the Niggli Catanorm and the Barth Mesonorm are given in Hutchison (1974).

Lamproites and the CIPW norm

Lamproite is a rare rock type which has risen to prominence in recent years as a source of natural diamonds (Atkinson et al., 1984). Geochemically the rocks are characterized by extremely high contents of K_2O, TiO_2, Zr, Sr, Ba, and F, combined with low levels of CaO and Al_2O_3, and extremely low Na_2O, and a K_2O/Al_2O_3 ratio that commonly exceeds unity (Jaques et al., 1986; Lewis, 1987). The affinity of these rocks with kimberlites is shown by the high content of MgO, Cr, and Ni, of the olivine lamproites which, except for high TiO_2 may be compared chemically with Group II Kimberlites (Dawson, 1987; Lewis, 1987).

The distinctive chemistry of the lamproites strains the credibility and usefulness of the CIPW norm. Rocks which consist essentially of leucite, phlogopite, diopside, and olivine, are reported as quartz normative, rich in orthoclase and hypersthene, but with no leucite or diopside. The simple modification of reporting excess TiO_2 as rutile rather than sphene is enough to restore minor amounts of diopside to the norm (Table 1, column A), but the normative mineralogy still includes many minerals which do not occur in reality. However, the CIPW system may be simply modified to accommodate any mineral of reasonably constant composition which might bring the normative mineralogy into better agreement with the modal mineralogy. Such a scheme was suggested by Lewis (1987), in which the calculation of pyrite, fluorite, sphene, rutile, and ilmenite, none of which occur modally, is eliminated. Zircon is replaced by wadeite ($Zr_2K_4Si_6O_{18}$); S is calculated as barite ($BaSO_4$); and TiO_2 and excess Ba are calculated as priderite ($K_2O.0.667BaO.Fe_2O_3.14TiO_2$). The result (Table 1, column B) is a slightly more realistic norm with respect to the minor minerals; less K_2O reported as potassium metasilicate, but there was no significant change in the proportion of diopside or hypersthene.

The only innovative feature of the modified CIPW norm of Lewis (1987) is the ability to set the 100 Mg/(Mg+Fe) ratio of the mafic minerals to any desired level. The standard CIPW calculation assumes a constant ratio for the mafic minerals, but its actual level is determined by the FeO remaining after the calculation of chromite, ilmenite, and magnetite. Furthermore, if the rock is oxidized, the FeO content is lowered, and there is often little FeO left for the mafic minerals. Greater realism is introduced if iron is allocated preferentially to MgO at the beginning of the calculation, with any deficiency taken up by converting Fe_2O_3 to FeO. The method used is outlined in rule 10 below, and the result illustrated in Table 1, column C, where an Mg number of 91 is adopted. This ratio is that commonly found in lamproite minerals of the West Kimberley lamproites (Jaques et al., 1986).

A norm calculation for lamproites

It is evident that the extent to which the CIPW norm can be modified to correspond with the reality of lamproite modal mineralogy is limited. Despite the presence of modal leucite, the leucite lamproites are quartz normative, and despite the absence of modal leucite, the olivine lamproites are strongly orthoclase normative. In addition, the CIPW norm calculation produces abundant acmite and K-metasilicate, which cannot easily be equated with the potassic richterite and phlogopite present in the mode. The actual mineralogy of lamproites results from the rapid cooling of a K_2O- and TiO_2-rich magma. At the high temperature of eruption, leucite and phlogopite were stable phases, and there was insufficient cooling time for the leucite to invert to microcline. Also, the modal mineralogy is the result of partial crystallization, as the lamproites commonly contain abundant glass, or its devitrification products, in the groundmass. The equilibrium mineralogy of slowly cooled lamproites is not known, as there are no plutonic members of the suite. Nevertheless, the magma is also relatively SiO_2-rich, and there is therefore no method for distributing the elements between phlogopite, diopside, and olivine, which would leave an undersaturated residue to form leucite by the usual CIPW style calculation.

If a norm that bears some relationship to the modal mineralogy is to be calculated for West Kimberley lamproites, then a radical approach must be taken. The mineralogy of the lamproites is relatively simple: leucite, phlogopite, potassic richterite, diopside, olivine; minor amounts of chrome spinel, priderite, perovskite, wadeite, barite, and calcite; and, in many specimens, abundant interstitial glass. Although phlogopite and potassic richterite are commonly zoned to more Ti- and Fe-rich margins, the bulk of each mineral is fairly constant in composition, with a reasonably constant 100 Mg/(Mg+Fe) ratio for the mafic minerals (Jaques et al., 1986). A norm which avoids allocation of oxides to theoretical minerals or to minerals not present in the mode may, therefore, be calculated on the basis of this limited list of minerals. Such a calculation, LAMPNORM,

TABLE 1. COMPARISON OF NORMS CALCULATED BY CIPWNORM AND LAMPNORM

	71366 Leucite lamproite Rice Hill					*71456A Olivine lamproite Ellendale 9*					*Chemical analyses and modal mineralogy*		
Mineral	*A*	*B*	*C*	*D*	*E*	*A*	*B*	*C*	*D*	*E*		71366	71456A
Quartz	1.78	0.96	0.50	(a)	(a)	....	....	....	(a)	(a)	SiO_2	51.00	36.81
Orthoclase	43.74	43.58	43.60	(a)	(a)	21.60	13.29	10.01	(a)	(a)	TiO_2	6.04	3.33
K-metasilicate	3.62	2.55	2.55	(a)	(a)	1.84	1.21	1.21	(a)	(a)	Al_2O_3	7.70	4.01
Leucite	....	....	....	29.64	27.83	1.64	8.15	10.75	....	....	Fe_2O_3	4.70	5.38
Acmite	6.28	6.26	6.26	(a)	(a)	3.79	3.79	3.79	(a)	(a)	FeO	1.84	4.00
Phlogopite	(a)	(a)	(a)	11.55	15.42	(a)	(a)	(a)	36.56	36.99	MnO	0.07	0.14
Al-phlogopite	(a)	(a)	(a)	(5.87)	(9.64)	(a)	(a)	(a)	(36.56)	(36.99)	MgO	9.18	23.40
Al,Fe-phlogopite	(a)	(a)	(a)	(5.68)	(5.78)	(a)	(a)	(a)	....	....	CaO	4.02	5.80
K-richterite	(a)	(a)	(a)	22.56	22.95	(a)	(a)	(a)	13.91	14.06	Na_2O	0.81	0.47
Diopside	14.30	14.83	14.90	7.85	7.97	8.00	9.95	10.01	4.58	4.62	K_2O	9.24	4.74
Ca-enstatite	(b)(14.30)	(13.78)	(13.38)	(7.85)	(7.16)	(8.00)	(9.30)	(8.99)	(4.36)	(4.15)	P_2O_5	0.45	2.85
Ca-ferrosillite	....	(1.05)	(1.52)	....	(0.81)	....	(0.65)	(1.02)	(0.22)	(0.47)	H_2O+	2.01	6.00
Hypersthene	17.16	18.84	19.79	(a)	(a)	....	....	....	(a)	(a)	H_2O^-	1.09	1.12
Enstatite	(17.16)	(17.32)	(17.51)	(a)	(a)	....	....	....	(a)	(a)	CO_2	0.06	0.15
Ferrosillite	....	(1.52)	(2.28)	(a)	(a)	....	....	....	(a)	(a)			
Olivine	....	....	....	....	....	41.61	44.80	47.23	22.42	25.46	Total	100.05	100.40
Forsterite	....	....	....	....	....	(41.61)	(41.16)	(41.31)	(21.08)	(22.27)			
Fayalite	....	....	....	....	....	....	(3.65)	(5.92)	(1.34)	(3.19)	Ba	11 673	13 465
Magnetite	....	2.63	2.05	5.73	3.97	4.22	5.79	3.97	8.31	5.66	Sr	1 197	1 341
Hematite	2.72	....	....	(a)	(a)	1.61	....	....	(a)	(a)	Zr	1 113	723
Chromite	0.19	0.19	0.19	(a)	(a)	0.25	0.25	0.25	(a)	(a)	Cr	832	1 084
Chrome spinel	(a)	(a)	(a)	0.23	0.23	(a)	(a)	(a)	0.31	0.31	Ni	224	1 200
Ilmenite	4.09	(a)	(a)	(a)	(a)	6.85	(a)	(a)	(a)	(a)	S	180	100
Priderite	(a)	8.26	8.26	5.67	5.39	(a)	4.75	4.76	0.99	0.99	F	2 745	6 450
Rutile	4.13	(a)	(a)	(a)	(a)	....	(a)	(a)	(a)	(a)	Cl	202	110
Apatite	1.09	1.09	1.09	1.11	1.11	7.17	7.16	7.17	7.30	7.31			
Zircon	0.23	(a)	(a)	(a)	(a)	0.16	(a)	(a)	(a)	(a)			
Wadeite	(a)	0.50	0.50	0.50	0.50	(a)	0.34	0.34	0.34	0.34	Leucite	30.1	....
Fluorite	0.50	(a)	(a)	(a)	(a)	0.87	(a)	(a)	(a)	(a)	Phlogopite	15.4	15.7
Pyrite	0.04	(a)	(a)	(a)	(a)	0.02	(a)	(a)	(a)	(a)	K-richterite	16.7	13.5
Calcite	0.14	0.14	0.14	0.14	0.14	0.37	0.37	0.37	0.37	0.37	Diopside	9.0	3.5
Barite	(a)	0.14	0.14	0.14	0.14	(a)	0.08	0.08	0.08	0.08	Olivine	2.5	26.3
											Opaques	tr	0.6
Remainder:											Priderite	4.5	....
SiO_2	(a)	(a)	(a)	14.88	14.36	(a)	(a)	(a)	4.83	3.80	Perovskite	....	2.1
											Wadeite	tr	0.8
Excess fluorine	(a)	0.25	0.25	(a)	(a)	(a)	0.43	0.43	(a)	(a)	Apatite	tr	tr
											Calcite	tr	1.1
100 Mg/(Mg+Fe^{2+})	100	93.7	91	100	91	100	94.2	91	95.8	91	Groundmass	21.2	36.4

KEY: A = CIPW norm. B = Modified CIPW (Lewis, 1987). C = Modified CIPW with Mg/Fe ratio set to 91. D = LAMPNORM. E = LAMPNORM with Mg/Fe ratio set to 91.

NOTES: (a) = Not calculated in the norm. (b) = Bracketed values are the Mg and Fe components of the mafic minerals.

is reported below, and the resulting norms given in Table 1, columns D and E. However, if only the named minerals are calculated there will commonly remain an excess of SiO_2 and, more rarely, Al_2O_3 and TiO_2, which are reported as "remainder".

The rules for calculation of LAMPNORM are given below, but the principles on which the rules are based are as follows:

(a) All normative minerals have a fixed composition.

(b) All mafic minerals have the same 100 Mg/(Mg+Fe^{2+}) ratio, which, if known, may be fixed at the outset of the calculation.

(c) All normative minerals are anhydrous, thus potassic richterite and phlogopite are calculated H_2O-free.

(d) Diopside and olivine are Al_2O_3-free.

(e) Only known modal minerals are calculated in the norm.

In outline, LAMPNORM calculates the minor minerals, wadeite, barite, apatite, chrome spinel, and calcite. before proceeding to distribute the components among the major minerals. Ba, K_2O, and TiO_2, are then allocated to provisional priderite, and after sufficient iron has been allocated to MgO to give the desired Mg number the remainder is allocated to provisional magnetite.

Despite its presence only in small amounts, Na_2O is an important determinant of the mineralogy of lamproites, combining with available CaO to form potassic richterite. If Na_2O is relatively abundant then diopside is suppressed in the norm, and excess Na_2O is calculated as potassic magnesioarfvedsonite, a mineral which often fringes diopside and potassic richterite. If CaO remains, it is calculated as diopside.

Al_2O_3 is then distributed to K_2O, and phlogopite calculated according to formulae which correspond to the Fe, Ti-rich marginal and groundmass phlogopite, and the relatively Al-rich cores of phlogopite phenocrysts and poikilitic plates. For leucite lamproites this exhausts the MgO available, suppressing the calculation of olivine. For both potassic richterite and phlogopite, provisional priderite may be used if the remaining TiO_2 is insufficient. Phlogopite analyses (Jaques et al., 1986) show the TiO_2/Ba molecular ratio to average about 21, the same as for priderite; and altered phlogopite is commonly fringed by needles of secondary priderite.

Any remaining K_2O and Al_2O_3 is converted to leucite; and priderite and magnetite are calculated from provisional priderite and provisional magnetite. Finally, any remaining MgO is converted to olivine, and oxides remaining are summed and reported as "remainder".

Norms calculated in this manner are shown in Table 1, columns D and E, and the results may be compared with the mode reported in the same table. The normative and modal mineralogy compare quite well, if it is presumed that the groundmass of the leucite lamproite contains much potassic richterite, while the groundmass of the olivine lamproite is largely phlogopite. This is probably true of the olivine lamproite, the groundmass of which contains abundant minute flakes of red-brown tetraferriphlogopite, but the groundmass of the leucite lamproite consists of altered glass and alteration products of leucite. In both specimens, apatite is present in the groundmass as extremely small needles, not easily visible in thin section.

A feature of the norm is the prominence of magnetite, compared with its absence in the mode. The excess of normative iron is probably accounted for by groundmass tetraferriphlogopite and disseminated secondary hematite. The small amount of olivine in the mode of the leucite lamproite does not appear in the norm because of the method of calculation. In K_2O-rich lamproites all the MgO is calculated as phlogopite, and only in MgO-rich rocks will there be sufficient to produce normative olivine. Essentially, either olivine or leucite is excluded by the calculation. Finally, it should be noted that perovskite is a modal mineral in the olivine lamproites, not priderite as calculated in the norm.

As with other norm calculations, LAMPNORM assumes that, within the limits of the minerals calculated, all mineral reactions have gone to finality—that early formed olivine and leucite have combined to form phlogopite and diopside has converted to potassic richterite. In the samples chosen—from the centre of a thick sill of leucite lamproite and the centre of a mass of olivine lamproite—this assumption is reasonably correct; but for the many glassy lamproites it is impossible to calculate the proportion of glass, which is of variable and unknown composition. The "remainder", which consists mostly of SiO_2, is not equivalent to the glassy matrix, but is entirely the excess of the various oxides over that required for the minerals calculated. The original glass was probably silica-rich, but the excess SiO_2 is presumably accommodated in the altered lamproites in the K-feldspar which pseudomorphs leucite, and in the groundmass clay minerals.

LAMPNORM has its limitations but it is useful when comparing a series of analyses on a uniform basis. It may also provide other indications of the origin of a particular lamproite. For example, if significant Al_2O_3 occurs in the remainder it suggests the assimilation of shale. Whereas the norm usually shows some relation to the mode of the lamproites, it is notable that the olivine-rich leucite lamproites of Mount Cedric and Mount Ibis (Jaques et al., 1986), which contain very little modal phlogopite, are normatively phlogopite-rich with very little leucite. The probability is that the olivine is xenocrystal and was incorporated at a late stage by a fully evolved lamproite magma.

LAMPNORM, as outlined above, was devised with the West Kimberley lamproites in mind, using mineral compositions appropriate to those rocks. It would probably prove useful for comparing lamproites from several areas, but it could be easily modified to accommodate other lamproites with differing mineral compositions.

Rules for calculating LAMPNORM

1. Calculate the molecular proportion of each oxide or element by dividing the weight per cent of each by the appropriate molecular weight (Table 2). The resulting amounts will be used throughout the following calculations.
2. (a) Add Mn + Ni to FeO

   (b) Add Sr to CaO

   (c) Add Cl to F

Calculate the following minerals:

3. **Wadeite, Wd.** Set Wd = Zr. Subtract Wd from K_2O, and 3Wd from SiO_2.
4. **Apatite, Ap.**

   (a) Set Ap = P_2O_5.

   (b) If CaO>3.33 Ap, subtract 3.33 Ap from CaO.

   (c) If CaO<3.33 Ap, set "CaO deficiency" = 3.33 Ap - CaO. Set CaO = 0.

   (d) Subtract 0.667 Ap from F, or if insufficient F, allocate all F to Ap and set F = 0.

5. **Calcite and magnesite, Cc, Ms.**

   (a) If CaO>CO_2, set Cc = CO_2, subtract Cc from CaO.

   (b) If CaO<CO_2, set Cc = CaO subtract Cc from CO_2, set CaO = 0.

   (c) If CO_2 remains after calculating calcite, set Ms = CO_2, subtract Ms from MgO.

6. **Barite, Br.** Set Br = S/SO_3. Subtract S/SO_3 from Ba.
7. **Provisional Priderite, Pd'.**

   (a) If TiO_2>21 Ba, set Pd' = 21 Ba. Subtract Pd' from TiO_2.

   (b) If TiO_2<21 Ba, set Pd' = TiO_2. Subtract Pd'/21 from Ba, add surplus Ba to CaO. Set TiO_2 = 0.

   (c) Subtract Pd'/14 from K_2O.

8. **Chrome spinel, Cm.** Set Cm = Cr_2O_3/11. Subtract 6 Cm from FeO; 10 Cm from MgO; and Cm from Fe_2O_3 and TiO_2. Set Cr_2O_3 = 0.

Two routes are possible from this point when calculating mafic minerals: (9) follows the CIPW procedure and first calculates magnetite; (10) allocates FeO/Fe_2O_3 to MgO to give a desired Mg/(Mg+Fe) ratio, before calculating magnetite.

9. **Provisional Magnetite, Mt'.**

   (a) If Fe_2O_3>FeO, set Mt' = FeO. Subtract Mt' from Fe_2O_3; set FeO = 0.

   (b) Fe_2O_3<FeO, set Mt' = Fe_2O_3. Subtract Mt' from FeO, set Fe_2O_3 = 0.

   (c) Allocate surplus FeO from (b) to MgO: (MgFe) = MgO + FeO. MG = MgO/(MgFe); FE = FeO/(MgFe) set MgO = 0, FeO = 0.

   (d) Fe' = 2 Fe_2O_3 + 3 Mt'. Proceed to rule 11.

10. **Allocate Fe to MgO to give a specific Mg number, Mgn**

    (a) The required iron, Ir, to give a particular Mg number is Ir = MgO (100-Mgn)/Mgn.

    (b) If Fe_2O_3>FeO then Fe' = 3 FeO. Subtract Fe'/3 from Fe_2O_3; set FeO = 0.

    (c) If Fe_2O_3<FeO then Fe' = 3 Fe_2O_3. Subtract Fe'/3 from FeO; set Fe_2O_3 = 0.

    (d) Allocate twice the Fe_2O_3 remaining, or FeO remaining, to fulfil the requirement for Ir. Excess FeO is added to Ir and lowers the Mg number.

    (e) If there is insufficient Fe_2O_3 or FeO to satisfy Ir then Fe' is reduced to fill Ir.

    (f) If there is insufficient Fe' to satisfy Ir then Ir is reduced and the Mg number raised.

    (g) (MgFe) = MgO + Ir. MG = MgO/(MgFe); FE = Ir/(MgFe).

    (h) Fe' = Fe' + 2Fe_2O_3

11. **Potassic richterite, Kr.**

    (a) Total TiO_2, Tt = Pd' + TiO_2

    (b) Determine which of Na_2O, Tt or CaO/2 is the lowest, and set Kr = Na_2O, Tt or CaO/2 as appropriate. Subtract Kr from Na_2O and K_2O; subtract 2 Kr from CaO, 9.5 Kr from (MgFe) and 15 Kr from SiO_2.

    (c) If Kr = Tt, set Tt, TiO_2 and Pd' = 0.

    (d) Allocate TiO_2 and Pd' to fill Kr.

    (e) If F>2 Kr, subtract 2 Kr from F.

    (f) If F<2 Kr allocate all F to Kr; set F = 0.

12. **Potassic magnesioarfvedsonite, Ka.**

    (a) If Na_2O remains, set Ka = Na_2O. Subtract Ka/2 from K_2O, Ka from Fe', 2 Ka from (MgFe), and 8 Ka from SiO_2; set Na_2O = 0.

13. **Diopside, Di.**

    (a) If CaO>(MgFe), set Di = (MgFe); subtract Di from CaO and 2 Di from SiO_2; set (MgFe) = 0.

    (b) If CaO<(MgFe), set Di = CaO, subtract Di from (MgFe) and 2 Di from SiO_2; set CaO = 0.

14. **Phlogopite, Pg, Ph.**

(a) Total TiO_2, Tt = TiO_2 + Pd'

(b) **Provisional Phlogopite plus Leucite, Phl:** (i) if Al_2O_3>K_2O, set Phl = K_2O; subtract Phl from Al_2O_3; set K_2O = 0. (ii) If Al_2O_3<K_2O, set Phl = Al_2O_3; subtract Phl from K_2O; set Al_2O_3 = 0. (iii) If K_2O remains, form provisional Al,Fe-phlogopite from Phl: subtract K_2O from Phl and make Phg = 2 K_2O; set K_2O = 0.

(c) **Al,Fe-Phlogopite, Pg:** determine which of Phg, (MgFe)/5 or Tt is lowest and set Pg = Phg, (MgFe)/5 or Tt, as appropriate. Subtract Pg from Phg, Tt, and Fe', 5 Pg from (MgFe), and 6 Pg from SiO_2. If Pg = Tt, set Tt = 0, TiO_2 = 0, and Pd' = 0.

(d) Allocate TiO_2 and Pd' to fill Pg.

(e) If F>Pg, subtract Phg from F.

(f) If F<Pg, allocate all F to Pg; set F = 0.

(g) If there is excess Phg half is added to Phl and half returned to K_2O

(h) **Al-Phlogopite, Ph:** determine which of Phl, (MgFe)/5.5 or 1.54 Tt is lowest, and set Ph = Phl, (MgFe)/5.5 or 1.54 Tt, as appropriate. Subtract Ph from Phl,5.5 Ph from (MgFe) and 5.85 Ph from SiO_2. If Ph = Tt, set Tt = 0, TiO_2 = 0 and Pd' = 0.

(i) Allocate TiO_2 and Pd' to fill 0.65 Ph.

(j) If F>Ph, subtract Ph from F.

(k) If F<Ph, allocate all F to Ph; set F = 0.

15. **Leucite, Lc.** Set remaining Phl = Lc; subtract 4 Lc from SiO_2.

16. **Priderite, Pd.**

(a) If Pd'/14>Fe'/2, Pd = Fe'/2; subtract 14 Pd from Pd' set Fe' = 0.

(b) If Pd'/14<Fe'/2, Pd = Pd'/14; subtract 2 Pd from Fe'; set Pd' = 0.

(c) If Pd' remains, add Pd' to TiO_2 remaining; excess Ba = Pd'/21 and add Pd'/14 to excess K_2O.

17. **Olivine, Ol.**

(a) If (MgFe)>2 SiO_2, set Ol = SiO_2, subtract 2 Ol from (MgFe); set SiO_2 = 0.

(b) If (MgFe)<2 SiO_2, set Ol = (MgFe)/2, subtract Ol from SiO_2, set (MgFe) = 0.

(c) If (MgFe) remains, MgO = MG(MgFe) and FeO = FE(MgFe).

18. **Magnetite, Mt.** Set Mt = Fe'/3.

19. Normative minerals are converted to weight per cent by multiplying the molecular proportion by the appropriate molecular weight of Table 2.

Note: Adjustments must be made to the final amounts of potassic richterite and phlogopite, to take account of the small, but variable, quantities of BaO and K_2O added by incorporating provisional priderite into the molecule, and the variable amount of F used in each case.

20. Any remaining SiO_2, Al_2O_3, FeO, MgO, K_2O, Ba or F, after the above calculations have been performed is first converted to weight per cent and then summed and reported as "remainder".

TABLE 2. NORMATIVE MINERALS AND FOR LAMPNORM

Mineral		*Formula*	*Mol.wt*
Leucite	Lc	$K_2O.Al_2O_3.4SiO_2$	436.49
Al-Phlogopite	Ph	$K_2O.Al_2O_3.0.65TiO_2.5.5MgO.5.85SiO_2$.(F)	821.26
		$K_2O.Al_2O_3.0.65TiO_2.5.5FeO.5.85SiO_2$.(F)	994.74
Al,Fe-Phlogopite	Pg	$K_2O.0.5Al_2O_3.TiO_2.0.5Fe_2O_3.5MgO.6SiO_2$.(F)	866.95
		$K_2O.0.5Al_2O_3.TiO_2$ $0.5Fe_2O_3.5FeO.6SiO_2$.(F)	1 024.66
K,Ti-Richterite	Kr	$K_2O.Na_2O.2CaO.TiO_2.9.5MgO.15SiO_2$.(2F)	1 632.38
		$K_2O.Na_2O.2CaO.TiO_2.9.5FeO.15SiO_2$.(2F)	1 932.03
K,Mg-Arfvedsonite	Ka	$K_2O.2Na_2O.Fe_2O_3.4MgO.16SiO_2$	1 500.41
		$K_2O.2Na_2O.Fe_2O_3.4FeO.16SiO_2$	1 626.58
Diopside	Di	$CaO.MgO.2SiO_2$	216.55
		$CaO.FeO.2SiO_2$	248.09
Olivine	Ol	$2MgO.SiO_2$	140.69
		$2FeO.SiO_2$	203.78
Magnetite	Mt	$FeO.Fe_2O_3$	231.54
Chrome spinel	Cm	$TiO_2.3Al_2O_3.Fe_2O_3.6FeO.11Cr_2O_3.10MgO$	3 051.48
Priderite	Pd	$K_2O.Fe_2O_3.0.667BaO.14TiO_2$	1 474.69
Wadeite	Wd	$ZrO_2.K_2O.3SiO_2$	397.67
Apatite	Ap	$3CaO.P_2O_5.0.333CaF_2$	336.21
Calcite	Cc	$CaO.CO_2$	100.09
Magnesite	Ms	$MgO.CO_2$	84.31
Barite	Br	$BaO.SO_3$	233.39

SiO_2	60.08	CaO	56.08	Zr	91.22
TiO_2	79.90	Na_2O	61.98	Cr	52.00
Al_2O_3	101.96	K_2O	94.20	Ni	58.71
Fe_2O_3	159.69	P_2O_5	141.94	S	32.06
FeO	71.85	CO_2	44.01	SO_3	80.06
MnO	70.94	Ba	137.33	F	19.00
MgO	40.30	Sr	87.62	Cl	35.45

References

ATKINSON, W. J., HUGHES, F. E., and SMITH, C. B., 1984, A review of the kimberlitic rocks of Western Australia, *in* Kimberlites I—Kimberlites and Related Rocks, *edited by* J. Kornprobst: Amsterdam, Elsevier, p. 195–224.

BARTH, T. F.W ., 1955, Presentation of rock analyses: Journal of Geology, v.63, p. 340–363.

CROSS, W., IDDINGS, J. P., PIRSSON, L. V., and WASHINGTON, H., 1903, Quantitative classification of igneous rocks: University of Chicago Press.

DAWSON, J. B., 1987, The kimberlite clan—Relationship with olivine and leucite lamproites, and inferences for upper mantle metasomatism, *in* Alkaline igneous rocks, *edited by* J.G. Fitton and B.G. Upton: London, Geological Society Special Publication 30, p. 95–101.

HUTCHISON, C. S., 1974, Laboratory handbook of petrographic techniques: New York, John Wiley, 527 pp.

JAQUES, A. L., LEWIS, J. D., and SMITH, C. B., The kimberlites and lamproites of Western Australia: Western Australia, Geological Survey, Bulletin 132, 268 pp.

JOHANNSEN, A., 1939, A descriptive petrography of the igneous rocks (2nd edn.): University of Chicago Press.

LEWIS, J. D., 1987, The geology and geochemistry of the West Kimberley Lamproite Province, Western Australia: University of Western Australia, M.Sc Thesis (unpublished).

NIGGLI, P., 1954, Rocks and mineral deposits: San Francisco, W. H. Freeman.

The Mount Pleasant Sill Eastern Goldfields, Western Australia Iron-rich granophyre in a layered high-Mg intrusion

by

W. K. Witt, R. Davy, and D. Chapman[1]

ABSTRACT

The Mt Pleasant Sill is one of a number of mafic to ultramafic sills in the Eastern Goldfields of Western Australia. Although affected by greenschist–facies metamorphism, relic textures and some relic minerals permit interpretation of the igneous history of the sill. Early crystallization on the floor of the sill, and later crystallization from the roof and the floor inwards, produced phase layering and textural zonation. Fractionation has yielded a cumulate-textured, ultramafic basal zone and an iron-rich granophyre (quartz gabbro) approximately 50 m below the roof of the 550 m-thick sill. Structurally controlled gold mineralization has been preferentially concentrated in the granophyre at several localities.

The calculated bulk composition of the Mt Pleasant Sill suggests the initial magma had a high-Mg basalt composition (about 11% MgO). Igneous layering and fractionation trends in gabbroic rocks above the basal ultramafic zone are similar to those of the Golden Mile Dolerite (bulk composition about 4% MgO). More extreme fractionation of the relatively magnesian Mt Pleasant magma produced an iron-rich granophyre similar to that found in the Golden Mile Dolerite.

Geochemical evidence and the presence of primary amphibole at the base of the sill suggest contamination of the melt by alkalis and water from enclosing sediments. Contamination may have had several important consequences, including the lowering of the melt viscosity—thus promoting convection and aiding fractionation; and the decreasing of liquidus temperatures below the roof of the sill—thereby promoting bottom-dominated crystallization. In addition, relatively high $P(H_2O)$ near the roof may have promoted crystallization of clinopyroxene while plagioclase and orthopyroxene were crystallizing towards the centre of the intrusion, leading to divergent geochemical trends for the upper and lower parts of the sill.

Key words: Mt Pleasant, mafic, ultramafic, sill, petrology, geochemistry

Introduction

Layered and differentiated mafic to ultramafic sills are significant components of Archaean greenstone belts in Canada (MacRae, 1969; Naldrett and Mason, 1968), South Africa (Anhaeusser, 1985), and Western Australia (McCall, 1973; Williams and Hallberg, 1973). In Western Australia, some differentiated sills are important hosts to structurally controlled gold mineralization, e.g. the Golden Mile Dolerite at Kalgoorlie (Travis et al., 1971), and the Defiance Dolerite at Kambalda (Clark et al., 1986). Regional mapping of the BARDOC 1:100 000 sheet (SH51-9-3137), northwest of Kalgoorlie, has revealed the presence of several conformable to semiconformable, layered mafic to ultramafic intrusions. One of these, the Mt Pleasant Sill, hosts gold mineralization at several localities in the Ora Banda–Broad Arrow area. These include the Golden Kilometre and Southern shoots at Mt Pleasant (Chapman, 1987), Lady Bountiful (Goode, 1987), the Ora Banda Mine, Lady Evelyn, and minor mineralization at Goongarrie (Fig. 1). This contribution describes the layering and geochemistry of the Mt Pleasant Sill and compares the sill with several other layered and differentiated, mafic to ultramafic *sills in the Eastern Goldfields*. Although the Mt Pleasant Sill and some of the other intrusions discussed may be slightly transgressive on a regional scale, their broadly conformable nature justifies use of the term *sill*.

Regional geology

The Ora Banda–Broad Arrow area is dominated by the north-northwest trending Goongarrie–Mt Pleasant Anticline (Fig. 1). Drilling in the Mt Pleasant area, near the nose of the fold, indicates a southerly plunge of 10–20°. The core of the anticline is monzogranite and granodiorite of the Goongarrie–Mt Pleasant dome.

Greenstones of the Ora Banda sequence (Witt, 1987) are regionally conformable with the strongly deformed margins of the granite dome. The Ora Banda sequence commences with basalt, which is progressively overlain by komatiitic volcanics, high-Mg basalt, and tholeiitic basalt. This lower, mafic to ultramafic part of the Ora Banda sequence is overlain by intermediate to felsic, epiclastic and volcaniclastic metasediments (Black Flag Group), and mature metasediments, including sandstone and conglomerate (Kurrawang Formation). Regional relationships suggest an unconformity between the Black Flag Group and the Kurrawang Formation. Layered mafic to ultramafic sills occur at or near the transition from high-Mg rocks to tholeiitic basalts (Mt Ellis Sill, Mt Pleasant Sill), and at or near the transition from mafic rocks to epiclastic and volcaniclastic metasediments (Ora Banda Sill, Orinda Sill).

[1] Mount Pleasant Gold Group. Present address: Kalgoorlie Gold Operations, Kalgoorlie, Western Australia.

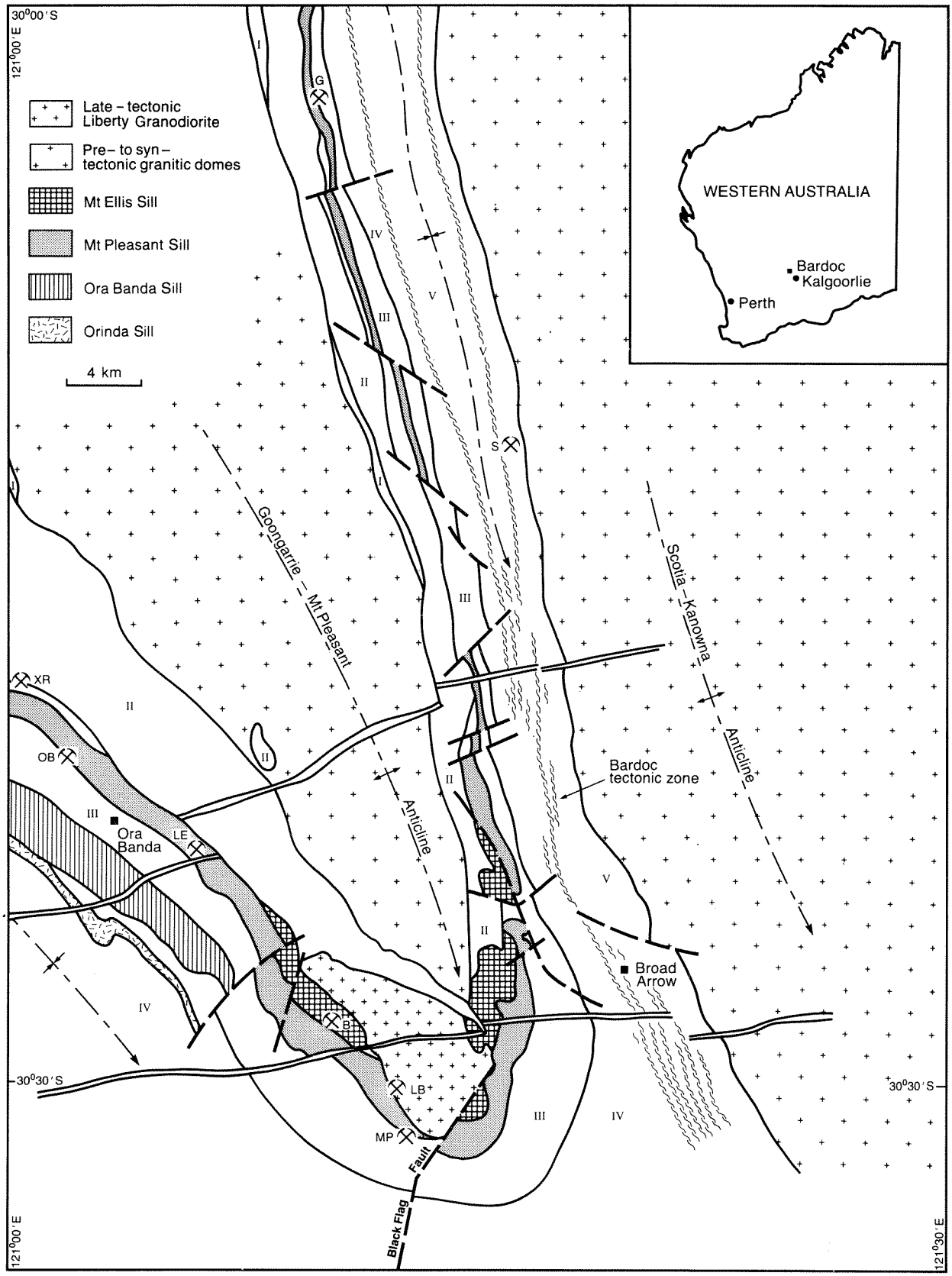

GSWA 25324

Figure 1. Map of Goongarrie–Mount Pleasant Anticline, showing the locations of layered mafic to ultramafic sills. For key to volcanosedimentary units see Figure 2. Unit V is unassigned greenstones on the eastern side of the Bardoc Tectonic Zone. Mines (all gold, except for Scotia nickel mine) are as follows: XR—Christmas Reef; OB—Ora Banda; LE—Lady Evelyn; B—Bellvue; LB—Lady Bountiful; MP—Mount Pleasant; G—Goongarrie; S—Scotia.

Recent publications have correlated the greenstone sequences at Kalgoorlie and Kambalda (Griffin et al., 1983; Gee et al., 1976; Clark et al., 1986). Figure 2 suggests a possible correlation between the Ora Banda sequence and the well-established stratigraphy for the Kalgoorlie and Kambalda areas (Travis et al., 1971; Gresham and Loftus-Hills, 1981). Mafic to ultramafic sills occur at similar stratigraphic levels. However, direct correlation of intrusive units over large distances may be unjustified, and one of the aims of this paper is to illustrate differences between intrusions at similar stratigraphic levels in the two areas.

The Mt Pleasant Sill is remarkably persistent and consistent, and is mappable over a strike length of more than 70 km (Fig. 1). A similar sill which occurs at a comparable stratigraphic horizon in the Goongarrie area may be part of the same intrusion. The ultramafic basal zone is absent in the Goongarrie area, perhaps because of structural complications. The Mt Pleasant Sill occurs at, or just above, the base of the Bent Tree Basalt over the entire distance. In the nose area of the Goongarrie–Mt Pleasant Anticline, the Mt Ellis Sill separates Big Dick Basalt from Bent Tree Basalt and the Mt Pleasant Sill. The Mt Pleasant Sill is characterized by phase layering, and this is the basis for the zoning described in this paper (Fig. 3). Further subdivisions can be erected on a textural basis. The thickness and stratigraphy of the sill and the relative thickness of each zone are very consistent, although some variations occur at its extremities. For example, northwest of Christmas Reef, the granophyre layer (zone 9) thickens at the expense of zone 8, and granophyric segregations are several centimetres thick rather than the more typical 1–2 mm.

Narrow metasedimentary horizons occur at both base and top of the sill. These metasediments probably formed as a single unit which was later split by intrusion of the sill. The Mt Pleasant Sill has not been dated, but the intrusion is considered to be broadly synvolcanic because it displays the same deformations as the enclosing volcanosedimentary succession.

Petrography

Layering in the Mt Pleasant Sill (Fig. 3) was first established in the Mt Pleasant area, where exploration drilling provided core from all but the peridotite layer. Regional mapping subsequently established the same features in surface exposures. Petrographic samples were taken from several localities between Mt Pleasant and Christmas Reef. Igneous textures are well preserved even though metamorphic mineralogy dominates most samples; and so igneous terminology is used, with the understanding

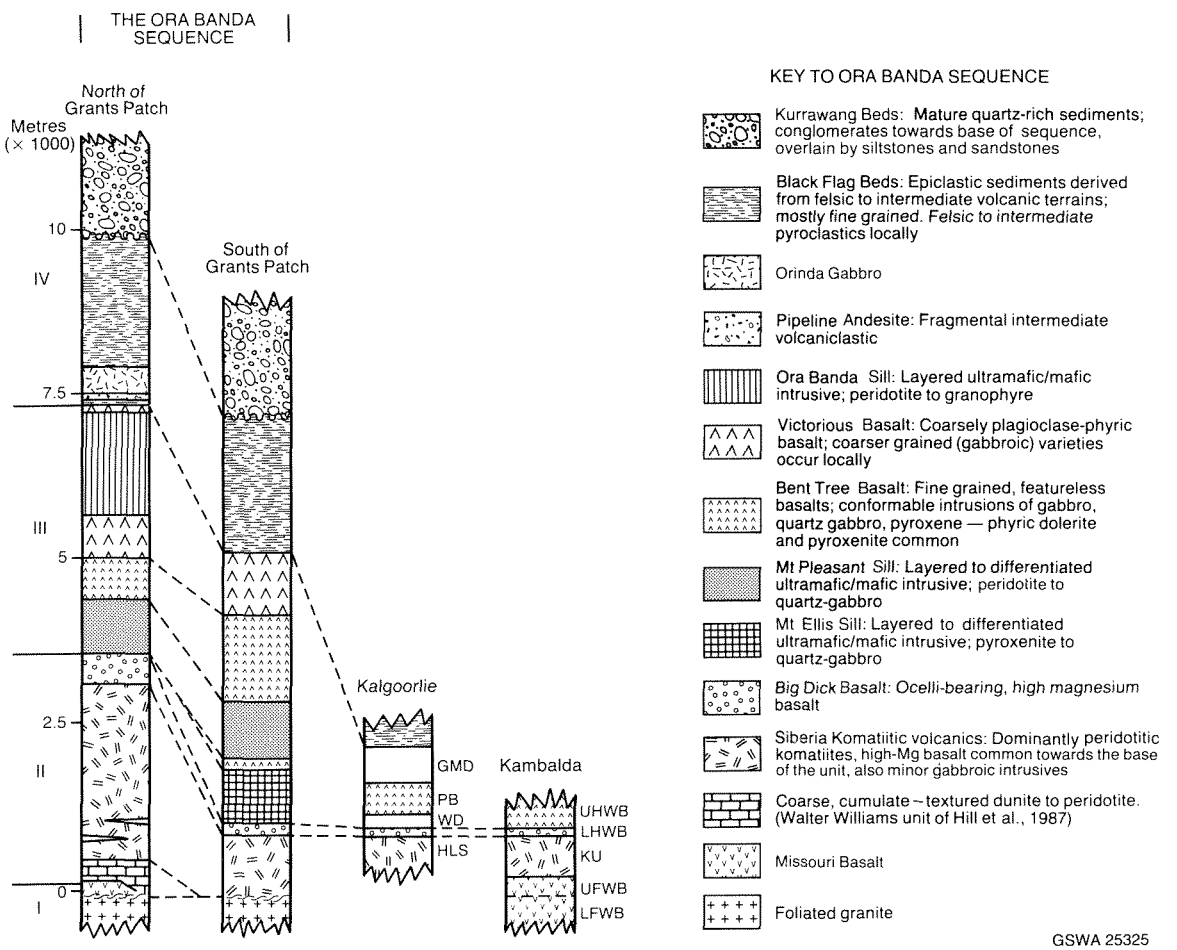

Figure 2. Stratigraphy of the Ora Banda sequence, and comparison with stratigraphic columns from Kalgoorlie and Kambalda (Redman and Keays, 1985). Key to sections at Kalgoorlie and Kambalda: GMD—Golden Mile Dolerite; PB—Paringa Basalt; WD—Williamstown Dolerite; HLS—Hannans Lake Serpentinite; UHWB—Upper hanging wall basalt; LHWB—Lower hanging wall basalt; KU—Kambalda ultramafics; UFWB—Upper footwall basalt; LFWB—Lower footwall basalt.

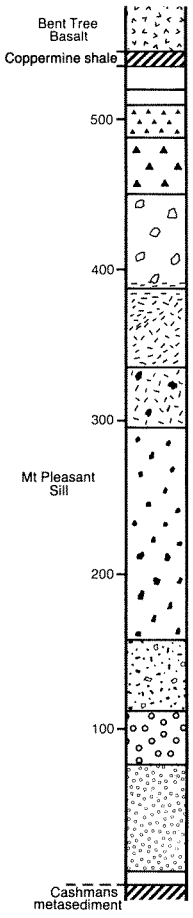

Metres	Zone	Rock Type	Silicate phases (in order of abundance)	Fe / Fe + Mg	Texture	Grain size	Oxide assemblage	Comments	Regional mapping unit
	12	Porphyritic dolerite		0.59					
	11	C.g. subophitic gabbro	CPX + PLAG	0.62	Subophitic	0.2-0.5 mm, oikocrysts to ~6 mm	Tr - 2% lcxn, mnr ilm	Proportion of pyroxene phenocrysts increases upwards.	UPPER GABBRO ZONE
500	10	C.g. subophitic gabbro (mnr qtz gabbro)		0.67 0.84		2-7 mm	2-3% lcxn, mnr ilm 2-3% lcxn, mnr ilm	Alternating layers of gabbro & qtz gabbro	
	9	Quartz gabbro (granophyre)	CPX + PLAG + QTZ	0.93	Granophyric	Variable to ~ 1.5 mm	4-5% ilmenite mnr mt	5-20% quartz; quartz-albite granophyre common	QUARTZ GABBRO ZONE
	8	Gabbro	PLAG + CPX	0.79	Variable, mostly subophitic?	Variable to ~ 1.5 mm	3-5% lcxn, mnr ilm	Coarse pegmatoidal segregations common	LOWER GABBRO ZONE
400	7	Flow-textured gabbro		0.64	Subophitic?	0.5 mm - 1 mm	~2% lcxn, sphene	Flow textures common	
	6	Glomeroporphyritic gabbronorite		0.52	Glomeroporphyritic	0.5 - 2 mm; phenocryst aggregates to 3cm across	Tr - 2% lcxn	Lath-shaped feldspars, flow textures towards top of zone	
300									
Mt Pleasant Sill	5	Porphyritic gabbronorite	PLAG + CPX + OPX	0.46	Porphyritic	0.5 - 2 mm, 2 - 3 mm phenocrysts	Tr - 1% lcxn	Layering (mm-scale) common at some localities	PORPHYRITIC GABBRO NORITE ZONE
200									
	4	C.g. gabbronorite	CPX + OPX + PLAG	0.43 0.42	Equigranular, cumulate lower section	2 - 4 mm	Tr - 1% lcxn	Modal plagiocase increases upwards from ~ 20% to 60%	COARSE GABBRO NORITE ZONE
100	3	Pyroxenite	CPX + OPX	0.42	Ortho to mesocumulate	3 - 4 mm	Tr - 1% lcxn	Cumulate textures	
	2	Hb-peridotite	OL + CPX + HB	0.40 0.39	Orthocumulate, post-cumulus hornblende	⩽1 mm	2-9% magnetite, mostly secondary? mnr chromite?	Hb decreases upwards	BASAL ULTRAMAFIC ZONE
Cashmans metasediment	1	Hb-mela-microgabbro	CPX + PLAG + HB	0.54	Equigranular	0.2-0.5 mm	Tr lcxn	Contamination?	FINE-GRAINED MARGIN

- Mafic patches, with or without relic pyroxene
- Quartz, or quartz-albite granophyre
- Pegmatoidal segregations
- Lath-shaped feldspars

Note: Fe/Fe + Mg = ΣFeO/ΣFeO + MgO

Abbreviations

mt	magnetite
ilm	ilmenite
lcxn	leucoxene
Tr	trace

Figure 3. Zoning in the Mt Pleasant Sill.

GSWA 25326

that the "meta" prefix has been dropped. Relic igneous minerals occur in some rocks, but primary mineralogy must frequently be inferred from the form and composition of metamorphic minerals (Williams, 1971; Jaques, 1976; Williams and Hallberg, 1973).

Contacts between some layers of the sill are transitional over several metres. Transitions are marked by alternating bands of adjacent rock types; some other features, such as pegmatoid gabbro, flow alignment, and coarse mafic (glomeroporphyritic) patches display some overlap. Petrographic features of the Mt Pleasant Sill are summarized in Figure 3, and detailed petrographic descriptions are given in Witt (1991).

Fine-grained margin

A narrow (≤410 m) fine-grained margin of equigranular hornblende-bearing melanocratic microgabbro (zone 1) at the base of the sill is generally poorly exposed, but can be identified west of the Bellvue mining centre where the sill has a flatter than normal attitude; this attitude is possibly related to emplacement of the Liberty Granodiorite, and associated movement on a system of accommodation faults (Grants Patch Fault Zone).

Ultramafic layer

Zone 2 is an olivine orthocumulate (peridotite) with intercumulus chlorite (after ?clinopyroxene), hornblende, and small amounts of chromite (Fig. 4). Widespread, disseminated, fine-grained, secondary magnetite formed during serpentinization of the olivine, and the peridotite layer has a strong magnetic expression. Sampling west of the Bellvue mining centre has indicated the presence of a thin, olivine–clinopyroxene mesocumulate at the top of zone 2 (zone 2A, Table 1). The rock consists of coarse (3–4 mm), cumulus olivine (serpentinized) and clinopyroxene, and intercumulus tremolite–actinolite. Stubby prisms (3–4 mm) of tremolite–actinolite, some with cores of relic clinopyroxene are dominant in zone 3. Aggregates of matted tremolite–actinolite, chlorite, and epidote (after ?orthopyroxene), appear first as rounded inclusions within clinopyroxene pseudomorphs and then, towards the top of zone 3, as subequant grains of similar size to the original clinopyroxene (3–4 mm) Fig. 5).

Gabbro-norite layer

Zones 4–6 are termed (leuco-) gabbro-norites on the assumption that the aggregates of matted tremolite, chlorite, and epidote, described above, are pseudomorphs after orthopyroxene. This assumption is based on the contrast between these assemblages and the coarse, prismatic tremolites which contain cores of relic clinopyroxene (Fig. 6). Zones 4–6 are the most plagioclase-rich layers of the sill. In areas of good outcrop, zone 4 generally forms steep ridges, and its distinctive texture (Fig. 7) makes it a valuable regional marker horizon. Subhedral ?orthopyroxene phenocrysts (2–3 mm) in zone 5 (Fig. 8) decrease upwards from about 5% at the base, and are commonly absent in the upper part of this zone. Rhythmically repeated layers consisting of a lower, plagioclase-rich section and an upper, pyroxene-rich section, define a millimetre-scale igneous lamination at some localities. Plagioclase-rich veinlets and irregular

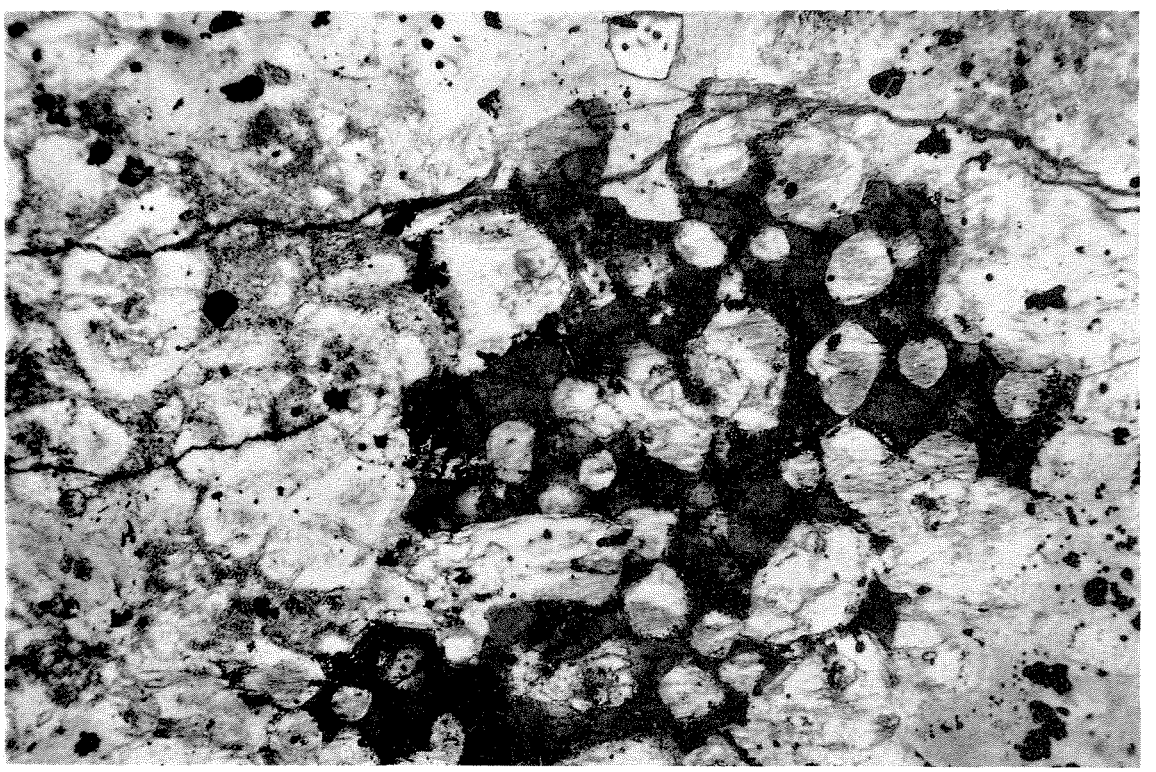

GSWA 25327

Figure 4. Olivine orthocumulate, zone 2; serpentine pseudomorphs after cumulus olivine with post-cumulus kaersutite; plane polarized light; long axis 4 mm.

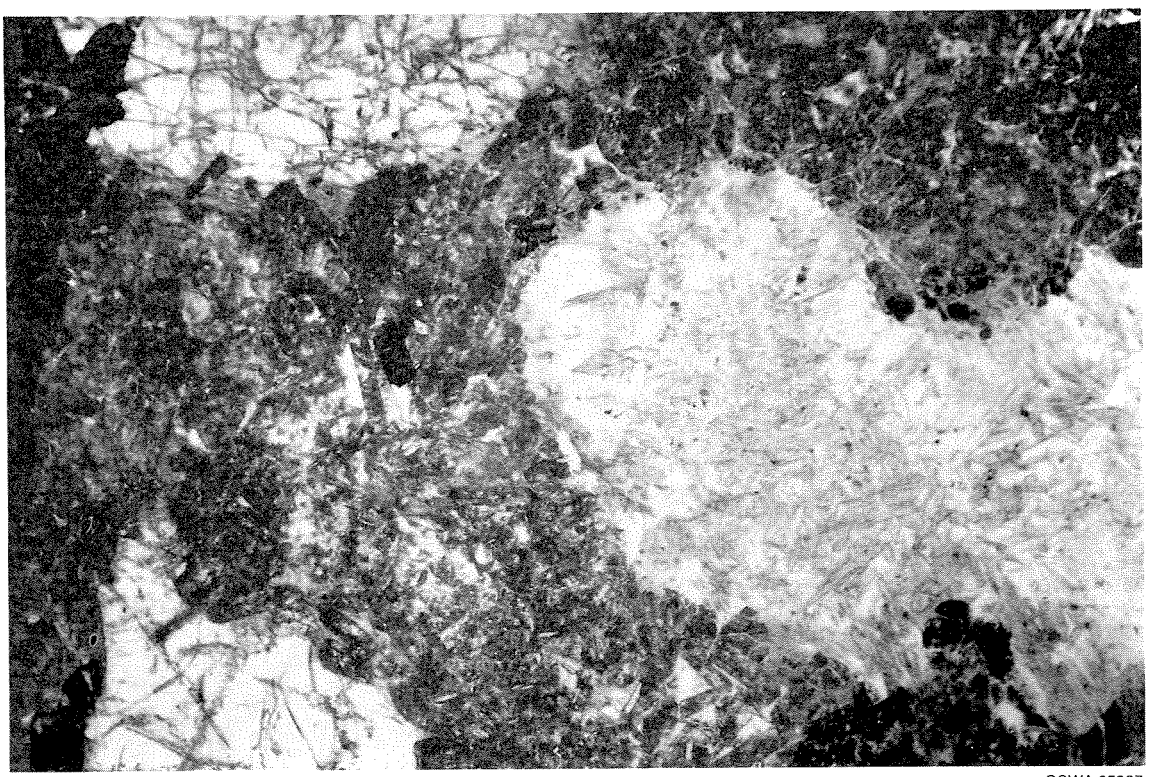

GSWA 25327

Figure 5: Uralitic assemblage (tremolite, chlorite, and epidote), probably after orthopyroxene, in a groundmass of saussuritized plagioclase grains, zone 4; large grains with prominent cleavage at left of photomicrograph are partly tremolitized augite; plane polarized light; long axis 4 mm.

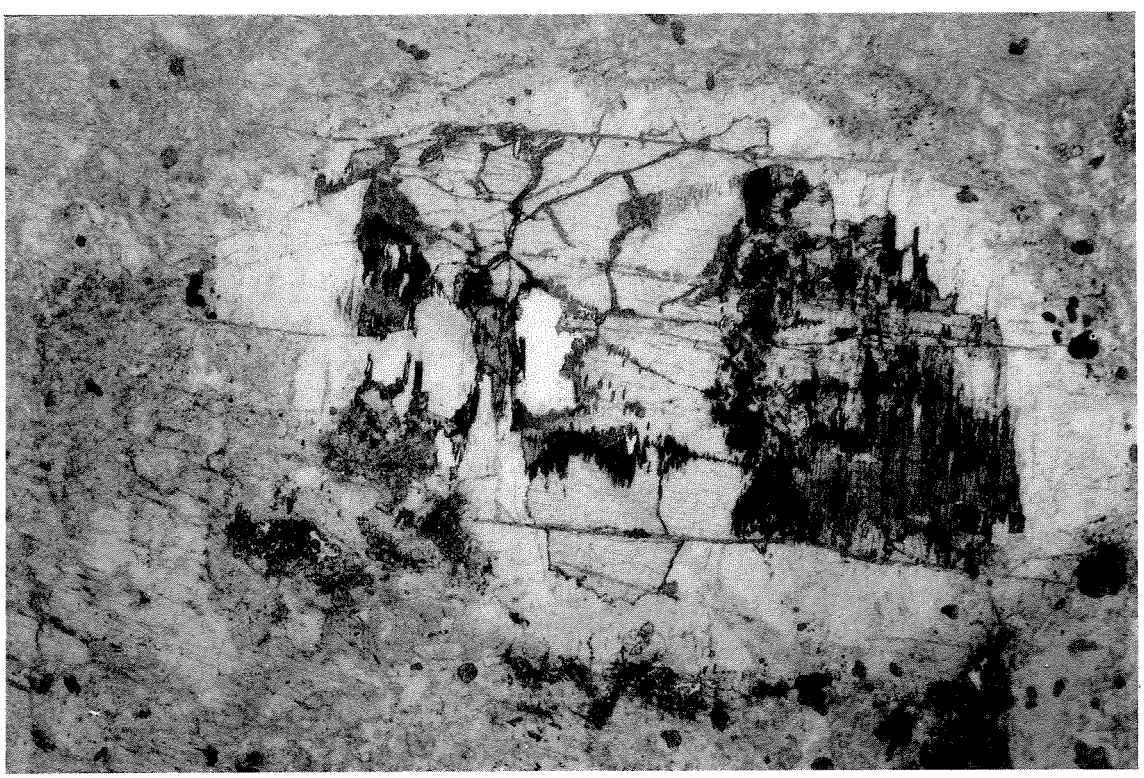

GSWA 25327

Figure 6. Relic augite in coarse, prismatic tremolite in intercumulus groundmass of fine-grained uralite, zone 3; note chloritic alteration of tremolite at margins of the original pyroxene grain, plane polarized light, long axis 4 mm.

segregations of plagioclase which cut across the igneous lamination are also common. Zone 6 is characterized by rounded, mafic patches consist of matted tremolite–actinolite–chlorite–epidote assemblages which display domainal extinction characteristics. They are interpreted to be glomeroporphyritic accumulations of orthopyroxene phenocrysts. Towards the top of zone 6, the proportion of mafic minerals increases, and plagioclase assumes a characteristic lath shape. Alignment of these laths in some sections produces a flow texture which sweeps around the mafic patches (Fig. 9).

Lower gabbro layer

Zones 7 and 8 are distinctly more melanocratic than zone 6. Trace quartz occurs in some zone 8 samples; most is confined to pegmatoidal segregations. Pegmatoid amphiboles tend to be plumose and strongly oriented, and may be several centimetres long.

Granophyre layer

Zone 9 is an ilmenite-rich quartz ferrogabbro; it represents the most fractionated layer of the Mt Pleasant sill. Quartz (5%) is an essential component and much of it occurs in granophyric intergrowth with albite.

Upper gabbro layer

Quartz gabbro layers containing <5% quartz alternate with quartz-deficient gabbro towards the base of zone 10. Zone 11 exhibits coarse (to about 1 cm), blotchy, chloritic patches after clinopyroxene. This zone is quite thin, and absent or difficult to detect, in poorly exposed areas. Zone 12 is a subophitic gabbro in which partly tremolitized clinopyroxene oikocrysts (to about 6 mm) increase in abundance towards the upper contact of the sill.

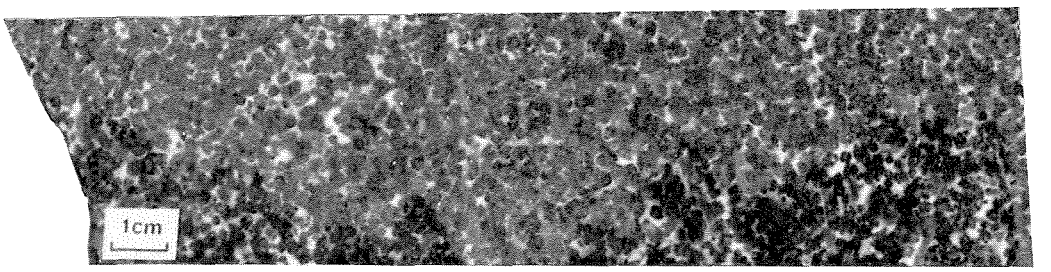

GSWA 25328

Figure 7. Coarse-grained equigranular gabbro-norite, zone 4; cumulate pyroxene phenocrysts in a groundmass of fine grained, saussuritized plagioclase.

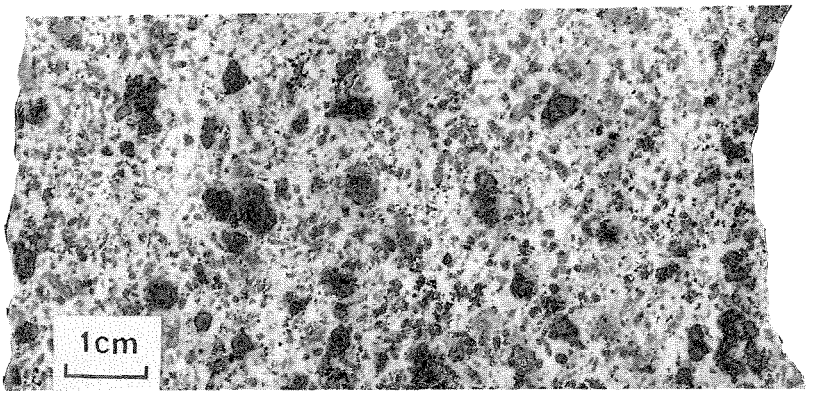

GSWA 25328

Figure 8. Subhedral (?ortho-)pyroxene pseudomorphs as phenocrysts in a groundmass of finer grained, saussuritized plagioclase, zone 5.

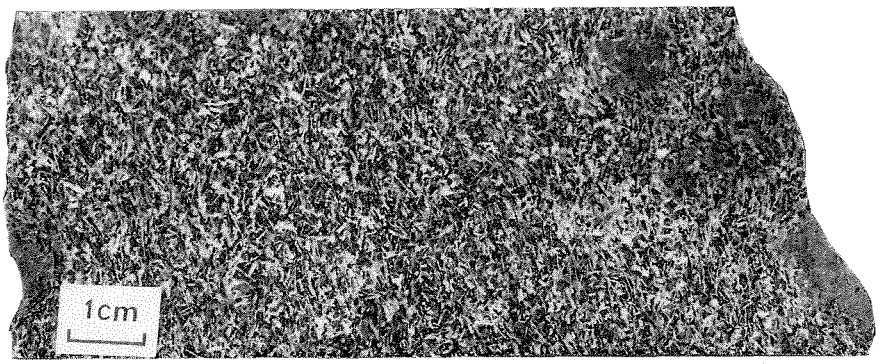

GSWA 25328

Figure 9. Dark, uralitized (?ortho-)pyroxene phenocrysts displaying glomeroporphyritic texture, in a gabbroic groundmass in which plagioclase exhibits flow alignment, zone 6.

Mineralogy

Table 1 summarizes mineralogical data for the Mt Pleasant Sill. Analyses were performed on a MAC electron microprobe at CSIRO, Floreat Park.

Relic olivine was not observed, but cumulate olivine is perfectly pseudomorphed by serpentine.

Clinopyroxene is replaced by tremolite–actinolite and, in the peridotite zone, by chlorite. Pale-green tremolite–actinolite is characteristic of the lower part of the sill; but dark-green, actinolitic margins appear in the upper part of zone 5; and actinolitic amphibole occurs in zones 8 and 9, above which amphiboles become paler again. These colour changes reflect increasing iron enrichment of the igneous pyroxenes from the base of the sill to zone 9. Relic clinopyroxene is relatively common. Cumulate clinopyroxene from zones 2 to 4, and subophitic clinopyroxene from zone 12 are chromian augite (approximately $Wo_{40}En_{50}Fs_{10}$). Clinopyroxene from zone 5 has a similar composition but contains less chrome.

Fine-grained masses of matted tremolite, sometimes accompanied by variable chlorite and epidote, are interpreted to be pseudomorphs after orthopyroxene, but relic orthopyroxene was not observed.

Orange-brown amphibole in zones 1 and 2 is considered a primary igneous mineral; this opinion is based on coarse-grained, well-preserved intercumulus texture in zone 2 olivine orthocumulate, and the absence of relics of earlier formed minerals. The orange-brown amphibole is partly altered to metamorphic tremolite–actinolite. Igneous amphibole from the lower part of the Mt Pleasant Sill is a titanium-rich edenitic hornblende. Amphibole from zone 2 (Table 1) contains sufficient titanium to be termed kaersutite (Deer, Howie, and Zussman, 1970). Most grains of primary amphibole, irrespective of which zone they occur in, have an irregular, pleochroic, orange-brown core, and a colourless margin. The coloured cores presumably reflect relatively titanium-rich compositions.

Saussuritization of plagioclase in most zones precludes accurate analysis; but fresh, to weakly altered, plagioclase is preserved in zones 7 and 9. Average compositions indicate andesine–labradorite (An_{52}) in zone 7, and albite (An_4) in the iron-rich granophyre (zone 9).

Secondary magnetite, released during serpentinization of olivine, is common in zone 2 but was not observed in other zones. Leucoxene (after skeletal ilmenite) increases from trace amounts in zone 3 to between 3 and 5% in zone 8; zone 9 contains 4–5% unaltered ilmenite and minor very fine-grained (<50 μm) magnetite containing 5–10% exsolution lamellae of ilmenite.

Geochemistry

Whole-rock major- and trace-element data, and CIPW norms are presented in Table 2. Each sample consists of approximately 1 m of drill core from the Mt Pleasant area. Sampled drillholes are within one or two kilometres of one another and several kilometres from known gold deposits. Care was taken to sample least-altered material but serpentinization and variable carbonatization in zones 2 and 3 are reflected in higher-than-normal values for both CO_2 and loss on ignition. Earlier studies of layered mafic to ultramafic sills in the Eastern Goldfields (Williams and Hallberg, 1973; Jaques, 1976) assumed isochemical metamorphism with regard to most major and trace elements. This assumption appears to be justified by the coherent fractionation trends described by the geochemical data, and is followed in this paper.

The geochemical data indicate a continuous fractionation of the melt from the roof (zone 12) and floor (zone 2) of the sill towards the granophyric zone (zone 9); this is shown by enrichment of SiO_2, TiO_2, $FeO+Fe_2O_3$, and P_2O_5 (Fig. 10). However, zones 8, 9 and 10 are all relatively iron-enriched and TiO_2 has a maximum value in zone 8 (pegmatoidal gabbro).

Analyses plotted on an AFM diagram (Fig. 11) demonstrate a distinct iron-enrichment trend. This trend is compared with those for several other layered and differentiated mafic to ultramafic bodies in the Eastern Goldfields of Western Australia, and overseas. The similarity between trends for the Mt Pleasant Sill and the Golden Mile Dolerite is striking. The trend of the Mt Pleasant Sill also resembles that of the Skaergaard Intrusion in Greenland (Wager, 1960) but lacks the pronounced enrichment in alkalis during the final stages of fractionation. Most other intrusions plotted on Figure 11 have a more basic composition and display a less pronounced iron enrichment. The data from the Mt Pleasant Sill describe a moderate calcium enrichment preceding iron enrichment on a CFM diagram (not reproduced).

The bulk composition of the Mt Pleasant Sill was calculated by summing analyses in Table 2 (on a volatile-free basis) after weighting them according to the thickness of the appropriate zone (see Fig. 3). Separate calculations were made using thicknesses estimated at Mt Pleasant, and average thicknesses estimated during regional mapping. Results are Table 3, which also compares these values with the fine-grained margin (zone 1) and with analyses of some other Archaean mafic rocks.

Petrogenesis

Selected oxides are plotted against silica in Figure 12, and Cr and Ni are plotted against MgO in Figure 13. The absence of pronounced reversals in these diagrams and in Figure 10, and in FeO/FeO+MgO values (Fig. 3) argue against a multiple-injection origin for layering in the Mt Pleasant Sill. Comparable chemistry for the fine-grained margin and calculated bulk composition of the sill also suggest a single pulse of magma was responsible for the layered intrusion. However, the fine-grained margin contains more MgO and Cr, and less CaO, SiO_2, TiO_2, than the calculated bulk composition of the sill (Figs 11, 12, 13, 14, 16). This suggests that the marginal zone is partly cumulate in origin, and is not a true chilled margin.

TABLE 1. SEM MICROPROBE ANALYSES OF RELIC IGNEOUS MINERALS MOUNT PLEASANT SILL

(All mineral compositions are the average of 3 to 6 analysed points; all results expressed as percentage.)

	Pyroxene in zone					*Amphibole in zone*			*Feldspar in zone*	
	2A(a)	3	4	5	12	1	2	2A(a)	7	9
SiO_2	52.91	52.81	52.31	52.96	52.10	45.20	44.06	47.41	55.20	64.05
TiO_2	0.26	0.08	0.16	0.17	0.21	2.89	4.67	2.51	....	....
Al_2O_3	2.72	2.51	2.37	1.79	3.28	9.77	9.99	9.55	28.53	19.17
Cr_2O_3	0.75	0.88	0.68	0.26	0.95	0.37	1.03	0.41	....	....
FeO(b)	6.64	5.03	5.71	5.91	5.95	10.32	8.45	6.95	0.24	0.44
MnO	0.15	0.06	0.17	0.17	0.11	0.15	0.12	0.09	....	....
MgO	16.90	17.26	17.12	17.49	17.14	14.89	15.84	18.25	....	....
CaO	19.97	20.74	20.03	20.00	19.63	11.21	11.21	11.36	10.67	0.86
Na_2O	0.16	bld	0.15	0.14	0.17	2.11	2.90	2.28	5.38	10.41
K_2O	....	....	....	....	....	0.51	0.69	0.11	0.08	0.06
Total	**100.46**	**99.37**	**98.70**	**98.89**	**99.54**	**97.42**	**98.96**	**98.92**	**100.10(c)**	**94.99**
Si	1.93	1.94	1.94	1.96	1.92	6.87	6.61	6.96	2.48	2.95
Al	....	....	....	....	....	....	....	....	1.51	1.04
Al^{IV}	0.06	0.06	0.06	0.04	0.08	1.12	1.39	1.04	....	....
Ti	0.01	bld	0.01	0.01	0.01	0.33	0.53	0.28	....	....
Mg	0.72	0.76	0.76	0.76	0.73	3.38	3.54	3.99	....	....
Fe	0.20	0.15	0.18	0.18	0.18	1.31	1.06	0.57	0.01	0.02
Mn	0.01	bld	0.01	0.01	bld	0.02	0.01	0.01	....	....
Cr	0.02	0.02	0.02	0.01	0.03	0.04	0.12	0.05	....	....
Al^{VI}	0.06	0.05	0.04	0.04	0.06	0.63	0.37	0.61	....	....
Ca	0.78	0.82	0.79	0.79	0.77	1.83	1.80	1.79	0.51	0.04
Mg	0.20	0.18	0.19	0.20	0.21	3.38	3.54	3.79	....	....
Na	0.01	bld	0.01	0.01	0.01	0.62	0.84	0.65	0.47	0.93
K	....	....	....	....	....	0.10	0.13	0.02	0.01	bld
Wo	40.9	42.6	41.4	40.8	40.7	....	....	....	....	....
En	48.2	49.3	49.2	49.6	49.5	....	....	....	....	....
Fs	10.9	8.1	9.5	9.7	9.8	....	....	....	....	....
An	....	....	....	....	....	....	....	....	52.1	4.3
Ab	....	....	....	....	....	....	....	....	47.5	95.3
Or	....	....	....	....	....	....	....	....	0.4	0.3

NOTE: (a) = Zone 2A is the olivine + augite mesocumulate and is not the same as Zone 2U (see Table 2).
(b) = Total iron as FeO. (c) = Low total may be due to incipient saussuritization. Repeated analyses were consistent, which suggests that the composition is valid. (bld) = Below limit of detection. (....) = Not determined.

Element variation diagrams, in general, support petrographic evidence for the primary crystallization history of the sill. The increasing concentration of incompatible elements (SiO_2, TiO_2, alkalis, P_2O_5, V, Y, Zr, and volatiles) towards zones 8 and 9 indicates that these zones represent the most fractionated part of the sill. The positions of these zones in the sill indicate that fractionation took place through crystallization, mainly at the floor of the intrusion. The amount of chromic oxide in the cumulus clinopyroxene (Table 1) provides a guide to the correlation of zones and suggests crystallization at the roof of the sill occurred simultaneously with the formation of zone 3.

Chromium versus MgO, and Ni versus MgO (Fig. 13) are consistent with abundant crystallization of olivine (with small amounts of chromite) in zone 2, and of pyroxenes in

TABLE 2. MAJOR- AND TRACE-ELEMENT GEOCHEMISTRY AND CIPW NORMS, MOUNT PLEASANT SILL

	Zone														
	1	*2L*	*2U*	*3*	*4L*	*4U*	*5*	*6*	*7*	*8*	*9*	*10*	*11*	*12L*	*12U*
							(per cent)								
SiO_2	46.7	39.8	38.8	44.8	48.1	47.8	47.6	47.1	48.2	47.1	54.7	50.2	49.2	49.4	48.5
TiO_2	0.59	0.27	0.27	0.28	0.30	0.30	0.26	0.35	0.59	1.75	1.46	1.46	0.82	0.81	0.74
Al_2O_3	11.8	5.5	5.3	9.3	11.0	13.0	17.4	16.9	16.5	12.7	12.3	12.7	14.0	14.3	14.7
Fe_2O_3	2.7	6.4	6.0	1.8	1.6	1.6	1.6	2.2	2.9	5.8	4.2	2.8	2.6	2.5	2.1
FeO	9.30	6.97	6.92	6.02	5.62	4.90	4.32	5.28	6.72	10.3	13.0	12.9	8.67	7.94	8.12
MnO	0.17	0.19	0.23	0.14	0.12	0.12	0.10	0.12	0.15	0.17	0.22	0.18	0.16	0.13	0.14
MgO	12.7	26.0	23.9	15.7	12.7	10.7	8.63	8.56	6.87	5.26	1.56	3.83	6.84	7.79	8.87
CaO	7.91	3.69	5.89	12.4	15.2	15.5	15.5	13.8	11.5	9.55	8.14	10.2	10.4	9.83	9.30
Na_2O	1.83	0.21	0.27	0.43	0.73	0.73	1.09	1.34	1.95	2.51	1.95	1.73	2.25	2.79	2.13
K_2O	0.38	0.04	0.01	0.27	0.17	0.35	0.03	0.12	0.18	0.23	0.20	0.21	0.28	0.43	0.44
CO_2	0.34	0.60	3.34	3.14	0.80	1.00	0.56	0.52	0.32	0.97	0.29	0.34	0.66	0.80	0.44
P_2O_5	0.11	0.08	0.06	0.08	0.10	0.09	0.09	0.10	0.12	0.15	0.28	0.18	0.12	0.12	0.12
FeS_2	0.03	0.02	0.06	0.05	0.05	0.23	0.11	0.15	0.05	0.03	0.07	0.25	0.10	0.10	0.13
LOI	4.47	8.94	7.53	4.77	2.98	2.57	3.01	3.57	3.35	3.01	1.58	2.55	3.06	2.92	3.38
Other	0.06	0.03	0.03	0.05	0.05	0.05	0.04	0.05	0.07	0.16	0.06	0.10	0.08	0.09	0.09
TOTAL	**99.09**	**98.74**	**98.61**	**99.23**	**99.52**	**98.94**	**100.34**	**100.16**	**99.47**	**99.69**	**100.01**	**99.63**	**99.24**	**99.95**	**99.20**
							(parts per million)								
Cr	952	2650	2500	1697	1515	955	471	42	14	17	<10	10	134	188	278
Ni	250	880	790	330	220	170	120	110	60	15	2	20	65	75	90
Co	55	110	110	55	45	40	35	45	45	65	45	60	45	50	50
V	220	133	125	157	162	160	136	164	203	698	37	335	257	249	241
Ba	84	33	<25	46	<25	<25	<25	<25	45	88	103	94	76	114	159
Sr	45	8	36	67	97	83	95	113	151	113	112	131	145	180	154
Rb	20	3	<5	16	12	26	<5	7	9	9	5	7	13	15	16
Cu	65	25	15	15	45	70	45	100	45	10	10	60	85	35	60
Zn	150	100	115	51	43	56	39	43	54	140	100	105	76	40	50
Zr	31	15	17	16	13	16	19	18	33	41	135	81	42	47	43
Y	16	7	7	9	7	10	8	10	16	22	47	32	20	23	20
							(per cent)								
Qz	....	....	....	....	....	....	....	....	1.92	3.75	18.68	8.72	2.23	....	....
Or	2.36	0.24	0.06	1.71	1.06	2.13	0.18	0.77	1.12	1.42	1.18	1.30	1.71	2.66	2.72
Ab	16.24	1.95	2.54	3.98	6.43	6.43	9.56	11.85	17.09	22.08	16.84	15.06	19.80	24.54	18.70
An	24.04	15.44	14.86	24.59	27.25	32.31	44.07	41.41	37.12	23.68	24.67	27.05	28.32	26.18	30.42
Di	13.24	3.32	13.78	33.19	40.21	37.42	28.11	23.65	17.32	20.30	12.67	20.25	20.18	19.27	13.62
Wo	6.85	1.76	7.30	17.41	21.04	19.57	14.69	12.31	8.91	10.29	6.10	9.98	10.28	9.89	7.00
En	4.41	1.40	5.74	12.73	15.03	13.97	10.36	8.38	5.45	5.32	1.15	3.39	5.67	5.90	4.26
Fs	1.98	0.16	0.75	3.05	4.14	3.88	3.07	2.97	2.95	4.69	5.42	6.87	4.23	3.48	2.36
Hy	26.45	38.34	26.50	19.80	17.22	16.25	14.40	16.35	18.97	15.68	16.13	19.43	20.99	18.35	27.32
En	18.26	34.39	23.45	15.97	13.50	12.72	11.11	12.07	12.30	8.33	2.81	6.42	12.01	11.55	17.59
Fs	8.19	3.95	3.05	3.83	3.72	3.53	3.29	4.27	6.67	7.35	13.32	13.01	8.98	6.81	9.73
Ol	11.05	28.25	30.10	12.19	3.97	0.87	0.76	1.74	....	....	....	....	....	3.12	1.25
Fo	7.39	25.08	26.33	9.64	3.04	0.67	0.57	1.25	....	....	....	....	....	1.89	0.78
Fa	3.65	3.17	3.77	2.55	0.92	0.20	0.19	0.49	....	....	....	....	....	1.23	0.48
Mt	4.12	10.25	9.76	2.83	2.41	2.41	2.41	3.32	4.36	8.76	6.21	4.18	3.91	3.77	3.16
Ilm	1.18	0.57	0.57	0.57	0.59	0.59	0.51	0.68	1.16	3.46	2.83	2.85	1.61	1.60	1.46
Ap	0.28	0.21	0.17	0.21	0.24	0.21	0.21	0.24	0.28	0.38	0.69	0.45	0.28	0.28	0.28

NOTE: Zones 2L, 4L, and 12L, refer to lower parts of zones 2, 4, and 12; 2U, 4U and 12U refer to upper parts.

zone 3. The work of Roeder and Emslie (1970) indicates that a melt with the bulk composition of the Mt Pleasant Sill should crystallize olivine with a forsterite content of Fo_{88-89}. Whole-rock silica is consistent with an average observed cumulus olivine content of about 70% in zone 2 peridotites, assuming the olivine has this composition. However, slightly low whole-rock values suggest possible leaching of MgO during serpentinization and carbonatization.

Zones 4 to 12 reflect depletion in the olivine- and pyroxene-forming components (MgO, Cr, Ni) from the melt. The high CaO values of zones 4 to 6 reflect high modal plagioclase. Relatively Cr-poor augite (Table 1), and small amounts of orthopyroxene also formed in zones 4 to 6. Dominant plagioclase crystallization in zones 5 and 6 caused rejection of Y (Fig. 14) which was concentrated in more fractionated liquids represented by zones 8 and 9,

TABLE 3. COMPOSITIONS OF SOME ARCHAEAN LAYERED AND DIFFERENTIATED SILLS

(Bulk compositions are calculated on a volatile-free basis)

	1	*2*	*3*	*4*	*5*	*6*	*7*	*8*	*9*	*10*	*11*	*12*	*13*
						(per cent)							
SiO_2	49.4	50.2	49.6	49.8	49.36	51.9	51.2	50.9	47.47	47.48	50.46	52.0	51.2
TiO_2	0.68	0.70	0.63	1.53	0.49	0.41	0.38	0.34	0.09	0.14	0.14	0.96	0.53
Al_2O_3	13.9	13.5	12.5	15.1	16.85	12.4	10.3	12.4	2.59	4.08	4.28	15.0	11.4
Fe_2O_3	3.58	3.50	(a)	2.21	2.9	(a)	(a)	(a)	(a)	(a)	(a)	(a)	(a)
FeO	7.6	8.0	9.87	14.12	8.06	9.7	10.2	9.3	10.82	9.94	9.50	10.6	9.9
MnO	0.16	0.16	0.18	0.2	0.19	0.17	0.15	0.16	0.19	0.17	0.15	bld	0.18
MgO	11.2	11.3	13.5	5.4	8.17	15.7	18.7	16.7	35.71	33.09	30.70	6.7	13.2
CaO	11.8	11.5	8.40	9.1	12.48	8.1	7.5	8.3	2.53	4.85	4.02	10.9	11.2
Na_2O	1.41	1.40	1.94	2.0	1.57	1.21	0.78	1.20	0.52	0.20	0.67	2.7	1.77
K_2O	0.16	0.18	0.40	0.1	0.13	0.34	0.21	0.14	0.06	0.04	0.04	0.18	0.14
P_2O_5	0.12	0.13	0.12	0.1	0.12	0.06	0.05	0.06	0.02	0.01	0.04	0.12	0.08
						(parts per million)							
Cr	674	761	953	....	....	1630	....	....	....	....	....	367	....
Ni	196	222	250	....	....	340	....	....	....	....	....	170	....
Y	15	17	16	....	....	....	....	....	....	....	....	....	....
Zr	34	42	31	....	....	41	....	....	....	....	....	61	....

KEY:
1 = Mount Pleasant Sill: calculated bulk composition (thickness of zones estimated from drill intersections at Mount Pleasant).
2 = Mount Pleasant Sill: calculated bulk composition (estimated from relative thicknesses of zones observed during regional mapping).
3 = Mount Pleasant Sill: fine-grained margin (zone 1).
4 = Golden Mile Dolerite: calculated bulk composition (Clark, 1980).
5 = Mount Kilkenny Sill (Leonora): calculated bulk composition (Jaques, 1976).
6 = Mount Monger Sill (Eastern Goldfields): calculated bulk composition (Williams and Hallberg, 1973).
7 = Mount Hunt (Eastern Goldfields): calculated bulk composition (Williams and Hallberg, 1973).
8 = Seabrook Hills Sill (Eastern Goldfields): calculated bulk composition (Williams and Hallberg, 1973).
9 = Koedoe Complex (South Africa): calculated bulk composition (Anhauesser, 1978).
10 = Ship Hill Complex (South Africa): calculated bulk composition (Anhauesser, 1978).
11 = Stolzburg Complex (South Africa): calculated bulk composition (Anhauesser, 1978).
12 = Average low-K tholeiite (Eastern Goldfields): (Hallberg and Williams, 1972).
13 = Mount Monger area (Eastern Goldfields): average of six high-Mg basalts (Williams, 1972)

NOTE:(a) = Total iron is expressed as FeO. (bld) = Below limit of detection. (....) = Not determined.

while clinopyroxene and orthopyroxene remove Cr from the melt. In Figure 14, the change in slope between zones 6 and 7 coincides with the change from crystallization of plagioclase + clinopyroxene + orthopyroxene to clinopyroxene + plagioclase only.

Contamination of the sill from sediments at the roof and the floor of the intrusion is evident from the anomalously high alkali contents in zones 1 and 12 (Fig. 10), and from the presence of primary amphibole in zones 1 and 2. Precipitation of ilmenite ahead of magnetite would have been promoted by high fO_2 and the availability of TiO_2 in the melt. Hydrous contamination of the melt, and shallow emplacement levels discussed below, may have maintained relatively high fO_2 during crystallization.

Asymmetric phase layering

Despite the apparent contemporaneity of zones 3 and 12, there is an absence of phase symmetry between these zones. Orthopyroxene is present in zones 3 to 6, but absent in the upper part of the sill. Plagioclase is the dominant mineral in zones 5 and 6, whereas clinopyroxene is dominant in zones 12 to 10. These differences and the contrasting partitioning behaviour of elements such as MgO, FeO, TiO_2, Y, Cr, and CaO, between clinopyroxene and plagioclase (Pearce and Norry, 1979) help explain the divergent geochemical trends displayed by zones 12 through 9, and zones 4 through 8 (Figs 14, 15). Textural evidence suggests a comparatively high proportion of trapped, intercumulus melt in the upper part of the sill, and this would accentuate the high FeO, TiO_2, and Y, caused by the dominant crystallization of clinopyroxene over plagioclase. In Figure 14, the change in slope of Cr versus Y between zones 10 and 9 in Figure 12 coincides with the beginning of crystallization of quartz.

Contrasting fractionation paths from the floor and roof of the sill may also contribute to the contrasting chemical characteristics of zones 8 and 9, both of which are highly fractionated. For example, TiO_2, alkalis, and volatiles (as indicated by pegmatoidal gabbro), reach maximum levels in zone 8, but SiO_2, FeO (total iron), and P_2O_5 reach maximum levels in zone 9. Figures 12B, D, E, 14, and 15

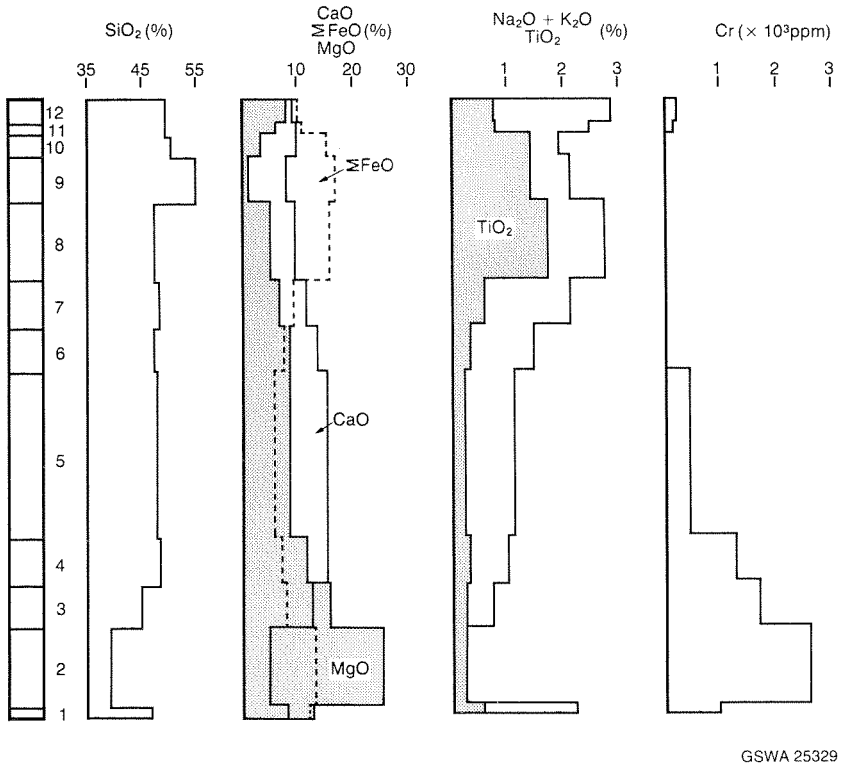

Figure 10. Variation in some geochemical parameters within the Mt Pleasant Sill.

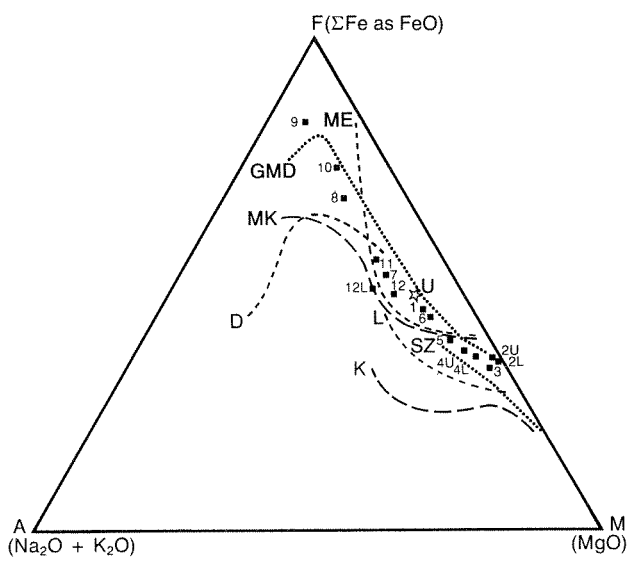

	Numbered squares denote zones of the Mount Pleasant Sill
☆	Calculated bulk composition of the Mount Pleasant Sill
GMD	Golden Mile Dolerite (Travis et al., 1971)
MK	Mount Kilkenny Sill (Jaques, 1976)
ME	Mount Ellis Sill (W. Witt, unpublished data)
L	Layered high–Mg sills of Williams and Hallberg (1973)
D	Dundonald Sill, Canada (from Anhaeusser, 1985)
SZ	Stolzburg trend, South Africa (Anhaeusser, 1985)
K	Kaapmuiden trend, South Africa (Anhaeusser, 1985), includes Ship Hill, Koekoe intrusions. etc.

GSWA 25330

Figure 11. AFM diagram comparing differentiation curves for the Mt Pleasant Sill and for some other Archaean layered sills. Note L and U after a zone number indicates upper and lower parts of the zone.

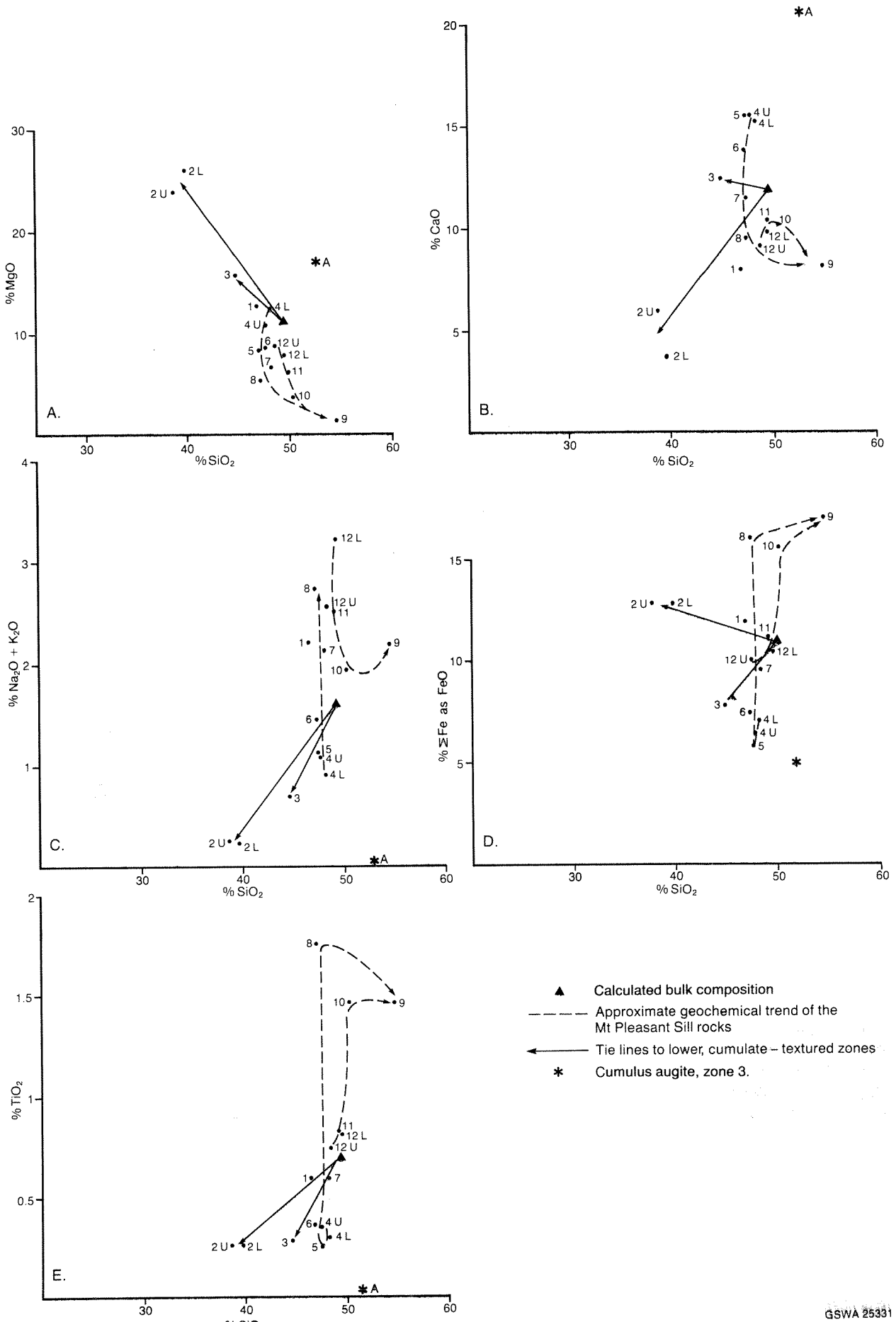

Figure 12. Variation diagrams, Mt Pleasant Sill.

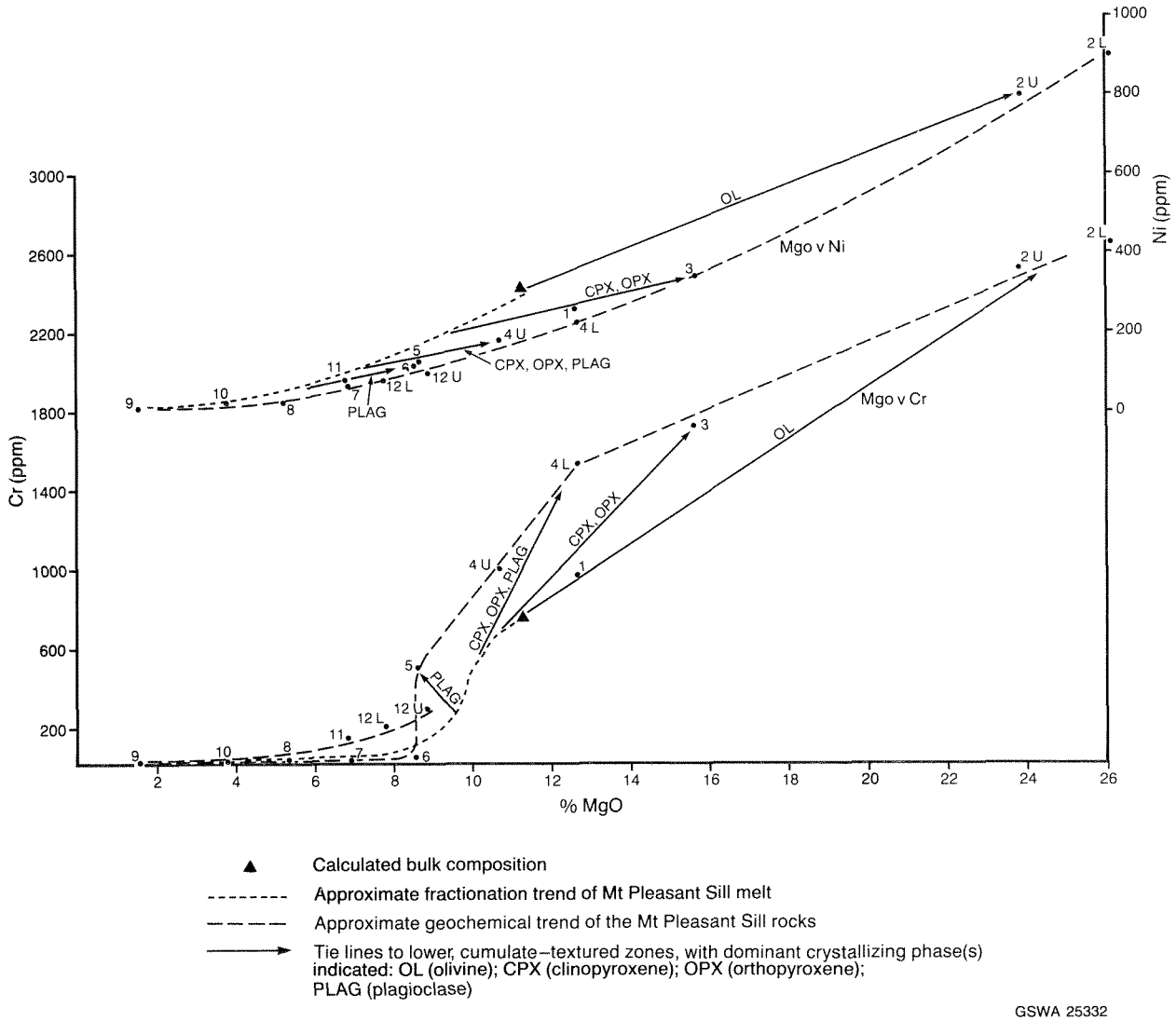

Figure 13. Cr and Ni versus MgO, Mount Pleasant Sill.

suggest that zone 8 may be the end product of fractionation from the base upwards, whereas zone 9 may be end product of fractionating from the top downwards. Homogenization of the melt is required for efficient fractionating. Flow textures in zone 7 suggest that convection currents were operating, and these would have helped to achieve melt homogenization. However, convection may have ceased to operate during the closing stages of crystallization of the sill (Shaw, 1965, Bartlett, 1969), giving rise to stratification of the melt with an upper, SiO_2-rich layer (zone 9) overlying a denser, SiO_2-depleted layer (zone 8).

The reasons for the contrasting crystallization histories at the floor and the roof of the intrusion are uncertain, but may involve greater activity of water near the roof which promoted crystallization of clinopyroxene ahead of plagioclase (Kushiro, 1972). Although contamination from both footwall and hangingwall sediments was likely, crystallization of primary amphiboles would have lowered the concentration of water in the melt by the time zone 3 had begun to crystallize. Relatively high water activity may have been maintained in melt directly below the roof of the intrusion.

Apart from the contrasting fractionation paths of the upper and lower parts of the sill, the preceding discussion indicates that:

(a) nucleation at the roof of the intrusion was delayed until after formation of the olivine-cumulate layer (zone 2);

(b) subsequent crystallization at the roof proceeded more slowly than crystallization at the floor of the intrusion; and

(c) relatively more intercumulus liquid was trapped in rocks forming at the roof of the intrusion, i.e. fractionation near the roof was less efficient than near the floor of the sill.

For thick, layered intrusions these features might be explained by the increase in the melting point of minerals with depth and pressure (Turner and Campbell, 1986). However, the melting-point gradient is only about 3°C/km, and unlikely to be effective in sills which are only 600 m

thick. Turner and Campbell (1986) refer to the local melting of roof rocks to form a stable layer of light felsic melt, which inhibits crystallization near the roof. There is good evidence that this has occurred at the top of the Ora Banda Sill, which has incorporated phenocrysts from the overlying basalt into a felsic granophyre and pegmatoidal gabbro layer at the top of the sill (Witt, 1987). A similar layer is not present at the top of the Mt Pleasant Sill, but contamination by water and alkalis from the hanging-wall shale may have had a similar effect because the addition of water lowers liquidus temperatures of a basaltic melt (Cox et al., 1979, Morse, 1980). Convection movements, which redistributed heat from the lower part of the magma chamber, may also have prevented crystallization at the top of the sill. The same convection currents would have efficiently removed relatively light rest-liquids produced by dominant crystallization of clinopyroxene at the floor of the intrusion. Similar liquids would be less efficiently removed from the crystal–Liquid interface at the roof of the sill since convection currents would have to work against gravity.

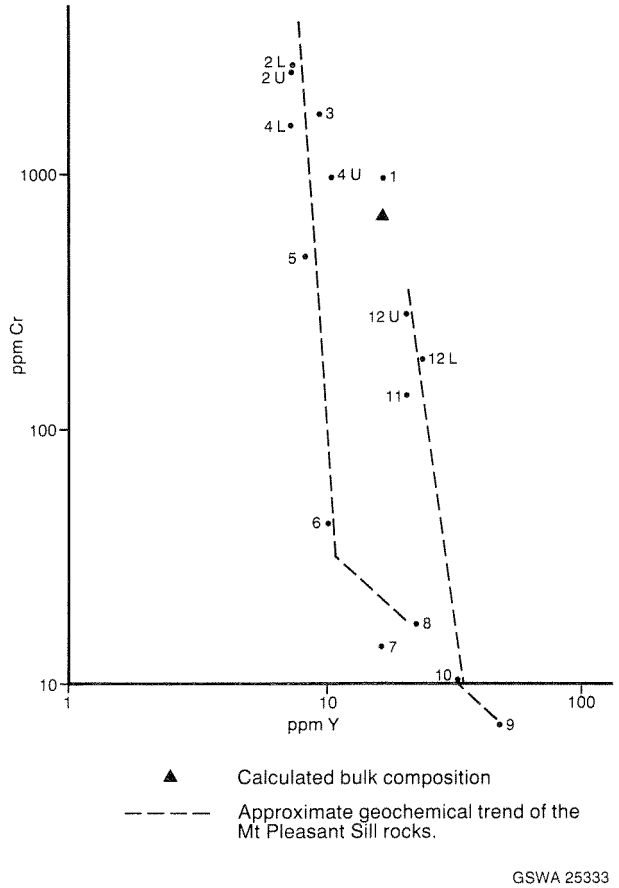

Figure 14. Cr versus Y, Mt Pleasant Sill.

Order of crystallization

The order of crystallization at the base of the sill, based on relic mineralogy and interpretation of metamorphic pseudomorphs, is olivine–clinopyroxene–orthopyroxene–plagioclase; plagioclase began to crystallize very shortly after orthopyroxene. The Mt Pleasant bulk composition (Table 3, col. 1) was plotted on triangular projections from the "system" ol–cpx–plag–SiO_2 (following Irvine, 1970). In Figure 16A, the Mt Pleasant Sill plots in the olivine field, this is consistent with the early crystallization of olivine in zone 2. Projection of the initial melt composition from the olivine corner intersects the orthopyroxene liquidus well before that of plagioclase at 450 MPa (4.5 kb), but passes close to the olivine–orthopyroxene–plagioclase triple point at 1 atmosphere (101.325 kPa). Thus, low confining pressures are indicated by the observed order of crystallization. Similarly, in Figure 16B, the bulk composition plots well into the orthopyroxene field for all but very low pressures. Even at 1 atmosphere, it plots in the plagioclase field rather than the clinopyroxene field, as predicted by the presence of cumulate augite towards the top of zone 2. A high activity of water in the melt, during formation of the cumulate-textured lower zones (2 and 3), consistent with the presence of primary amphibole, expands the clinopyroxene field at the expense of plagioclase (Kushiro, 1972) and could explain the apparent discrepancy.

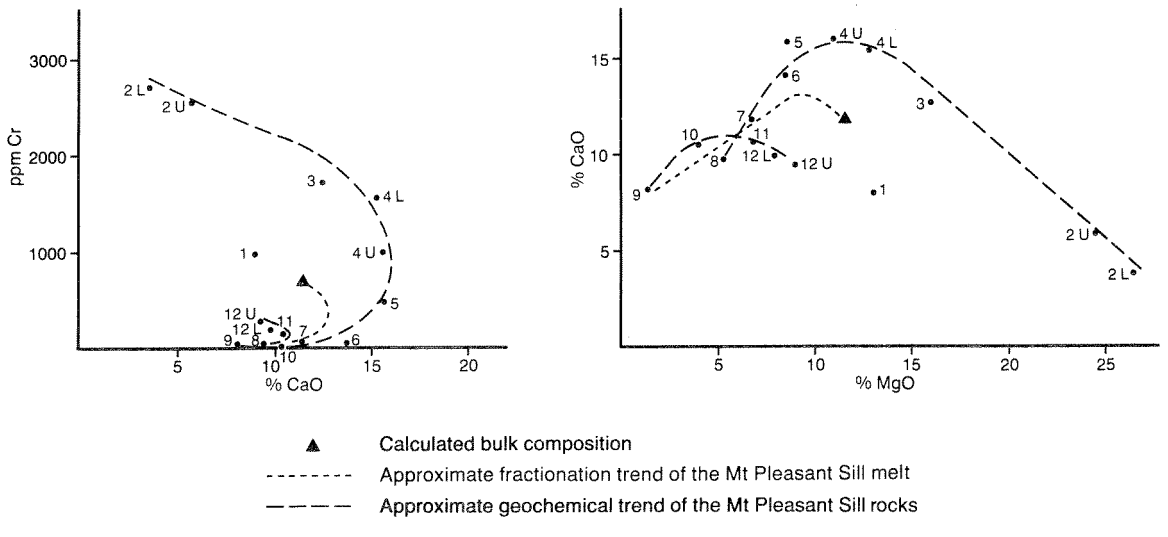

Figure 15. Cr versus CaO and CaO versus MgO, Mt Pleasant Sill.

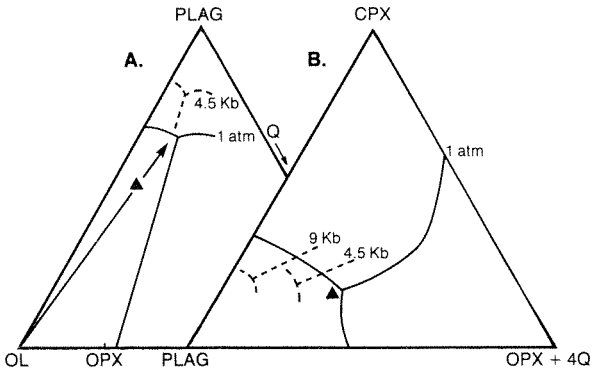

Figure 16. Bulk composition of the Mount Pleasant Sill in the system olivine-clinopyroxene-plagioclase-silica (diagrams after Irvine, 1970). A—projection from the clinopyroxene corner. B—projection from the olivine corner.

Crystal settling or crystallization of cumulus minerals *in-situ*

Current thinking explains cumulate textures in terms of crystal nucleation and growth rates (Irvine, 1980; Campbell, 1978; McBirney and Noyes, 1979; Turner and Campbell, 1986). Whilst most aspects of the Mt Pleasant Sill can be explained by such models, some features challenge crystal settling as a dominant mechanism for fractionation.

Cumulate olivine in zone 2 ranges from about 0.1 to 0.5 mm in diameter. The small size of the cumulate olivine grains prohibits settling through any but the lowest viscosity liquids (McBirney and Noyes, 1979). McBirney and Noyes concluded that olivine may sink in hot, agitated flows and sills, but not in a static body that has begun to nucleate other phases. This introduces doubts about a crystal settling origin for the olivine–clinopyroxene cumulate (zone 2A). Contamination by water may have aided crystal settling by lowering melt viscosity.

Millimetre-scale rhythmic laminations in zone 5 are unlikely to have been formed by crystal settling because the leucogabbros do not display cumulate textures. The laminations could be explained by boundary-layer effects and rapid diffusion rates (Turner and Campbell, 1986; McBirney and Noyes, 1979). Each cycle would have begun with a pulse of plagioclase nucleation and growth. Crystallization would have produced a boundary layer depleted in components needed to form plagioclase. This boundary layer would have been relatively dense and would have ponded above the plagioclase layer. When the cooling front had advanced into the boundary layer, augite would have crystallized until equilibrium had been re-established and another cycle started.

Millimetre-scale lamination did not develop in the ultrabasic zones because the boundary layer was relatively light and convected away from the crystallization front. Alternatively, or additionally, the laminations could have been produced prior to crystallization by opposing temperature and compositional density gradients. McBirney and Noyes (1979) and Turner and Campbell (1986) reviewed experimental work which indicates a magma chamber might become stratified if a temperature gradient destabilizes a density gradient that is the result of composition. Convection resulting from the temperature gradient opposes the tendency for a relatively dense boundary layer produced by crystallization of plagioclase to pond at the bottom of the magma chamber.

North of Ora Banda, exposures several metres across reveal irregular mixing structures at the transition between zones 3 and 4. Inclusions of zone 4 rocks display chilled margins against zone 3 pyroxenite. This feature would seem to require, as suggested by Irvine et al. (1983), some compositional zoning of the sill-forming melt prior to crystallization. It is best explained by convective or tectonic disturbance at the floor of the sill at a stage when zone 3 had formed as a pyroxene-rich crystal mush, and zone 4 had formed as a compositionally distinct melt layer overlying the mush.

Sill or flow?

The remarkable strike length of the sill, and the consistent zoning sequence, are difficult to reconcile with an intrusive origin. However, the evidence for contamination of the upper part of the sill from hangingwall sediments requires roof rocks to have been deposited prior to emplacement of the intrusion. These apparently conflicting observations may reflect shallow emplacement of the melt into unconsolidated sediments, consistent with low confining pressure and high fO_2 during crystallization.

Geochemical affinities

On a MgO–Al_2O_3–CaO diagram after Groves and Gee (1980), the Mt Pleasant Sill plots in the field of overlap between komatiitic basalts and tholeiitic basalts, but close to the limits of the tholeiite field (Fig. 17). This contrasts with the Golden Mile Dolerite (Travis et al., 1971; Clark, 1980) and the Mt Kilkenny Sill (Jaques, 1976), which plot well within the field of tholeiitic rocks. Layered sills studied by Williams and Hallberg (1973), though generally basaltic, are more magnesian than the Mt Pleasant Sill, while the ultramafic sills of South Africa (Anhaeusser, 1985) plot within the komatiitic (peridotite) field.

Redman and Keays (1985) distinguished high-Mg series basalts and siliceous high-Mg series basalts in the Yilgarn Block. The latter are characterized by relatively high SiO_2 and large-ion-lithophile element (LIL) contents, which are interpreted to reflect hydrous melting of LIL-enriched mantle (Redman and Keays, 1985) or crustal contamination (Compston et al., 1986). Titanium versus Zr plots (Fig. 18), and several other discriminatory plots suggested by Redman and Keays (1985) identify the Mt Pleasant Sill melt as a high-Mg series basalt, compositionally comparable to lower footwall basalts at Kambalda. These have Ti:Zr, TiO_2:Al_2O_3 and TiO_2:CaO marginally higher than chondritic ratios. They may have formed by partial melting of a slightly LIL-depleted mantle source, or fractionation of a komatiitic melt.

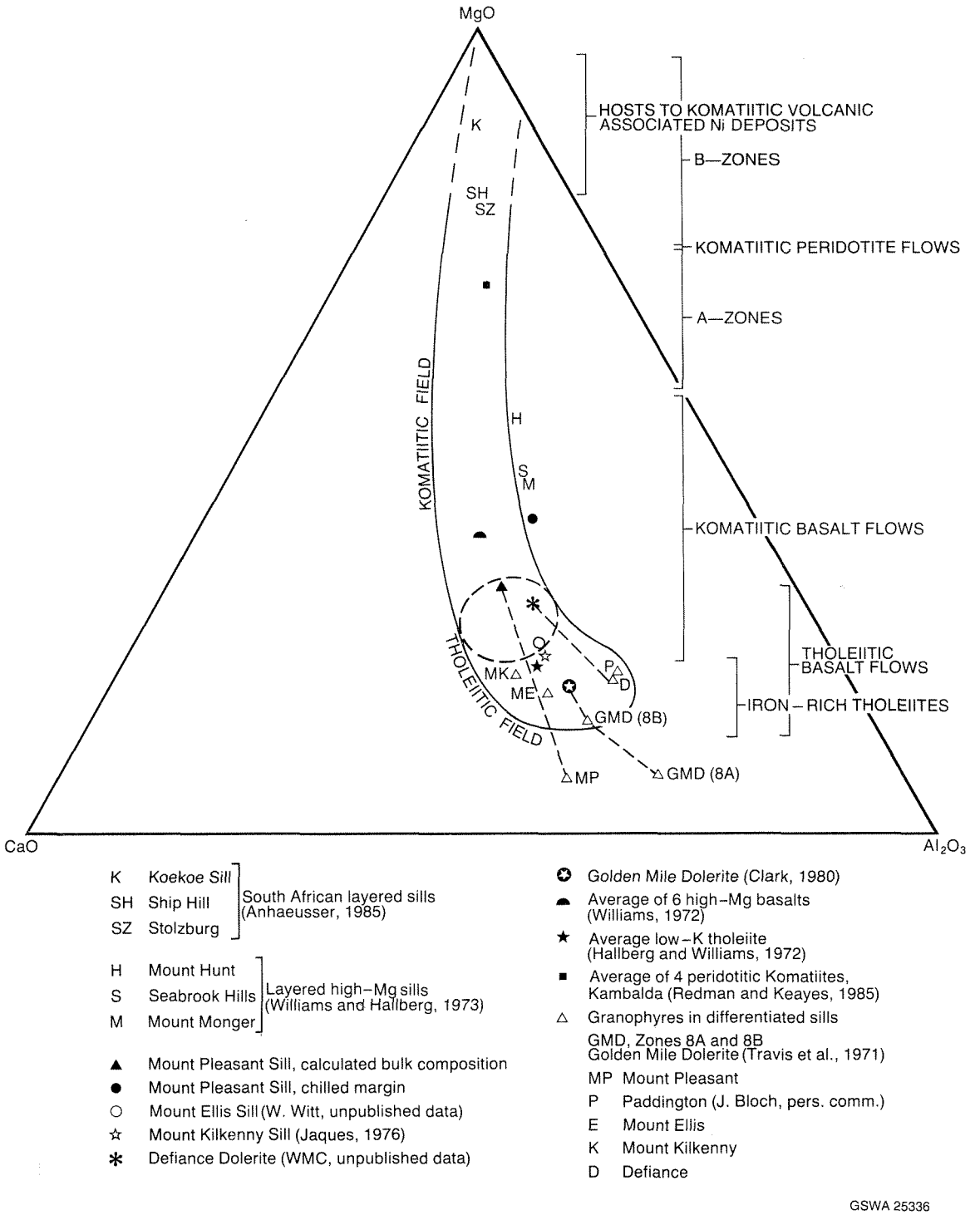

Figure 17. Calculated bulk compositions, Archaean layered mafic to ultramafic sills and related granophyres, plotted on a $MgO–Al_2O_3–CaO$ diagram (after Groves and Gee, 1980).

Discussion

Archaean layered mafic to ultramafic sills display a range of bulk compositions corresponding to the range of Archaean volcanic rocks, from iron-rich tholeiites through to komatiitic compositions. Figure 17 suggests that, for layered sills, there may be a compositional gap between komatiitic basalt and peridotitic komatiite, similar to that for volcanic rocks.

Williams and Hallberg (1973) recognized two types of mafic intrusion in the Eastern Goldfields. These authors described layered intrusions (Ora Banda, Mt Hunt, Mt Monger, Mission, Mt Thirsty, Seabrook Hills, Yilmia) with high-Mg (komatiitic) geochemical affinities; and distinguished these from differentiated sills with tholeiitic affinities. They cited the Golden Mile Dolerite as an example of a differentiated sill and Clark (1980) subsequently confirmed its tholeiitic chemistry. However, cumulate textures

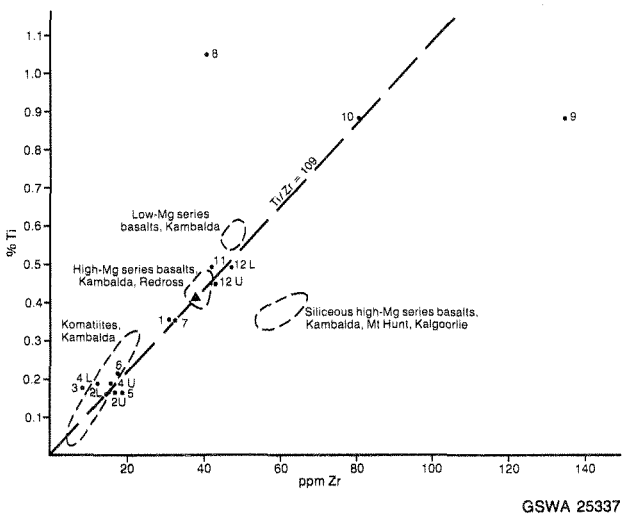

Figure 18. Comparison of Ti:Zr ratios for the Mt Pleasant Sill with selected basalts and komatiites in the Kalgoorlie–Kambalda region. Basalt fields from Redman and Keays (1985).

and phase layering in the Mt Ellis Sill (Witt, 1987; in prep.) and the Mt Kilkenny Sill (Jaques, 1976) indicate that some tholeiitic intrusions may also be layered.

Layered mafic to ultramafic sills in the Eastern Goldfields can be classified according to the order of crystallization of their main cumulus minerals. The crystallization sequence for the Mt Pleasant Sill contrasts with that of the Ora Banda Sill and other layered intrusions described by Williams and Hallberg (1973). These intrusions were described as "Stillwater type" because the order of crystallization was that shown by the Stillwater intrusion in Montana (olivine–orthopyroxene–plagioclase–clinopyroxene). The crystallization sequence shown by the Mt Pleasant Sill is the same as that shown by several Archaean layered sills in the Abitibi region of Canada (Naldrett and Mason, 1968; MacRae, 1969). The sequence, olivine–clinopyroxene–orthopyroxene–plagioclase, is also similar to that displayed by some parts of the Muskox intrusion (Irvine, 1970) and sills showing this order of crystallization could be termed "muskox-type" to distinguish them from the sills described by Williams and Hallberg (1973). A third type of sill in which plagioclase is the first phase to crystallize, is represented by the Mt Kilkenny Sill (Jaques, 1976) and the Mt Ellis Sill (Witt, 1987). Ultimately, this scheme could become unwieldy since a wide variety of crystallization sequences are theoretically possible (Irvine, 1970).

Gee et al. (1976), Griffin et al. (1983), Redman and Keayes (1985) and Clark et al. (1986) correlate greenstone sequences at Kalgoorlie and Kambalda on the basis of a similar succession of lithological units. Although supporting chemical data are presently lacking, the evolution of volcanic units in the Ora Banda sequence is superficially very similar to that in the Kalgoorlie–Kambalda area, and layered mafic to ultramafic units occur at similar stratigraphic levels (Fig. 2). However, the composition and nature of sills at the equivalent stratigraphic levels in each area are quite different.

At Kalgoorlie, the Williamstown Dolerite (Mt Hunt Sill) occurs at the transition from komatiitic to less magnesian volcanic rocks. Detailed published descriptions of the Williamstown Dolerite are not available, but Williams and Hallberg (1973) included it amongst their layered high-Mg sills. In contrast, the Mt Pleasant and Mt Ellis Sills are less magnesian. At Kambalda, the Defiance Dolerite has a composition similar to that of the Mt Pleasant Sill.

At Kalgoorlie, the Golden Mile Dolerite occurs at or near the transition from mafic volcanic rocks to sediments derived from felsic and intermediate volcanics. The Ora Banda sill occupies a position equivalent to the Golden Mile Dolerite, but is far more magnesian. Reference has already been made to the difference between bulk compositions of the Golden Mile Dolerite and the Mt Pleasant Sill: in spite of that difference, the chemical fractionation trends in both units are similar. Other petrographic features in common include mafic-rich basal zones followed by relatively plagioclase-rich zones and granophyre towards the roof of the intrusion. Flow textures caused by alignment of lath-like plagioclase and pegmatoidal patches also occur at similar levels in both sills.

Witt et al. (1988) discussed the role of the Mt Pleasant Sill as a host to gold mineralization in the Ora Banda–Broad Arrow area. Iron-rich granophyre in the upper part of layered mafic to ultramafic sills is an important host to gold mineralization in some mining centres (e.g. Mt Pleasant Sill at Mt Pleasant, Golden Mile Dolerite at Kalgoorlie, the Triumph Gabbro at Celebration, and the Defiance Dolerite at Kambalda). The iron-rich granophyres are believed to fix sulphur as pyrite, thus destablizing soluble thio-complexes of gold (Groves et al., 1984). The sills cited include differentiated tholeiitic sills (e.g. Golden Mile Dolerite) and layered high-Mg sills (e.g. Mt Pleasant Sill), but are all characterized by fractionating from both the floor and the roof of the sill to produce iron-rich granophyre towards the top of but within the intrusion.

Iron-rich granophyres were not recorded for the layered sills studied by Williams and Hallberg (1973). These intrusions appear to have crystallized only from the bottom upwards, and some (e.g. the Ora Banda Sill) have developed a felsic granophyre directly below the roof of the intrusion. Presently available data (Fig. 17) suggest there is a critical composition separating sills which crystallize from both top and bottom inwards and develop iron-rich granophyres from those which only crystallize from base upwards and do not develop iron-rich granophyres. The critical composition seems to fall between that of the Mt Pleasant Sill (11% MgO) and that of the Mt Monger Sill (16% MgO). However, other factors such as size and wall-rock interaction may also be important in controlling the degree of fractionating undergone by a sill.

Primary amphibole has been recognized at the base of both the Golden Mile Dolerite and the Mt Pleasant Sill. Contamination of sill-forming melts from above and below may have aided fractionating and the generation of iron-rich granophyres by lowering the viscosity of the melt and promoting convection. Flow-textured gabbros similar to those of zone 7 in the Mt Pleasant Sill, occur at similar stratigraphic positions within the Golden Mile Dolerite and Triumph Gabbro suggesting that convection currents are active in sills with generate iron-rich granophyres.

Acknowledgements

The Mt Pleasant Gold Group of companies is thanked for assistance and access to drillcore samples. Whole-rock analyses were performed by the Chemistry Centre (W.A.). Bruce Robinson (CSIRO) assisted with microprobe analyses. Neil Harrison (BHP) is thanked for drawing our attention to the "mixing" occurrences north of Ora Banda, and for more general discussions. Jim Cleghorn (Kalgoorlie Mining Associates) and Ian Glacken (Western Mining Corporation) are thanked for permission to examine core from the Golden Mile Dolerite and the Victory Dolerite, respectively. John Clout (Western Mining Corporation) provided the bulk composition of the Victory Dolerite. Steve Barnes (CSIRO) read an early version of the manuscript and offered some valuable comments. The manuscript has also benefited from reviews by John Blockley, Arthur Hickman and Paul Morris of the GSWA, and Jack Hallberg.

References

ANHAEUSSER, C. R., 1985, Archaean layered ultramafic complexes in the Barberton Mountain Land, South Africa, *in* Evolution of Archaean supracrustal sequences, *edited by* L. D. Ayres, P. C. Thurston, K. D. Card, and W. Weber: Geological Association Canada, Special Paper 28.

BARTLETT, R. W., 1969, Magma convection, temperature distribution and differentiation: American Journal Science, v. 267, p. 1067–1082.

CAMPBELL, I. H., 1978, Some problems with the cumulus theory: Lithos, v. 11, p. 311–328.

CHAPMAN, D. M., 1987, Mount Pleasant Gold Project—Golden Kilometer Mine, *in* Second Eastern Goldfields Geological Field Conference, Kalgoorlie: Geological Society Australia (Western Australian Division), Abstracts and Excursion Guide, p. 86–91.

CLARK, M. E., 1980, Localisation of gold, Mt Charlotte, Kalgoorlie, Western Australia: University Western Australia, Unpublished B.Sc. (Hons) thesis.

CLARK, M. E., ARCHIBALD, N. J., and HODGSON, C. J., 1986, The structural and metamorphic setting of the Victory Mine, Kambalda, Western Australia, *in* Gold '86 Symposium, Toronto, Canada: Proceedings, p. 243–254.

COMPSTON, W., WILLIAMS, I. S., and GRESHAM, J. J., 1986, Zircon xenocrysts from the Kambalda volcanics: Age constraints and direct evidence for older continental crust below the Kambalda–Norseman greenstones: Earth Planetary Science Letters, v. 76, p. 299–311.

COX, K. G., BELL, J. D., and PANKHURST, R. J., 1979, The Interpretation of igneous rocks: London, George Allen and Unwin Ltd., 450 pp.

DEER, W. A., HOWIE, R. A., and ZUSSMAN, J., 1970, An Introduction to the rock-forming minerals, Sixth Impression: London, Longman.

GEE, R. D., GROVES, D. I., and FLETCHER, C. I., 1976, Archaean geology and mineral deposits of the Eastern Goldfields: 25th International Geological Congress Excursion Guidebook no. 42A.

GOODE, A. H., 1987, The Lady Bountiful Gold Mine, *in* Second Eastern Goldfields Geological Field Conference, Kalgoorlie: Geological Society Australia (Western Australian Division), Abstracts and Excursion Guide, p. 73–77.

GRESHAM, J. J. and LOFTUS-HILLS, G. D., 1981, The geology of the Kambalda nickel field, Western Australia: Economic Geology, v. 76. p. 1373–1416.

GRIFFIN, T. J., HUNTER, W. M., and KEATS, W., 1983, Geology of the Kalgoorlie–Widgiemooltha district, *in* Eastern Goldfields Geological Field Conference, Kalgoorlie *edited by* P. Muhling: Geological Society Australia (Western Australian Division), Abstracts and Excursion Guide, p. 7–8.

GROVES, D. I. and GEE, R. D., 1980, Regional geology and mineral deposits of the Kalgoorlie–Norseman region, *in* Second International Archaean Symposium, Perth, 1980: Geological Society Australia (Western Australian Division), Excursion Guide, 112 pp.

GROVES, D. I., PHILLIPS, G. N., HO, S. E., HENDERSON, C. A., CLARK, M. E., and WOAD, G. M., 1984, Controls on the distribution of Archaean hydrothermal gold deposits in Western Australia, *in* Gold '82 — The geology, geochemistry and genesis of gold deposits, *edited by* R. P. Foster: Geological Society Zimbabwe, Special Publication 1, p. 689– 712.

HALLBERG, J. A. and WILLIAMS, D. A. C., 1972, Archaean mafic and ultramafic rock associations in the Eastern Goldfields region, Western Australia: Earth Planetary Science Letters, v. 15, p. 191–200.

HILL, R. E. T., GOLE, M. J., and BARNES, S. J., 1987, Physical volcanology of komatiites: Geological Society Australia (Western Australian Division), Excursion Guide Book 1, 74 pp.

HUNTER, W. M., 1988, Kalgoorlie W.A.: Western Australia, Geological Survey, 1:100 000 Geological Series—Map.

IRVINE, T. N., 1970, Crystallization sequences in the Muskox Intrusion and other layered intrusions: Geological Society South Africa, Special Publication 1, p. 441–476.

IRVINE, T. N., 1980, Magmatic infiltration metasomatism, double diffusive fractional crystallisation, and adcumulus growth in the Muskox Intrusion and other layered intrusions, *in* Physics of magmatic processes, *edited by* R. B. Hargraves: Princeton University Press, p. 325–383.

IRVINE, T. N., KIETH, D. W., and TODD, S. G., 1983, The J-M platinum-palladium reef of the Stillwater Complex, Montana: II. Origin by double diffusive convective magma mixing and implications for the Bushveld complex: Economic Geology, v. 78, p. 1287–1334.

JAQUES, A. L., 1976, An Archaean tholeiitic layered sill from Mt Kilkenny, Western Australia: Geological Society Australia, Journal, v. 23, p. 157–168.

JAHNS, R. H. and BURNHAM, C. W., 1969, Experimental studies of pegmatite genesis: I. A model for the derivation and crystallisation of granitic pegmatites: Economic Geology, v. 64, p. 843–864.

KUSHIRO, I., 1972, Effects of water on the composition of magmas formed at high pressure: Journal Petrology, v. 13, p. 311–334.

MACRAE, N. D. 1969, Ultramafic intrusions of the Abitibi area, Ontario: Canadian Journal Earth Science, v. 6, p. 281–303.

McBIRNEY, A. R. and NOYES, R. M., 1979, Crystallisation and layering of the Skaergaard Intrusion: Journal Petrology, v. 20, p. 487–554.

McCALL, G. J. H., 1973, Geochemical characteristics of some Archaean greenstone suites of the Yilgarn structural province, Australia: Chemical Geology, v. 11, p. 243–269.

MORSE, S. A., 1980, Basalts and phase diagrams: New York, Springer Verlag, 493 pp.

NALDRETT, A. J. and MASON, G. D., 1968, Contrasting Archaean ultramafic igneous bodies in Dundonald and Clergue Townships, Ontario: Canadian Journal Earth Science, v. 5, p. 11–143.

PEARCE, J. A. and NORRY, M. J., 1979, Petrogenetic implications of Ti, Zr, Y and Nb variations in volcanic rocks: Contributions Mineralogy Petrology, v. 69, p.. 33–47.

REDMAN, B. A. and KEAYS, R. R., 1985, Archaean basic volcanism in the Eastern Goldfields Province, Yilgarn Block, Western Australia: Precambrian Research, v. 30, p. 113–152.

ROEDER, P. L. and EMSLIE, R. F., 1'970, Olivine–liquid equilibrium: Contributions Mineralogy Petrology, v. 29, p. 275–289.

SHAW, H. R., 1965, Comments on viscosity, crystal settling and convection in granitic magmas: American Journal Science, v. 263, p. 120–152.

TRAVIS, G. A., WOODALL, R., and BARTRAM, G. D., 1971, The geology of the Kalgoorlie Goldfield, *in* Symposium on Archaean rocks, Perth, 1970, *edited by* J. E. Glover: Geological Society Australia, Special Publication 3, p. 175–190.

TURNER, J. J. and CAMPBELL, I. H., 1986, Convection and mixing in magma chambers: Earth Science Reviews, v. 23, p. 255–352.

WAGER, L. R., 1960, The major element variation of the layered series of the Skaergaard intrusion and a re-estimation of the average composition of the hidden layered series and of the successive residual magmas: Journal Petrology, v. 1, p. 364–398.

WILLIAMS, D. A. C., 1971, Determination of primary mineralogy and textures in ultramafic rocks from Mt Monger, Western Australia, *in* Symposium on Archaean Rocks, Perth, 1970, *edited by* J. E. Glover: Geological Society Australia, Special Publication 3, p. 259–268.

WILLIAMS, D. A. C., 1972, Archaean ultramafic, mafic, and associated rocks, Mount Monger, Western Australia: Geological Society Australia, Journal, v. 19, p. 163–188.

WILLIAMS, D. A. C. and HALLBERG, J. A., 1973, Archaean layered intrusions of the Eastern Goldfields, Western Australia: Contributions Mineralogy Petrology, v. 38, p. 45–70.

WITT, W. K., 1987, Stratigraphy and layered mafic/ultramafic intrusions of the Ora Banda sequence, Bardoc 1:100 000 sheet, Eastern Goldfields: An excursion guide, *in* Second Eastern Goldfields Geological Field Conference, Kalgoorlie: Geological Society Australia (Western Australian Division), Abstracts and Excursion Guide, p. 49–63.

WITT, W. K., 1991, Geology of the Bardoc 1:100 000 sheet, Western Australia, Geological Survey, Record 1990/14.

WITT, W. K., CHAPMAN, D. M., and FISH, B. L., 1988, The role of layered mafic/ultramafic intrusions as hosts to gold mineralization in the Eastern Goldfields, Western Australia, with particular reference to the Mount Pleasant sill, *in* Bicentennial Gold 88 Extended Abstracts Poster Programme, Vol. 1: Geological Society Australia, Abstracts no. 23, p. 51–53.

2474/6/91-500-L/5425

GARRY L. DUFFIELD, Government Printer, Western Australia